The helicase-like domain from *Thermotoga maritima* reverse gyrase: catalytic cycle and contribution to DNA supercoiling

Inauguraldissertation

zur

Erlangung der Würde eines Doktors der Philosophie

vorgelegt der

Philosophisch-Naturwissenschaftlichen Fakultät

der Universität Basel

von

Yoandris del Toro Duany

aus

Santiago de Cuba, Kuba

Basel 2011

Genehmigt von der Philosophisch-Naturwissenschaftlichen Fakultät

auf Auftrag von

Prof. Dr. Dagmar Klostermeier

Prof. Dr. Nenad Ban

Basel, den 21. Juni 2011

Prof. Dr. M. Spiess

(Dekan)

Table of Contents

I. Summary

Reverse gyrases are the only topoisomerases capable of introducing positive supercoils into circular DNA. Their exclusive presence in thermophilic and hyperthermophilic organisms indicates a DNA thermoprotective role *in vivo*. In spite of the efforts to improve our knowledge of reverse gyrase, modest progress has been made since its discovery. Currently, only one crystal structure of the enzyme is available, and the most widely accepted reaction mechanism is a hypothetical one, mostly derived from the functions of enzymes related to reverse gyrase domains.

In the present work we address mechanistic aspects of the reaction by exploiting the capabilities of a wide range of techniques, to elucidate the role of one module of *T. maritima* reverse gyrase. Reverse gyrase consists of an N-terminal helicase-like domain, fused to a C-terminal topoisomerase domain. We selected the helicase-like domain as a model of study due to its capacity to couple ATP binding and hydrolysis to DNA processing. Exploiting of these features by reverse gyrase turns this region into a key player at virtually every step of DNA supercoiling.

Steady-state ATPase assays and equilibrium binding titrations with the helicase-like domain and the full-length enzyme, enabled us to prove for the first time a harnessing effect of the topoisomerase over the helicase-like domain. We showed that properties intrinsic to the helicase-like domain, like DNA-stimulated ATP hydrolysis, nucleotide-dependent affinity switch for DNA, and thermodynamic coupling between DNA binding and ATP binding and hydrolysis, are strongly reduced in the context of reverse gyrase. At that time apparent contradictions arose, from reports stating that the isolated helicase-like domain is less active than within the context of the full-length enzyme. We reconciled these differences by demonstrating that the presence of the putative N-terminal Zn-finger in the helicase-like domain construct is the cause for the decreased activity. Furthermore, we have elucidated the thermodynamic and conformational cycle of the helicase-like domain, and predicted the stages fulfilling the requirements for interdomain communication,

local duplex DNA unwinding, and the stages where DNA is in a suitable state to support the supercoiling reaction. Finally, besides the use of smFRET as a tool to investigate conformational changes in solution, we have also provided high-resolution snapshots of the helicase-like domain *via* X-ray crystallography. We have provided the most detailed structures of this region to this date, in the apo and ADP-bound forms. They also revealed high flexibility of the linker joining the RecA domains with relative orientations far from random, and local differences in secondary structure motifs that discard the assumption of all reverse gyrases having a “monolithic” build-up.

We also created a deletion mutant of the latch, region with a *sui generis* location, perfectly suited for interdomain communication. Previous reports stated that its deletion from reverse gyrase abolishes positive supercoiling. We demonstrated its strong involvement in DNA binding, DNA-stimulated ATP hydrolysis, and thermodynamic coupling between these processes in the isolated helicase-like domain. We also revealed its role in presenting the ssDNA to the topoisomerase domain and in guiding the strand passage and resealing, ensuring the directionality leading to the introduction of positive supercoils. Additionally, we also elucidated the nucleotide cycle and conformational transitions for this helicase-like domain mutant, which gave the first indications of why no positive supercoiling can be performed by the full-length reverse gyrase lacking the latch, and only DNA relaxation is allowed.

Finally, our pre steady-state kinetic studies allowed us to fully describe the unstimulated ATPase activity of the isolated helicase-like domain. We also demonstrated for the first time its DNA unwinding activity, shedding light on the rarely documented local B-DNA duplex destabilization of helicase-like modules, appended to bigger enzymes. Additionally, the sequence of ssDNA strand release, and identification of secondary structure motifs involved in ssDNA binding at different stages were determined. Together with the finding of new conformational states *via* smFRET, and “targeted” supercoiling assays with the full-length enzyme, we end up proposing a detailed catalytic mechanism, similar to the one derived from the reverse gyrase structure, only this time based on and supported by a combination of kinetic, thermodynamic, and structural data.

II. Introduction

Reverse gyrase is an enzyme exclusive to thermophilic and hyperthermophilic organisms[1] that exerts a DNA-thermoprotective role and thus facilitates life at high temperatures[2]. Although this enzyme has the unique capability of introducing positive supercoils into the DNA in an ATP-dependent manner[3], its main role *in vivo* is still debated. Positive DNA supercoiling may prevent spontaneous local unwinding of the double helix, but does not protect DNA from chemical degradation, the main hazard at high temperatures[4]. More recently it has also been reported that reverse gyrase may act as a DNA chaperone by binding to the nicked regions and thus preventing DNA from melting[5], and even to act as a DNA renaturase by re-annealing single-stranded regions[6]. Most probably its contribution to DNA thermostability is the combination of all these individual effects, and maybe others not yet identified. On the other hand, it has been shown that the deletion of the reverse gyrase gene is not lethal for hyperthermophiles, although it induces growth retardation in culture[2]. Overall, hyperthermophiles seem to have redundant mechanisms to ensure DNA homeostasis, and the cooperation of reverse gyrase with partners like the DNA repair machinery is most probably the key to ensure it[5]. Nevertheless, the main contribution of reverse gyrase is still most likely topological, since the plasmid DNA of hyperthermophiles has been mostly found either in a relaxed or a positively supercoiled state[7,8].

Due to its length, and in the case of prokaryotes its circular nature, DNA topology poses a challenge to DNA readout, remodeling, and replication[9]. In its relaxed form, B-DNA has 10.4 base pairs per turn (bp/turn) at 25°C and low magnesium concentration, whereas 10.6 bp/turn at 83°C under the same salt conditions[10]. This implies that at higher temperatures relaxed double-stranded DNA (dsDNA) is more prone to unwinding due to a reduction of the energetic barrier for strand separation. The circular nature of bacterial DNA prevents alleviation of the torsional stress introduced by virtually all proteins involved in DNA processing[11]. Only strand breakage, controlled strand passage, and resealing ensure a dynamic regulation of the DNA torsional state, compatible with the metabolic processes that affect it[12]. The degree of

torsion is commonly expressed in terms of the linking number (L), which depends on the twist (T) of the single strands on each other, and the writhe (W) of the double helix on itself, as follows[13]:

$$L = T + W \quad (1)$$

If L is smaller than the amount of bp/turn corresponding to the relaxed dsDNA, the DNA is negatively supercoiled, and if L is larger it is called positively supercoiled DNA (Figure 1). Since the structure of relaxed dsDNA in hyperthermophiles is less stable than its equivalent in mesophiles, the introduction of positive supercoils seems to be an adaptation to cope with life at high temperatures[14].

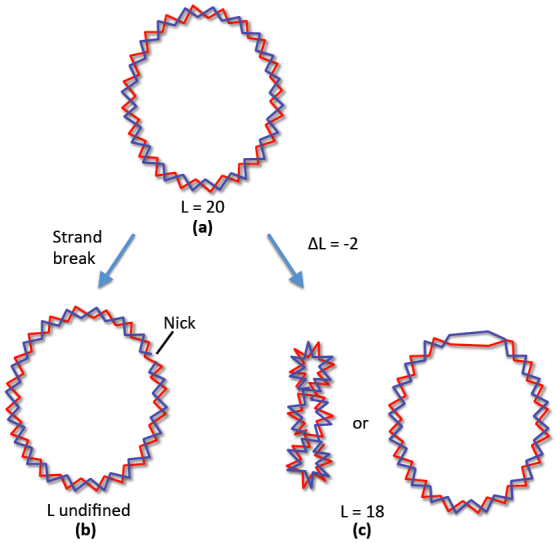

Figure 1. Interconversions between relaxed and supercoiled circular DNA. (**a**) Given a relaxed circular DNA with a linking number of 20, after strand breakage (**b**), depending on the direction the resealing is made, positive or negative supercoils are introduced. (**c**) If the resealed DNA has a linking number smaller that 20 a negative supercoiled was introduced. The torsional stress can be compensated with local unwinding or negative supercoils. Picture adapted from[49].

Reverse gyrase was first identified in *Sulfolobus acidocaldarius* [15] and is one of the enzymes that regulate the topological state of DNA in thermophiles and hyperthermophiles. Its structural signature is the fusion of a topoisomerase domain to a helicase-like domain[16], the last one harboring an insertion that plays a key role in interdomain communication[17]. To date, the only high-resolution structure available of a full-length reverse gyrase is from *Archaeoglobus fulgidus*[18]. It shows an N-terminal helicase-like module with homology to the superfamily 2 of helicases, linked to a C-terminal topoisomerase domain that shares 30 % sequence identity with the topoisomerase I from *E. coli* (Figure 2). Like other members of the IA family, the topoisomerase domain possesses two putative Zn-fingers, probably implicated in DNA binding[9]. Interestingly, the N-terminal Zn-finger appears before the helicase-like domain in the primary structure, although it belongs to the topoisomerase domain in the tertiary structure[18]. This is the first report of these modules expressed in the same polypeptide chain, which otherwise

appear independently in nature, although many processes require their cooperation in trans.

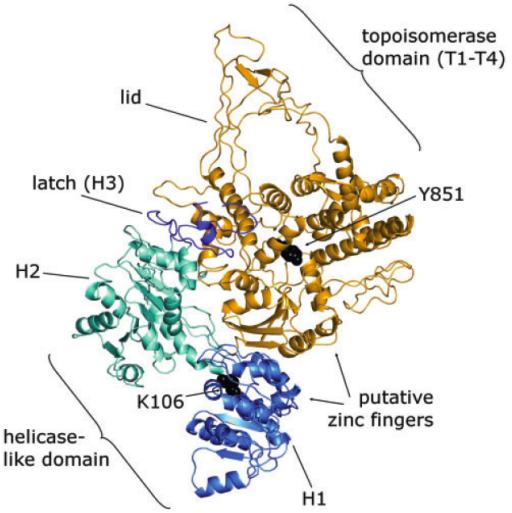

Figure 2. Homology model of *T. maritima* reverse gyrase. It shows the RecA domains of the N-terminal helicase-like module in dark blue and green. Additionally, the latch domain, an insertion into the H2 domain is shown in dark blue. The topoisomerase domain shows a Rossman fold called domain T1, followed by domains T4, T2, and T3T2, which constitute the so-called lid. The location of the putative Zn-fingers is indicated with arrows.

Reverse gyrase is a type IA topoisomerase *i.e.*, it increases the linking number by one after cleavage, passage, and resealing of only one strand of the DNA duplex, with formation of a transient covalent link to the 5' phosphate. Combining the known functions of helicases and topoisomerases a catalytic mechanism for reverse gyrase has been proposed. It starts with processive DNA unwinding by the helicase-like domain that generates positive supercoils ahead of the direction of propagation, and negative supercoils behind. Finally, the negative supercoils are removed by the topoisomerase domain with a net generation of positive supercoils[16]. Studies with the isolated modules reveal that the topoisomerase domain is able to relax DNA on its own[19], and the helicase-like domain acts as a nucleotide-dependent switch to synchronize the DNA preference with the nucleotide state[20]. Another catalytic mechanism has been proposed from the reverse gyrase crystal structure and the available biochemical data at the time. This last mechanism also assumed conformational changes, derived from the crystal structures of DNA topoisomerase I from *E. coli*[21], and PcrA helicase from *B. stearothermophilus* in complex with ssDNA and ADPNP[22]. First, a conformational change in the helicase-like domain upon DNA and ATP binding triggers the release of the lid in the topoisomerase domain. The resulting conformation exposes the catalytic tyrosine that breaks a DNA strand and covalently binds to the 5'-end of the nick. Afterwards, the intact chain is "relocated" within the cavity of the topoisomerase domain and at the resealing step, a positive supercoil is introduced. Finally, the initial conformation is regained to allow product

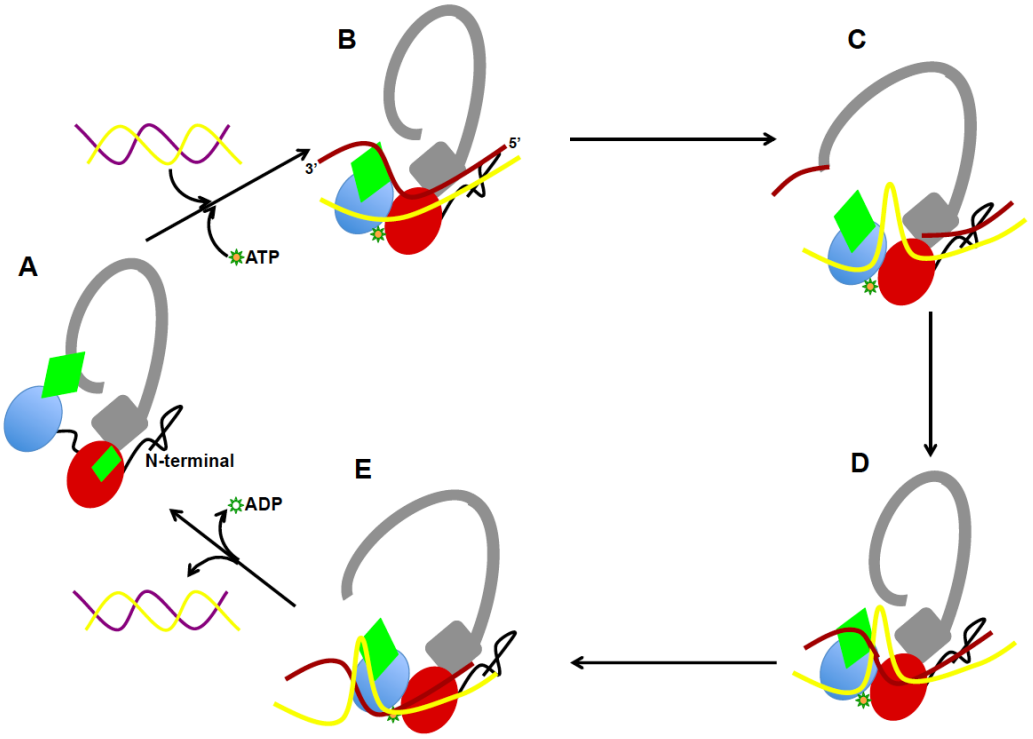

Figure 3. Hypothetic catalytic cycle of reverse gyrase. **A** It starts with the enzyme in the conformation of the apo form in the crystal structure. **B** Upon ATP and DNA binding the helicase-like domain adopts a closed conformation that disengages the latch from the contact with the lid and unwinding occurs. **C** The lid is able to break a strand and remain attached to the 5' end of the ssDNA. At the same time the intact ssDNA strand is relocated within the cavity of the topoisomerase domain. **D** The cleaved strand is resealed with the introduction of a positive supercoil. **E** The lid re-opens to allow release of the supercoiled DNA. Adapted from[18].

release[18] (Figure 3). Although this model has an undoubted merit, it does not provide necessary information to understand the supercoiling reaction. Since ATP hydrolysis fuels the supercoiling reaction, the energetic aspects related to the nucleotide cycle are relevant. Each step is supposed to be controlled by the nucleotide state. Therefore it is important to know the simultaneous progression of DNA and nucleotide through the cycle, and how they influence each other. Also, structural details like which regions of the enzyme are involved in binding to specific DNA segments at each point of the cycle, are likely to be more precisely assigned as more biochemical and structural data become available.

It has been reported that the topoisomerase and helicase-like domains interact extensively, and their functions are strongly modulated by the presence of the other domain[17,19,20]. Both modules share a common substrate – the DNA. As a result, individual contributions of the domains are difficult to spot due to their overlap during the reaction cycle. The electrostatic surface potential also shows large positively charged grooves and patches that

indicate extensive interaction with DNA (Figure 4). Untangling of the reaction mechanism requires further characterization of the isolated domains and proper identification of their contributions to the reaction. The present work addresses the characterization of different constructs of the isolated helicase-like domain from *Thermotoga maritima* reverse gyrase, as a first approach to investigate its contribution to DNA supercoiling. Furthermore, specific properties were successfully assigned to individual regions of the domain[17].

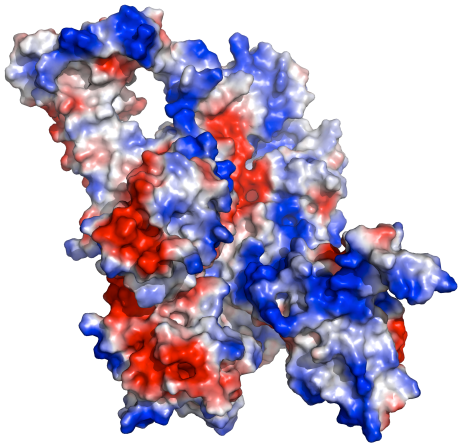

Figure 4. Electrostatic surface potential of *T. maritima* reverse gyrase homology model. It shows large positively charged patches and grooves in blue. They are potential DNA binding sites. Generated with Pymol (http://www.pymol.org).

Helicases are a widely distributed group of enzymes that couple the energy of hydrolysis of triphosphate nucleotides (NTP) to nucleic acids processing[23]. Historically, it has been assumed that their role *in vivo* consists of unwinding double helix structures, as it was the case for the first members of the group identified[24]. Over time, many new helicases and helicase-like enzymes have been identified where such an unwinding activity has not been detected. For some of them translocation along DNA/RNA strands, protein displacement[25], and DNA/RNA annealing[26] activities have been demonstrated instead. So far, the best characterized helicases are the ones involved in functions like DNA replication and transcription, where they processively unwind dsDNA, while helicase-like enzymes or helicase-like domains from larger proteins are only beginning to be understood. Overall, helicases are known to be involved in virtually every step of nucleic acids metabolism, like DNA read-out, replication, repair, remodeling, and recombination; as well as RNA splicing, editing, ribosome biogenesis, among others[27,28,29,30].

Assignation of enzymes to the group of helicases is based on their structural signatures. They share the distinctive Walker A motif, which is a seven amino acids consensus sequence (GXGXGK[T/S]) related to ATP binding. This motif normally appears in a loop (P loop) at the interface of a bipartite nucleotide binding site [31]. Located at the same side of the nucleotide-binding pocket is

the Walker B motif, another conserved region among all helicases. Its main feature is the presence of an aspartate residue (D) that for many members of the group appears in the context of a “DEAD” sequence, also involved in interaction and hydrolysis of NTP [32]. Helicases are further sub-classified into 5 superfamilies, based on the presence of additional group-specific conserved sequences[33]. These consensus sequences normally appear at both sides of the nucleotide binding site, at the interface between two domains arranged either in RecA folds [34] or in some cases AAA+ folds [35]. In the case of monomeric and dimeric helicases this interface is intramolecular. For hexameric helicases however, it appears at the contact regions of adjacent monomers. Reverse gyrase helicase-like domain belongs to the superfamily 2 (SF2) of helicases, which comprise DExD/H helicases, the RecQ family and SWI/SNF family[28].

Helicases come in different flavors, not only determined by their primary structure, but also their oligomeric state[31]. There are hexameric, dimeric, monomeric helicases, and they can even be found as domains of bigger proteins[30]. There are also reports of helicases that change their oligomeric state upon binding to nucleic acids[36]. This broad spectrum of oligomeric states also correlates with the way the unwinding reaction is performed. While hexameric helicases are highly processive[31], dimeric helicases are an intermediate case with members that processively unwind[29] and members that locally destabilize the double helix. Monomeric helicases on the other hand, have been reported to either lack unwinding activity or locally destabilize the double helix, although more recently a few members of this group have also been reported to achieve processive unwinding[37]. Another source of diversity is the insertion of accessory domains or secondary structure motifs to the archetypical core. These regions have been reported to be responsible for substrate specificity and recognition of accessory proteins[38].

There are currently two widely accepted models to explain the unwinding mechanism of processive non-hexameric helicases. Biochemical data of the Rep helicase led to the proposal of a “rolling mechanism”[29], while mostly based on crystallographic data from PcrA an “inchworm mechanism”[22] has been proposed (Figure 5). Both models include the requirement of two DNA

binding sites with different preferences at a given point of the catalytic cycle, *i.e.*, ssDNA and dsDNA binding sites that simultaneously interact with the

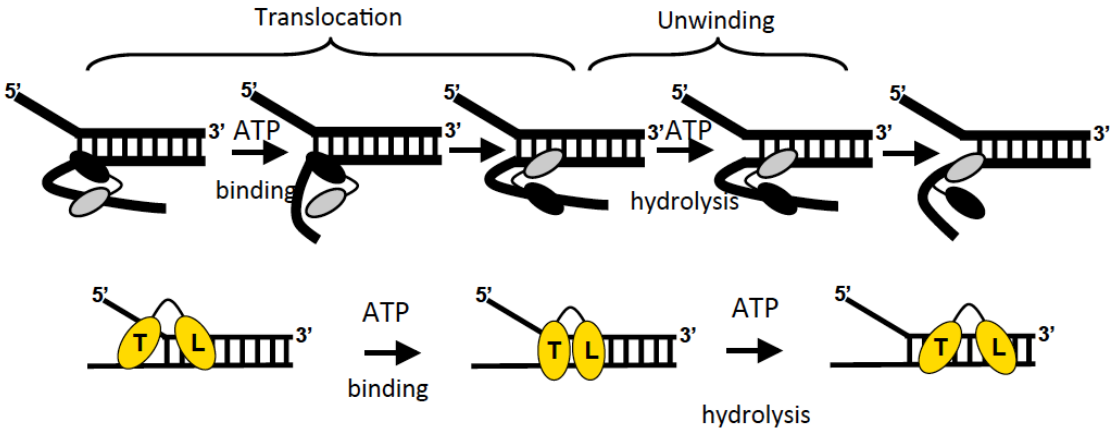

Figure 5. The most accepted models for processive unwinding of non-hexameric helicases. **Top**: rolling mechanism, where the units of a dimer alternate between ss- ds-DNA preferences and upon ATP hydrolysis the monomer bound to dsDNA locally unwinds it. **Bottom**: inchworm mechanism where the sites with ss- and dsDNA preferences are located within the same monomer. ATP-driven conformational changes switch the affinity of the site with preference for dsDNA promoting local unwinding. The dsDNA preference is regained after nucleotide exchange and so the cycle is repeated. Adapted from[28].

substrate. The rolling mechanism contemplates alternate nucleotide states of helicases forming a dimer, where the ATP-bound helicase has a preference for dsDNA and promotes local unwinding during nucleotide hydrolysis, undergoing a preference switch for ssDNA in the post-hydrolysis state and therefore hindering re-annealing of the unwound segment by remaining attached to one of the generated ssDNA regions. At that point the other monomer is able to bind ATP and therefore resume unwinding by attaching itself to the next dsDNA segment at the junction, repeating the cycle described for the first monomer. The inchworm mechanism on the other hand, contemplates the existence of a catalytic form of a monomer with the regions that bind ssDNA and dsDNA contained in the same polypeptide chain. It involves the presence of a trailing binding site with constitutive ssDNA preference and a leading site with a nucleotide-dependent DNA preference. The cycle starts with a closed conformation of the enzyme in the ATP-bound state, where the leading site preferably binds to and unwinds dsDNA during ATP hydrolysis. After hydrolysis the enzyme, anchored at the trailing site, returns to the open conformation and thus relocates the leading site in a position suited for another round of unwinding after nucleotide exchange.

Hexameric helicases on the other hand, unwind dsDNA by translocating a ssDNA strand in the interior of their ring-shaped structure. The monomers contact the ssDNA strand with either loops or hairpins that project to the interior cavity, in an orientation that depends on the nucleotide-state. That way, with every round of ATP hydrolysis of each unit within the hexamer, the complex is pulled forward one base along the ssDNA, producing unwinding of the duplex[30].

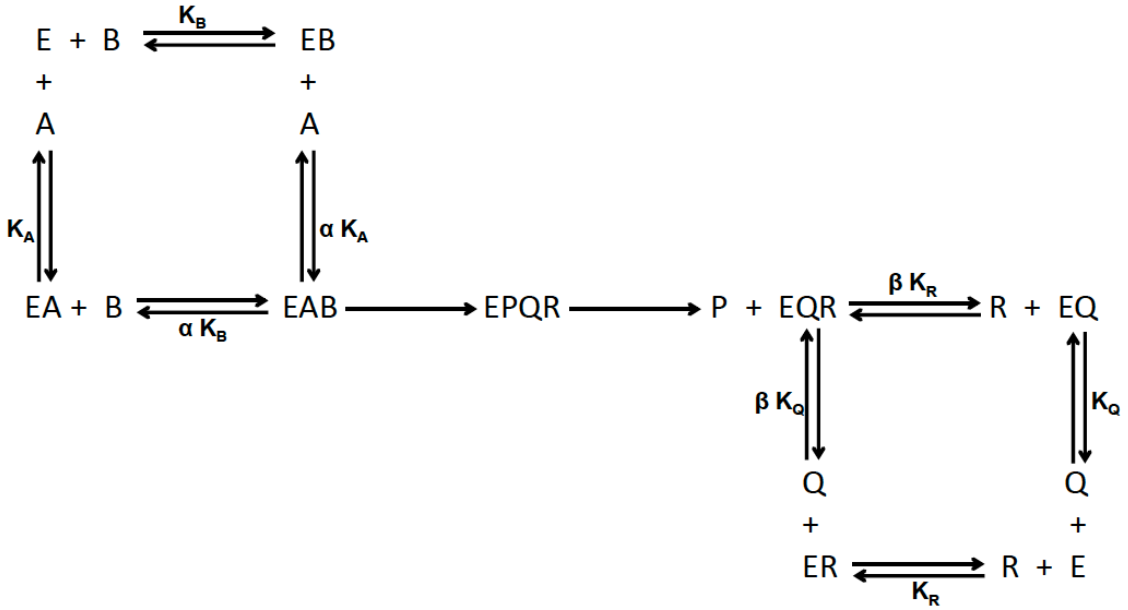

Figure 6. Reactions thermodynamically coupled from an enzymological point of view. Binding of the substrates should cooperatively increase the affinity for the second in the same factor α. On the other hand, release of the substrates should also be favored by a negative effect of binding of the first substrate on the second, also in the same factor β. If the equilibrium constant compared are the K_Ds, the conditions $\alpha < 1$ and $\beta > 1$ should be fulfilled. Adapted from[39].

In spite of the structural and mechanistic differences, from an enzymological point of view all helicases are random bi-reactant systems[39]. They bind two substrates (dsDNA/dsRNA and ATP) to yield three products (ssDNA/ssRNA, ADP, and Pi). Since the energy of ATP hydrolysis is transduced in mechanical work by helicases, these parallel reactions are thermodynamically coupled. The conditions for thermodynamic coupling are: binding of one substrate increases the affinity for the other in the same factor for both, they mutually decrease the activation energies of the rate-limiting steps in the parallel reaction paths, and the products mutually decrease their affinities for the enzyme and thus favor release (Figure 6).

Although substantial knowledge about structures and mechanisms of helicases from different superfamilies has been gained to date, much less is known about the non-processive helicase-like enzymes that largely differ from the representative members due to large deviations of the consensus sequences. The helicase-like module of reverse gyrase is one of those cases. The lesson learnt from the research in the field of helicases is that projects like the elucidation of reverse gyrase catalytic mechanism at the molecular level will require the confluence of many individual techniques from different fields. On the other hand, the intrinsic structural complexity of reverse gyrase renders a dissection of the contributions of its parts almost impossible. The present work is a compromise between the use of a wide spectrum of fields and techniques to study a simplified model of the enzyme. The selection of the helicase-like domain as starting point is justified by its capacity to bind and hydrolyze ATP, coupled to DNA processing. As a consequence, it has a key involvement at every point of the catalytic cycle, fueling the supercoiling reaction and synchronizing the nucleotide-state to its progression. Detailed knowledge of the reaction the helicase-like domain performs on its own would also lay the ground work to identify the most likely check points for interdomain communication and cooperation, that would help delineate more accurate models for the reaction mechanism and generate sound hypothesis susceptible to be tested in the context of the full-length enzyme.

Aims of research

The present study focuses on elucidating the catalytic cycle of reverse gyrase by getting a deeper understanding of the intrinsic properties of the helicase-like domain and its contribution to the overall supercoiling reaction. The helicase-like module fuels the supercoiling reaction by hydrolyzing ATP, and is therefore strongly involved in every step of the cycle.

In spite of the interest in reverse gyrase, very little is known about the mechanistic details of supercoiling. To date, the most widely accepted model for the reaction is based in little direct biochemical experimentation, and mostly on the only crystal structure available of a reverse gyrase and on extrapolation of the knowledge from related proteins[18]. Given the unique structural arrangement of reverse gyrase that enables the enzyme to perform an unprecedented reaction, some distinctive features are also expected of the mechanism of catalysis.

We therefore use a combination of structural, kinetic, and thermodynamic approaches to characterize the helicase-like domain from *Thermotoga maritima* reverse gyrase and the reaction it performs on its own. Structurally, we use smFRET as a tool to track the conformational dynamics of the enzyme in solution, as well as the effect of substrates. The crystal structures of the apo form of the enzyme and in complex with substrates also provide snapshots of the reaction at different points of the cycle. The study of the transitions during the reaction, identification of individual steps, quantification of their relative rates, and assigning of the rate-limiting steps, is performed *via* steady state and pre-steady state kinetics. On the other hand, thermodynamic studies allow quantification of the energetic barriers between intermediates, and elucidation of the reaction pathway by comparison of the relative affinities of the enzyme for putative substrates in each nucleotide state[40]. Last but not least, generating deletion mutants allows us to assign individual functions to specific regions within the molecule.

Overall, this approach should provide the first indications of how the helicase module might contribute to supercoiling, guiding and presenting the DNA substrate to the active site in the topoisomerase domain, synchronized to the

nucleotide state. It should also unravel which general properties of the helicases are being exploited and which are being suppressed, in order to achieve compatibility with the supercoiling reaction.

III. Materials and Methods

Oligonucleotides

Primers used for mutagenesis (Microsynth). The nomenclature of the names include the target gene (*rGyr* stands for reverse gyrase, *rGh* for helicase-like domain of reverse gyrase)_type of modification (numbers stand for start position of amplification, number between single letters for point mutations, *Δlatch* for latch deletion, *Δhelix9* for helix9 deletion, *latch* for generation of the isolated latch)_directionality (*for*, *f* and *5* stand for forward; *rev*, *r*, and *3* for reverse). All sequences are listed in the 5' ➔ 3' direction.

rGyr_1_for:	GCGCCATGGCAGTGAATTCCAAATACC
rGyr_541_rev:	GGCCTCGAGTTATCTTGACGTGTCGGT CAG
rGyr_59_for:	GCGCCATGGAATTCTGGAACGAGTACG
rGyr_S169C_5:	GAAAAGTTCGAGAAATGCTTTGAAGAAGACG
rGyr_S169C_3:	CGTCTTCTTCAAAGCATTTCTCGAACTTTT C
rGyr_D173C_5:	GCTTTGAAGAATGCGATTACCATATCCTGG
rGyr_D173C_3:	CCAGGATATGGTAATCGCATTCTTCAAAGC
rGyr_Y328C_5:	GAGCTTTATGAGTGCTTGAAAAGATTC
rGyr_Y328C_3:	GAATCTTTTCAAGCACTCATAAAGCTC
rGyr_F332C_5:	GTACTTGAAAAGATGCAAATTCAATGTGGG
rGyr_F332C_3:	CCCACATTGAATTTGCATCTTTTCAAGTAC
rGyr_S341C_5:	GGGAGAGACCTGGTGCGAATTTGAG
rGyr_S341C_3:	CTCAAATTCGCACCAGGTCTCTCCC
rGyr_E59C_5:	GAGATATACCATGTGCTTCTGGAACGAG
rGyr_E59C_3:	CTCGTTCCAGAAGCACATGGTATATCTC
rGyr_N188C_5:	GTTCGTTTCGAAATGCAGAGAAAAGC
rGyr_N188C_3:	GCTTTTCTCTGCATTTCGAAACGAAC
rGyr_Q194C_5:	CAGAGAAAAGCTTTCCTGCAAAAGATTTGACTTTG

rGyr_Q194C_3:	CAAAGTCAAATCTTTTGCAGGAAAGCTTTTCTCTG
rGyr_S297C_5:	CTCCTCCAGATGCAAAGAAAAACTG
rGyr_S297C_3:	CAGTTTTTCTTTGCATCTGGAGGAG
rGyr_E422C_5:	GGAGAACCCAGATGTCTGTGAGCTCAG
rGyr_E422C_3:	CTGAGCTCACAGACATCTGGGTTCTCC
rGh_Δlatch_1_r:	GGAAGGAGTTCCCCAGAAGATCACG
rGh_Δlatch_1_f:	CCA GAT GTT TAC ACC TAC ATA CAA GC
rGh_Δlatch_2_r:	CGTGATCTTCTGGGGAACTCCTTCCGGCCCAGATGT TTACACCTACATACAAGC
rGh_Δlatch_2_f:	GCTTGTATGTAGGTGTAAACATCTGGGCCGGAAGGA GTTCCCCAGAAGATCACG
rGh_Δhelix9_1_r:	TCCAACCATCATGAGCAAAGTG
rGh_Δhelix9_1_f:	CCAGGTATTCTTGTGGTTTCTTC
rGh_Δhelix9_2_f:	CACTTTGCTCATGATGGTTGGACCAGGTATTCTTGT GGTTTCTTC
rGh_Δhelix9_2_r:	GAAGAAACCACAAGAATACCTGGTCCAACCATCATG AGCAAAGTG
rGyr_latch_for:	GCGCCATGGCCATGAGATTTTCACTGG
rGyr_latch_rev:	GGCCTCGAGTTAGATGATCAGCTCCAGGT

Primers used for sequencing (Microsynth).

T7-Promotor:	TAATACGACTCACTATAGGG
T7-Terminator:	GCTAGTTATTGCTCAGCGG

Primers used for activity assays (Microsynth). The letter at the end of the name indicates the direction (*a* stands for forward, *b* is the complementary strand with opposite directionality).

sbstr_rg_a: AAGCCAAGCTTCTAGAGTCAGCCCGTGATATTCATT
ACTTCTTATCCTAGGATCCCCGTT

sbstr_rg_b: AACGGGGATCCTAGGATAAGAAGTAATGAATATCAC
GGGCTGACTCTAGAAGCTTGGCTT

20nt_rg_b: GATAAGAAGTAATGAATATC

20nt_rg_b5: TGACTCTAGAAGCTTGGCTT

20nt_rg_b3: AACGGGGATCCTAGGATAAG

20nt_jxn_b: ACGGGCTGACTCTAGAAGCT

30nt_fork_b: GATAAGAAGTAATGAATATCTGCCCGACTG

rGyr_bubble_b: AACGGGGATCCTAGGATAGCCTTTTTTTTTTTTTTT
CCGACTCTAGAAGCTTGGCTT

Fluorescently labeled primers used for activity assays (Purimex). Labeled form of some of the primers, used for activity assays. Names starting with *Unw* describe unwinding substrates, not used in the unlabeled form (*Unw* is followed by *primer length_dye*).

sbstr_rg_a_FAM: 5'-(fluorescein)-sbstr_rg_a

sbstr_rg_a_FAM_3: sbstr_rg_a-(fluorescein)-3'

40nt_ jxn_a_FAM: 5'-(fluorescein)-AGCTTCTAGAGTCAGCCCGTGATATT
CATTACTTCTTATC

35nt_jxn_a_FAM: 5'-(fluorescein)-CTAGAGTCAGCCCGTGATATTCATTA
CTTCTTATC

30nt_jxn_a_FAM: 5'-(fluorescein)-GTCAGCCCGTGATATTCATTACTTCTT
ATC

25nt_jxn_a_FAM: 5'-(fluorescein)-CCCGTGATATTCATTACTTCTTATC

rGyr_bubble_a: 5'-(fluorescein)-AAGCCAAGCTTCTAGAGTCGGTTTTTT
TTTTTTTTTGGCTATCCTAGGATCCCCGTT

Unw_9_Cy5: 5’-(Cy5)-CGTTACGCA

Unw_14_Cy5: 5’-(Cy5)-CGTTACGCATTATC

Unw_9_Cy3: TGCGTAACG-(Cy3)-3’

Unw_14_Cy3: GATAATGCGTAACG-(Cy3)-3’

Cell strains

E. coli XL1-Blue strain (Stratagene) used for plasmid propagation:

endA1 gyrA96(nalR) thi-1 recA1 relA1 lac glnV44 F'[::Tn10 proAB+ lacIq Δ(lacZ)M15] hsdR17(rK- mK+)

E. coli Rosetta (DE3) strain (Merck), used for expression of recombinant proteins:

F^- ompT $hsdS_B(R_B^- m_B^-)$ gal dcm λ(DE3 [lacI lacUV5-T7 gene 1 ind1 sam7 nin5]) pLysSRARE (Cam^R)

Plasmid vectors

pET-based cloning and expression vectors possess a multiple cloning site under control of the bacteriophage T7-promoter. Due to the high processivity of the T7 RNA polymerase, inserts are over-expressed to levels even higher than 50 % of the total protein content of the host cell. Expression of this RNA polymerase can be induced by addition of Isopropyl-β-D-thiogalactopyranosid (IPTG) to the growth medium of host strains that contain the gene for the T7 RNA polymerase in their genomes, under the *lac*UV5 promoter.

The pET28a construct confers resistance to kanamycin and gives the option of attaching an N-terminal or C-terminal His-tag to the insert, while the pETM30 plasmid allows the introduction of an N-terminal His-GST-tag (Figure 7).

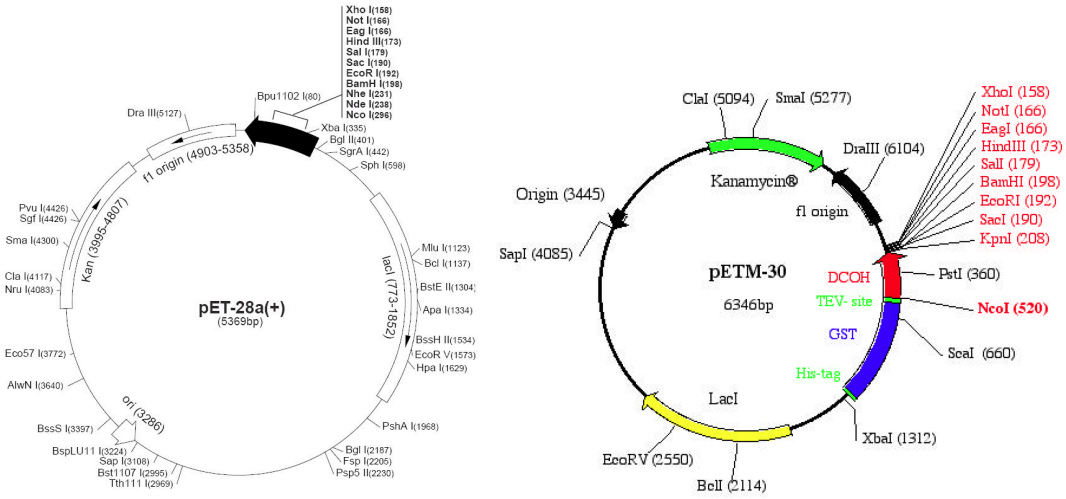

Figure 7. Maps of the plasmid vectors used during this work. It shows the multiple cloning sites and the all the restriction sites it contains. Taken from Novagen User Manual.

Solutions for culture media

Proliferation of freshly transformed cells was promoted by 60 min incubation at 37°C in LB medium containing 10g peptone, 5 g yeast extract, and 10 g NaCl, per liter. Selection of the transformed clones was performed by overnight incubation at 37°C on LB plates containing 19 g agar per liter, and supplemented with 20 µg/ml kanamycin for *E. coli* XL1-Blue cells, or 20 µg/ml kanamycin and 5 µg/ml chloramphenicol for *E. coli* Rosetta (DE3) cells. Overnight cultures for plasmid propagation on XL1-Blue cells or biomass generation of Rosetta (DE3) cells, were performed on LB medium supplemented with the appropriate antibiotics.

High recombinant proteins expression levels were achieved by 24 hours incubation of 10 ml LB overnight-grown Rosetta (DE3) cells, in 1 l auto-inducing medium[41], supplemented with kanamycin and chloramphenicol.

General methods

Agarose gel electrophoresis

Size-based detection and evaluation of PCR-generated DNA regions encoding for the helicase-like domain constructs were performed on 0.8 % agarose gels, or 2% agarose gels in the case of the latch construct. The PCR-generated fragments were mixed with 6x Sample Buffer Stock, and the final solution (10 mM EDTA, pH 8.0, 50 % glycerin, 0.02 % bromophenol blue, and 0.02 % Xylene cyanol) was then loaded on a gel. The runs were performed on 0.5x TBE buffer (89 mM Tris, 89 mM boric acid, 2 mM EDTA, pH 8.3) over 20 min at 16 V/cm. Detection of the migration bands was achieved by illumination of the gel under UV light after ethidium bromide staining.

SDS-PAGE

Stacking gel:	125 mM Tris/HCl, pH 6.8, 4.5 % acrylamide, 0.1 % bis-acrylamide, 0.06 % sodium dodecyl sulfate (SDS), 0.1 % TEMED, 0.1 % ammonium persulfate
Resolving gel:	375 mM Tris/HCl, pH 8.8, 15 % acrylamide, 0.4 % bis-acrylamide, 0.1 % SDS, 0.06 % TEMED, 0.086 % ammonium persulfate
Running buffer:	24 mM Tris, 200 mM glycine, 0.1 % SDS
4x sample buffer:	130 mM Tris/HCl, pH 6.8, 200 mM dithiothreitol (DTT), 4 % SDS, 0.01 % bromophenol blue, 20 % glycerol
Staining solution:	50 % methanol, 10 % acetic acid, 0.1 % Brilliant Blue R250
Destaining solution:	20 % ethanol, 10 % acetic acid

Detection of target proteins and evaluation of their purity was performed *via* SDS-PAGE[42]. 4x sample buffer was added to give a final volume of 10 µl. The

samples were denatured by heating for 1 min at 95°C to allow optimal interaction of the proteins with the hydrophobic chains of SDS molecules.

The negative surface charge of the SDS coated proteins contained in the sample and the molecular sizes determine the relative mobility within the gel in an electric field. Thus, under a 30 mA current the proteins are concentrated while migrating through the stacking gel due to its pH value of 6.8, the use of glycine in the running buffer, and the absence of sieving effect as a consequence of the large pore size. Glycine protonates at pH 6.8 and therefore has no net charge. That way, inside the stacking gel the Cl^- ions migrate first due to their small size, followed by the protein-SDS micelles, and finally the glycine zwitterions. Between the fronts formed by Cl^- ions and glycine a zone of low conductance and high field strength is generated, which moves forward the lagging protein-SDS micelles, while the micelles closer to the Cl^- front are slowed down as a consequence of the high conductance in this region. Once these molecules enter the 15 % resolving gel the glycine regains its negative charge and the pore size is reduced, allowing for protein separation based on molecular weight after 20 min, with the smallest moving farther from the application point than the biggest. The Roti-Mark molecular weight standard (Roth) containing 200, 119, 66, 43, 29, 20, and 14.5 kDa proteins was run simultaneously for identification of the target protein.

Afterwards, the protein bands on the gels were developed by 30 min incubation on staining solution and then 20 min in destaining solution.

Light absorption-based methods

The DNA and protein concentrations were determined by direct UV-absorption at 260 nm and 280 nm respectively, applying the Lambert-Beer law:

$$c = \frac{A}{\varepsilon \cdot d} \qquad (2)$$

where c – concentration in ng/ml, A – absorption at the corresponding wavelength, ε – extinction coefficient in $M^{-1} \cdot cm^{-1}$, and d – path length in cm.

The dsDNA concentration was determined from the relation: 1 AU (absorbance unit) = 50 ng/ml.

The protein concentration was determined by using the calculated extinction coefficient, performed by ProtParam at the ExPASy Proteomics Server (http://expasy.org/tools/protparam.html).

Due to the lack of aromatic amino acids, the concentration of the latch construct was determined *via* the Bradford method[43] (Bradford *et al*, 1976). This colorimetric assay is based on the shift in the absorption maximum of Coomassie brilliant Blue G250 upon interaction with proteins. First, a calibration curve of absorption at λ_{595} was plotted for known concentrations of bovine serum albumin (BSA), and then the concentration of the latch was estimated by interpolation.

Mutagenesis

Before the beginning of this project, the reverse gyrase helicase-like domain from *Thermotoga maritima* had been sub-cloned into the pET28a plasmid, carrying the gene of the full-length enzyme as an insert in the multiple cloning site under the T7-promoter. The gene segments encoding the regions M1-R541 and E59-R541 (rGyr_hel) were amplified by PCR using Phusion DNA polymerase with the combination of primers *rGyr_1_for/ rGyr_541_rev* and *rGyr_59_for/ rGyr_541_rev*, respectively. These oligonucleotides introduced Nco I and Xho I restriction sites at the 5' and 3' ends respectively, as four-nucleotides overhangs, non-complementary to the template. The targets generated were inserted into the multiple cloning site of the plasmid vector pET28a (Figure 8A).

Mutants of the helicase-like domain lacking the N-terminal Zn-finger (ΔM1-H58), the latch (ΔM389-I459) or the helix 9 (ΔI224-K249), were created in a sequence of three PCR reactions (25 µl) using *Phusion* DNA polymerase. First, the rGyr_hel gene regions flanking the deletion segment were amplified and the Nco I/ Xho I restriction overhangs were introduced, in a reaction mixture (1 ng/µl template, 0.5 µM of each primer, 0.2 mM of each dNTP, 0.02 U/µl Phusion DNA polymerase, 1x High Fidelity (HF) Buffer) containing the

combination of primers *rGyr_59_for/ rGh_dlatch_1_r*, *rGh_dlatch_1_f/ rGyr_541_rev*, *rGyr_59_for/ rGh_Dhelix9_1_r*, and *rGh_Dhelix9_1_f/ rGyr_541_rev*; to generate the gene segments coding for E59-S388, P460-R541, E59-G223, and P250-R541, respectively. For this purpose the following thermal cycles were used:

- 30 s 98°C
- 10 s 98°C
- 10 s gradient 56°C - 62°C
- 35 s 72°C (30 nested cycles from the second step)
- 300 s 72°C

DNA segments were purified with a PCR purification kit (Promega). The concentrations of the eluates were determined from the absorption at 260 nm. Afterwards, the second PCR cycle was performed, using the primers and template combinations *rGyr_59_for/ rGh_dlatch_2_r/ gene_E59-S388* and *rGh_dlatch_2_f/ rGyr_541_rev/ gene_P460-R541* for the latch deletion mutant; and the combination *rGyr_59_for/ rGh_Dhelix9_2_r/ gene_E59-G223* and rGh_Dhelix9_2_f*/ rGyr_541_rev/ gene_P250-R541* for the helix9 deletion mutant, to introduce overlapping sequences flanking the deleted regions, followed by another PCR clean-up step. Afterwards, the DNA fractions containing the segments encoding for E59-S388/ P460-R541, and E59-G223/ P250-R541 were mixed, denatured at 98°C for 5 min, incubated at room temperature for 5 min to promote annealing of the complementary overhangs, and mixed with 0.2 mM of each dNTP, 0.02 U/µl Phusion DNA polymerase, 1x HF (high fidelity) buffer, to promote synthesis of the complementary strands at 72°C for 10 min. On the third and last PCR step, the use of the primers *rGyr_59_for* and *rGyr_541_rev* on the reaction mixtures allowed for selective amplification of the heterogeneously annealed DNA containing the coding sequence of the latch and helix9 deletion mutants (Figure 8B). At this point the following thermal cycles were used:

- 30 s 98°C
- 10 s 98°C
- 10 s 60°C
- 45 s 72°C (30 nested cycles from the second step)
- 300 s 72°C

The generation of the region coding for the latch was achieved in a single PCR reaction step, consisting of the amplification of the region S388-P460 and addition of the Nco I and Xho I restriction sites, using the primers

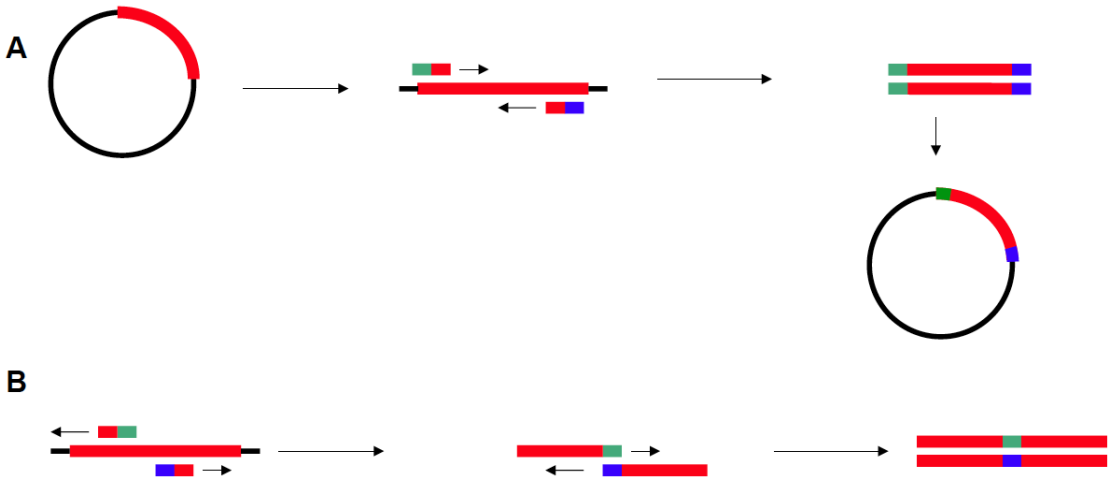

Figure 8. Schemes depicting the cloning strategies followed in this study. **A** Cloning strategies to produce continuous fragments of the gene encoding reverse gyrase. **B** Strategy to achive deletion of internal sequences from the final construct.

rGyr_latch_for and *rGyr_latch_rev* in the reaction mixture as previously described (Figure 8A).

The generated inserts and the pET28a plasmid in the case of the helicase-like domain constructs, or the pETM30 plasmid for the case of the latch, were then incubated with the Nco I and Xho I restriction enzymes in NEB2-Buffer for two hours at 37°C to generate the ssDNA sticky ends.

Afterwards, the reaction product was again purified and ligation of the plasmid with the insert was performed with 400 units of NEB-ligase. A 6-fold excess of plasmid DNA, in base pairs content, over the insert was used. The reaction mixture in 1x ligase buffer was incubated at 16°C overnight.

Site-directed mutagenesis of single and double Cys mutants was achieved by following the Quickchange protocol (Stratagene). This protocol uses complementary primers containing a 1-2 bp mismatch at the position on the template that encodes the amino acid to be replaced. The 25 µl reaction mixture contained: 1 ng/µl template, 0.2 µM of each primer, 0.2 mM of each dNTP, 0.04 U/µl *Pfu* DNA polymerase, 1x Pfu-Buffer. The *Pfu* DNA polymerase PCR thermal cycles were:

- 5 min 95°C
- 30 s 95°C
- 30 s gradient 55°C-68°C (depending on the annealing temperature of the primers)
- 14.5 min 68°C (25 nested cycles from the second step)
- 300 s 68°C

Heat-shock transformation

Heat-shock competent *E. coli* XL1-Blue cells were mixed with the PCR product and incubated for 30 min on ice. Afterwards, the cells were incubated at 37°C for 3 min, mixed with 800 µl LB medium, and placed on a Minitron incubator (INFORS, AG), shaking. After 60 min the cells were centrifuged (Eppendorf) at 6 000 rpm using an F45-24-11 rotor, for 2 min. Then 600 µl of the supernatant was removed, cells were re-suspended on the remaining liquid volume, and finally spread on LB-agar plates supplemented with kanamycin.

Plasmid DNA extraction from the expression vector for sequencing and cloning was performed with the MiniPrep kit from Quiagen, as described in the user manual.

Rosetta DE3 cells were transformed with the pET28a or pETM30 plasmid carrying the insert. Cells were thawed by incubation on ice for 5 min, then 1 µl plasmid was added and the mixture was incubated at 42°C for 1.5 min. Finally 100 µl LB medium was added, followed by 60 min incubation at 37°C, shaking.

Afterwards, the cells were plated on LB-agar medium supplemented with kanamycin and chloramphenicol, and incubated at 37°C overnight.

Protein expression and purification

Solution for purification

Buffer: 50 mM Tris/HCl, pH 7.5, 10 mM $MgCl_2$, 10 µM $Zn(OAc)_2$, 2 mM β-mercaptoethanol

Cells expressing the recombinant constructs were inoculated into 10 ml LB medium at 37°C with shaking overnight. This culture was used to inoculate 1l auto-inducing (AIM) medium.

The AIM culture was incubated 24 h at 37°C with shaking at 140 rpm. Cells were harvested by 15 min centrifugation at 4 800 rpm using a SLA3000 rotor. All centrifugation steps during the purification were performed on a Sorvall RC 5C centrifuge. Cells were re-suspended in 30 ml Buffer containing 0.5 M NaCl and 0.25 units of the protein inhibitor cocktail Complete EDTA-free (Roche). Harvested cells were disruptured on a microfluidizer (M-110L) and the debris was pelleted by centrifugation at 18 000 rpm for 30 min using a SS34 rotor. The supernatant was stored, and the pellet was re-suspended in Buffer containing 1 M NaCl for 30 min at room temperature. After a second centrifugation step, both supernatants were mixed and the NaCl concentration was adjusted to 250 mM by addition of Buffer. Heating for 10 min at 65°C isolated the heat-resistant recombinant protein from the host E *coli* proteins. After an additional centrifugation step, the supernatant was collected for the subsequent chromatographic runs.

The cleared protein solution was applied to consecutive cationic and anionic exchange columns to eliminate protein and DNA contaminants, respectively. In both cases Buffer containing 0.2 M NaCl was used to equilibrate and load the columns. The sample was first loaded onto a 10 ml SP-Sepharose column. Elution was achieved by exchange to Buffer containing 1 M NaCl, which increased the ionic strength. The collected fraction was dialyzed overnight

against Buffer with 0.2 M NaCl and applied to a 10 ml Q-Sepharose column. The flow-through was collected and concentrated with a spin-column (Vivaspin, 10 000 MWCO) to a final volume of 2 ml, and applied to a S200 size exclusion chromatography column. The protein eluted as a single peak at a volume corresponding to the molecular size of the monomer.

The latch was produced as an N-terminal GST-fusion protein in the pETM30 vector. Cell culture and protein extraction were performed as for the helicase-like domain constructs. Only the heating step was excluded from the protocol due to the thermal instability of the GST-tag. Afterwards, the obtained protein solution was applied to a 10 ml Glutathione-Sepharose column and elution was performed by supplementing the Buffer with 20 mM reduced glutathione (GSH). The collected fraction was then incubated overnight at room temperature with TEV protease for removal of the GST-tag. Finally the isolated latch protein was separated from the GST-tag by size exclusion chromatography on an S75 column. Due to the absence of aromatic residues, elution of the latch was detected with UV-light of wavelength 230 nm, selective for the peptide bond.

After each purification step, samples of the fractions were taken and run on a SDS-PAGE gel. The final protein solutions were shock-frozen on liquid nitrogen and stored at - 80°C.

DNA unwinding assay

DNA unwinding was detected *via* FRET between the Cy3 and Cy5 dyes. The 5’ and 3’ ends were labeled with Cy5 and Cy3 respectively, at the duplex side of the junction or dsDNA. Unwinding was detected by decrease of the acceptor fluorescence emission at 666 nm (1 nm bandwidth), after excitation at 554 nm (1 nm bandwidth) on a Fluoromax-3 fluorimeter (Jobin Yvon). 0.5 µM DNA was incubated with 5 µM of the enzyme at 37°C for 1 min in buffer 50 mM Tris/HCl, pH 7.5, 0.15 M NaCl, 10 mM $MgCl_2$, 10 µM $Zn(OAc)_2$, 2 mM β-mercaptoethanol, prior to addition of 1.5 mM nucleotide.

Fluorescence equilibrium titrations

The assay for determination of the K_D values for rGyr_hel complexes with fluorescently labeled mant-nucleotides were determined as described[20]. The data was fitted with the equation describing a 1:1 binding mode:

$$F = F_0 + \frac{\Delta F_{max}}{[mA]}\left(\frac{[hel]+[mA]+K_D}{2} - \sqrt{\left(\frac{[hel]+[mA]+K_D}{2}\right)^2 - [hel][mA]}\right) \quad (3)$$

where $\mathrm{F_0}$ is the initial fluorescence of the nucleotide, $\Delta \mathrm{F_{max}}$ is the amplitude of the increase upon binding to the enzyme, $[\mathrm{hel}]$ is the enzyme concentration, and $[\mathrm{mA}]$ is the labeled nucleotide concentration.

Fluorescein-labeled DNA binding was measured *via* fluorescence anisotropy, at 37°C in buffer 50 mM Tris/HCl, pH 7.5, 0.15 M NaCl, 10 mM $MgCl_2$, 10 µM $Zn(OAc)_2$, 2 mM β-mercaptoethanol. Data was evaluated using the same equation as previously described[20].

Stopped-flow nucleotide binding kinetics

Measurements were performed on an Applied Photophysics SX 20 stopped-flow apparatus using 0.1 µM rGyr_hel at 37°C in buffer 50 mM Tris/HCl, pH 7.5, 0.15 M NaCl, 10 mM $MgCl_2$, 10 µM $Zn(OAc)_2$, 2 mM β-mercaptoethanol. Binding and dissociation kinetics of mant-nucleotides was detected *via* FRET between the tryptophans contained in rGyr_hel and the mant group. The excitation wavelength was 280 nm and for detection a long pass cut-off filter for the wavelength 335 nm was used.

Fluorescence time courses of binding kinetics were fitted to the equation:

$$k_{obs} = k_{on}[mdADP] + k_{off} \quad (4)$$

describing the dependence of k_{obs} on the association (k_{on}) and dissociation (k_{off}) rate constants.

Time courses of mant-d-ADP fluorescence decay for direct determination of the dissociation rate constant were fitted with the equation:

$$Fl = A \cdot e^{-k_{off} \cdot t} + c \quad (5)$$

where *Fl* is the monitored fluorescence signal, *A* is the amplitude, and *c* the fluorescence value where the plateau is reached. The value determined this way was substituted on equation 4 to obtain a better estimate of the association rate constant.

Kinetic competition assays between mant-d-ADP and ADPNP, were performed by rapid mixing of the enzyme solution with pre-incubated mdADP/ADPNP solutions, of varying ADPNP concentrations and 2 μM mdADP.

Measurements in the presence of DNA were performed with saturating DNA concentrations in both solutions before rapid mixing.

CD spectroscopy

The CD spectra of the helicase-like domain constructs were recorded (ChiraScan CD spectrometer), in order to exclude an effect of the deletions on the secondary structure. 3 μM protein solutions were measured within the 195 – 260 nm range at 37°C, in 50 mM Tris/HCl, pH 7.5, 0.15 M NaCl, 10 μM $MgCl_2$, 10 mM $Zn(OAc)_2$, 2 mM β-mercaptoethanol. The measured ellipticity was converted to molar residual ellipticity by means of the equation:

$$[\Theta]_{MRW} = \frac{\Theta \cdot 100}{N \cdot c \cdot d} \quad (6)$$

where $[\Theta]_{\mathrm{MRW}}$ – molar ellipticity, Θ – measured ellipticity, c – concentration, d – path length, and N – number of residues.

Single molecule fluorescence resonance energy transfer (smFRET)

Single molecule FRET (smFRET) measurements were performed on an in-house built confocal setup[44]. The dyes used were maleimide derivates, which ensures the formation of a stable bond with the thiol group of cysteines[45]. The helicase-like domain Cys mutants were labeled by addition of a 10-fold

excess of Alexa 488 and TMR to a 40 µM protein solution, in buffer: 50 mM Tris/HCl, pH 7.5, 0.2 M NaCl, 10 mM $MgCl_2$, 10 µM $Zn(OAc)_2$, 1 mM Tris(2-carboxyethyl)phosphine (TCEP). After 15 min incubation at 25°C, the free dye was removed by buffer exchange on Microspin columns (BioRad), to 50 mM Tris/HCl, pH 7.5, 0.2 M NaCl, 10 mM $MgCl_2$, 10 µM $Zn(OAc)_2$, 2 mM β-mercaptoethanol. The labeling efficiencies and protein concentration were determined from the absorption maxima at 280, 493, and 550 nm. The concentration values were corrected for the contributions of the acceptor (TMR) to the absorption at 280 and 493 nm, and the contribution of the donor (Alexa 488) to the absorption at 280 nm.

Measurements were performed in the reaction buffer: 50 mM Tris/HCl, pH 7.5, 0.15 M NaCl, 10 mM $MgCl_2$, 10 µM $Zn(OAc)_2$ after treatment with active charcoal to remove fluorescent impurities. Cuvettes (Nalge Nunc International) were saturated with 200 µl, 10 µM rGyr_hel_K106Q, an ATPase-deficient mutant of the helicase-like domain, for 1 h. Afterwards, 200 µl 50 pM of the labeled protein was prepared, and the measurements were performed at 475 nm, 75 µW, until 10 000 000 photons were recorded after approximately 20 min.

Confocal microscopy allows for single molecule detection (SMD) of freely diffusing molecules. It has the advantage of not requiring surface immobilization, and it also enables longer observation times due to the relatively short diffusion time of the molecules through the confocal volume, which reduces the occurrence of fluorescence quenching. However, data analysis is not straightforward, and the recorded FRET efficiencies (E) should be corrected for donor signal detected on the acceptor APD (α), acceptor signal detected on the donor APD (β), sensitivity to both acceptor and donor dyes (γ), and direct excitation of the acceptor (δ) at 475 nm. The final equation to calculate E, accounting for all these effects is as follows[44]:

$$E = \frac{(1+\beta\gamma\delta)\cdot\left(I_A - \frac{\alpha+\gamma\delta}{1+\beta\gamma\delta} I_D\right)}{(1+\beta\gamma\delta)\cdot\left(I_A - \frac{\alpha+\gamma\delta}{1+\beta\gamma\delta} I_D\right) + (\gamma+\gamma\delta)\cdot(I_D - \beta I_A)} \qquad (7)$$

where I_A is the background-corrected intensity detected by the acceptor APD, and I_D is the intensity detected by the donor APD.

The correction parameters were determined experimentally, using the helicase-like domain single Cys mutants. Each one was labeled with donor (Alexa 493) and acceptor (TMR) dyes as previously described, and the absorption spectrum was recorded. This enables determination of the direct acceptor excitation at 475 nm, *i.e.*, determination of the δ value for a Cys mutants pair, for both possible label combinations, given the equation:

$$\delta = \frac{{OD_A}^{475\,nm}/_{[Acceptor]}}{{OD_D}^{475\,nm}/_{[Donor]}} \tag{8}$$

where OD is the absorption, and $[\mathrm{Acceptor}]$, $[\mathrm{Donor}]$ are the concentrations of acceptor and donor dyes, respectively.

The relative signal intensities of the labeled single Cys mutants as well as the buffer background were determined on the confocal smFRET microscope. The labeled protein solutions were adjusted to give a dye concentration of 100 nM, measurements were performed at 75 µW, 25°C temperature, and using a neutral filter on the detection part. The correction parameters α, β, and γ, were determined using the equations:

$$\alpha = \frac{I_A^{Donor} - I_A^{Buffer}}{I_D^{Donor} - I_D^{Buffer}} \tag{9}$$

$$\beta = \frac{I_D^{Acceptor} - I_D^{Buffer}}{I_A^{Acceptor} - I_A^{Buffer}} \tag{10}$$

$$\gamma = \frac{I_A^{Acceptor} - I_A^{Buffer}}{I_D^{Donor} - I_D^{Buffer}} \delta^{-1} \tag{11}$$

where I_D signifies counts on the donor channel and I_A signifies counts on the acceptor channel[44].

FRET efficiencies were converted to distances (r) using the equation:

$$r = R_0 \cdot \sqrt[6]{1/E - 1} \quad (12)$$

where R_o is the distance at which E is 0.5, also known as Förster distance[46].

The Förster distance can be experimentally determined from the spectral properties of the dyes bound to the protein and the donor quantum yield, according to the equation:

$$R_0 = \sqrt[6]{8.785 \cdot 10^{-5} \cdot \frac{\phi_D \cdot \kappa^2 \cdot J}{n^4}} \quad (13)$$

where Φ_D is the quantum yield of the donor, κ is the orientation factor, J is the overlap integral between the donor emission and acceptor absorption spectra, and n is the refractive index. The variables κ and n are 2/3 for a freely rotating dye and 1.33 for an aqueous solution, respectively.

The quantum yield of the donor was determined by comparison with fluorescein as a standard (ref) using the equation:

$$\phi_D = \frac{F_D \cdot \varepsilon_R \cdot \phi_R}{F_R \cdot \varepsilon_D} \quad (14)$$

where F – fluorescence emission of a 10 nM dye concentration solution, ε – extinction coefficient, and Φ is the quantum yield. The sub-indexes D or R indicate donor labeled protein (Alexa 493) or reference dye (fluorescein), respectively.

The overlap integral was determined using the equation:

$$J(\lambda) = \int_0^\infty F_D(\lambda) \cdot \varepsilon_A(\lambda) \cdot \lambda^4 d\lambda \quad (15)$$

where F_D and ε_A represent the donor fluorescence and acceptor extinction coefficient at a given wavelength (λ), respectively.

IV. Results

Chapter 1. Article

The reverse gyrase helicase-like domain is a nucleotide-dependent switch that is attenuated by the topoisomerase domain.

The effect of different DNAs and negatively charged polymers on the steady-state ATPase activity of *Thermotoga maritima* reverse gyrase and the isolated helicase-like domain was investigated. Comparison of the kinetic parameters of the reaction for both constructs revealed for the first time an inhibitory effect of the topoisomerase domain on the helicase domain DNA-stimulated ATP hydrolysis. Nucleotide and DNA binding measurements for the same constructs also revealed that the helicase domain ATP-dependent switch properties were also strongly reduced in the context of reverse gyrase. Overall, these were the first indications of a deceleration of ATP hydrolysis and DNA processing by the helicase-like domain in the context of reverse gyrase, in order to make it compatible with the DNA supercoiling reaction of the full-length enzyme.

5882–5895 *Nucleic Acids Research, 2008, Vol. 36, No. 18* *Published online 16 September 2008*
doi:10.1093/nar/gkn587

The reverse gyrase helicase-like domain is a nucleotide-dependent switch that is attenuated by the topoisomerase domain

Yoandris del Toro Duany, Stefan P. Jungblut, Andreas S. Schmidt and Dagmar Klostermeier*

University of Basel, Biozentrum, Biophysical Chemistry, Klingelbergstrasse 70, 4056 Basel, Switzerland

Received July 9, 2008; Revised and Accepted September 1, 2008

ABSTRACT

Reverse gyrase is a topoisomerase that introduces positive supercoils into DNA in an ATP-dependent manner. It is unique to hyperthermophilic archaea and eubacteria, and has been proposed to protect their DNA from damage at high temperatures. Cooperation between its N-terminal helicase-like and the C-terminal topoisomerase domain is required for positive supercoiling, but the precise role of the helicase-like domain is currently unknown. Here, the characterization of the isolated helicase-like domain from *Thermotoga maritima* reverse gyrase is presented. We show that the helicase-like domain contains all determinants for nucleotide binding and ATP hydrolysis. Its intrinsic ATP hydrolysis is significantly stimulated by ssDNA, dsDNA and plasmid DNA. During the nucleotide cycle, the helicase-like domain switches between high- and low-affinity states for dsDNA, while its affinity for ssDNA in the ATP and ADP states is similar. In the context of reverse gyrase, the differences in DNA affinities of the nucleotide states are smaller, and the DNA-stimulated ATPase activity is strongly reduced. This inhibitory effect of the topoisomerase domain decelerates the progression of reverse gyrase through the nucleotide cycle, possibly providing optimal coordination of ATP hydrolysis with the complex reaction of DNA supercoiling.

INTRODUCTION

Reverse gyrase is the only topoisomerase that introduces positive supercoils into DNA at the expense of ATP hydrolysis (1). It is unique to hyperthermophilic archaea and eubacteria. Deletion of the reverse gyrase gene in a hyperthermophilic archaeon leads to growth retardation at higher temperatures, but the organism is still able to survive at 90°C, demonstrating that reverse gyrase is not strictly required for hyperthermophilic life (2,3). The *in vivo* function of reverse gyrase is not clear. A heat-protective DNA chaperone activity (4) and a DNA renaturase activity (5) have been reported, indicating that reverse gyrase protects DNA from damage at high temperatures.

Reverse gyrase consists of an N-terminal helicase-like domain, fused to a C-terminal topoisomerase I domain. While most reverse gyrases are monomeric, a covalent connection between the two domains is not required for positive supercoiling activity. The *Methanopyrus kandleri* reverse gyrase is a dimeric enzyme, with the helicase-like and part of the topoisomerase domain in one subunit, and the remainder of the topoisomerase domain provided by the second subunit (6,7). Furthermore, an active reverse gyrase can be reconstituted by mixing separately produced helicase-like and topoisomerase domains (8; Hilbert,M. and Klostermeier,D., unpublished data). Nevertheless, a functional cooperation of helicase-like and topoisomerase domains is required for positive supercoiling by reverse gyrase (8,9).

The helicase-like domain shares the three-dimensional structure with helicases of the superfamily (SF) 2, namely two tandem RecA-folds (H1, H2) connected by a linker (Figure 1). In reverse gyrase, the subdomain H2 is interrupted by the so-called latch domain (H3) that shows homology to the region of the transcription termination factor Rho that is involved in RNA binding (10). The reverse gyrase helicase-like domain comprises all signature motifs of SF2 helicases, but the sequences of these motifs show large deviations from the consensus (Supplementary Figure S1). These sequence variations may be responsible for the lack of unwinding activity by reverse gyrase or the isolated helicase-like domain (8). Reverse gyrase does not catalyze relaxation in the absence of nucleotides, whereas the topoisomerase domain on its own can relax DNA in

*To whom correspondence should be addressed. Tel: +41 61 267 2381; Fax: +41 61 267 2189; Email: dagmar.klostermeier@unibas.ch

The authors wish it to be known that, in their opinion, the first two authors should be regarded as joint First Authors.

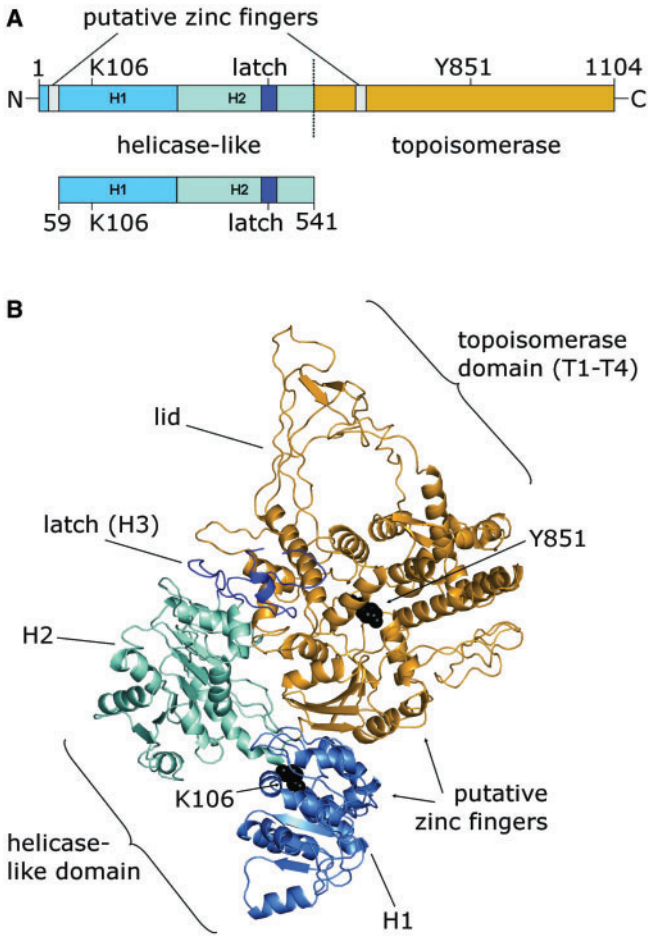

Figure 1. Reverse gyrase and its helicase-like domain. (**A**) Full-length reverse gyrase, consists of an N-terminal helicase-like domain [H1, light blue, H2, cyan, H3 (latch), blue] and a C-terminal topoisomerase domain (orange). The helicase-like domain construct comprises the helicase-like domain (H1 and H2), and the latch-domain H3 that is inserted into H2. The positions of K106 in the Walker A motif and of the catalytic tyrosine, Y851 (black), and the putative zinc fingers (gray) are indicated. (**B**) Structure of *A. fulgidus* reverse gyrase [PDB-ID 1GKU, Ref. (10)], color-coded as in (A). The regions carrying the putative zinc fingers are missing in the electron density.

the absence of nucleotides, but lacks supercoiling activity (8,11). It has been suggested that the latch domain suppresses relaxation in reverse gyrase in the absence of nucleotides (12).

Based on the crystal structure of the reverse gyrase from *Archaeoglobus fulgidus* (10), a mechanism for positive supercoiling has been postulated that is based on a conformational change of the helicase-like domain as the initiating step, leading to a closure of the cleft between the two RecA-like subdomains. This conformational change may then allow for release of the latch domain, and for swinging-up of the 'lid' region in the topoisomerase domain, which is required for strand passage (Figure 1B). We have recently shown that such a conformational change occurs in SF2 helicases in response to the cooperative binding of ATP and nucleic acid substrates (13). Furthermore, we have demonstrated that reverse gyrase can use ATP or ATPγS as the energy source for positive supercoiling, suggesting that both nucleotides can power the conformational cycle (14). This ATPγS-dependent activity has also been observed for the translation factor eIF4A, a member of the SF2 helicase family (15), which further indicates mechanistic similarities of the reverse gyrase helicase-like domain and SF2 helicases. Although the helicase-like domain is a crucial element for ATP-dependent positive supercoiling by reverse gyrase, its role is currently not well understood. We present here the characterization of nucleotide binding, ATP hydrolysis, DNA binding and DNA-stimulation of the ATPase activity for the isolated helicase-like domain of *Thermotoma maritima* reverse gyrase and compare it to the properties of reverse gyrase. The helicase-like domain confers nucleotide-dependent DNA binding to reverse gyrase. The isolated domain is an efficient DNA-stimulated ATPase, but the topoisomerase domain in reverse gyrase exerts a moderating effect onto the ATPase activity, slowing down the nucleotide cycle by a factor of 10. This intra-molecular inhibition suggests that the helicase-like domain is harnessed by reverse gyrase to provide efficient coupling of ATPase activity with the supercoiling reaction.

MATERIALS AND METHODS

Cloning, mutagenesis, protein production and purification

The region encoding the helicase-like domain of reverse gyrase (E59-R541, rGyr_hel) was PCR-amplified from the full-length gene and cloned into pET28a using NcoI and XhoI restriction sites. Site-directed mutagenesis was performed according to the Quikchange protocol (Stratagene, La Jolla, CA, USA).

rGyr_hel was produced at 37°C in *Escherichia coli* Rosetta (DE3) (Invitrogen, Paisley, U.K) in autoinducing medium (16), and cells were harvested after 24 h. All purification steps were performed at room temperature. Cells were disrupted in a Microfluidizer in 50 mM Tris/HCl, pH 7.5, 1 M NaCl, 10 mM $MgCl_2$, 10 μM $Zn(OAc)_2$, 2 mM BME and the crude extract was cleared by centrifugation. The NaCl concentration of the supernatant was adjusted to 0.2 M, and it was applied to a SP sepharose column equilibrated in 50 mM Tris/HCl, pH 7.5, 0.2 M NaCl, 10 mM $MgCl_2$, 10 μM $Zn(OAc)_2$, 2 mM BME. rGyr_hel was eluted in a linear gradient from 0.2–1 M NaCl, dialyzed against 50 mM Tris/HCl, pH 7.5, 0.2 M NaCl, 10 mM $MgCl_2$, 10 μM $Zn(OAc)_2$, 2 mM BME, and applied to a Q sepharose column equilibrated in the same buffer. rGyr_hel was collected in the flowthrough. Final purification was achieved via size-exclusion chromatography on a calibrated S200 column in 50 mM Tris/HCl, pH 7.5, 0.2 M NaCl, 10 mM $MgCl_2$, 10 μM $Zn(OAc)_2$, 2 mM BME. rGyr_hel elutes as a monomer from a calibrated size-exclusion chromatography column (apparent molecular weight: 49.8 kDa, calculated: 56.3 kDa). Protein concentration was determined photometrically using the calculated extinction coefficient at 280 nm of 56 309 M^{-1} cm^{-1}. From 1 l of bacterial culture, 4 mg of rGyr_hel with >98% purity (as judged from SDS–PAGE with Coomassie staining) were obtained. The pure protein was concentrated,

shock-frozen in liquid nitrogen, and stored at −80°C. Full-length reverse gyrase was purified as described (14).

Adenine nucleotides and RNA and DNA substrates

Adenine nucleotides were purchased from Pharma Waldhof (Mannheim, Germany) or Jena Bioscience (Jena, Germany), and checked for impurities by reverse-phase HPLC on a C18 column in 0.1 M sodium phosphate, pH 6.5. Oligonucleotides for ssDNA or dsDNA substrates were obtained from Purimex (Grebenstein, Germany). The sequence of the 60-base ssDNA was 5′-(fluorescein)-AAGC CAAGCT TCTAGAGTCA GCCCGTGATA TTCATT ACTT CTTATCCTAG GATCCCCGTT-3′, and the dsDNA substrate was formed by annealing the complementary strand. These substrates contain a preferred cleavage site (17,18) for reverse gyrase; cleavage occurs between the two underlined nucleotides. PolyU-RNA was purchased from Sigma (Hamburg, Germany).

ATPase assays

Steady state ATPase activity was measured in a spectroscopic enzymatic assay that couples ADP production to the oxidation of NADH as described (14). Assay conditions were 50 mM Tris/HCl, pH 7.5, 0.15 M NaCl, 10 mM $MgCl_2$, 100 μM $Zn(OAc)_2$, 2 mM BME, 0.4 mM PEP and 0.2 mM NADH, 23 μg ml^{-1} LDH, 37 μg ml^{-1} PK. ATPase activity at 75°C was determined in 50 mM Tris/HCl, pH 7.5, 0.15 M NaCl, 10 mM $MgCl_2$, 100 μM $Zn(OAc)_2$, 2 mM BME, 10% (w/v) PEG 8000 by mixing 1 μM enzyme, 2 mM ATP and the respective nucleic acid substrate, taking aliquots at different time points, and analyzing the nucleotide composition by reverse-phase HPLC as described (14).

Fluorescence measurements

Dissociation constants of rGyr_hel/nucleotide complexes were determined in fluorescence equilibrium titrations at 37°C using 1 μM of the fluorescent ADP analog mantADP (19) and in competitive titrations of the mantADP/rGyr_hel complex with ADP, ATPγS, ADPNP, ADPCP and ATP, and analyzed as described (14).

Dissociation constants of reverse gyrase/DNA complexes were determined using 5′-fluorescein-labeled DNA and the steady-state anisotropy of fluorescein as a probe for binding. The DNA concentrations were 25 nM for titrations with rGyr_hel, and 10 nM for rGyr_fl, unless stated otherwise. Dissociation constants were obtained by analysis of the data using the solution of a quadratic equation describing a one-site binding model as described (14), or with the Hill equation.

Helicase assay

Helicase activity was tested via the displacement of a 10-mer from a 10/50-mer substrate (2 nM) by 10 μM rGyr_hel in 20 mM HEPES/NaOH, pH 7.5, 70 mM KCl, 1 mM MgOAc, 10% (v/v) glycerol, 2 mM DTT and 1 mg/ml BSA as described for eIF4A (20). The ATP concentration was 2 mM.

RESULTS

Nucleotide binding and ATPase properties of the helicase-like domain

The role of the helicase-like domain for DNA supercoiling by reverse gyrase is currently unknown. A detailed understanding of nucleotide binding and hydrolysis by the helicase-like domain and its interaction with DNA, isolated and in the context of reverse gyrase, is a pre-requisite to delineate its function within reverse gyrase. To this end, we subcloned a DNA fragment coding for amino acids 59–541 of *T. maritima* reverse gyrase (rGyr_hel). This construct comprises the two RecA-like domains H1 and H2, and the so-called latch domain H3, but lacks the N-terminal putative zinc finger (Figure 1). The nucleotide binding properties of rGyr_hel were investigated in fluorescent equilibrium titrations using the fluorescent ADP analog mantADP (Figure 2), which we previously used as a probe for nucleotide binding to reverse gyrase (14). Upon binding to rGyr_hel, the mant fluorescence increases 1.5-fold (Figure 2A). The fluorescence signal returns to the value for free mantADP upon displacement with ADP, confirming that mantADP binds to the ADP binding site and is thus suitable to study nucleotide binding to rGyr_hel. The K_d value of the mantADP/rGyr_hel complex determined from the titration curves is 1.1 ± 0.1 μM. In the displacement titration with ADP (Figure 2B), a K_d value of 2.6 ± 0.8 μM was determined for the ADP complex. The K_d value of the rGyr_hel/AMP complex is three orders of magnitude higher (1600 ± 231 μM), demonstrating that interactions with the β-phosphate provide high affinity binding of adenine nucleotides to rGyr_hel. The ATP analogs ATPγS, ADPNP and ADPCP are bound less tightly than ADP (Figure 2B), with K_d values for the complexes of 10.9 ± 0.8 μM (ATPγS), 20 ± 4.9 μM (ADPNP) and 18 ± 3.8 μM (ADPCP), respectively, indicating that the binding energy from additional interactions with the γ-phosphate is converted into conformational changes. The corresponding K_d values for the full-length reverse gyrase (rGyr_fl) are virtually identical in the case of the mantADP, ADP and AMP complexes, and of the ATP analog ATPγS, and 2- to 4-fold higher for the complexes with the nonhydrolyzable ATP analogs ADPNP and ADPCP (14). The similar K_d values confirm that all determinants for nucleotide binding are contained in the helicase-like domain. A summary of the K_d values for rGyr_fl and rGyr_hel is given in Table 1.

In a steady state ATPase assay, rGyr_hel exhibits a low intrinsic ATPase activity (Figure 3). As with rGyr_fl (14), the rate constant k_{cat} of ATP hydrolysis by rGyr_hel is independent of the protein concentration (<10 μM, data not shown), consistent with a monomer as the active species. The dependence of the ATP hydrolysis rate on ATP concentration follows Michaelis–Menten behavior, with a k_{cat} for ATP hydrolysis of 30 (± 2) × 10^{-3} s^{-1}, and a K_M value for ATP of 77 ± 23 μM. The corresponding values for reverse gyrase are very similar with a k_{cat} of 20 (± 0.8) × 10^{-3} s^{-1} and a K_M of 44 ± 6 μM (14).

These results demonstrate that the nucleotide binding properties and the intrinsic ATPase activity of reverse

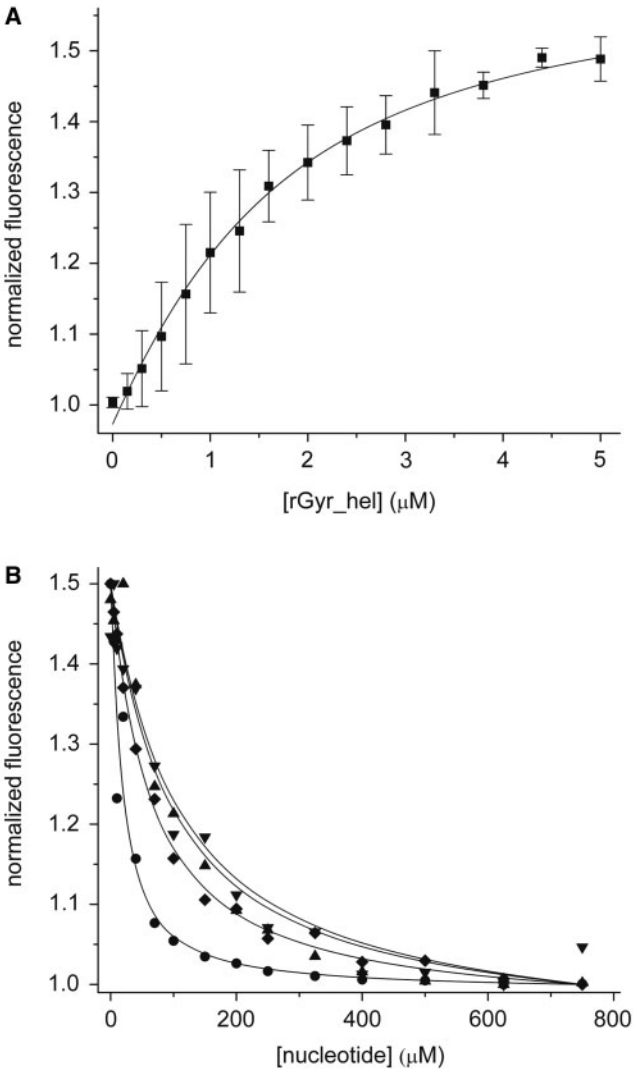

Figure 2. Interaction of rGyr_hel with nucleotides. (**A**) Titration of 1 μM mantADP with rGyr_hel. Description of the binding curve using a one-site binding model yields a K_d of the mantADP/rGyr_hel complex of 1.1 ± 0.1 μM. (**B**) Displacement titrations of the mantADP/rGyr_hel complex with ADP (circles), ADPCP (triangle), ADPNP (inverted triangle), and ATPγS (diamond). The K_d values are summarized in Table 1.

Table 1. Dissociation constants for nucleotide complexes of full-length reverse gyrase and the helicase-like domain

Nucleotide	rGyr_fl K_d (μM)	rGyr_hel K_d (μM)	rGyr_fl K106Q/Y851F K_d (μM)	rGyr_hel K106Q K_d (μM)
mantADP	1.0 ± 0.1[a]	1.1 ± 0.1	22 ± 2	67 ± 5
AMP	1549 ± 375	1600 ± 231	ND	ND
ADP	1.6 ± 0.2[a]	2.6 ± 0.8	36 ± 5	150 ± 85
ATP	ND	ND	98 ± 12	570 ± 300
ATPγS	14.3 ± 1.5[a]	10.9 ± 0.8	ND	ND
ADPNP	43.2 ± 2.0[a]	19.8 ± 4.9	ND	ND
ADPCP	74.7 ± 7.3	17.5 ± 3.8	ND	ND

[a]Data from Ref. (14).

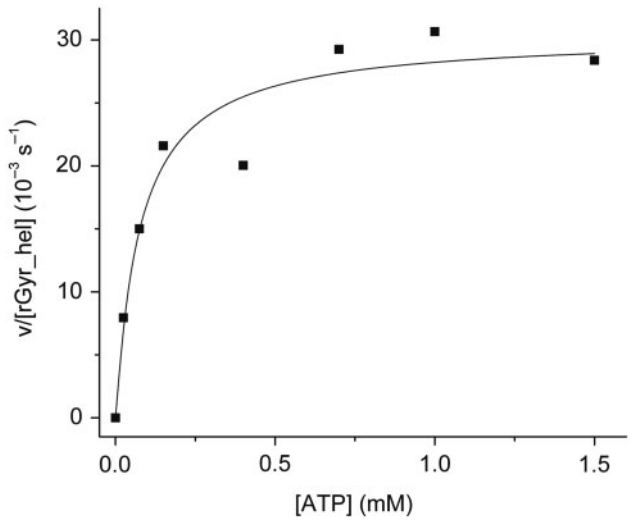

Figure 3. Steady state ATPase activity of rGyr_hel. rGyr_hel is a Michaelis–Menten enzyme with a k_{cat} of 30 $(\pm 2) \times 10^{-3}$ s^{-1}, and a $K_{M,ATP}$ of 77 ± 23 μM.

gyrase are a property of the helicase-like domain and are not significantly affected by the topoisomerase domain.

Stimulation of the rGyr_hel and rGyr_fl ATPase activities by nucleic acids

Reverse gyrases are DNA-stimulated ATPases (21). To investigate the effect of nucleic acid substrates on the ATPase activity of rGyr_hel, steady state ATPase assays were performed in the presence of a 60-base ssDNA substrate, a 60 bp dsDNA, pUC18 plasmid DNA, and polyU-RNA at saturating ATP concentrations (Figure 4A). All substrates led to a significant acceleration of ATP hydrolysis. Saturating concentrations of ssDNA or linear dsDNA increased the k_{cat} by a factor of 40–50, with a slightly higher stimulation by dsDNA. The apparent K_M values are 0.07 ± 0.04 μM for ssDNA (corresponding to 4 μM in terms of bases) and 0.18 ± 0.03 μM for dsDNA (11 μM base pairs), respectively. In the presence of negatively supercoiled pUC18 plasmid, the k_{cat} value increased 22-fold (K_M 0.046 ± 0.006 μM, corresponding to 124 μM base pairs).

Interestingly, polyU-RNA also stimulated the intrinsic ATPase activity of rGyr_hel tremendously (~100-fold). With 25 μM (bases), the apparent K_M value for polyU-RNA was in the same range as for the pUC18 plasmid. PolyU-RNA binding might reflect nonspecific interactions with the negatively charged phosphoribose backbone, and we therefore repeated the steady state ATPase assay in the presence of increasing concentrations of heparin as a model for a negatively charged polymer. Indeed, heparin increased the k_{cat} of rGyr_hel for ATP hydrolysis ~80-fold and thus had a comparable effect to the polyU-RNA. The K_M value for heparin was 0.20 ± 0.05 μM (8 μM monomeric units) and thus also similar to polyU.

To compare ATPase properties of the helicase-like domain with reverse gyrase, the steady state ATPase rates in the presence of ssDNA, dsDNA, pUC18 and

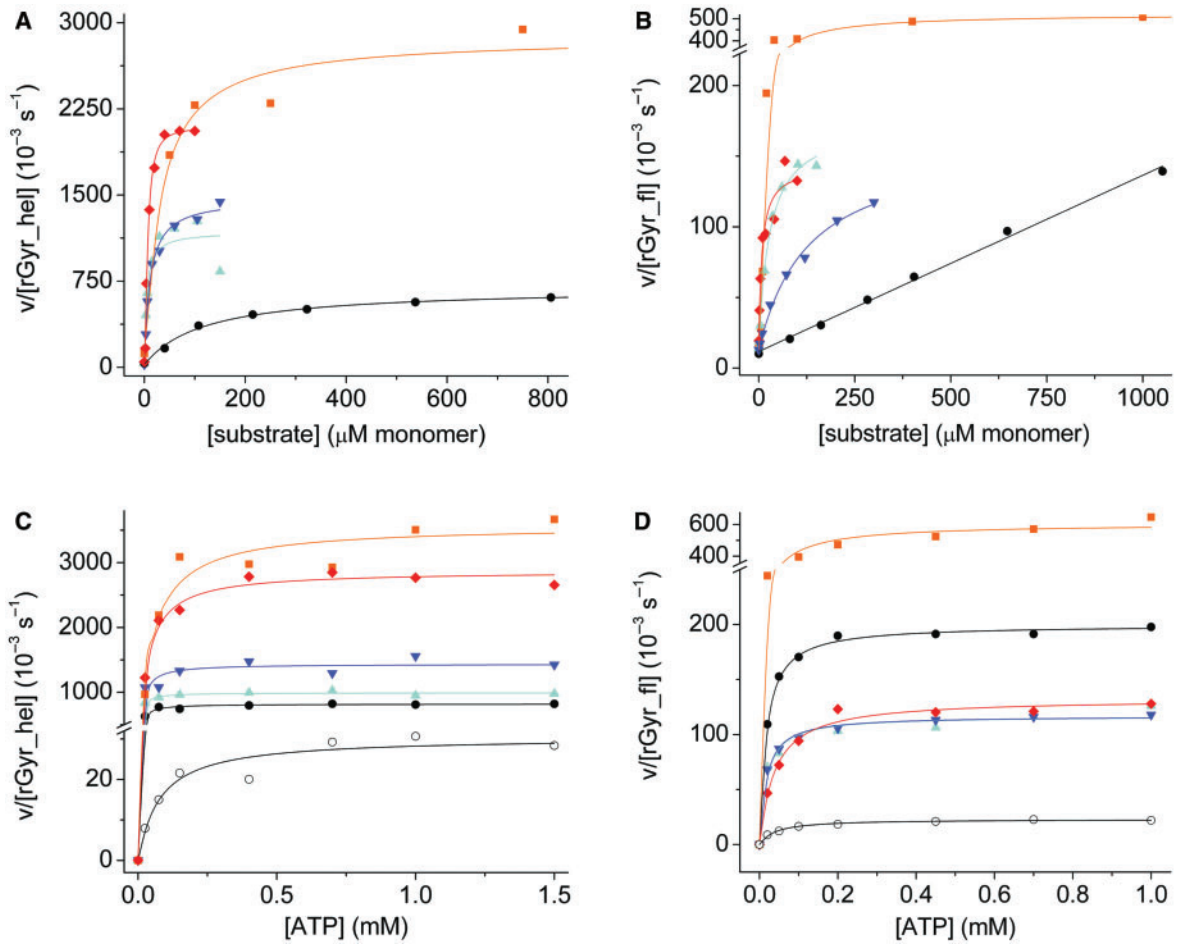

Figure 4. Effect of nucleic acid substrates on the steady state ATPase activity of rGyr_hel and rGyr_fl. (**A** and **B**) The effect of nucleic acid substrates on the ATPase rate at saturating (1 mM) ATP. (**C** and **D**) The ATP-dependence of the ATPase rate at saturating concentrations of nucleic acids. Substrates are indicated as follows: ssDNA (cyan, triangles), dsDNA (blue, inverted triangles), pUC18 (black, circles), polyU-RNA (orange, squares) and heparin (red, diamond). The open symbols in (C and D) indicate data in the absence of DNA. All steady state ATPase parameters are summarized in Tables 2 and 3. (A) Stimulation of the rGyr_hel ATPase by nucleic acids and heparin. The ATPase activity is significantly stimulated by all substrates. (B) Stimulation of the rGyr_fl ATPase by nucleic acids and heparin. The ATPase activity is significantly stimulated by all substrates, but in contrast to rGyr_hel, no saturation is observed with pUC18. (C) Cooperativity between ATP and nucleic acid binding in rGyr_hel. The steady state ATPase activity was measured as a function of ATP concentration in the presence of saturating concentrations of ssDNA (2 μM,), dsDNA (2.5 μM), pUC18 (300 nM), polyU-RNA (1.5 mM monomers) and heparin (40 μM monomers). (D) Cooperativity between ATP and nucleic acid binding in rGyr_fl. The steady state ATPase activity was measured as a function of ATP concentration in the presence of saturating concentrations of ssDNA (2 μM,), dsDNA (5 μM), pUC18 (300 nM), polyU-RNA (0.5 mM monomers) and heparin (60 μM monomers).

polyU-RNA were also determined for rGyr_fl (Figure 4B). As with rGyr_hel, linear ssDNA and dsDNA showed a similar effect on the ATPase rate of rGyr_fl. Importantly, the stimulation of the ATPase activity by ssDNA and dsDNA was only 7- to 8-fold. The ATPase rate of rGyr_fl increases linearly up to a pUC18 concentration of 400 nM (1.1 mM bases), and saturation is not observed (14). In contrast to rGyr_hel, pUC18 only showed a moderate stimulation of the rGyr_fl ATPase rate (7-fold at 400 nM pUC18, compared to 22-fold at saturation for rGyr_hel). As with rGyr_hel, polyU-RNA showed the highest degree of stimulation of the reverse gyrase ATPase activity, with k_{cat} increased 25-fold (K_M 30 μM bases), and heparin showed a 6-fold stimulation (K_M 6 μM monomeric units). These data indicate that interactions with nonspecific substrates are similar for rGyr_hel and rGyr_fl. The k_{cat} values for rGyr_fl and rGyr_hel in the absence and presence of nucleic acids and the apparent K_M values are summarized in Table 2.

Reverse gyrase is an enzyme unique to hyperthermophilic organisms, which thrive at temperatures of 75°C and higher. To investigate if the results from experiments at 37°C reflect the properties of reverse gyrase at its optimum temperature, the ATPase activity was determined at 75°C in the absence of DNA, and in the presence of ssDNA, dsDNA and pUC18 (Figure 5). In the absence of DNA, the ATPase activities of rGyr_fl and rGyr_hel are similar, with initial rates of 0.28 μM s^{-1} (rGyr_hel) and 0.48 μM s^{-1} (rGyr_fl). While we have determined the affinities for DNA substrates at 37°C and could therefore ensure saturating DNA concentrations in ATPase assays, a quantitative comparison of the ATPase stimulation at 75°C is difficult as the corresponding K_d values cannot easily be determined, and the DNA concentrations may not

Table 2. Steady state ATPase parameters for rGyr_hel and rGyr_fl, and the influence of nucleic acid substrates

	Nucleic acid	k_{cat} (10^{-3} s^{-1})	$K_{M,DNA}$ (μM)	K_M (μM base/bp)
rGyr_hel	–	30 ± 2	NA	NA
	ssDNA	1160 ± 188	0.07 ± 0.04	4.2 ± 2.4
	dsDNA	1450 ± 64	0.18 ± 0.03	10.8 ± 1.8
	pUC18	673 ± 21	0.046 ± 0.006	124 ± 16
	polyU-RNA	3264 ± 304	NA	25 ± 10
	Heparin	2420 ± 160	0.20 ± 0.05	8.0 ± 0.04
rGyr_fl	–	20 ± 0.8	NA	NA
	ssDNA	160 ± 6.7	0.45 ± 0.06	27 ± 4
	dsDNA	148 ± 9.1	2.2 ± 0.30	129 ± 18
	pUC18	No saturation for conc. <400 nM		
	polyU-RNA	507 ± 27	NA	30 ± 7
	Heparin	120 ± 10	0.15 ± 0.06	6 ± 2.4

be saturating. In addition, the thermodynamic stability of the 60 bp duplex is limited (T_m = 70°C), and at 75°C more than 50% single strand are expected. Qualitatively, the rGyr_hel ATPase activity at 75°C is stimulated to a similar extent by ssDNA and dsDNA at 75°C, and about 2-fold less by pUC18. Overall, the ATPase activity is increased only 3-fold by DNA substrates, compared to 50-fold at 37°C. The rGyr_fl ATPase is most efficiently stimulated by ssDNA, and to a smaller extent by dsDNA or pUC18. As observed at 37°C, the overall stimulation is smaller for rGyr_fl than for rGyr_hel. Thus, the rGyr_hel and rGyr_fl ATPase activities at 75°C show the same response to DNA as at 37°C.

In summary, the basal ATP hydrolysis rates are very similar for rGyr_hel and rGyr_fl, confirming that all determinants for ATP binding and hydrolysis are confined to the helicase-like domain. The intrinsic ATPase of rGyr_hel is efficiently stimulated by ssDNA, dsDNA and plasmid DNA. All substrates also stimulate the intrinsic ATP hydrolysis of rGyr_fl, but generally to a lesser extent. These data point towards an inhibitory effect of the topoisomerase domain on the ATPase activity of the helicase-like domain in the presence of DNA substrates. The apparent K_M values for DNA are higher for rGyr_fl than for rGyr_hel. This effect seems to be slightly more pronounced for dsDNA, leading to a 5-fold higher apparent K_M for dsDNA over ssDNA for rGyr_fl, compared to an only 2.5-fold difference for rGyr_hel. Both enzymes thus appear to interact more tightly with ssDNA. Interestingly, the apparent K_M values for polyU-RNA and heparin are identical for rGyr_fl and rGyr_hel, indicating similar interactions with nonspecific substrates.

Coupling between DNA and ATP binding to rGyr_hel and rGyr_fl

The interaction of SF2 helicases with ATP and their DNA substrate is cooperative: ATP binding increases the affinity for the DNA substrate, and vice versa (13,22–24). To test whether any of the nucleic acid substrates shows such a cooperative effect on ATP binding to rGyr_hel or rGyr_fl, we determined the effect of DNA on K_M values for ATP by measuring the steady state ATPase rate with increasing

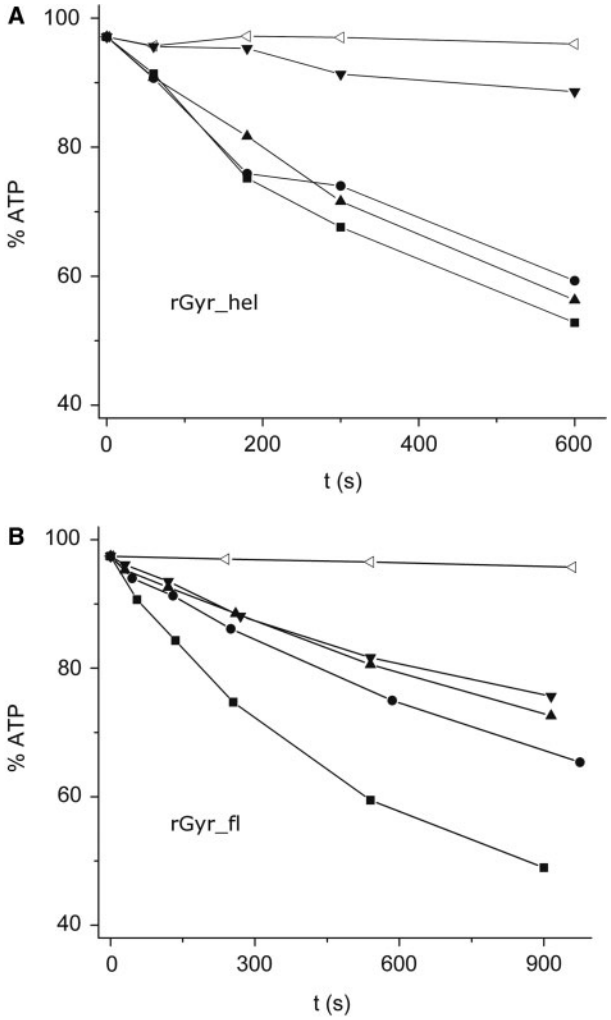

Figure 5. DNA-stimulated ATPase activity at 75°C. ATPase activity of rGyr_hel (**A**) and rGyr_fl (**B**) at 75°C in the absence of enzyme (open triangles), in the presence of 1 μM enzyme without DNA (inverted triangles) and in the presence of ssDNA (100 nM, squares), dsDNA (100 nM, circles), or pUC18 (15 nM, triangles). The ATP concentration was 1 mM.

concentrations of ATP and saturating concentrations of the nucleic acid (Figure 4C and D). In all cases, the k_{cat} values are in good agreement with the values in the DNA-dependent experiments at saturating ATP concentrations (Table 2), confirming that saturation is reached in both series of experiments. In the presence of ssDNA, the apparent $K_{M,ATP}$ value of rGyr_hel is decreased 16-fold, demonstrating cooperative binding of ATP and ssDNA to rGyr_hel. For dsDNA, this cooperativity is lower than for ssDNA, with $K_{M,ATP}$ decreased 7-fold. The effect of pUC18 plasmid is intermediate, with a 10-fold decrease in the apparent $K_{M,ATP}$. Hence, all DNA substrates promote ATP binding to rGyr_hel. PolyU-RNA and heparin only affect the apparent $K_{M,ATP}$ slightly (1.8-fold and 2.5-fold, respectively) and thus do not show significant cooperativity. These data corroborate the notion that the stimulating effect of polyU-RNA and heparin on the ATPase activity of rGyr_hel is due to a nonspecific interaction.

For rGyr_fl, limited cooperativity of DNA and ATP binding was detected (Figure 4D). The reduction of the $K_{M,ATP}$ was 3.8-fold for ssDNA and 2.8-fold for dsDNA. Hence, as for rGyr_hel, the cooperativity with ATP binding is highest for ssDNA. However, the cooperativity of DNA and ATP binding to rGyr_fl is smaller for ssDNA and dsDNA compared to rGyr_hel. For pUC18, it was not possible to perform the experiment under saturating conditions. At 300 nM pUC18, $K_{M,ATP}$ was reduced 2.8-fold. This is similar to the effect of linear dsDNA, whereas for rGyr_hel, pUC18 shows intermediate cooperativity to ssDNA and dsDNA. However, a more pronounced effect of pUC18 on $K_{M,ATP}$ for rGyr_fl at higher plasmid concentrations cannot be excluded. Overall, rGyr_fl shows cooperative interactions with DNA and ATP, but to a lesser extent than rGyr_hel. PolyU-RNA and heparin had a negligible effect on ATP binding (1.4-fold and 1.2-fold, respectively), consistent with a nonspecific interaction. The k_{cat} and $K_{M,ATP}$ values are summarized in Table 3.

Altogether, the interaction of rGyr_hel and rGyr_fl with polyU-RNA or heparin and ATP is noncooperative and most likely reflects a nonspecific interaction. Substantial cooperativity is observed for ssDNA, dsDNA or plasmid DNA and ATP binding to rGyr_hel. rGyr_fl also binds ssDNA or dsDNA and ATP cooperatively, but the effect of the DNA on $K_{M,ATP}$ is only 3- to 4-fold, compared to 7- to 16-fold for rGyr_hel. Again, this points towards a moderating effect of the topoisomerase domain on the helicase-like domain in full-length reverse gyrase.

Influence of the nucleotide state on DNA binding to rGyr_hel

During their nucleotide cycle, SF2 helicases switch between low affinity and high affinity states for their nucleic acid substrate (22,25,26). We therefore investigated the influence of the nucleotide state of rGyr_hel and rGyr_fl on their interaction with DNA. To this end, the affinity of rGyr_hel for nucleic acids was determined in fluorescence anisotropy titrations of a 5′-fluorescein-labeled 60-base ssDNA or a fluorescein-labeled 60 bp dsDNA in the absence of nucleotides, and in the presence of saturating concentrations of ADP, ADPCP, ADPNP and ATPγS (Figure 6, Table 4).

First, we characterized binding of ssDNA to rGyr_hel (Figure 6A). The K_d value for the rGyr_hel/ssDNA complex was 0.20 ± 0.03 μM in the absence of nucleotide, and varied only moderately with the nucleotide state. The non-hydrolyzable ATP analogs ADPNP and ATPγS showed the largest effect on ssDNA binding, with 3-fold (ADPNP) or 6-fold (ATPγS) increased K_d values, respectively, indicating that the affinity for ssDNA is slightly reduced in the ATP state of rGyr_hel. The ADP state of rGyr_hel binds ssDNA 1.5-fold less tightly than the nucleotide-free state, but 2- to 4-fold more tightly than the ATP-state (mimicked by ADPNP and ATPγS). ADPCP has a similar effect on ssDNA binding as ADP, suggesting that ADPCP is not a suitable mimic for ATP.

When the concentration of ssDNA in the titration with rGyr_hel was increased to 2 μM, a sigmoidal binding curve was obtained, indicating that more than one

Table 3. Steady state ATPase parameters for rGyr_hel and rGyr_fl: the influence of nucleic acid substrates on $K_{M,ATP}$

	Nucleic acid (saturating)	k_{cat} (10^{-3} s^{-1})	$K_{M,ATP}$ (μM)
rGyr_hel	–	30 ± 2	77 ± 23
	ssDNA	992 ± 12	4.8 ± 1.0
	dsDNA	1435 ± 57	11 ± 4
	pUC18	818 ± 10	7.4 ± 1.1
	polyU-RNA	3402 ± 79	42 ± 5.5
	Heparin	2869 ± 63	31 ± 4
rGyr_fl	–	20 ± 0.8	44 ± 6
	ssDNA	108 ± 2.1	12 ± 1.5
	dsDNA	117 ± 1.6	16 ± 1.5
	pUC18 (300 nM)	199 ± 1.6	15.6 ± 0.9
	polyU-RNA	565 ± 19	32 ± 5.1
	Heparin	133 ± 7	37 ± 6.7

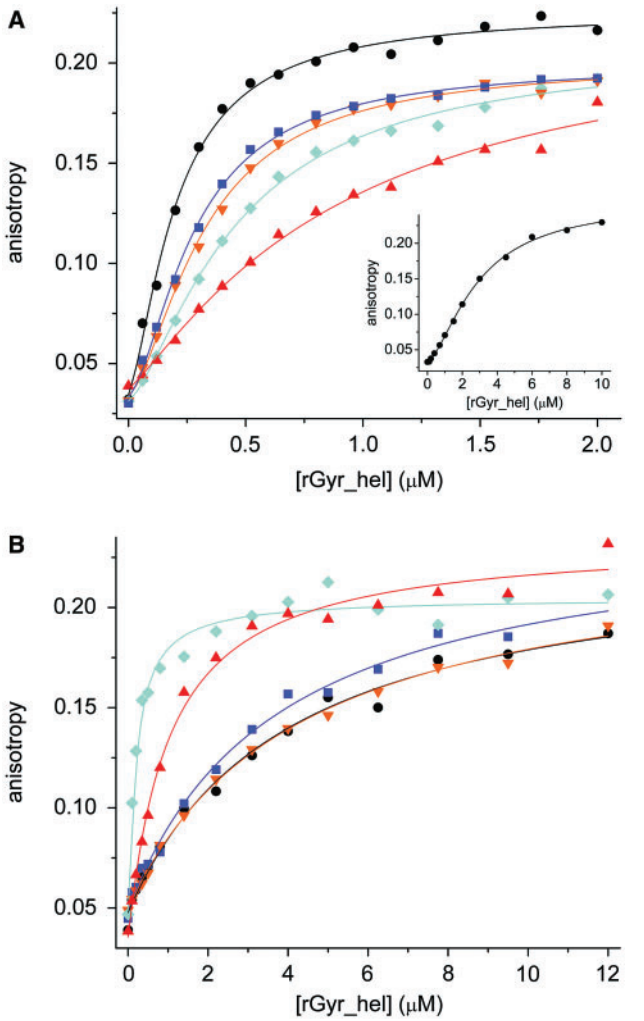

Figure 6. DNA binding and coupling to nucleotide binding (rGyr_hel). Titrations of DNA with rGyr_hel in the absence of nucleotide (black, circles), and in the presence of ADP (100 μM, blue, squares), ADPCP (500 μM, orange, inverted triangles), ATPγS (500 μM, red, triangles) and ADPNP (500 μM, cyan, diamonds). All K_d values and Hill coefficients are summarized in Table 4. (**A**) ssDNA (25 nM). The binding curves are described with the Hill equation. The inset shows the stoichiometric titration of 2 μM ssDNA with rGyr_hel. (**B**) dsDNA (25 nM). The binding curves are described with a one-site binding model.

Table 4. DNA binding properties of different nucleotide states of rGyr_hel

K_d (μM)	nucleotide-free	ADP state		ATP state	
ssDNA					
wt	0.20 ± 0.03[a]	ADP	0.31 ± 0.04[a]	ADPNP	0.60 ± 0.07[a]
	0.20 ± 0.01[b]		0.28 ± 0.01[b]		0.46 ± 0.03[b]
	$n = 1.4 \pm 0.1$		$n = 1.6 \pm 0.1$		$n = 1.4 \pm 0.1$
		ADPCP	0.38 ± 0.05[a]	ATPγS	1.2 ± 0.2[a]
			0.33 ± 0.01[b]		0.92 ± 0.21[b]
			$n = 1.6 \pm 0.1$		$n = 1.2 \pm 0.2$
K106Q	0.18 ± 0.03[a]		0.25 ± 0.03[a]		0.19 ± 0.02[a]
	0.18 ± 0.03[b]		0.24 ± 0.02[b]		0.20 ± 0.02[b]
	$n = 1.3 \pm 0.2$		$n = 1.3 \pm 0.1$		$n = 1.1 \pm 0.1$
dsDNA					
wt	3.9 ± 0.6[a]	ADP	3.7 ± 0.5[a]	ADPNP	0.19 ± 0.03[a]
		ADPCP	4.2 ± 0.3[a]	ATPγS	1.0 ± 0.1[a]
K106Q	3.8 ± 0.6[a]		2.9 ± 0.6[a]		1.7 ± 0.2[a]

[a]One-site.
[b]Hill analysis.

rGyr_hel molecule interacts with each ssDNA (Figure 6A, inset). The data were well-described by the Hill equation, with a Hill coefficient of 1.6 ± 0.1, and a K_d of 2.9 ± 0.1 μM. Analysis of all ssDNA titration curves with the Hill equation gave similar K_d values as the analysis with the one-site binding model (Table 4), and Hill coefficients of 1.2–1.6, indicating that the cooperativity is moderate.

Next, binding of rGyr_hel to dsDNA was characterized (Figure 6B, Table 4). DsDNA was bound 10- to 20-fold less tightly by rGyr_hel than ssDNA, consistent with the observed higher K_M value for dsDNA. The K_d value for dsDNA was ~3.9 μM in the absence of nucleotide, or in the presence of ADP or ADPCP. Only in the presence of ADPNP or ATPγS was a significant change observed: the K_d value of the dsDNA/rGyr_hel complex was decreased 20-fold by ADPNP, or 4-fold by ATPγS. This decrease is consistent with ADPNP and ATPγS mimicking the ATP state. Overall, the ATP state of rGyr_hel thus binds dsDNA 4- to 20-fold more tightly than the ADP state.

Comparison of DNA binding to different nucleotide states (Table 4) reveals that the nucleotide-free form of rGyr_hel shows 20-fold higher affinity for ssDNA over dsDNA. In the ATP state, the affinity for ssDNA remains similar, but the dsDNA affinity increases compared to the nucleotide-free state. Thus, the ATP state exhibits similar affinities for ssDNA and dsDNA. In the ADP state, the affinity for ssDNA is similar to the nucleotide-free or ATP states, but the affinity for dsDNA is reduced compared to the ATP state. As a consequence, ssDNA binding is favored 11- to 13-fold in the ADP state. Hence, during the nucleotide cycle, rGyr_hel does not discriminate between ssDNA and dsDNA prior to ATP hydrolysis, but will preferentially interact with ssDNA after hydrolysis.

Due to thermodynamic coupling, the observed increased affinity of the ATP state for dsDNA requires a reciprocal effect of DNA on ATP binding. Comparison with the steady state ATPase data (Figure 4A and C, Table 3) shows that this coupling is indeed present: the $K_{M,ATP}$ of rGyr_hel is decreased 7-fold in the presence of dsDNA, which is in good agreement with the 4- to 20-fold increased dsDNA affinity in the ATP state of rGyr_hel. The comparison for the ssDNA seems to be inconsistent: the ATP state of rGyr_hel binds ssDNA 3- to 6-fold less tightly than the nucleotide-free form, but $K_{M,ATP}$ is decreased 16-fold when ssDNA is bound. However, the observed differences most likely reflect differences of the ADPNP or ATPγS states compared to the ATP state. This is partly supported by experiments with a hydrolysis-deficient mutant (see below), where ATP binding does not reduce the ssDNA affinity.

Influence of the nucleotide state on DNA binding to rGyr_fl

To test whether the helicase-like domain also acts as a nucleotide-dependent switch with different affinities for dsDNA in the ATP and ADP states in reverse gyrase, we performed DNA binding experiments with rGyr_fl (Figure 7). Quantification of DNA binding to rGyr_fl is complicated by the existence of several potential DNA binding sites that could be located in the helicase-like domain, in the cleft of the topoisomerase domain near the catalytic tyrosine, and possibly at the two putative zinc fingers. To ensure equilibrium conditions, we used the Y851F mutant of reverse gyrase in DNA binding experiments, which is deficient in covalent binding to the DNA.

Again, we first addressed binding of ssDNA to rGyr_fl (Figure 7, Table 5). In a titration of the 60-base ssDNA with rGyr_fl(Y851F), a sigmoidal dependence of the fluorescence anisotropy on the concentration of enzyme was observed (Figure 7A). The binding isotherm was well-described by the Hill equation, with a Hill coefficient of 2.3 (± 0.2) and a K_d of 36 ± 1 nM for nucleotide-free rGyr_fl(Y851F), pointing towards cooperative binding of at least two reverse gyrase molecules to the DNA. To confirm the existence of cooperativity, the titration was repeated at 300 nM of ssDNA, where the sigmoidality became much more prominent (Figure 7A, inset). Description with the Hill equation yielded $K_d = 0.33 \pm 0.02$ μM, and $n = 2.0 \pm 0.14$). In the presence of saturating concentrations of ADP, ADPCP, ADPNP or ATPγS, binding isotherms for ssDNA to rGyr_fl remained sigmoidal (Figure 7A), with Hill coefficients from 1.8 ± 0.10 to 2.1 ± 0.16, again consistent with two reverse gyrase molecules binding to one ssDNA molecule.

Overall, rGyr_fl binds ssDNA 6-fold more tightly than rGyr_hel. In the presence of ADP, the interaction with ssDNA is only slightly affected, and it is virtually unchanged in the presence of nonhydrolyzable ATP analogs. Consequently, the affinity of rGyr_fl for ssDNA is not significantly modulated by the nucleotide state.

Next, the interaction of rGyr_fl(Y851F) with dsDNA was characterized (Figure 7, Table 5). Interestingly, the cooperativity was less pronounced for rGyr_fl binding to dsDNA (Figure 7B). In this case, the binding isotherm could be described by a simple one-site model with a K_d of 490 ± 60 nM. Thus, rGyr_fl interacts 8-fold more tightly with dsDNA than rGyr_hel. dsDNA bound to rGyr_fl was displaced upon addition of an excess of

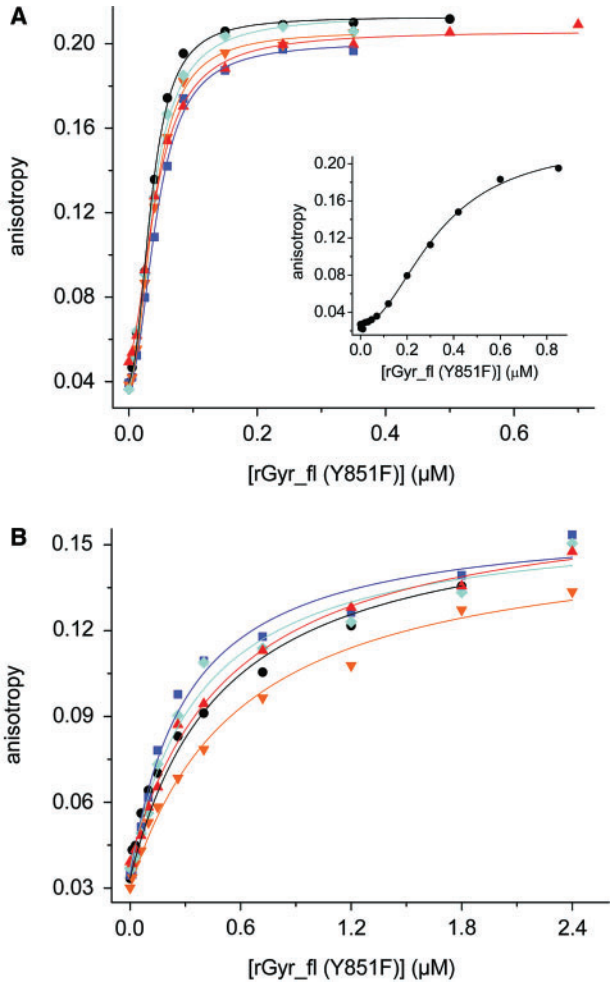

Figure 7. DNA binding and coupling to nucleotide binding (rGyr_fl). Titration of DNA with rGyr_fl in the absence of nucleotide (black, circles), and in the presence of ADP (100 μM, blue, squares), ADPCP (500 μM, orange, inverted triangles), ATPγS (500 μM, red, triangles) and ADPNP (500 μM, cyan, diamonds). All K_d values and Hill coefficients are summarized in Table 5. (**A**) ssDNA (10 nM). The binding curves are described with the Hill equation. The inset shows the stoichiometric titration of 300 nM ssDNA with rGyr_fl. (**B**) dsDNA (10 nM). The binding curves are described with a one-site binding model.

ssDNA (data not shown), demonstrating that both types of nucleic acids interact with the same binding site.

In the presence of nucleotides, the cooperativity of dsDNA binding appeared to increase slightly, as indicated by a slightly improved fit with the Hill equation. Hill coefficients varied between 0.7 and 1.7, consistent with a lower cooperativity compared to ssDNA (or a reduced number of binding sites). However, the experimental data were already reasonably well described with the one-site binding model. The presence of ADP, ADPNP, ADPCP or ATPγS affects the affinity of rGyr_fl for dsDNA <2-fold.

Comparison of DNA binding to different nucleotide states of rGyr_fl (Table 5) shows that the nucleotide-free form binds dsDNA 14-fold less tightly than ssDNA. In the ATP or state, ssDNA or dsDNA binding are not affected. However, the ADP state binds dsDNA 2-fold more tightly than the nucleotide-free and the ATP states. In the nucleotide cycle, both the ATP and the ADP state bind ssDNA more tightly than dsDNA. The preference for ssDNA is slightly reduced after hydrolysis (from 10-fold in the ATP state to 4-fold in the ADP state). The small effect of nucleotides on DNA binding to rGyr_fl is consistent with the small effect of ssDNA and dsDNA on ATP binding according to the steady state ATPase data (Figure 4B and D, Table 3).

In summary, the ATP state of rGyr_hel binds ssDNA and dsDNA with equal affinities, whereas the ADP state interacts preferentially with ssDNA. rGyr_fl binds DNA ~10-fold more tightly than rGyr_hel, but the differences between the nucleotide states are far less pronounced. Both the ATP and the ADP states bind preferentially to ssDNA.

DNA binding to different nucleotide states of a hydrolysis-deficient mutant of rGyr_fl and rGyr_hel

As complexes with the nonhydrolyzable ATP analogs might not perfectly mimic the ATP states, we analyzed the effect of nucleotides on the interaction with DNA using hydrolysis-deficient mutants of rGyr_hel and rGyr_fl. A conserved lysine in the Walker A motif of

Table 5. DNA binding properties of different nucleotide states of rGyr_fl

K_d (μM)	nucleotide-free	ADP state		ATP state	
ssDNA					
Y851F	0.035 ± 0.005[a]	ADP	0.060 ± 0.015[a]	ADPNP	0.041 ± 0.009[a]
	0.036 ± 0.001[b]		0.045 ± 0.002[b]		0.038± 0.002[b]
	n = 2.3 ± 0.2		n = 2.1 ± 0.2		n = 2.1 ± 0.2
		ADPCP	0.049 ± 0.012[a]	ATPγS	0.046 ± 0.008
			0.039 ± 0.001[b]		0.041 ± 0.001[b]
			n = 2.1 ± 0.1		n = 1.8 ± 0.1
K106Q/Y851F	0.047 ± 0.005[a]		0.053 ± 0.007[a]		0.037 ± 0.004[a]
	0.044 ± 0.003[b]		0.044 ± 0.002[b]		0.035 ± 0.002[b]
	n = 1.4 ± 0.1		n = 1.5 ± 0.1		n = 1.4 ± 0.1
dsDNA					
Y851F	0.49 ± 0.06[a]	ADP	0.25 ± 0.04[a]	ADPNP	0.33 ± 0.07[a]
		ADPCP	0.59 ± 0.06[a]	ATPγS	0.53 ± 0.07[a]
K106Q/Y851F	0.71 ± 0.11[a]		0.46 ± 0.07[a]		0.49 ± 0.09[a]

[a]one-site.
[b]Hill analysis.

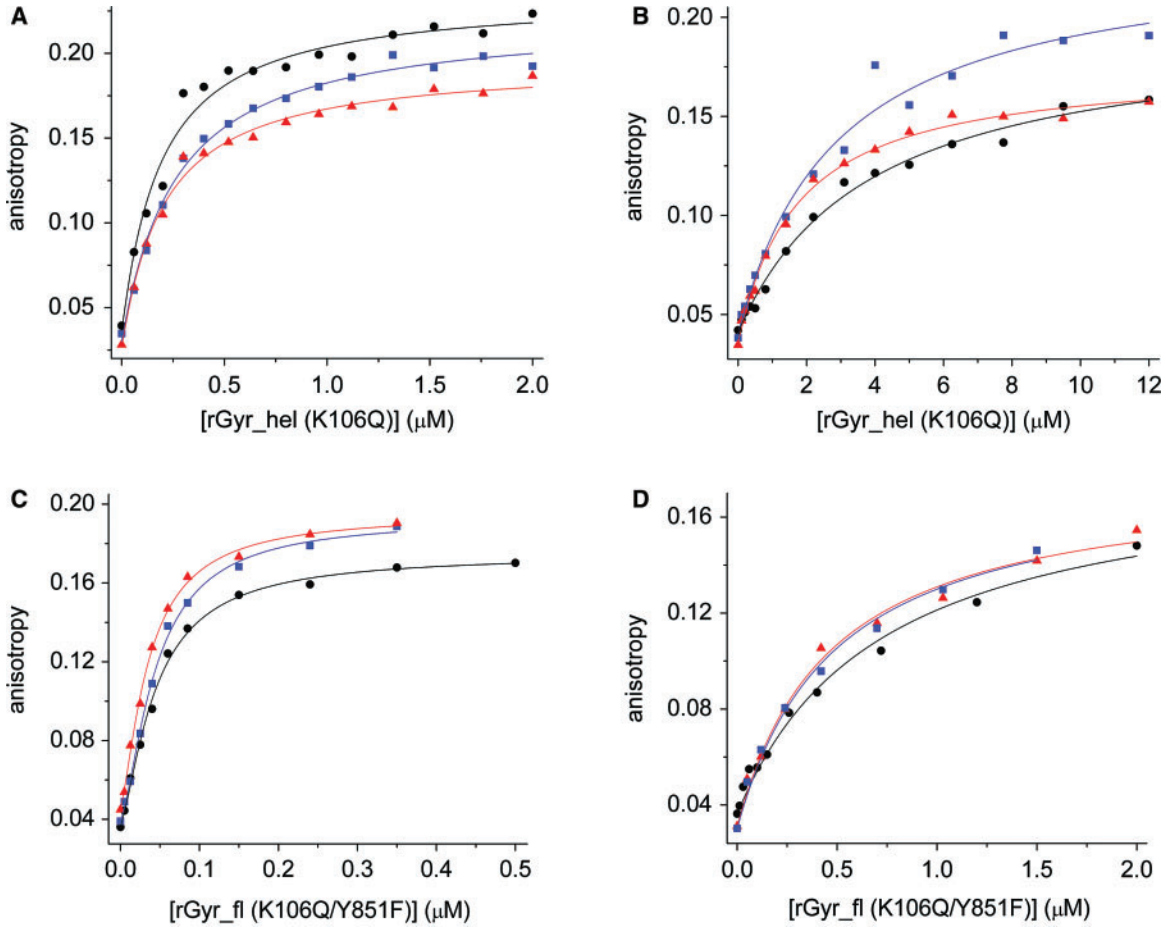

Figure 8. Binding of ssDNA and dsDNA to rGyr_hel(K106Q) and rGyr_fl(K106Q/Y851F). Titrations of ssDNA (**A**, **C**) and dsDNA (**B**, **D**) with rGyr_hel(K106Q) (A, B) or rGyr_fl(K106Q/Y851F) (C, D) in the absence of nucleotide (black, circles), and in the presence of ADP (2 mM, blue, squares) or ATP (4 mM, red, triangles). The DNA concentration was 25 nM in (A and B), and 10 nM in (C and D). The K_d values are summarized in Table 5.

ATPases contacts the β- and γ-phosphates of ATP, and stabilizes negative charges during ATP hydrolysis. In the rGyr_fl(K106Q) mutant, ATP hydrolysis is abolished, but nucleotides are still bound, albeit with reduced affinity (14). The rGyr_fl(K106Q/Y851F) double mutant was created to stably generate ATP and ADP states of reverse gyrase that do not covalently bind to DNA. The absence of ATP hydrolysis was confirmed, and the K_d values of the nucleotide complexes were determined to be $22 \pm 2\,\mu M$ (mantADP), $36 \pm 5\,\mu M$ (ADP) and $98 \pm 12\,\mu M$ (ATP) in equilibrium titrations (Table 1). Overall, nucleotide binding to rGyr_fl(K106Q/Y851F) is reduced ~20-fold compared to wild-type.

The DNA binding properties of this ATP-hydrolysis- and DNA-cleavage-deficient mutant were studied using the 60-base ssDNA and 60 bp dsDNA as a substrate (Figure 8, Table 5). ssDNA was bound independent of the nucleotide state, with K_d values of 44 ± 3 nM (no nucleotide), 44 ± 2 nM (ADP state) and 35 ± 2 nM (ATP state). K_d values for the corresponding dsDNA complexes were higher, consistent with the lower affinity of rGyr_fl for dsDNA. Similar to ssDNA binding, interaction of rGyr_fl(K106Q/Y851F) with dsDNA is independent of the nucleotide state. The K_d values of the dsDNA complexes are $0.71 \pm 0.11\,\mu M$ (no nucleotide), $0.46 \pm 0.07\,\mu M$ (ADP state) and $0.49 \pm 0.09\,\mu M$ (ATP state). Consistent with the wild-type data, the hydrolysis-deficient mutant of rGyr_fl thus shows ~10-fold tighter binding of ssDNA to all nucleotide states.

The data for the wild-type enzyme and nonhydrolyzable ATP analogs (Figure 7, Table 5) support a slightly decreased preference for ssDNA after hydrolysis. The increased preference for ssDNA in the ADP state of rGyr_fl(K106Q/Y851F) results from a 2-fold increased K_d of 0.46 μM for the dsDNA complex, compared to a K_d of 0.25 μM for rGyr_fl(Y851F), and suggests differences between the ADP state of wild-type rGyr_fl and the K106Q/Y851F mutant. Previous work already pointed towards such a difference: Reverse gyrase relaxes negatively supercoiled DNA in the presence of ADP, whereas the K106Q mutant lacks such a relaxation activity (14). Most likely, lysine 106 functions as a nucleotide sensor that triggers an ADP-dependent conformational change that is required for relaxation. If this conformational change is absent in the K106Q mutant, the ADP state will be different, leading to different DNA binding properties.

To compare the DNA binding properties of the nucleotide states of rGyr_hel with rGyr_fl, the corresponding

K106Q mutation in the Walker A motif of rGyr_hel was introduced, and the absence of hydrolysis was confirmed (data not shown). Fluorescence equilibrium titrations revealed a K_d value for the mantADP complex of $67 \pm 5\,\mu M$, and $150 \pm 85\,\mu M$ and $570 \pm 300\,\mu M$ for the ADP and ATP complexes, respectively (Table 1). Thus, the nucleotide affinity of the K106Q mutant of rGyr_hel is ~60-fold reduced compared to the wild-type. This effect is more pronounced than for rGyr_fl (20-fold).

rGyr_hel(K106Q) binds ssDNA 20-fold more tightly than dsDNA ($K_d = 0.18 \pm 0.03$ and $3.8 \pm 0.6\,\mu M$, respectively). In the presence of ADP or ATP, ssDNA binding is not significantly affected, and dsDNA binding is only slightly increased (ADP: 1.3-fold, $K_d = 2.9 \pm 0.6\,\mu M$; ATP: 2.2-fold, $K_d = 1.7 \pm 0.2\,\mu M$). As a consequence, ssDNA interacts more tightly than dsDNA with both nucleotide states (12-fold, ADP state; 9-fold, ATP state), implying a slightly stronger preference for ssDNA after ATP hydrolysis. Similarly, the data from wild-type rGyr_hel suggest a stronger interaction with ssDNA after ATP hydrolysis. However, wild-type rGyr_hel in complex with nonhydrolyzable ATP analogs binds ssDNA and dsDNA with similar affinities, while the ATP state of rGyr_hel(K106Q) interacts 9-fold more tightly with ssDNA. This discrepancy arises from a reduced affinity of the rGyr_hel(K106Q) ATP state for dsDNA compared to the ADPNP or ATPγS state of the wild-type rGyr_hel (Figure 6, Table 4), suggesting structural differences between the ATP state of rGyr_hel(K106Q) and the corresponding complexes of wild-type with nonhydrolyzable analogs.

Altogether, rGyr_hel shows similar affinities for ssDNA and dsDNA in the ATP state, and a 10-fold preference for ssDNA in the ADP state due to a decrease in dsDNA affinity. Thus, the helicase domain switches from a 'high affinity' state with respect to dsDNA to a 'low affinity' state upon ATP hydrolysis, and back to the 'high affinity' state after nucleotide exchange, while the ssDNA affinity remains constant. In rGyr_fl, both nucleotide states show a preference for ssDNA, indicating that the switch to the 'low affinity' state for dsDNA upon ATP hydrolysis is suppressed in the full-length enzyme. Figure 9 summarizes the properties of rGyr_hel and rGyr_fl. The K106Q mutants of rGyr_hel and rGyr_fl show similar DNA preferences, with a 10-fold higher affinity for ssDNA compared to dsDNA in both nucleotide states. These results argue for a critical role of lysine 106 as a nucleotide sensor in the helicase domain, and for inter-domain communication between the helicase-like and the topoisomerase domains.

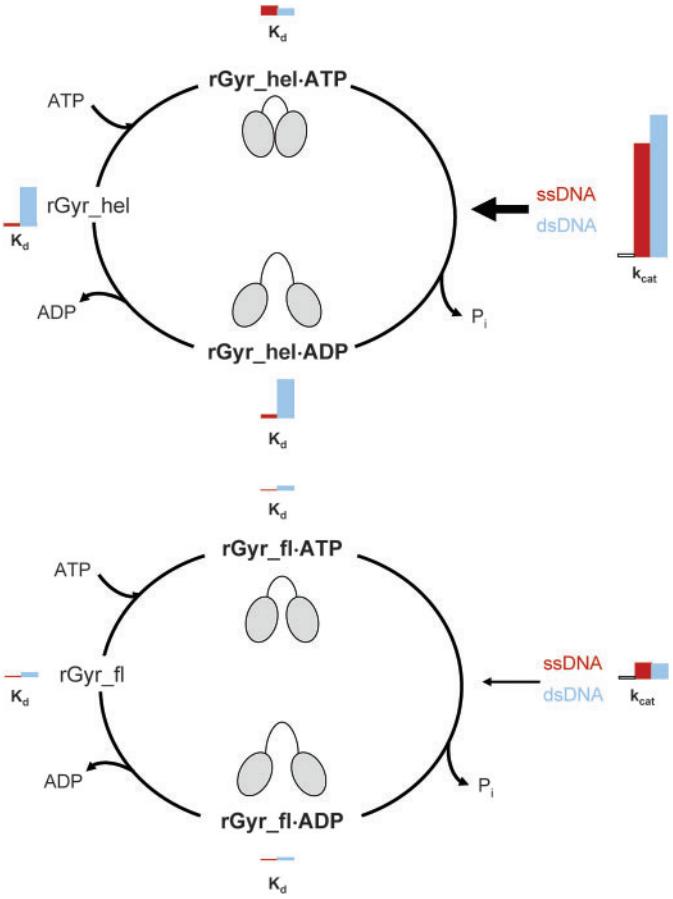

Figure 9. Overview of the nucleotide cycle of rGyr_hel and rGyr_fl. The K_d values of the nucleotide states for ssDNA (red) and dsDNA (blue) are displayed as bars with a size proportional to their value. Analogously, a red bar denotes the k_{cat} value in the presence of ssDNA, a blue bar corresponds to the k_{cat} value in the presence of dsDNA. For reference, an additional bar represents the intrinsic k_{cat} in the absence of DNA. A cartoon indicates possible conformations of the helicase-like domain in the different nucleotide states of rGyr_hel and rGyr_fl. rGyr_hel (upper panel) shows similar affinities for ssDNA and dsDNA in the ATP state, and a preference for ssDNA in the ADP state due to a decrease in dsDNA affinity. This corresponds to a switch from a 'high affinity' state with respect to dsDNA to a 'low affinity' state upon ATP hydrolysis. Both dsDNA and ssDNA efficiently stimulate ATP hydrolysis (arrow). Most likely, the helicase-like domain switches between a closed conformation (cartoon) in the presence of DNA and ATP that hydrolyzes ATP efficiently, and an open conformation in the ADP state, as observed for SF2 helicases. In rGyr_fl (lower panel), both nucleotide states show a preference for ssDNA, indicating that the switch to the 'low affinity' state for dsDNA upon ATP hydrolysis is suppressed in the full-length enzyme. The ATPase stimulation by DNA is 10-fold smaller than in rGyr_hel. Possibly, steric hindrance by the topoisomerase domain prevents a complete closure of the helicase-like domain (cartoon) in the context of full-length reverse gyrase. The progression through the nucleotide cycle with moderate velocity may be required for efficient coupling of ATP hydrolysis and positive supercoiling.

DISCUSSION

The helicase-like domain confers nucleotide-dependent DNA binding to reverse gyrase

We have shown here that the nucleotide binding properties of reverse gyrase are a function of the N-terminal helicase-like domain. Nucleotide affinities and ATP hydrolysis rates are virtually identical for the isolated helicase-like domain and for the full-length enzyme in the absence of nucleic acids. Thus, all determinants for nucleotide binding and hydrolysis are contained within the helicase-like domain, and its characteristics are unaltered in the context of reverse gyrase. The similar ATPase rates suggest that the conformations of the helicase-like domains are similar, indicating that the arrangement of

the catalytic residues in the isolated helicase-like domain and in context of reverse gyrase are the same.

Our results demonstrate that the helicase-like domain mediates nucleotide-dependent interactions of reverse gyrase with ssDNA and dsDNA, and with plasmid DNA. In the ATP state, dsDNA and ssDNA are bound with similar affinities, whereas after ATP hydrolysis, ssDNA is preferentially bound. The DNA substrates influence the rate of switching between these states by stimulating the intrinsic ATPase activity of the helicase-like domain. Thus, the helicase-like domain is a module that confers nucleotide-dependent DNA binding to reverse gyrase. The topoisomerase domain has no influence on nucleotide binding and hydrolysis by the helicase-like domain in the absence of DNA, but modulates the ATPase properties in the presence of DNA. In the context of reverse gyrase, the ATPase activity of the helicase-like domain is still stimulated by the same DNA substrates, but to a much lesser extent. The DNA-stimulated ATPase activity of reverse gyrase is 10-fold lower than that in the isolated domain, demonstrating that the activity of the helicase-like domain is strongly suppressed by the topoisomerase domain.

The nucleic acid-stimulated ATPase activity of SF2 helicases results from a conformational change upon binding of both ligands that leads to a closure of the cleft between the two helicase subdomains. In this closed conformation, the catalytic residues are correctly positioned for efficient ATP hydrolysis. It has been proposed that such a conformational change in the helicase-like domain initiates supercoiling by reverse gyrase (10,14). The observed similar ATPase activities of the helicase-like domain and reverse gyrase suggest a similar open conformation of the helicase in both enzymes (Figure 9). In the presence of DNA, the isolated helicase-like domain adopts a closed conformation that rapidly hydrolyzes ATP. Possibly, in full-length reverse gyrase the topoisomerase domain provides a steric hindrance for the conformational change in the helicase-like domain. This steric hindrance may confine the helicase-like domain to a more open form even in the presence of nucleic acids, and consequently to less efficient ATP hydrolysis by reverse gyrase compared to the isolated helicase-like domain. A restriction of this conformational change by the topoisomerase domain would also readily explain the lower cooperativity between ATP and nucleotide binding in rGyr_fl.

Inter-domain communication in reverse gyrase: DNA binding and ATPase stimulation

The helicase-like domain and reverse gyrase interact more tightly with ssDNA than with dsDNA. This preference for ssDNA is reminiscent of other type I DNA topoisomerases (27). The high affinity of reverse gyrase for ssDNA may allow for sensing of single-stranded regions (5), and lead to stabilization of these regions for strand cleavage and the subsequent strand-passage reaction during catalysis. It has been shown previously that the presence of single-stranded regions in the DNA substrate favors positive supercoiling by reverse gyrase (5). Reverse gyrase contains several potential interaction sites for nucleic acids, located in the helicase-like domain, or in a cleft close to the catalytic tyrosine. In addition, the latch region may contact DNA (10,12), and a transient interaction of the putative zinc fingers with the DNA during supercoiling has been proposed (10). However, nucleic acid binding to these different interaction sites of reverse gyrase has not been characterized in detail. By using the Y851F mutant of reverse gyrase in DNA binding studies, we excluded the covalent binding of DNA *via* the catalytic tyrosine. In general, the DNA affinity of reverse gyrase is about 10-fold higher than that for the helicase-like domain. This increased affinity could either reflect tight DNA binding to the helicase-like domain in reverse gyrase, or point towards simultaneous interactions of DNA with the topoisomerase domain that increase the overall affinity. Clearly, a more detailed analysis of DNA binding to reverse gyrase would be required to further understand the relation between DNA binding to different sites and stimulation of ATP hydrolysis. However, in this context it is important to note that the cooperativity observed for ssDNA binding does not reflect two DNA molecules binding to one molecule of reverse gyrase (as would be possible if one ssDNA molecule interacts with the helicase-like domain and one with the topoisomerase domain). Instead, the data is consistent with the interaction of two reverse gyrase molecules with one ssDNA molecule, pointing towards a possible interaction between reverse gyrase molecules on the same substrate DNA. The fact that this cooperative effect is more pronounced for the full-length enzyme than for the isolated helicase-like domain, and only observed for ssDNA but not for dsDNA, suggests a functional role of this protein–protein interaction during the supercoiling reaction.

Is the ATPase activity of the helicase-like domain modulated to achieve optimal coupling of ATP hydrolysis to positive supercoiling?

Our results demonstrate that the helicase-like domain of reverse gyrase meets most criteria for a bona fide helicase: it has a DNA-dependent ATPase activity, and the nucleotide-state determines its affinity for ssDNA and dsDNA. However, as already reported for other reverse gyrase homologs, we did not detect DNA unwinding activity for the helicase-like domain of *T. maritima* reverse gyrase (data not shown). Altogether, the helicase-like domain of reverse gyrase acts as a nucleotide-dependent switch reminiscent of the nonprocessive DEAD box helicases that constitute a subfamily of SF2 helicases (28).

Helicase domains frequently occur in conjunction with additional domains that mediate substrate specificity or the interaction with protein partners, or regulate helicase activity (29–33). For instance, the DEAD box helicase RIG-I consists of a helicase domain and two N-terminal caspase activation and recruitment domains that connect the helicase function to the caspase signaling pathway, and these additional domains inhibit the RIG-I helicase activity (33). Conversely, the internal helicase domain of dicer inhibits its RNase activity (32), demonstrating that the domains can mutually influence their respective activities. Likewise, the ATPase activity of the helicase-like

domain in the presence of DNA is attenuated in the context of reverse gyrase, and the differences in nucleic acid affinities of the nucleotide states are smaller (Figure 9). A repression of relaxation activity of the topoisomerase domain in the absence of nucleotides by the helicase-like domain, mediated by the latch region (11,12), has been demonstrated earlier. The inhibition of the helicase-like domain we describe here seems to be the reciprocal effect. Deletion of the latch region increases the ATPase activity of reverse gyrase in the presence of ssDNA (11), suggesting a simultaneous role of the latch for the inhibitory effect of the topoisomerase domain on the helicase-like domain. Both effects emphasize the importance of communication between the reverse gyrase domains. The fact that the differences between switching of the helicase-like domain and reverse gyrase are mostly lost in the K106Q mutants suggests a critical contribution of the Walker A motif to inter-domain communication.

As a consequence of the inhibitory effect of the topoisomerase domain on the helicase-like domain in reverse gyrase, the progression through the nucleotide cycle in the presence of DNA is strongly decelerated. DNA supercoiling is a complex multi-step process, and the current model of DNA supercoiling by type IA topoisomerases such as reverse gyrase involves DNA cleavage, strand passage and re-ligation of the cleaved strand. This reaction will most likely require substantial conformational changes in reverse gyrase, and supercoiling is therefore an intrinsically slow process. Thus, a rapid cycling between the nucleotide states may not be necessary or could even be detrimental for supercoiling. Instead, the precise coordination of ATP hydrolysis and supercoiling may require matching rates for both processes, and hence a moderate ATP turnover. The inhibitory effect of the topoisomerase domain on the helicase-like domain emphasizes the role of inter-domain communication for efficient coupling between ATP hydrolysis and positive DNA supercoiling by reverse gyrase.

SUPPLEMENTARY DATA

Supplementary Data are available at NAR Online.

ACKNOWLEDGEMENTS

We thank Manuel Hilbert for performing the unwinding experiment with rGyr_hel and Markus Rudolph for discussions.

FUNDING

VolkswagenStiftung; Swiss National Science Foundation. Funding for open access charge: Swiss National Science Foundation.

Conflict of interest statement. None declared.

REFERENCES

1. Kikuchi,A. and Asai,K. (1984) Reverse gyrase–a topoisomerase which introduces positive superhelical turns into DNA. *Nature*, **309**, 677–681.
2. Forterre,P. (2002) A hot story from comparative genomics: reverse gyrase is the only hyperthermophile-specific protein. *Trends Genet.*, **18**, 236–237.
3. Atomi,H., Matsumi,R. and Imanaka,T. (2004) Reverse gyrase is not a prerequisite for hyperthermophilic life. *J. Bacteriol.*, **186**, 4829–4833.
4. Kampmann,M. and Stock,D. (2004) Reverse gyrase has heat-protective DNA chaperone activity independent of supercoiling. *Nucleic Acids Res.*, **32**, 3537–3545.
5. Hsieh,T.S. and Plank,J.L. (2006) Reverse gyrase functions as a DNA renaturase: annealing of complementary single-stranded circles and positive supercoiling of a bubble substrate. *J. Biol. Chem.*, **281**, 5640–5647.
6. Krah,R., Kozyavkin,S.A., Slesarev,A.I. and Gellert,M. (1996) A two-subunit type I DNA topoisomerase (reverse gyrase) from an extreme hyperthermophile. *Proc. Natl Acad. Sci. USA*, **93**, 106–110.
7. Krah,R., O'Dea,M.H. and Gellert,M. (1997) Reverse gyrase from *Methanopyrus kandleri*. Reconstitution of an active extremozyme from its two recombinant subunits. *J. Biol. Chem.*, **272**, 13986–13990.
8. Declais,A.C., Marsault,J., Confalonieri,F., de La Tour,C.B. and Duguet,M. (2000) Reverse gyrase, the two domains intimately cooperate to promote positive supercoiling. *J. Biol. Chem.*, **275**, 19498–19504.
9. Confalonieri,F., Elie,C., Nadal,M., de La Tour,C., Forterre,P. and Duguet,M. (1993) Reverse gyrase: a helicase-like domain and a type I topoisomerase in the same polypeptide. *Proc. Natl Acad. Sci. USA*, **90**, 4753–4757.
10. Rodriguez,A.C. and Stock,D. (2002) Crystal structure of reverse gyrase: insights into the positive supercoiling of DNA. *EMBO J.*, **21**, 418–426.
11. Rodriguez,A.C. (2002) Studies of a positive supercoiling machine. Nucleotide hydrolysis and a multifunctional "latch" in the mechanism of reverse gyrase. *J. Biol. Chem.*, **277**, 29865–29873.
12. Rodriguez,A.C. (2003) Investigating the role of the latch in the positive supercoiling mechanism of reverse gyrase. *Biochemistry*, **42**, 5993–6004.
13. Theissen,B., Karow,A.R., Kohler,J., Gubaev,A. and Klostermeier,D. (2008) Cooperative binding of ATP and RNA induces a closed conformation in a DEAD box RNA helicase. *Proc. Natl Acad. Sci. USA*, **105**, 548–553.
14. Jungblut,S.P. and Klostermeier,D. (2007) Adenosine 5'-O-(3-thio)-triphosphate (ATPgammaS) promotes positive supercoiling of DNA by *T. maritima* reverse gyrase. *J. Mol. Biol.*, **371**, 197–209.
15. Peck,M.L. and Herschlag,D. (2003) Adenosine 5'-O-(3-thio)triphosphate (ATPgammaS) is a substrate for the nucleotide hydrolysis and RNA unwinding activities of eukaryotic translation initiation factor eIF4A. *RNA*, **9**, 1180–1187.
16. Studier,F.W. (2005) Protein production by auto-induction in high density shaking cultures. *Protein Expr. Purif.*, **41**, 207–234.
17. Kovalsky,O.I., Kozyavkin,S.A. and Slesarev,A.I. (1990) Archaebacterial reverse gyrase cleavage-site specificity is similar to that of eubacterial DNA topoisomerases I. *Nucleic Acids Res.*, **18**, 2801–2805.
18. Jaxel,C., Duguet,M. and Nadal,M. (1999) Analysis of DNA cleavage by reverse gyrase from *Sulfolobus shibatae* B12. *Eur. J. Biochem.*, **260**, 103–111.
19. Hiratsuka,T. (1983) New ribose-modified fluorescent analogs of adenine and guanine nucleotides available as substrates for various enzymes. *Biochim. Biophys. Acta*, **742**, 496–508.
20. Rogers,G.W. Jr, Richter,N.J. and Merrick,W.C. (1999) Biochemical and kinetic characterization of the RNA helicase activity of eukaryotic initiation factor 4A. *J. Biol. Chem.*, **274**, 12236–12244.
21. Shibata,T., Nakasu,S., Yasui,K. and Kikuchi,A. (1987) Intrinsic DNA-dependent ATPase activity of reverse gyrase. *J. Biol. Chem.*, **262**, 10419–10421.
22. Lorsch,J.R. and Herschlag,D. (1998) The DEAD box protein eIF4A. 1. A minimal kinetic and thermodynamic framework reveals coupled binding of RNA and nucleotide. *Biochemistry*, **37**, 2180–2193.

23. Lorsch,J.R. and Herschlag,D. (1998) The DEAD box protein eIF4A. 2. A cycle of nucleotide and RNA-dependent conformational changes. *Biochemistry*, **37**, 2194–2206.
24. Polach,K.J. and Uhlenbeck,O.C. (2002) Cooperative binding of ATP and RNA substrates to the DEAD/H protein DbpA. *Biochemistry*, **41**, 3693–3702.
25. Yang,Q. and Jankowsky,E. (2006) The DEAD-box protein Ded1 unwinds RNA duplexes by a mode distinct from translocating helicases. *Nat. Struct. Mol. Biol.*, **13**, 981–986.
26. Yang,Q. and Jankowsky,E. (2005) ATP- and ADP-dependent modulation of RNA unwinding and strand annealing activities by the DEAD-box protein DED1. *Biochemistry*, **44**, 13591–13601.
27. Kirkegaard,K. and Wang,J.C. (1985) Bacterial DNA topoisomerase I can relax positively supercoiled DNA containing a single-stranded loop. *J. Mol. Biol.*, **185**, 625–637.
28. Pyle,A.M. (2008) Translocation and unwinding mechanisms of RNA and DNA helicases. *Annu. Rev. Biophys.*, **37**, 317–336.
29. Morlang,S., Weglohner,W. and Franceschi,F. (1999) Hera from *Thermus thermophilus*: the first thermostable DEAD-box helicase with an RNase P protein motif. *J. Mol. Biol.*, **294**, 795–805.
30. Rogers,G.W. Jr, Richter,N.J., Lima,W.F. and Merrick,W.C. (2001) Modulation of the helicase activity of eIF4A by eIF4B, eIF4H, and eIF4F. *J. Biol. Chem.*, **276**, 30914–30922.
31. Kossen,K., Karginov,F.V. and Uhlenbeck,O.C. (2002) The carboxy-terminal domain of the DExDH protein YxiN is sufficient to confer specificity for 23S rRNA. *J. Mol. Biol.*, **324**, 625–636.
32. Ma,E., MacRae,I.J., Kirsch,J.F. and Doudna,J.A. (2008) Autoinhibition of human dicer by its internal helicase domain. *J. Mol. Biol.*, **380**, 237–243.
33. Gee,P., Chua,P.K., Gevorkyan,J., Klumpp,K., Najera,I., Swinney,D.C. and Deval,J. (2008) Essential role of the N-terminal domain in the regulation of RIG-I ATPase activity. *J. Biol. Chem.*, **283**, 9488–9496.

Chapter 2. Article

The latch modulates nucleotide and DNA binding to the helicase-like domain of *Thermotoga maritima* reverse gyrase and is required for positive DNA supercoiling

From crystallographic studies the latch domain, an insertion in the H2 RecA fold of the helicase-like domain, has been proposed to be involved in interdomain communication between the topoisomerase and the helicase-like domain in reverse gyrase. A putative DNA-binding role was also assumed from its homology to the Rho factor. Effects of a latch deletion had been documented almost exclusively for the full enzyme, and mostly the effect on the overall supercoiling reaction had been characterized. In the present article we demonstrate for the first time how it is involved in the intrinsic properties of the helicase-like domain. Deletion of the latch from the isolated helicase-like domain uncouples DNA binding and ATP binding and hydrolysis, as demonstrated *via* steady-state ATPase measurements. Furthermore, the latch deletion abolishes almost completely the nucleotide-dependent DNA preference switch property of the isolated helicase-like domain. In the full-length enzyme removal of the latch allows only DNA relaxation. This is a reaction that the isolated topoisomerase domain can perform on its own. Overall, we confirmed the role of the latch in communicating the nucleotide state to the topoisomerase domain, we directly demonstrated the ability of the isolated latch to bind either ss- or ds-DNA, and we also reported the extent of its involvement in the intrinsic properties of the helicase-like domain.

Published online 4 November 2010

Nucleic Acids Research, 2011, Vol. 39, No. 5 ***1789–1800***
doi:10.1093/nar/gkq1048

The latch modulates nucleotide and DNA binding to the helicase-like domain of *Thermotoga maritima* reverse gyrase and is required for positive DNA supercoiling

Agneyo Ganguly[1], Yoandris del Toro Duany[1], Markus G. Rudolph[2] and Dagmar Klostermeier[1,*]

[1]Department of Biophysical Chemistry, University of Basel, Biozentrum, Klingelbergstrasse 70, CH–4056 Basel and [2]Hoffmann-La Roche AG, Grenzacher Strasse 124, CH-4070 Basel, Switzerland

Received July 16, 2010; Revised October 8, 2010; Accepted October 12, 2010

ABSTRACT

Reverse gyrase is the only topoisomerase that can introduce positive supercoils into DNA in an ATP-dependent process. It has a modular structure and harnesses a helicase-like domain to support a topoisomerase activity, thereby creating the unique function of positive DNA supercoiling. The isolated topoisomerase domain can relax negatively supercoiled DNA, an activity that is suppressed in reverse gyrase. The isolated helicase-like domain is a nucleotide-dependent switch that is attenuated by the topoisomerase domain. Inter-domain communication thus appears central for the functional cooperation of the two domains. The latch, an insertion into the helicase-like domain, has been suggested as an important element in coordinating their activities. Here, we have dissected the influence of the latch on nucleotide and DNA binding to the helicase-like domain, and on DNA supercoiling by reverse gyrase. We find that the latch is required for positive DNA supercoiling. It is crucial for the cooperativity of DNA and nucleotide binding to the helicase-like domain. The latch contributes to DNA binding, and affects the preference of reverse gyrase for ssDNA. Thus, the latch coordinates the individual domain activities by modulating the helicase-like domain, and by communicating changes in the nucleotide state to the topoisomerase domain.

INTRODUCTION

DNA topoisomerases catalyze the inter-conversion of DNA topoisomers in processes such as DNA replication, recombination and repair (1). Reverse gyrase, first identified in the hyperthermophilic archaeon *Sulfolobus acidocaldarius* (2), is the only topoisomerase that can introduce positive supercoils into DNA in an ATP-dependent process. Reverse gyrases are unique to thermophiles and hyperthermophiles, and presumably protect their DNA at high temperatures via DNA chaperone and renaturase activities (3,4). In general, reverse gyrases have a modular structure, comprised of an N-terminal helicase-like domain covalently linked to a C-terminal topoisomerase I domain (Figure 1) (5). The helicase-like domain consists of two RecA-like subdomains (H1 and H2) that harbor all signature motifs of superfamily (SF) two helicases, though with altered sequences (6). The H2 domain is interrupted by an insertion called the 'latch' (H3), which structurally resembles the RNA-binding region of the transcription termination factor Rho (7,8). The C-terminal topoisomerase domain is homologous to prokaryotic type IA DNA topoisomerases, and consists of four subdomains (T1–T4) equivalent to domains I-IV of *Escherichia coli* topoisomerase I (9). The isolated topoisomerase domain can relax negatively supercoiled DNA *in vitro* (10). By contrast, neither the isolated helicase-like domain nor reverse gyrase exhibits any nucleic acid unwinding activity (10,11). The helicase-like domain is a nucleotide-dependent switch that exhibits a strong preference for ssDNA in the nucleotide-free and ADP state, but binds ssDNA and dsDNA with similar affinities in the

*To whom correspondence should be addressed. Tel: +41 61 267 2381; Fax: +41 61 267 2189; Email: dagmar.klostermeier@unibas.ch

The authors wish it to be known that, in their opinion, the first two authors should be regarded as joint First Authors.

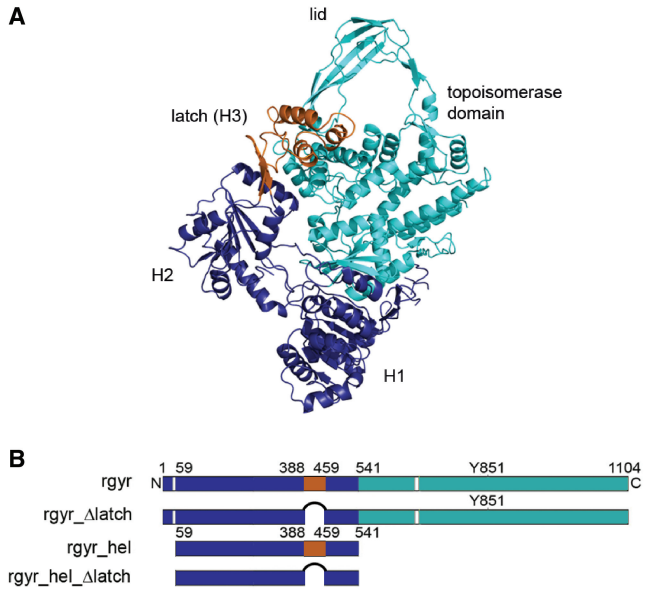

Figure 1. Reverse gyrase structure and constructs used. (**A**) Structure of reverse gyrase from *A. fulgidus* (PDB-ID 1gku) (6). The helicase-like domain is shown in dark blue (H1, H2) and orange (H3, latch, residues 389–459), and the topoisomerase domain (T1-T4) in cyan. The figure was created with Pymol (www.pymol.org). (**B**) Constructs used in this study. rgyr: reverse gyrase, rgyr_Δlatch: reverse gyrase lacking the latch region H3, rgyr_hel: helicase-like domain comprising H1, H2 and H3 (latch), rgyr_hel_Δlatch: helicase-like domain comprising H1 and H2.

ATP state (11). Reverse gyrase, in contrast, preferentially interacts with ssDNA in all states, and it has been shown that positive supercoiling is more efficient with a plasmid containing single-stranded regions (4). Furthermore, the DNA-stimulated ATPase activity of the helicase-like domain of *Thermotoga maritima* reverse gyrase is 10-fold higher than that of full-length reverse gyrase, pointing toward a suppression of the activity of the helicase-like domain by the topoisomerase domain (11). Harnessing a helicase-like domain to support a topoisomerase activity creates the unique function of positive DNA supercoiling and thus generates an enzyme that is clearly more than the sum of its parts. Undoubtedly, inter-domain communication is central for the combined activities of the helicase-like and topoisomerase domains in the supercoiling reaction.

Based on biochemical data and structural information, a strand-passage mechanism, similar to DNA relaxation by type IA topoisomerases, has been proposed for positive supercoiling of DNA by reverse gyrase (6). The salient features of this putative mechanism are a conformational change in the helicase-like domain that brings domains H1 and H2 closer together, and a movement of the latch domain away from the topoisomerase domain that allows the lid (T3) to swing up. The latch has thus been suggested as an important element in inter-domain communication, and was shown to inhibit the DNA relaxation activity of the topoisomerase domain of *Archaeoglobus fulgidus* reverse gyrase (12). Moreover, mutants lacking the latch exhibited altered DNA-dependent ATPase activity, indicating a role of the latch in coupling ATP hydrolysis to the supercoiling reaction. By contrast, the latch was not required for the positive supercoiling activity of the enzyme (13).

Here, we have dissected the influence of the latch on nucleotide and DNA binding to the helicase-like domain, and on DNA supercoiling by reverse gyrase. The latch can be deleted without affecting the structure of the H2 domain. We find that the latch contributes to DNA binding, and inhibits nucleotide binding, but not ATP hydrolysis. The latch is crucial for the cooperativity of DNA and nucleotide binding to the helicase-like domain, and affects the preference of reverse gyrase for ssDNA. Most importantly, the latch is required for positive DNA supercoiling. Our data demonstrate that the latch modulates the properties of the helicase-like domain, and communicates changes in the nucleotide state to the topoisomerase domain, Thereby, it coordinates and couples individual domain activities to allow for positive supercoiling of DNA.

MATERIALS AND METHODS

Cloning, protein production and purification

Reverse gyrase lacking the latch region (aa 389–459) was constructed by inverse polymerase chain reaction (PCR) using pET28a with the reverse gyrase gene inserted into the NcoI and XhoI sites (14) as a template, and primers containing a BamH1 restriction site and the region downstream from the codon for aa 459 (forward primer), or upstream from the codon for aa 389 (reverse primer). The amplified DNA was restricted with BamH1, and circularized by ligation, resulting in pET28a with the gene for reverse gyrase lacking the latch domain (rgyr_Δlatch). The helicase-like domain lacking the latch (rgyr_hel_Δlatch) was constructed by overlap extension PCR with pET28 containing the coding region for aa 59–541 as a template. The generated fragment was amplified using primers containing NcoI and XhoI restriction sites, and ligated into the NcoI and XhoI sites of pETM28. The region coding for the latch (aa 388–459) was amplified using primers containing NcoI and XhoI restriction sites and ligated into the NcoI and XhoI sites of pETM30 (G. Stier, EMBL Heidelberg). Reverse gyrase (rgyr) and the rgyr_Δlatch were produced in *E. coli* BL21(DE3) Star RIL and were purified as described (11). Rgyr_hel, rgyr_hel_Δlatch and the isolated latch domains were produced in *E. coli* Rosetta(DE3). Rgyr_hel and rgyr_hel_Δlatch were purified as described (11). Cells overproducing the latch as a GST fusion were disrupted in a Microfluidizer in 50 mM Tris/HCl, pH 7.5, 1 M NaCl, 10 mM $MgCl_2$, 10 mM $Zn(OAc)_2$, 2 mM β-mercaptoethanol, and the crude extract was cleared by centrifugation. All purification steps were performed at room temperature. The NaCl concentration of the supernatant was adjusted to 0.2 M, and it was applied to a Glutathione sepharose column equilibrated in 50 mM Tris/HCl, pH 7.5, 0.2 M NaCl, 10 mM $MgCl_2$, 10 mM $Zn(OAc)_2$, 2 mM β-mercaptoethanol. The GST fusion protein was eluted with the same buffer containing 20 mM reduced glutathione, and cleaved overnight with TEV protease. Remaining fusion protein and GST were

removed by purification via size-exclusion chromatography on a calibrated S75 column in 50 mM Tris/HCl, pH 7.5, 0.2 M NaCl, 10 mM $MgCl_2$, 10 mM $Zn(OAc)_2$, 2 mM β-mercaptoethanol. As the latch does not contain tryptophans, the protein concentration was determined with the Bradford method.

Protein crystallization, data collection and structure determination

Diffraction quality crystals for rgyr_hel_Δlatch were obtained at 25°C from the PEG/ion screen (Hampton). 20 mg ml^{-1} protein was mixed 1:1 (v/v) with reservoir consisting of 0.2 M magnesium formate, 20% PEG 3350. Crystals were cryo-protected with paraffin oil, mounted in an arbitrary orientation and data were collected at SLS beamline X06DA on a MAR-CCD detector. Data were indexed in a primitive orthorhombic lattice, integrated with XDS (15), scaled with MOSFLM (16) and corrected for anisotropy with XPREP (Bruker). Data statistics are collected in Table 1. Systematic absences identified space group $P2_12_12_1$. A Matthews coefficient of 2.8 $Å^3$/Da corresponding to 56% solvent content indicated two rgyr_hel_Δlatch molecules per asymmetric unit.

The structure was determined by molecular replacement using the truncated (termini and loops were removed, the sequence of conserved residues was adjusted to match *T. maritima* reverse gyrase) H1 and H2 domains of *A. fulgidus* reverse gyrase as separate search models with PHASER (16). Both H2 domains, but only one H1 domain, were found. Refinement of this model with BUSTER (17) resulted in spurious electron density for the second H1 domain, which could be placed manually.

Table 1. Data collection, phasing and refinement statistics

Data set	3OIY
Data collection	132.7–2.35
Resolution range (Å)[a]	(2.44–2.35)
Space group	$P2_12_12_1$
Cell dimensions (Å)	a = 59.6, b = 126.5, c = 132.7
Unique reflections	42 547 (4453)
Multiplicity	7.1 (7.4)
Completeness (%)	99.6 (100)
R_{sym} (%)[b]	9.9 (65.9)
Average $I/\sigma(I)$	9.7 (1.3)
Refinement	44.4–2.35
Resolution range (Å)	(2.41–2.35)
R_{cryst} (%)[c]	20.8 (39.4)
R_{free} (%)[c]	25.1 (41.5)
# of residues/waters	807/99
Phase/coordinate errors (°/Å)[d]	28.3/0.38
rmsd bonds/angles (Å/ °)	0.012/1.56
Ramachandran plot (%)[e]	96.8/3.1/0.1

[a]Values in parentheses correspond to the highest resolution shell.
[b]$R_{sym} = 100 \cdot \Sigma_h\Sigma_i|I_i(h) - <I(h)>|/\Sigma_h\Sigma_i I_i(h)$, where $I_i(h)$ is the *i*-th measurement of reflection *h* and $<I(h)>$ is the average value of the reflection intensity.
[c]$R_{cryst} = \Sigma||F_o| - |F_c||/\Sigma|F_o|$, where F_o and F_c are the structure factor amplitudes from the data and the model, respectively; R_{free} is R_{cryst} with 5% of test set structure factors.
[d]Based on maximum likelihood.
[e]Calculated using COOT (19); numbers reflect the percentage amino acid residues of the core, allowed and disallowed regions, respectively.

Further refinement using PHENIX (18) and rebuilding in COOT (19) enabled tracing of the connections between the H1 and H2 domains to generate a model of two complete helicase modules. Refinement statistics are summarized in Table 1. The coordinates and structure factors have been deposited in the Protein Data Bank (accession code 3oiy).

Nucleotides and nucleic acid substrates

Nucleotides were purchased from Jena Biosciences. Oligonucleotides for ssDNA or dsDNA substrates were purchased from Purimex. The 60 b ssDNA was 5′-(Fl)-AAG CCA AGC TTC TAG AGT CAG CCC GTG ATA TTC ATT ACT TCT TAT CCT AGG ATC CCC GTT-3′. The 60-bp dsDNA substrate was formed by annealing with the complementary strand. Negatively supercoiled pUC18 was purified from transformed *E. coli* XL1-Blue cells.

Fluorescence equilibrium titrations

Dissociation constants of enzyme/nucleotide complexes at 37°C were determined in fluorescence equilibrium titrations with a Fluoromax-3 fluorimeter (Jobin Yvon) using the fluorescent ADP analog mantADP (20). In titrations of 1 μM mantADP in 50 mM Tris/HCl, pH 7.5, 0.15 M NaCl, 10 mM $MgCl_2$, 100 μM $Zn(OAc)_2$, 2 mM β-mercaptoethanol, binding was monitored via Förster resonance energy transfer (FRET) from tryptophan to the mant group. Tryptophan fluorescence was excited at 295 nm (3 nm bandwidth), and mant fluorescence was detected at 440 nm (3 nm bandwidth). The K_d value was determined using the solution of the quadratic equation describing a 1:1 complex formation [Equation (1)].

$$F = F_0 + \frac{\Delta F_{max}}{[L]_{tot}} \cdot \left(\frac{[E]_{tot} + [L]_{tot} + K_d}{2} - \sqrt{\left(\frac{[E]_{tot} + [L]_{tot} + K_d}{2} \right)^2 - [E]_{tot}[L]_{tot}} \right) \quad (1)$$

where F_0 is the fluorescence of free mantADP, ΔF_{max} is the amplitude, $[E]_{tot}$ is the total enzyme concentration and $[L]_{tot}$ is the total ligand concentration.

DNA binding was measured in fluorescence anisotropy titrations of DNA labeled with fluorescein at the 5′-end in 50 mM Tris/HCl, pH 7.5, 0.15 M NaCl, 10 mM $MgCl_2$, 100 μM $Zn(OAc)_2$, 2 mM β-mercaptoethanol, and analyzed as described (11).

Steady-state ATPase activity

The steady-state ATPase activity was measured in a coupled ATPase assay via the decrease in A_{340} due to oxidation of NADH to NAD^+ (21) as described (11). Assay conditions were 50 mM Tris/HCl, pH 7.5, 0.15 M NaCl, 10 mM $MgCl_2$, 2 mM β-mercaptoethanol, 0.4 mM phosphoenolpyruvate and 0.2 mM NADH, 23 μg ml^{-1} lactate dehydrogenase, 37 μg ml^{-1} pyruvate kinase. Initial velocities v (in μM ATP s^{-1}) were calculated from the absorbance change $\Delta A_{340}/\Delta t$ with $\varepsilon_{340,\,NADH} = 6220\ M^{-1}\,cm^{-1}$, and converted to k_{cat}. Data

were analyzed according to the Michaelis–Menten equation.

Topoisomerase activity

Relaxation and supercoiling activities were measured in 50 mM Tris/HCl, pH 7.5, 0.15 M NaCl, 10 mM $MgCl_2$, 100 μM $Zn(OAc)_2$, 2 mM β-mercaptoethanol, 10% (w/v) polyethylene glycol 8000 and 15 nM negatively supercoiled pUC18 plasmid as a substrate. Reactions were started by adding 2 mM ATP, ADP, ATPγS or ADPNP to 1 μM reverse gyrase at 75°C, and samples taken at different time points were analyzed on a 1.2% (w/v) agarose gel run at 11 V cm^{-1}. To separate positively and negatively supercoiled species, two-dimensional electrophoresis in 2% agarose gels was performed in the presence of 10 μg ml^{-1} chloroquine in the second dimension.

RESULTS

The latch interferes with nucleotide binding, but contributes to DNA binding to the helicase-like domain

We have previously shown that the helicase-like domain, rgyr_hel, is a nucleotide-dependent switch that binds DNA and ATP cooperatively (11). In the ATP state of rgyr_hel, the affinities for ssDNA and dsDNA are comparable, whereas in the ADP state, ssDNA is bound preferentially. In the context of full-length rgyr, the differences in affinities for ssDNA and dsDNA are reduced, as is the cooperativity between ATP and DNA binding.

To dissect the role of the latch region in positive DNA supercoiling, we constructed a latch deletion mutant of *T. maritima* reverse gyrase in which residues 389–459 of the helicase-like domain are replaced by a glycine (Figure 1, rgyr_hel_Δlatch). Residues 387 and 460 are prolines in *T. maritima* reverse gyrase (Pro352 and Pro424 in *A. fulgidus* numbering) that are conserved among reverse gyrases. In the structure of *A. fulgidus* reverse gyrase, Pro352 and Pro424 mark the beginning and end, respectively, of β-strands leading into and out of the latch domain. These β-strands are part of a β-sheet that connects the latch domain to H2. The C_α-atoms of the prolines are 0.66 nm apart, a distance that can be covered by two amino acids. To confirm that the replacement of the latch domain by a glycine does not alter the overall structure of reverse gyrase, we determined the crystal structure of rgyr_hel_Δlatch to 2.35-Å resolution (Table 1, Figure 2). The H2 domains of *T. maritima* and *A. fulgidus* reverse gyrases superpose with an rmsd of 1.6 Å over 181 residues, proving that the deletion of the latch domain does not significantly alter the structure of the H2 domain (Figure 2A). Importantly, the glycine residue replacing the latch domain is well defined by electron density (Figure 2B). The region around the conserved proline residues is similar in both structures with a C_α–C_α distance of 0.57 nm for Pro387 and Pro460. Thus, the deletion of the latch region does not alter the RecA fold of H2, and, consequently, should not have any undesired effects on the overall structure of reverse gyrase.

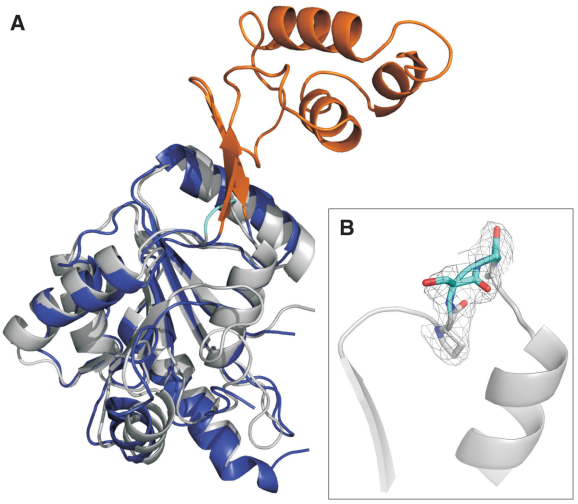

Figure 2. Structure of H2 in rgyr_hel_Δlatch. (**A**) Superposition of the H2 domain in rgyr_hel_Δlatch (*T. maritima*, gray) and H2/H3 of *A. fulgidus* reverse gyrase. H2 is depicted in dark blue, the latch domain (H3) in orange. (**B**) Close-up of the deletion region. P387, S388 and P460, as well as the introduced glycine are shown in stick representation; S388 and the glycine are highlighted in cyan. The σ_A-weighted $2mF_o$–DF_c electron density in this region is contoured at the 1σ level and depicted as a gray mesh. The figure was created with Pymol (www.pymol.org).

We also measured far-ultraviolet (UV) circular dichroism (CD) spectra of rgyr and rgyr_Δlatch at 37°C, 50°C and 70°C (Supplementary Figure S1). The CD spectra indicate that the two proteins are thermostable and have similar folds in this temperature range. Both enzymes are active topoisomerases at 75°C (see below). Overall, we thus have no indication for large structural changes in rgyr_Δlatch.

As the helicase-like domain is responsible for ATP binding and hydrolysis, we first analyzed the effect of the latch on adenine nucleotide binding (Figure 3). We have previously established that mantADP is a suitable analog to monitor adenine nucleotide binding to rgyr and rgyr_hel (11,14). Deletion of the latch in rgyr led to a 7-fold increase in affinity for mantADP, and a 2-fold increase in the affinity for ADPNP (Table 2). In the context of the isolated helicase-like domain, deletion of the latch led to a 1.6-fold increase in mantADP affinity, and a 2.7-fold in (mant)ADPNP affinity. Thus, the latch insertion in H2 affects adenine nucleotide binding.

To dissect contributions of the latch domain to DNA binding, anisotropy titrations of fluorescently labeled ssDNA and dsDNA were performed (Figure 4). Ideally, DNA binding studies should be performed with a reverse gyrase mutant in which the catalytic tyrosine involved in DNA cleavage is replaced by a phenylalanine to prevent covalent binding of the DNA. However, the DNA-cleavage-deficient rgyr_Δlatch_Y851F mutant was not soluble. Therefore, we performed comparative DNA-binding studies with rgyr_Δlatch and wild-type reverse gyrase that also contained the catalytic tyrosine (Table 3) to dissect the influence of the latch. The effects of the latch deletion on DNA binding to rgyr were small, with a 2-fold reduction of ssDNA affinity (K_d 17 nM for

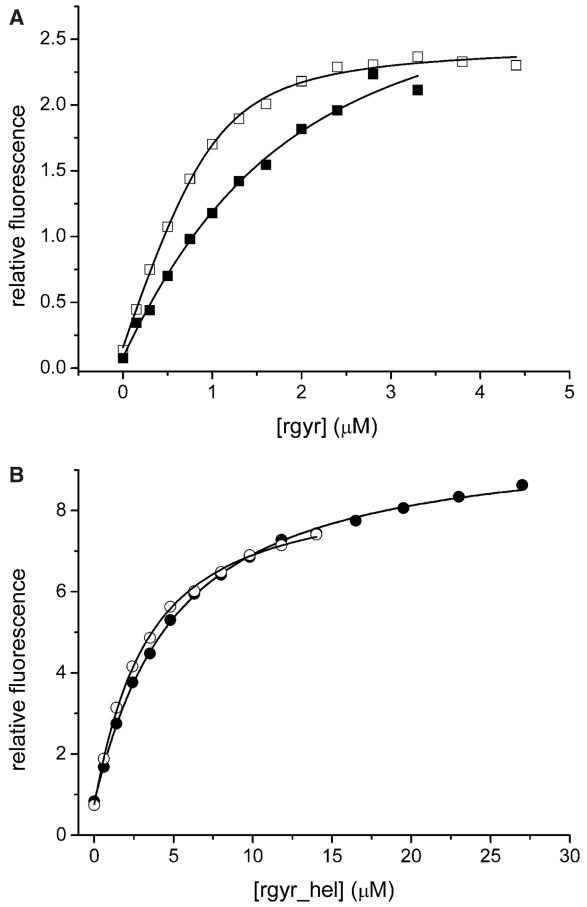

Figure 3. Nucleotide binding. (**A**) Titration of 1 μM mantADP with rgyr (filled squares) and rgyr_Δlatch (open squares). The K_d values are 1.1 ± 0.3 μM (rgyr) and 0.16 ± 0.02 μM (rgyr_Δlatch). (**B**) Titration of 1 μM mantADP with rgyr_hel (filled circles) and rgyr_hel_Δlatch (open circles). The K_d values are 4.4 ± 0.2 μM (rgyr_hel) and 2.7 ± 0.1 μM (rgyr_hel_Δlatch). Binding was detected via energy transfer from tryptophans to the mant group. For K_d values in the presence of DNA, see Table 2.

Table 2. Nucleotide binding

mADP		
	rgyr[a] K_d (μM)	rgyr_Δlatch K_d (μM)
–	1.1 ± 0.3	0.16 ± 0.02
ssDNA	2.2 ± 0.4	0.67 ± 0.05
dsDNA	0.5 ± 0.2	0.13 ± 0.03
	rgyr_hel K_d (μM)	rgyr_hel_Δlatch K_d (μM)
–	4.4 ± 0.2	2.7 ± 0.1
ssDNA	10 ± 1	2.6 ± 0.7
dsDNA	1.7 ± 0.4	0.9 ± 0.4
ADPNP		
	rgyr K_d (μM)	rgyr_Δlatch K_d (μM)
–	10 ± 0.8	4.7 ± 0.8
ssDNA	12 ± 3	12 ± 2
dsDNA	8 ± 1	8 ± 1
	rgyr_hel[b] K_d (μM)	rgyr_hel_Δlatch[b] K_d (μM)
–	36 ± 8	13 ± 4
ssDNA	12 ± 2	16 ± 8
dsDNA	1.9 ± 0.4	11 ± 4

[a]Data from ref. (11) .[b]Titrations were performed with mADPNP.

rgyr versus 33 nM for rgyr_Δlatch), and a 1.3-fold reduction of dsDNA affinity (74 nM versus 96 nM). These differences in K_d values correspond to a small energetic contribution of the latch to DNA binding by <2 kJ/mol. For rgyr_hel, the effects of the latch deletion on DNA binding were more pronounced. The ssDNA affinity was decreased 2.1-fold (K_d 0.20 μM for rgyr_hel versus 0.42 μM for rgyr_hel_Δlatch), and the dsDNA affinity was decreased 5.4-fold (3.9 μM versus 21 μM), corresponding to small but significant energetic contributions of the latch to DNA binding by 2–4 kJ/mol. To test directly for DNA binding to the latch, we produced the isolated latch domain, and determined its affinities for ssDNA and dsDNA (Figure 4E). The isolated latch binds both ssDNA and dsDNA with low affinities (K_d 64 ± 29 μM for ssDNA, 78 ± 39 μM for dsDNA), confirming that it contributes to DNA binding. Although differences in the helicase-like domain reflect contributions of the latch to DNA binding to the helicase-like domain only (and suggest that the latch is involved in DNA binding to this site), K_d values for the full-length enzyme also contain contributions from the (nucleotide-independent) DNA-binding sites in the topoisomerase domain, masking the influence of the latch and rendering a dissection of effects difficult.

Deletion of the latch diminishes cooperativity in the helicase-like domain

We next characterized the effect of the latch on ATP hydrolysis, and stimulation of ATP hydrolysis by DNA in steady-state ATPase assays (Figure 5, Table 4). The k_{cat} values for the intrinsic ATPase activities of rgyr and rgyr_Δlatch are small, with $30 \times 10^{-3}\,s^{-1}$ and $18 \times 10^{-3}\,s^{-1}$, respectively, indicating that the latch is not involved in ATP hydrolysis. The K_M value for ATP is slightly reduced in rgyr_Δlatch (44 μM for rgyr, 26 μM for rgyr_Δlatch). In the context of the isolated helicase-like domain, the analogous deletion of the latch also does not affect the intrinsic ATPase activity much ($k_{cat} = 30 \times 10^{-3}\,s^{-1}$, $K_{M,ATP} = 77$ μM for rgyr_hel, and $k_{cat} = 20 \times 10^{-3}\,s^{-1}$, $K_{M,ATP} = 67$ μM for rgyr_hel_Δlatch). The small reduction in $K_{M,ATP}$ upon deletion of the latch is in-line with the interference of the latch with nucleotide binding (see above, Table 2). The effect is more pronounced for rgyr than for rgyr_hel. The similar k_{cat} values demonstrate that the latch does not play a role in basal ATP hydrolysis within the helicase-like domain of reverse gyrase.

In the presence of ssDNA, dsDNA or pUC18 plasmid, the k_{cat} values for ATP hydrolysis by reverse gyrase are increased 5–10-fold (Table 4, ref. 11). Similar to wild-type reverse gyrase, ATP hydrolysis by rgyr_Δlatch was stimulated 6–9-fold by DNA (Table 4), excluding a role of the latch for stimulation of the ATPase activity by DNA. At 75°C, similar effects of ssDNA and plasmid DNA on ATP hydrolysis by rgyr and rgyr_Δlatch were observed (Supplementary Figure S2).

Rgyr binds ATP and DNA cooperatively, reflected in a 2.8–3.7-fold decrease of the $K_{M,ATP}$ in the presence of DNA (Table 4, ref. 11). By contrast, decreases in $K_{M,ATP}$ values in the presence of ssDNA, dsDNA or pUC18 plasmid are

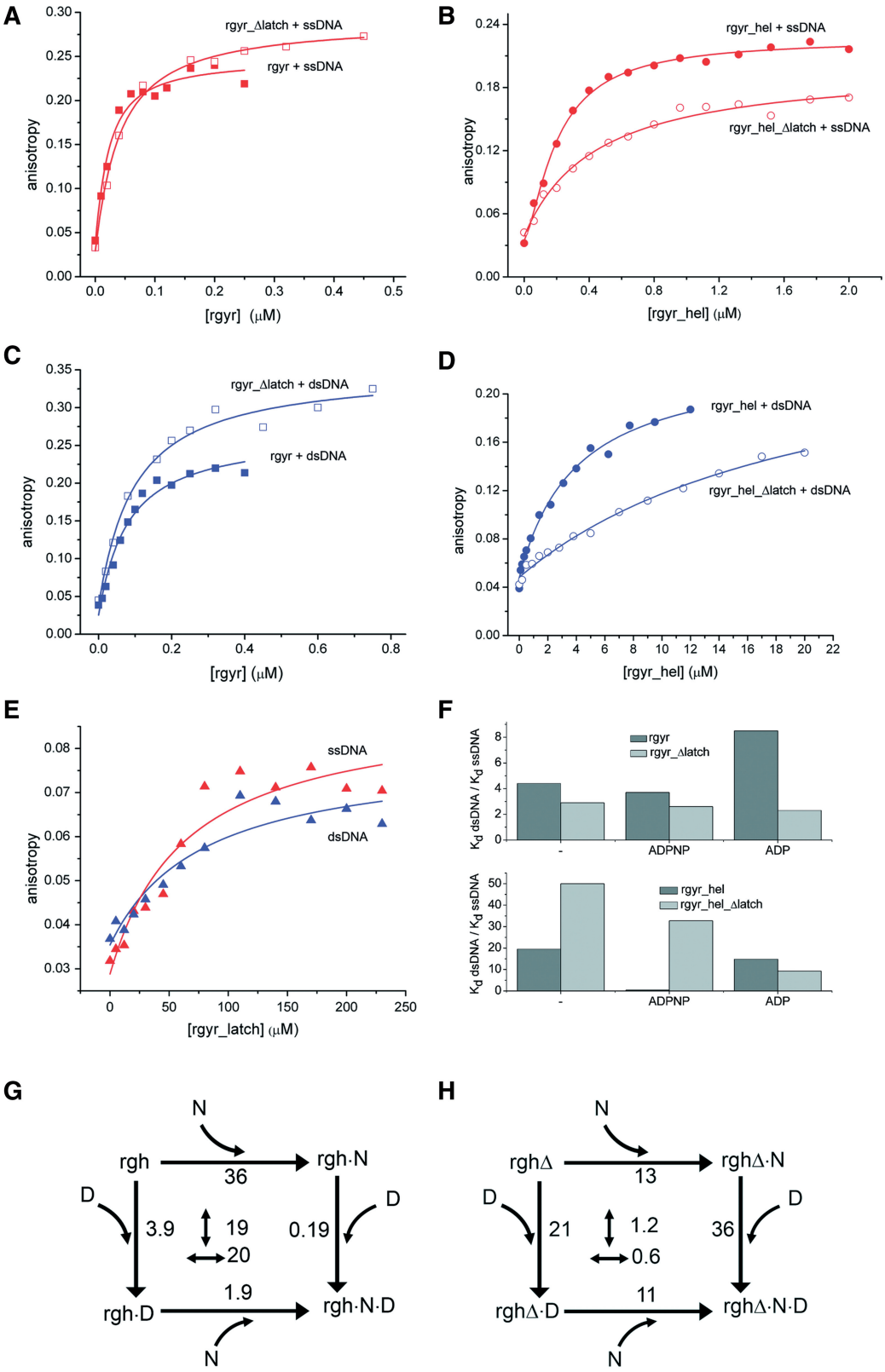

Figure 4. DNA binding. (**A**) Titration of 10 nM ssDNA with rgyr (filled squares) and rgyr_Δlatch (open squares). (**B**) Titration of 25 nM ssDNA with rgyr_hel (filled circles) and rgyr_hel_Δlatch (open circles). (**C**) Titration of 10 nM dsDNA with rgyr (filled squares) and rgyr_Δlatch (open squares). (**D**) Titration of 25 nM dsDNA with rgyr_hel (filled circles) and rgyr_hel_Δlatch (open circles). (**E**) Titration of 25 nM ssDNA (red) or dsDNA (blue) with the isolated latch domain. Binding curves for ssDNA are shown in red, binding curves for dsDNA are depicted in blue. For K_d values from the depicted data and K_d values in different nucleotide states, see Table 3. (**F**) Preference for ssDNA in rgyr and rgyr_Δlatch (upper panel) and rgyr_hel and rgyr_hel_Δlatch (lower panel) in different nucleotide states. (**G**) Thermodynamic cycle for ADPNP (N) and dsDNA (D) binding to rgyr_hel (rgh). The K_d values in μM are indicated. Numbers in the center refer to the coupling factor (n-fold decrease in K_d when the first ligand is already bound). The coupling factor for binding of ADPNP and dsDNA to rgyr_hel is ~20. (**H**) Thermodynamic cycle for ADPNP (N) and dsDNA (D) binding to rgyr_hel_Δlatch (rghΔ). The coupling factor for ADPNP and dsDNA binding is ~1, indicating that coupling is lost upon latch deletion.

Table 3. DNA binding

	rgyr		rgyr_Δlatch	
	K_d (μM)	rel.	K_d (μM)	rel.
ssDNA				
–	0.017 + 0.004	1	0.033 ± 0.077	1
ADP state	0.013 ± 0.003	0.8	0.025 ± 0.005	0.8
ATP state (ADPNP)	0.015 ± 0.006	1.2	0.040 ± 0.010	1.2
dsDNA				
–	0.074 ± 0.016	4.3	0.096 ± 0.019	2.9
ADP state	0.11 ± 0.02	6.5	0.058 ± 0.010	1.8
ATP state (ADPNP)	0.055 ± 0.015	3.2	0.104 ± 0.015	3.2
	rgyr_hel[a]		rgyr_hel_Δlatch	
	K_d (μM)	rel.	K_d (μM)	rel.
ssDNA				
–	0.20 ± 0.01	1	0.42 ± 0.07	1
ADP state	0.28 ± 0.01	1.4	2.6 ± 0.3	6.2
ATP state (ADPNP)	0.46 ± 0.03	2.3	1.1 ± 0.1	2.6
dsDNA				
–	3.9 ± 0.6	20	21 ± 5	50
ADP state	3.7 ± 0.5	19	24 ± 5	57
ATP state (ADPNP)	0.19 ± 0.03	1	36 ± 8	86

[a]Data from ref. (11).

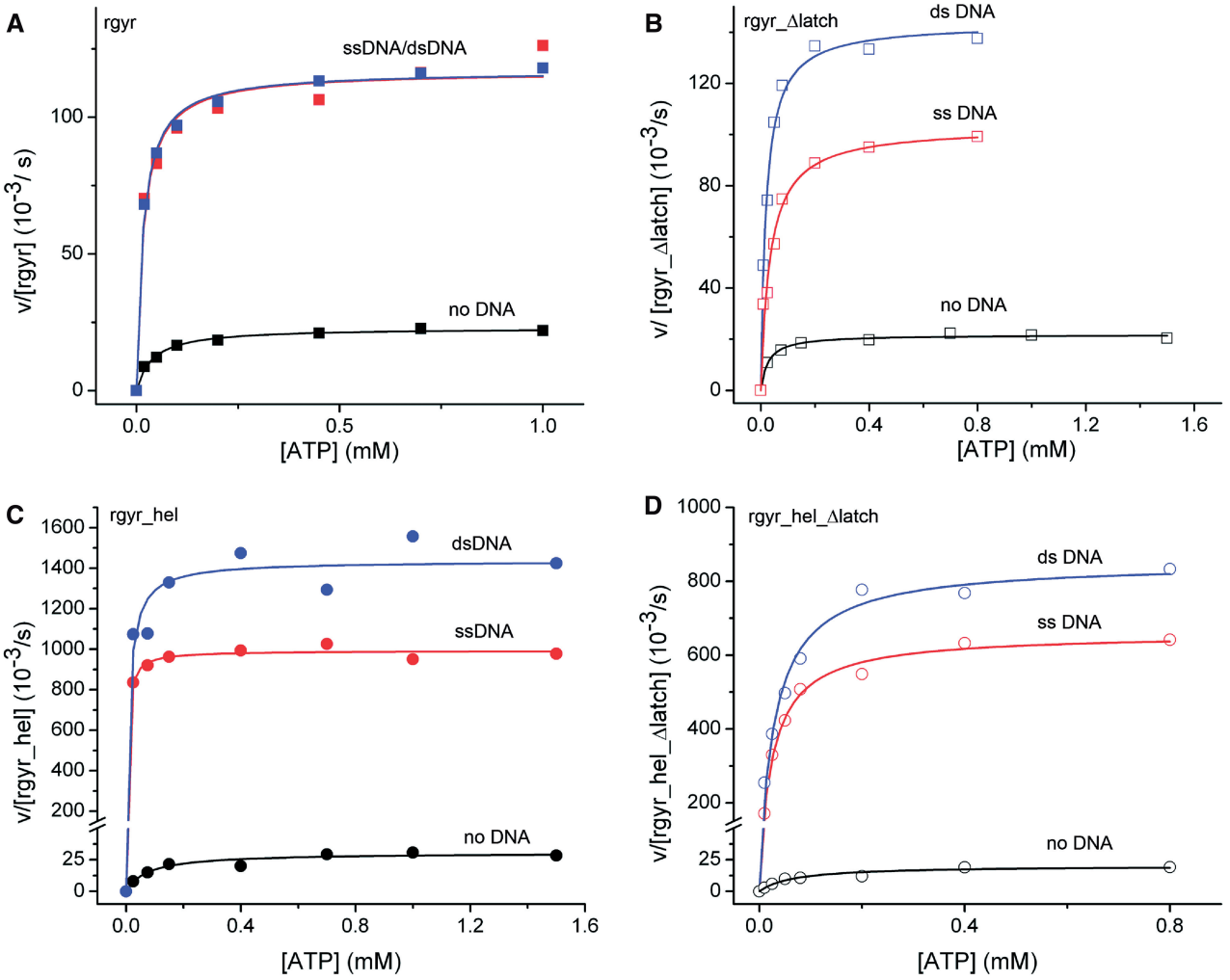

Figure 5. ATPase activity. Steady-state ATPase activity as a function of the ATP concentration. (**A**) rgyr, (**B**) rgyr_Δlatch, (**C**) rgyr_hel, (**D**) rgyr_hel_Δlatch. Black: no DNA, red: ssDNA, blue: dsDNA. Data for rgyr are depicted with squares, data for rgyr_hel with circles. Data for wild-type proteins are depicted with filled symbols, data for latch deletions with open symbols. For k_{cat} and K_M values, see Tables 4 and 5.

Table 4. Steady state ATPase parameters (ATP dependence)

	rgyr[a]		rgyr_Δlatch	
	$K_{M,ATP}$ (μM)	k_{cat} (10^{-3} s^{-1})	$K_{M,ATP}$ (μM)	k_{cat} (10^{-3} s^{-1})
–	44 ± 6	20 ± 0.8	26.5 ± 3.5	18 ± 0.5
ssDNA	12 ± 1.5	108 ± 2.1	33.3 ± 5.5	101 ± 4
dsDNA	16 ± 1.5	117 ± 1.6	18.3 ± 4.1	131 ± 6
pUC18	15.6 ± 0.9	199 ± 1.6	42.1 ± 2.3	164 ± 3
	rgyr_hel[a]		rgyr_hel_Δlatch	
	$K_{M,ATP}$ (μM)	k_{cat} (10^{-3} s^{-1})	$K_{M,ATP}$ (μM)	k_{cat} (10^{-3} s^{-1})
–	77 ± 23	30 ± 2	67 ± 18	20 ± 2
ssDNA	4.8 ± 1	992 ± 12	27 ± 2	660 ± 10
dsDNA	11 ± 4	1435 ± 57	30 ± 4	850 ± 20
pUC18	7.4 ± 1.1	818 ± 10	n.d.	n.d.

[a]Data from ref. (11).

Table 5. Steady state ATPase parameters (DNA dependence)

	rgyr[a]		rgyr_Δlatch	
	$K_{M,DNA}$ (μM)	k_{cat} (10^{-3} s^{-1})	$K_{M,DNA}$ (μM)	k_{cat} (10^{-3} s^{-1})
–	n.a.	20 ± 0.8	n.a.	18 ± 0.5
ssDNA	0.45 ± 0.06	160 ± 7	0.271 ± 0.024	108 ± 2
dsDNA	2.2 ± 0.30	148 ± 9	0.124 ± 0.039	98 ± 8
pUC18	No sat.	No sat.	0.020 ± 0.013	104 ± 14
	rgyr_hel[a]		rgyr_hel_Δlatch	
	$K_{M,DNA}$ (μM)	k_{cat} (10^{-3} s^{-1})	$K_{M,DNA}$ (μM)	k_{cat} (10^{-3} s^{-1})
–	n.a.	30 ± 2	n.a.	20 ± 2
ssDNA	0.07 ± 0.04	1160 ± 188	0.25 ± 0.03	780 ± 20
dsDNA	0.18 ± 0.03	1450 ± 64	0.29 ± 0.06	780 ± 40
pUC18	0.046 ± 0.006	673 ± 21	n.d.	n.d.

[a]Data from ref. (11).

only 0.7–1.3-fold for rgyr_Δlatch (Table 4), pointing toward a complete loss in cooperativity upon deletion of the latch region. A similar effect is observed with rgyr_hel, where the cooperativity of DNA and ATP binding leads to a large, 16- and 7-fold decrease of the $K_{M,ATP}$ in the presence of ssDNA and dsDNA, respectively. Deletion of the latch reduces the cooperativity, and the decrease is only 2.5- and 2.2-fold. Thus, the latch is crucial for coupling ATP and DNA binding within the helicase-like domain of reverse gyrase.

Measuring the steady-state ATPase activity as a function of the DNA concentration allows for the determination of apparent K_M values for DNA. These values provide a relative measure for DNA affinity to the predominant states populated under steady-state conditions. For reverse gyrase, the ATP state should be the predominant form as ATP hydrolysis is the rate-limiting step in the nucleotide cycle of reverse gyrase (14) (in the absence of DNA). In contrast to K_d values above that describe overall DNA binding to all sites, the K_M values only report on DNA-binding sites on reverse gyrase that are coupled to ATP hydrolysis. The $K_{M,DNA}$ values for rgyr are 0.45 μM (ssDNA), and 2.2 μM (dsDNA), respectively (Table 5, ref. 11). The corresponding $K_{M,DNA}$ values for rgyr_Δlatch are 0.27 μM (ssDNA), and 0.12 μM (dsDNA), corresponding to a slight increase in affinity for ssDNA (1.7-fold), and a significant increase for dsDNA (18-fold). The affinity for pUC18 plasmid was also increased by deleting the latch (Table 5). These data suggest an inhibitory effect of the latch on (ds)DNA binding to the ATP state of rgyr. The $K_{M,DNA}$ values for rgyr contain contributions from DNA binding to the helicase-like domain and to the topoisomerase domain, if these are coupled to ATP hydrolysis. We therefore dissected the contribution of the latch to DNA binding by performing the same experiments with rgyr_hel. Interestingly, the effects observed with rgyr are not paralleled by rgyr_hel (Table 5). Here, the $K_{M,DNA}$ values are increased 3.6-fold for ssDNA and 1.6-fold for dsDNA upon latch deletion, in-line with a contribution of the latch to DNA binding to the helicase-like domain in the ATP state. Overall, these findings are thus consistent with contributions of the latch to ssDNA and dsDNA binding to the helicase-like domain of reverse gyrase, in agreement with the findings from anisotropy titrations of DNA (see above). The decrease in $K_{M,DNA}$ of rgyr_Δlatch that is not

observed for rgyr_hel_Δlatch suggests that the latch (negatively) coordinates dsDNA binding within the topoisomerase domain to ATP hydrolysis by the helicase-like domain.

The effect of the latch on coupling nucleotide and DNA binding

The loss of cooperativity between ATP and DNA binding upon deletion of the latch region suggests a role of the latch for coupling DNA binding to the nucleotide state. We next determined the effect of the latch on nucleotide-dependent DNA binding (Table 3). In the nucleotide-free state, the latch contributes to ssDNA and dsDNA binding to the helicase-like domain of rgyr (see above, 1.3–2-fold loss in affinity by deleting the latch in rgyr, 2.1–5.4-fold in rgyr_hel). In the ADP state, deletion of the latch leads to a modest (2-fold) decrease in affinity for ssDNA, and an equally modest 2-fold increase in affinity of rgyr for dsDNA. These values suggest a contribution of the latch to ssDNA binding, but interference with dsDNA binding, in the ADP state. In the ADPNP state, in contrast, deletion of the latch causes a 2.7-fold and 1.9-fold loss in ssDNA and dsDNA affinity, in-line with a positive contribution of the latch to ssDNA and dsDNA binding to reverse gyrase.

Similar to the $K_{M,DNA}$ values, K_d values for rgyr/DNA complexes contain contributions from (nucleotide-dependent) DNA binding to the helicase-like domain and (nucleotide-independent) DNA binding to the topoisomerase domain, as well as possible coupling effects. To dissect the contribution of the latch to DNA binding within the helicase-like domain, we therefore also performed titrations with rgyr_hel. Here, the deletion of the latch consistently leads to a decrease in both ssDNA and dsDNA affinity in all nucleotide states (Table 3). In the ADP state, this loss in affinity is 9-fold for ssDNA and 7-fold for dsDNA; in the ADPNP state it is 2.4-fold for ssDNA and 190-fold for dsDNA. These values demonstrate that the latch contributes to ssDNA and dsDNA binding to the helicase-like domain in all nucleotide states. The largest contribution of the latch to DNA binding is observed for dsDNA in the ADPNP state.

As a reciprocal approach to monitoring DNA binding in different nucleotide states, we also measured nucleotide binding to different DNA-bound forms of rgyr and rgyr_hel (Table 2). Consistent with the observation in the absence of DNA, the affinity of rgyr and rgyr_hel for mantADP was increased in all DNA-bound states upon deletion of the latch, with more pronounced effects for rgyr (3–7-fold) than for rgyr_hel (2–4-fold). For rgyr, the increase in nucleotide affinity was most pronounced in the DNA-free state, whereas for rgyr_hel it was most pronounced in the ssDNA-bound state. The increased affinity of the latch deletions for (mant)ADPNP was alleviated in the presence of DNA, with identical nucleotide affinities for rgyr and rgyr_Δlatch, and similar values for rgyr_hel and rgyr_hel_Δlatch. The only exception is mantADPNP binding to rgyr_hel_Δlatch in the presence of dsDNA. Here, the latch deletion decreases the nucleotide affinity 5.8-fold. In combination with the nucleotide-dependent DNA binding studies (Table 3), thermodynamic cycles of DNA and nucleotide binding can be constructed (Figure 4). Coupling of overall DNA binding and nucleotide binding is small in reverse gyrase, and only small effects of the latch are observed. Coupling is larger for rgyr_hel, however, and here the effect of the latch becomes apparent. In rgyr_hel, ADPNP and dsDNA binding are thermodynamically coupled, with a coupling factor of 20 (Figure 4G). Upon deletion of the latch, this coupling is lost completely (Figure 4H). Some coupling is also present for ADPNP and ssDNA binding to rgyr_hel, which is also lost upon deletion of the latch. Overall, the data are thus consistent with a major effect of the latch on coupling (ds)DNA binding and ADPNP binding to the helicase-like domain.

The latch contributes to the discrimination between ssDNA and dsDNA

Reverse gyrase exhibits a clear (4–8-fold) preference for ssDNA over dsDNA in the nucleotide-free, the ADP and the ATP-state (Figure 4F, Table 3, ref. 11). Deletion of the latch reduces the preference for ssDNA significantly, and leads to a similar (2–3-fold) small preference for ssDNA in the nucleotide-free, the ADP- and the ADPNP state. In rgyr_hel, the latch deletion leads to a further increase of the preference for ssDNA in the nucleotide-free and the ADPNP state, but slightly reduces the preference in the ADP state (Figure 4F, Table 3). The preference of rgyr_hel_Δlatch for ssDNA in the ADPNP state is in stark contrast to similar affinities of rgyr_hel for ssDNA and dsDNA in the ADPNP state (11), strongly suggesting a role of the latch in this switch in DNA affinities upon ATP binding (switch from nucleotide-free to ADPNP state), and upon ATP hydrolysis/product release (switch from ADPNP to ADP state). This switch is suppressed in context of rgyr (11), and the effect of the latch can thus only be studied with the isolated helicase-like domain. Overall, our results point toward a role of the latch in coupling nucleotide and DNA-binding sites within the helicase-like domain, and in coordinating DNA binding within the topoisomerase domain with ATP hydrolysis in the helicase-like domain.

The latch is required for positive supercoiling of DNA by *T. maritima* reverse gyrase

Finally, we investigated the effect of the latch on the topoisomerase activities of reverse gyrase (Figure 6, Supplementary Figure S3). Similar to the wild-type enzyme, rgyr_Δlatch does not show significant relaxation activity in the absence of nucleotides, even at a large excess of enzyme (Supplementary Figure S3). In the presence of ATP and ATPγS, rgyr_Δlatch relaxes negatively supercoiled DNA, but is not capable of introducing positive supercoils as the wild-type enzyme (14). The relaxation activity of rgyr_Δlatch is also observed in the presence of ADP and ADPNP, indicating that it does not depend on ATP hydrolysis. Consequently, the latch region is required for the positive supercoiling reaction. Interestingly, this observation sets *T. maritima* reverse gyrase apart from the *A. fulgidus* homolog, which does

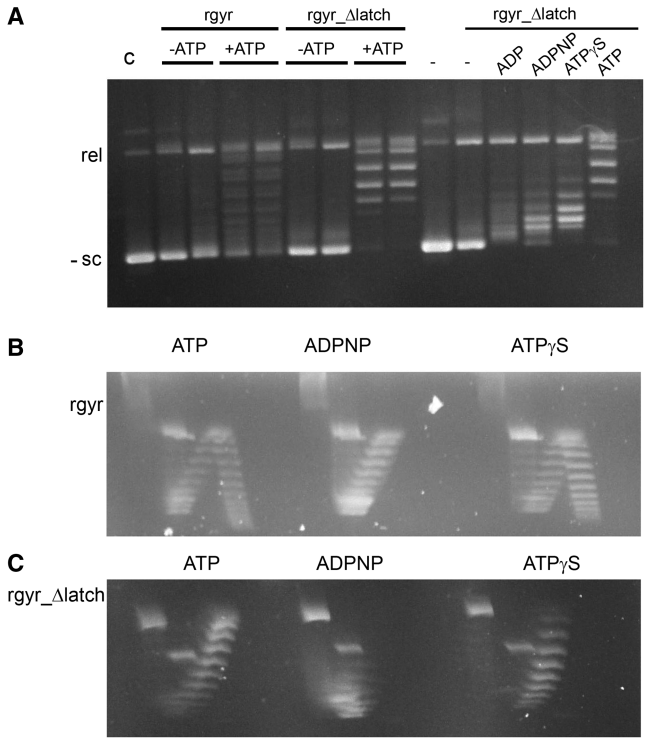

Figure 6. Topoisomerase activity. (**A**) Topoisomerase activity of rgyr and rgyr_Δlatch. (**B**) Topoisomerase activity of rgyr with ATP, ATPγS and ADPNP. Rgyr introduces positive supercoils in the presence of ATP and ATPγS, but only relaxes DNA in the presence of ADPNP. (**C**) Topoisomerase activity of rgyr_Δlatch with ATP, ATPγS and ADPNP. Rgyr_Δlatch relaxes DNA in the presence of ATP and ATPγS, and exhibits weak relaxation activity in the presence of ADPNP. In (A), reaction products from incubation of rgyr or rgyr_Δlatch with negatively supercoiled DNA were separated via one-dimensional gel electrophoresis. When two lanes are depicted for the same experimental conditions, the left lane corresponds to 1 h incubation time, the right lane to 2 h. In (B) and (C), reaction products were separated via two-dimensional gel electrophoresis ('Material and Methods' section). The species in the left arm of the arch represent negatively supercoiled DNA, the right arm of the arch represent positively supercoiled DNA. For analysis via one-dimensional gel electrophoresis in the presence of chloroquine, see Supplementary Figure S3.

not seem to require the latch for the positive supercoiling reaction (13).

DISCUSSION

The latch modulates the properties of the helicase-like domain in reverse gyrase

Studies on reverse gyrase from *A. fulgidus* have suggested that the latch region is involved in communication between the helicase-like and the topoisomerase domain and coordination of their activities, even though it was not required for positive supercoiling (13). Here, we have dissected the contributions of the latch to nucleotide binding and hydrolysis, DNA binding, and cooperativity in the isolated helicase-like domain of *T. maritima* reverse gyrase, as well as in the full-length enzyme. The latch affects nucleotide binding to the helicase-like domain, but does not alter the intrinsic or the DNA-stimulated ATPase activities. Coupling between DNA binding and ATP binding and hydrolysis in the helicase-like domain is lost when the latch is deleted, demonstrating that the latch is crucial for cooperativity within the helicase-like domain of reverse gyrase.

The helicase-like domain of reverse gyrase resembles DEAD box proteins. Members of this protein family within the SF2 helicases mediate ATP-dependent structural rearrangements of RNA, and typically exhibit cooperativity between nucleotide and DNA/RNA binding (22). This cooperativity has been rationalized from DEAD box protein structures that reveal a bipartite nucleic acid binding site that covers the surface of both RecA domains (corresponding to H1 and H2 in reverse gyrase) and a nucleotide binding site that is formed in the inter-domain cleft by residues from both domains (23). The similar spatial distribution of conserved motifs (6), mutational studies on the contributions of these motifs to supercoiling (24), as well as the existing cooperativity between DNA and ATP binding in the helicase-like domain of reverse gyrase altogether suggest similar concerted conformational changes upon ATP (and DNA) binding (11) in the helicase-like domain in reverse gyrase. The observation that the latch is involved in cooperativity of DNA and nucleotide binding suggests that it contributes to the DNA binding site within H2. On the other hand, the latch interferes with nucleotide binding. In the structure of *A. fulgidus* reverse gyrase with ADPNP bound to the helicase-like domain, the nucleotide only interacts with residues in H1, but not H2 (6), again supporting the notion that, similar to SF2 helicases, a closure of the cleft between H1 and H2 in response to nucleotide (and DNA) binding may lead to an increased nucleotide affinity. The interference of the latch with nucleotide binding to the helicase-like domain in the absence and presence of DNA suggests that the latch modulates the underlying conformational change, possibly by reducing the flexibility of the helicase-like domain. Consistent with the effect on the isolated helicase-like domain, inhibition of nucleotide binding by the latch is also observed in reverse gyrase. Here, binding of DNA and nucleotide is less cooperative, which may reflect an inhibition of the underlying conformational change in the helicase-like domain by the topoisomerase domain (11). In line with this scenario, the effect of the latch on nucleotide binding in reverse gyrase is less severe. In addition, it is alleviated in the presence of ssDNA and dsDNA. It is conceivable that nucleotide and DNA binding alleviate conformational restrictions caused by interactions between the helicase-like and the topoisomerase-like domains, consistent with a possible release of the latch from the topoisomerase domain in the presence of DNA (6), and a concomitant loss of conformational restrictions in the helicase-like domain.

The latch affects the discrimination between ssDNA and dsDNA

The DNA-binding site on the helicase-like domain exhibits a preference for ssDNA in the nucleotide-free and the ADP state, but switches to similar affinities for

ssDNA and dsDNA in the ATP state. By contrast, in the absence of the latch the preference for ssDNA is high in the nucleotide-free and ATP state, but reduced for the ADP state, implicating the latch in the switching properties of the helicase-like domain. In line with the effect of the latch on cooperativity, it indeed contributes to DNA binding to the helicase-like domain in reverse gyrase, and it is capable of weak DNA binding on its own. The latch is structurally homologous to a region of the transcription termination factor Rho that is involved in RNA binding (7,8), but for *A. fulgidus* reverse gyrase no effect of the latch on DNA binding was observed (13). This may be due to the presence of various different DNA-binding sites within reverse gyrase that contribute to the overall DNA affinity, hiding contributions from the latch. These effects thus only become detectable in DNA-binding studies with the isolated helicase-like domain as we have performed here, and may have been missed in studies of the *A. fulgidus* enzyme. Even though the latch provides minor contributions to DNA binding, it is not required for high-affinity DNA binding to reverse gyrase. Its contribution may be relevant for transient contacts of the latch with DNA that have been proposed (6), consistent with a guiding effect of the latch for DNA during supercoiling and strand passage. Most importantly, the latch affects the discrimination of reverse gyrase between ssDNA and dsDNA. The strong preference of reverse gyrase for ssDNA in all nucleotide states (11) is thought to be important for sensing single-stranded regions in DNA at high temperatures (4). Upon deletion of the latch in reverse gyrase, this preference is reduced, and is now similar for the nucleotide-free, ATP and ADP states, consistent with the latch being involved in communicating the nucleotide state of the helicase-like domain to the DNA-binding sites on the topoisomerase domain.

The latch is required for positive supercoiling

It has been suggested previously that a conformational change bringing H1 and H2 close together may lead to a movement of the latch and to a release of the lid of the topoisomerase domain during positive supercoiling (6). In light of this scenario (that has not been proven experimentally as yet), a crucial role of the latch in positive supercoiling is expected. Interestingly, a deletion of the latch in *A. fulgidus* reverse gyrase did not abolish positive supercoiling, though the activity was significantly reduced (13). By contrast, we have shown here that the latch is absolutely required for positive supercoiling by *T. maritima* reverse gyrase. The latch deletion construct we used here does not contain the two-stranded β-sheet connecting the latch to the H2 domain. This region is absent in SF2 helicases, but was retained in the deletion construct of *A. fulgidus* reverse gyrase (13). On the other hand, the latch region shows less sequence conservation among reverse gyrases than the H1 and H2 domains, and may have different roles in different enzymes. It is thus unclear whether the different effects of the latch deletions in *A. fulgidus* and *T. maritima* reverse gyrase are due to different deletions studied, or reflect genuine differences between these enzymes.

Despite its requirement for positive DNA supercoiling by *T. maritima* reverse gyrase, the latch is not required for nucleotide-mediated relaxation of DNA in the presence of ATP, ATPγS and ADPNP, and is thus not necessary *per se* for strand passage in general, or for strand passage toward a higher linking number. The latch has been implicated in repressing relaxation of DNA by the topoisomerase domain (13) in the absence of nucleotides. However, deletion of the latch in *T. maritima* reverse gyrase does not lead to DNA relaxation in the absence of nucleotides, arguing against a general role of the latch in repressing this activity. Deletion of the latch leads to relaxation in the presence of all nucleotides tested, suggesting an important role of the latch in coupling ATP hydrolysis to strand passage towards positive DNA supercoiling. To dissect how DNA is guided toward positive DNA supercoiling, future studies will have to address DNA binding to individual sites on reverse gyrase, and their contributions to DNA binding at different stages of the supercoiling.

SUPPLEMENTARY DATA

Supplementary Data are available at NAR Online.

ACKNOWLEDGEMENTS

We thank the staff at SLS beamlines PX-II and PX-III for support during data collection.

FUNDING

VolkswagenStiftung (to D.K.); Swiss National Science Foundation (to D.K.); Marie Curie postdoctoral fellowship (to A.G.). Funding for open access charge: University of Basel.

Conflict of interest statement. None declared.

REFERENCES

1. Schoeffler,A.J. and Berger,J.M. (2008) DNA topoisomerases: harnessing and constraining energy to govern chromosome topology. *Q. Rev. Biophys.*, **41**, 41–101.
2. Kikuchi,A. and Asai,K. (1984) Reverse gyrase–a topoisomerase which introduces positive superhelical turns into DNA. *Nature*, **309**, 677–681.
3. Kampmann,M. and Stock,D. (2004) Reverse gyrase has heat-protective DNA chaperone activity independent of supercoiling. *Nucleic Acids Res.*, **32**, 3537–3545.
4. Hsieh,T.S. and Plank,J.L. (2006) Reverse gyrase functions as a DNA renaturase: annealing of complementary single-stranded circles and positive supercoiling of a bubble substrate. *J. Biol. Chem.*, **281**, 5640–5647.
5. Confalonieri,F., Elie,C., Nadal,M., de La Tour,C., Forterre,P. and Duguet,M. (1993) Reverse gyrase: a helicase-like domain and a type I topoisomerase in the same polypeptide. *Proc. Natl Acad. Sci. USA*, **90**, 4753–4757.
6. Rodriguez,A.C. and Stock,D. (2002) Crystal structure of reverse gyrase: insights into the positive supercoiling of DNA. *EMBO J.*, **21**, 418–426.

7. Dolan,J.W., Marshall,N.F. and Richardson,J.P. (1990) Transcription termination factor rho has three distinct structural domains. *J. Biol. Chem.*, **265**, 5747–5754.
8. Dombroski,A.J. and Platt,T. (1988) Structure of rho factor: an RNA-binding domain and a separate region with strong similarity to proven ATP-binding domains. *Proc. Natl Acad. Sci. USA*, **85**, 2538–2542.
9. Lima,C.D., Wang,J.C. and Mondragon,A. (1994) Three-dimensional structure of the 67K N-terminal fragment of E. coli DNA topoisomerase I. *Nature*, **367**, 138–146.
10. Declais,A.C., Marsault,J., Confalonieri,F., de La Tour,C.B. and Duguet,M. (2000) Reverse gyrase, the two domains intimately cooperate to promote positive supercoiling. *J. Biol. Chem.*, **275**, 19498–19504.
11. Del Toro Duany,Y., Jungblut,S.P., Schmidt,A.S. and Klostermeier,D. (2008) The reverse gyrase helicase-like domain is a nucleotide-dependent switch that is attenuated by the topoisomerase domain. *Nucleic Acids Res.*, **36**, 5882–5895.
12. Rodriguez,A.C. (2003) Investigating the role of the latch in the positive supercoiling mechanism of reverse gyrase. *Biochemistry*, **42**, 5993–6004.
13. Rodriguez,A.C. (2002) Studies of a positive supercoiling machine. Nucleotide hydrolysis and a multifunctional "latch" in the mechanism of reverse gyrase. *J. Biol. Chem.*, **277**, 29865–29873.
14. Jungblut,S.P. and Klostermeier,D. (2007) Adenosine 5′-O-(3-thio)triphosphate (ATPgammaS) promotes positive supercoiling of DNA by *T. maritima.* reverse gyrase. *J. Mol. Biol.*, **371**, 197–209.
15. Kabsch,W. (1993) Automatic processing of rotation diffraction data from crystals of initially unknown symmetry and cell constants. *J. Appl. Crystallog.*, **26**, 795–800.
16. CCP4. (1994) The Collaborative Computational Project Number 4, suite programs for protein crystallography. *Acta Cryst.*, **D50**, 760–763.
17. Blanc,E., Roversi,P., Vonrhein,C., Flensburg,C., Lea,S.M. and Bricogne,G. (2004) Refinement of severely incomplete structures with maximum likelihood in BUSTER-TNT. *Acta Cryst.*, **D60**, 2210–2221.
18. Zwart,P.H., Afonine,P.V., Grosse-Kunstleve,R.W., Hung,L.W., Ioerger,T.R., McCoy,A.J., McKee,E., Moriarty,N.W., Read,R.J., Sacchettini,J.C. *et al.* (2008) Automated structure solution with the PHENIX suite. *Methods Mol. Biol.*, **426**, 419–435.
19. Emsley,P., Lohkamp,B., Scott,W.G. and Cowtan,K. (2010) Features and development of Coot. *Acta Crystallogr. D Biol. Crystallogr.*, **D66**, 486–501.
20. Hiratsuka,T. (1983) New ribose-modified fluorescent analogs of adenine and guanine nucleotides available as substrates for various enzymes. *Biochim. Biophys. Acta*, **742**, 496–508.
21. Adam,H. (1962) *Methoden der enzymatischen Analyse*, Bergmeyer, H.U.(Hrsg.), Verlag Chemie, Weinheim, pp. 573–577.
22. Hilbert,M., Karow,A.R. and Klostermeier,D. (2009) The mechanism of ATP-dependent RNA unwinding by DEAD box proteins. *Biol. Chem.*, **390**, 1237–1250.
23. Sengoku,T., Nureki,O., Nakamura,A., Kobayashi,S. and Yokoyama,S. (2006) Structural basis for RNA unwinding by the DEAD-box protein Drosophila Vasa. *Cell*, **125**, 287–300.
24. Bouthier de la Tour,C., Amrani,L., Cossard,R., Neuman,K., Serre,M.C. and Duguet,M. (2008) Mutational analysis of the helicase-like domain of *Thermotoga maritima* reverse gyrase. *J. Biol. Chem.*, **283**, 27395–27402.

Chapter 3. Article

Nucleotide-driven conformational changes in the reverse gyrase helicase-like domain couple the nucleotide cycle to DNA processing.

In this article, simultaneous equilibrium binding studies of the helicase-like domain to nucleotide analogs along the catalytic cycle and different DNA constructs were reported. By using this approach we unraveled the lowest energy path along the thermodynamic landscape of all possible complexes. Combined with smFRET data, also the conformational transitions along this nucleotide cycle were determined. The helicase-like domain is responsible for the nucleotide-dependent behavior of the DNA positive supercoiling reaction performed by reverse gyrase. From this characterization a picture emerged on which mechanistic details of the helicase-like domain fulfill the requirements for duplex DNA unwinding, and nucleotide- and conformational-controlled ssDNA strand presentation to the topoisomerase domain to perform the supercoiling reaction.

PCCP

View Online
Dynamic Article Links

Cite this: DOI: 10.1039/c0cp02859b

www.rsc.org/pccp

PAPER

Nucleotide-driven conformational changes in the reverse gyrase helicase-like domain couple the nucleotide cycle to DNA processing†

Yoandris del Toro Duany and Dagmar Klostermeier*‡

Received 12th December 2010, Accepted 2nd February 2011
DOI: 10.1039/c0cp02859b

Reverse gyrase introduces positive supercoils into DNA in an ATP-dependent process. It has a modular structure comprising a helicase-like and a topoisomerase domain. The helicase-like domain consists of two RecA-like subdomains and thus structurally resembles members of the helicase superfamily 2. It is a nucleotide-dependent switch that alters between an ATP state with a slight preference for dsDNA, and an ADP state with a high preference for ssDNA. Inter-domain communication between the helicase-like and the topoisomerase domain is central for their functional cooperation in reverse gyrase. The latch, an insertion into the helicase-like domain, has been suggested as an important element in coordinating their activities. Here, we have dissected the nucleotide cycle of the reverse gyrase helicase-like domain in the absence and presence of different DNA substrates. With this comprehensive thermodynamic characterization of the nucleotide cycle of the helicase-like domain, in combination with single molecule FRET data on the conformation of the helicase-like domain at all stages of the catalytic cycle, a picture emerges as to how the helicase-like domain may guide ATP-dependent positive supercoiling by reverse gyrase.

Introduction

Reverse gyrase is the only topoisomerase that can introduce positive supercoils into DNA in an ATP-dependent process. It was first identified in the hyperthermophilic archaeon *Sulfolobus acidocaldarius*,[1] and is unique to thermophiles and hyperthermophiles.[2] *In vivo*, reverse gyrases protect DNA at high temperatures *via* DNA chaperone and renaturase activities.[3,4] Reverse gyrases have a modular structure, with an N-terminal helicase like domain covalently linked to a C-terminal topoisomerase I domain.[5] The helicase-like domain consists of two RecA-like subdomains (H1 and H2) that harbor all signature motifs of superfamily (SF) 2 helicases, though with altered sequences.[6] The isolated helicase-like domain and reverse gyrase do not exhibit nucleic acid unwinding activity.[7,8] The helicase-like domain of *Thermotoga maritima* reverse gyrase is a nucleotide-dependent switch that exhibits a strong preference for ssDNA in the nucleotide-free and ADP state, but has a small (2-fold) preference for dsDNA in the ATP state.[8] The DNA-stimulated ATPase activity of the helicase-like domain is 10-fold higher than that of full-length reverse gyrase, pointing towards a suppression of the activity of the helicase-like domain by the topoisomerase domain.[8] The "latch" (H3), an insertion in the H2 domain resembling the RNA binding region of the transcription termination factor Rho,[9,10] is required for thermodynamic coupling of DNA and nucleotide binding in the helicase-like domain, and for positive DNA supercoiling by *T. maritima* reverse gyrase.[11] A strand-passage mechanism similar to other type IA topoisomerases has been suggested for positive DNA supercoiling by reverse gyrase.[6] The model postulates as the initial event a conformational change in the helicase-like domain that brings domains H1 and H2 closer together, and a subsequent movement of the latch domain away from the topoisomerase domain that allows the lid region of the topoisomerase domain to swing up.

Here we have dissected the nucleotide cycle of the isolated helicase-like domain of *T. maritima* reverse gyrase, the influence of DNA on the nucleotide cycle, as well as coupling between DNA and nucleotide binding. In addition, we have correlated the nucleotide cycle with conformational changes in the helicase-like domain. We show that the cleft between H1 and H2 closes upon binding of ATP and DNA, and re-opens upon ATP hydrolysis and thus prior to phosphate release. Thus, the helicase-like domain undergoes similar conformational cycles as DEAD box proteins, the largest family within the helicase SF2. However, the triggering events for opening

University of Basel, Biozentrum, Dept. of Biophysical Chemistry, Klingelbergstrasse 70, CH–4056 Basel, Switzerland.
E-mail: dagmar.klostermeier@unibas.ch; Fax: 0041 61-267 2189; Tel: 0041 61-267 2381

† Electronic supplementary information (ESI) available. See DOI: 10.1039/c0cp02859b

‡ Present address: University of Muenster, Institute for Physical Chemistry, Corrensstrasse 30, D-48149 Muenster, Germany. E-mail: dagmar.klostermeier@uni-muenster.de; Fax: 0049-251-83 29138; Tel: 0049-251-83 23421.

and closing of the inter-domain cleft differ. Implications of our results for positive supercoiling of DNA by reverse gyrase are discussed.

Material and methods

Cloning, protein production and purification

Rgyr_hel and rgyr_hel_Δlatch were purified as described.[8,11] Cysteine mutants were constructed using the Quikchange protocol (Stratagene), and were purified as wild-type protein.

Nucleotides and nucleic acid substrates

Nucleotides were purchased from Jena Biosciences. Oligonucleotides for DNA substrates were purchased from Purimex. The sequences were: 5′-(fluorescein)-AAGCCAAGCT TCTAGAGTCA GCCCGTGATA TTCATTACTT CTTATCCTAG GATCCCCGTT-3′ (60mer) and 5′-GATAAGAAGT AATGAATATC-3′ (20mer). Double-stranded DNA substrates were formed by annealing the 60mer with the complementary strand. The ss/dsDNA junction was formed by annealing the 60mer with the 20mer. The complementary part is underlined in the 60mer sequence. The dsDNA substrate containing a single-stranded bubble was generated by annealing the strands 5′-AAGCCAAGCT TCTAGAGTCG GTTTTTTTTT TTTTTTGGCT ATCCTAGGAT CCCCGTT-3′ and 5′-AACGGGGATC CTAGGATAGC CTTTTTTTTT TTTTTTCCGA CTCTAGAAGC TTGGCTT-3′.

Fluorescence equilibrium titrations

Dissociation constants of enzyme/nucleotide complexes were determined in fluorescence equilibrium titrations with a Fluoromax-3 fluorimeter (Jobin Yvon) using the fluorescent nucleotide analogs mantADP, mantADPNP, mantADP·BeF_x, and mantADP·MgF_x.[12] The fluorescent analogs mantADP·BeF_x, and mantADP·MgF_x were generated as described.[13] In titrations of 1 μM mant nucleotides in 50 mM Tris/HCl, pH 7.5, 0.15 M NaCl, 10 mM $MgCl_2$, 100 μM $Zn(OAc)_2$, 2 mM β-mercaptoethanol, binding was monitored *via* Förster Resonance Energy Transfer (FRET) from tryptophan to the mant group. Tryptophan fluorescence was excited at 295 nm (3 nm bandwidth), and mant fluorescence was detected at 440 nm (3 nm bandwidth). The temperature was 37 °C if not indicated otherwise. The K_d value was determined using the solution of the quadratic equation describing a 1 : 1 complex formation (eqn (1)).

$$F = F_0 + \frac{\Delta F_{max}}{[mA]_{tot}}\left(\frac{[E]_{tot} + [mA]_{tot} + K_d}{2} - \sqrt{\left(\frac{[E]_{tot} + [mA]_{tot} + K_d}{2}\right)^2 - [E]_{tot}[mA]_{tot}}\right) \quad (1)$$

where F_0 is the fluorescence of free mantADP, ΔF_{max} is the amplitude, $[E]_{tot}$ is the total enzyme concentration, and $[mA]_{tot}$ is the total nucleotide concentration.

DNA binding was measured in fluorescence anisotropy titrations at 37 °C of DNA labeled with fluorescein at the 5′-end in 50 mM Tris/HCl, pH 7.5, 0.15 M NaCl, 10 mM $MgCl_2$, 100 μM $Zn(OAc)_2$, 2 mM β-mercaptoethanol, or phosphate buffer (12 mM phosphate pH 7.5, 137 mM NaCl, 27 mM KCl, 10 mM $MgCl_2$), and analyzed using the corresponding form of eqn (1) as described.[8]

Single-molecule FRET experiments

The S169C/F332C and S169C/S341C cysteine mutants were labeled in 50 mM Tris/HCl, pH 7.5, 0.2 M NaCl, 10 mM $MgCl_2$, 100 μM $Zn(OAc)_2$ with a mixture of a 10-fold molar excess of A488- (donor) and tetramethylrhodamine (TMR) maleimide (acceptor), respectively, for 15 min at 25 °C in the presence of 0.5 mM Tris(2-carboxyethyl)phosphine. Labeling efficiencies were determined from absorbance ratios at 495 nm (A488, corrected for TMR contributions) and 280 nm (protein, corrected for dye contributions), or at 550 nm (TMR) and 280 nm. SmFRET experiments were performed in a home-built confocal microscope as described.[14] Only fluorescence bursts above a threshold of 50–100 photons were considered in the analysis. Measured fluorescence intensities were corrected for background, for cross-talk from donor fluorescence into the acceptor channel and *vice versa*, for different detection efficiencies and quantum yields of donor and acceptor, and for direct excitation of the donor as described.[14] Correction parameters and Förster radii R_0 were determined for each construct as described.[14] All measurements were performed at 37 °C in 50 mM Tris/HCl, pH 7.5, 0.15 M NaCl, 10 mM $MgCl_2$, 100 μM $Zn(OAc)_2$, treated with active charcoal, with 50 pM fluorescently labeled rgyr_hel (concentration of donor fluorophore).

Results

Dissecting the nucleotide cycle of rgyr_hel

We have previously shown that the helicase-like domain, rgyr_hel, is a nucleotide-dependent switch[8] that binds DNA and ATP cooperatively. In the ADPNP-state, rgyr_hel shows a slight (2-fold) preference for dsDNA, whereas in the ADP state, ssDNA is bound preferentially. In the context of full length reverse gyrase (rgyr), the differences in affinities for ssDNA and dsDNA are reduced, as is the cooperativity between ATP and DNA binding.

mantADP and mantADPNP are suitable analogs to monitor adenine nucleotide binding to rgyr and rgyr_hel.[8,11,15] To establish that binding data determined at 37 °C can be extrapolated to the physiological temperature of *T. maritima* (75 °C), and thus the temperature at which reverse gyrase exerts its DNA-protective function, we first addressed the temperature dependence of mantADP binding in the range of 25–50 °C (Fig. 1). The K_d value of the mantADP complex changes less than three-fold from 25–50 °C. The van't Hoff plot for mantADP binding is linear in this temperature range, and a binding enthalpy ΔH^0 of −26.1 kJ mol^{-1} is obtained. The binding entropy is positive (ΔS^0 = 30 J mol^{-1} K^{-1}). For mantADPNP, dissociation constants were determined in the temperature range of 20–37 °C (Fig. 1B). Again, the K_d values increase only slightly (less than 2-fold) over this temperature range. The van't Hoff plot is linear, and the binding enthalpy ΔH^0 is −24.7 kJ mol^{-1}, the binding entropy ΔS^0 = 16.4 J mol^{-1} K^{-1}. As a consequence of the small temperature

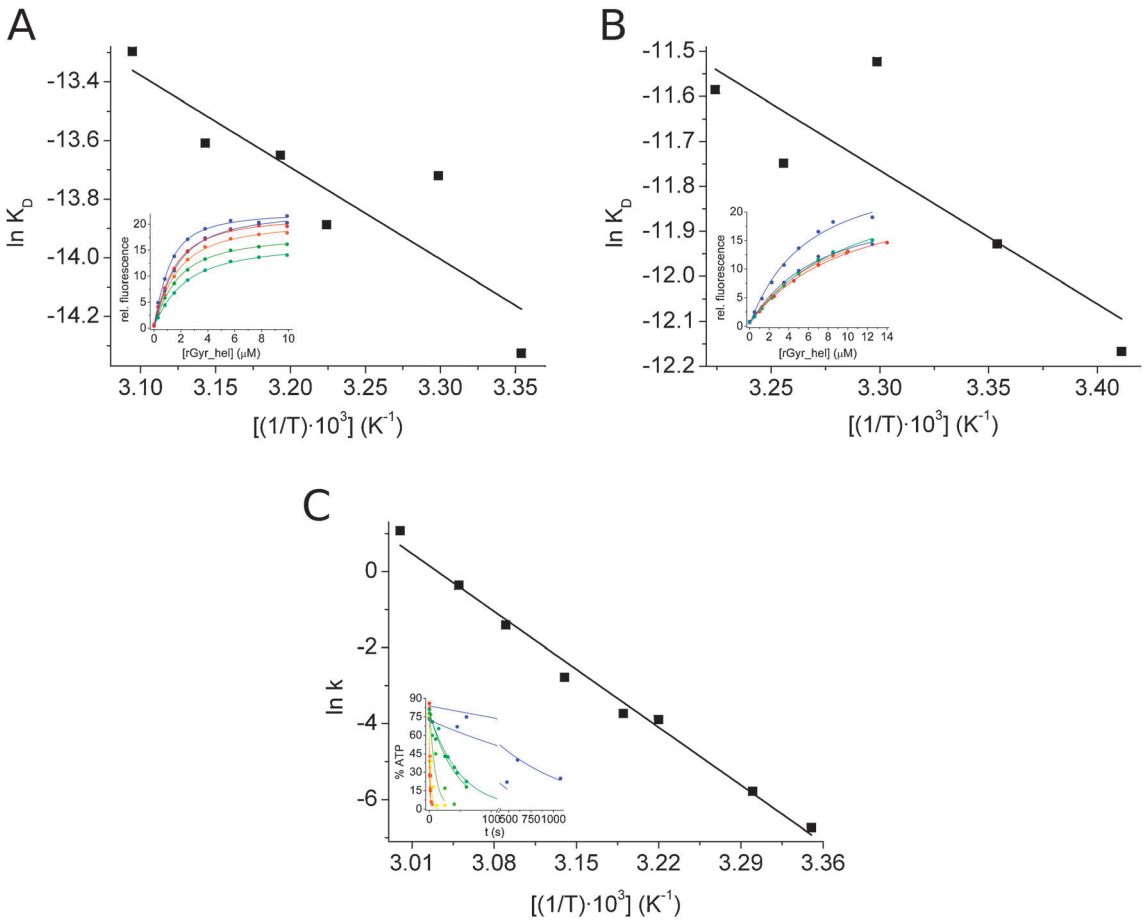

Fig. 1 Temperature dependence of nucleotide binding and ATP hydrolysis. (A) van't Hoff plot of dissociation constants for the mantADP/rgyr_hel complex in the temperature range of 25–50 °C. The binding enthalpy ΔH^0 is −26.1 kJ mol^{-1}, the binding entropy is ΔS^0 is 30 J mol^{-1} K^{-1}. The inset shows the titrations curves of mantADP at different temperatures, color-coded with a gradient from blue (25 °C) to red (50 °C). The dissociation constants show little temperature dependence, and with a 2.5-fold change from 25 °C to 50 °C. Dissociation constants are 0.6 μM (25 °C), 1.1 μM (30 °C), 0.93 μM (37 °C), 1.2 μM (40 °C), 1.2 μM (45 °C), and 1.7 μM (50 °C). (B) van't Hoff plot of dissociation constants for the mantADPNP/rgyr_hel complex in the temperature range of 20–37 °C. The binding enthalpy ΔH^0 is −24.7 kJ mol^{-1}, the binding entropy ΔS^0 is 16.4 J mol^{-1} K^{-1}. The inset shows the titrations curves of mantADP at different temperatures, color-coded with a gradient from blue (25 °C) to red (37 °C). As for mantADP, the dissociation constants show little temperature dependence, and change less than two-fold from 25 °C to 37 °C. Dissociation constants are 5.2 μM (20 °C), 6.6 μM (25 °C), 9.9 μM (30 °C), 7.9 μM (34 °C), and 9.3 μM (37 °C). (C) Arrhenius plot for ATP hydrolysis by rgyr_hel in the temperature range of 25–60 °C. The single turnover rate constant at 37 °C is $20 \pm 3 \times 10^{-3}$ s^{-1}, and thus similar to the steady state ATPase rate ($k_{cat} = 30 \pm 2 \times 10^{-3}$ s^{-1}),[8] indicating that ATP hydrolysis is the rate-limiting step in the nucleotide cycle of rgyr_hel at 37 °C. The linearity of the Arrhenius plot is in agreement with no change in the rate-limiting step within this temperature range. The inset shows the kinetics of ATP hydrolysis at different temperatures, color-coded with a gradient from blue (25 °C) to red (60 °C).

dependence of mantADP and mantADPNP binding, equilibrium constants at 37 °C are very similar (within 3–4-fold) to those at 75 °C.

Finally, we analyzed ATP hydrolysis under single turnover conditions as a function of temperature (Fig. 1C). Here, the temperature range of 25–60 °C was covered. The single turnover rate constant for ATP hydrolysis at 37 °C was $20 \pm 3 \times 10^{-3}$ s^{-1}. This value is similar to the k_{cat} value of $30 \pm 2 \times 10^{-3}$ s^{-1} determined for the steady state ATPase activity,[8] in-line with ATP hydrolysis as the rate-limiting step in the cycle. At 60 °C, ATP was hydrolyzed at a rate constant of 1.1 ± 0.1 s^{-1}, corresponding to a 900-fold increase compared to 25 °C. The Arrhenius plot of the rate constants is linear, indicating that the rate-limiting step is not changing in this temperature range. Thus, these temperature-dependent studies suggest that data on nucleotide binding and hydrolysis determined at 37 °C can be extrapolated safely to the physiological temperature of *T. maritima* of 75 °C.

Next, we determined K_d values for all nucleotide complexes relevant for the nucleotide cycle (Fig. 2). Since ATP is hydrolyzed, we have previously used (mant)ADPNP as a non-hydrolyzable nucleotide analog. In this study, we now mimicked nucleotide states before and after ATP hydrolysis using (mant)ADP·BeF$_x$ (Fig. 2A) as a pre-hydrolysis (ground state) state ATP analog, and (mant)ADP·MgF$_x$ as a post-hydrolysis (product state) analog mimicking the ADP·P$_i$ state. The K_d values were 1.9 (±0.1) μM (mantADP·BeF$_x$), and 2.1 (±0.1) μM (mantADP·MgF$_x$), demonstrating that rgyr_hel binds these nucleotides with

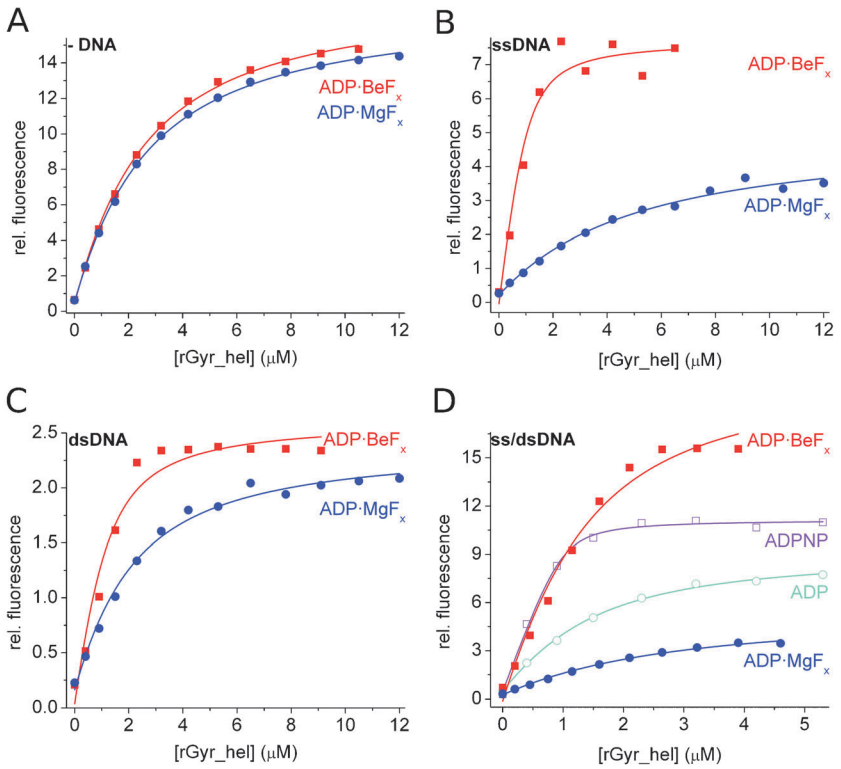

Fig. 2 Nucleotide binding to rgyr_hel. The K_d values for all nucleotide complexes are summarized in Table 1. Titrations of mantADPNP are depicted in magenta (open squares), of mantADP in cyan (open circles), of mantADP·BeF$_x$ in red (squares) and of mantADP·MgF$_x$ in blue (circles). (A) Fluorescence equilibrium titrations of mantADP·BeF$_x$ and mantADP·MgF$_x$ in the absence of DNA. The K_d values are 1.9 ± 0.1 μM (mantADP·BeF$_x$) and 2.1 ± 0.1 μM (mantADP·MgF$_x$). (B) Fluorescence equilibrium titrations of mantADP·BeF$_x$ and mantADP·MgF$_x$ in the presence of 5 μM ssDNA. The K_d values are 0.2 ± 0.1 μM (mantADP·BeF$_x$) and 4.5 ± 0.9 μM (mantADP·MgF$_x$). (C) Fluorescence equilibrium titrations of mantADP·BeF$_x$ and mantADP·MgF$_x$ in the presence of 10 μM dsDNA. The K_d values are 0.5 ± 0.2 μM (mantADP·BeF$_x$) and 1.6 ± 0.2 μM (mantADP·MgF$_x$). (D) Fluorescence equilibrium titrations of mantADPNP, mantADP·BeF$_x$, mantADP·MgF$_x$, and mantADP in the presence of 5 μM ss/dsDNA. The K_d values are 0.06 ± 0.02 μM (mantADPNP), 0.8 ± 0.3 μM (mantADP·BeF$_x$), 2.1 ± 0.4 μM (mantADP·MgF$_x$) and 0.9 ± 0.1 μM (mantADP).

Table 1 Nucleotide binding to rgyr_hel and the effect of DNA on nucleotide affinities

	K_d/μM			
Nucleotide	No DNA	ssDNA	dsDNA	ss/dsDNA
ADPNP[b]	36 ± 8[a]	12 ± 2[a]	1.9 ± 0.4[a]	0.06 ± 0.02
ADP·BeF$_x$[b]	1.9 ± 0.1	0.2 ± 0.1	0.5 ± 0.2	0.8 ± 0.3
ADP·MgF$_x$[b]	2.1 ± 0.1	4.5 ± 0.9	1.6 ± 0.2	2.1 ± 0.4
ADP[b]	4.2 ± 0.2[a]	10 ± 1[a]	1.7 ± 0.4[a]	0.9 ± 0.1

[a] From ref. 11. [b] All nucleotides are mant-nucleotides.

higher affinity than ADPNP and ADP. K_d values for the all rgyr_hel/nucleotide complexes are summarized in Table 1.

Effect of DNA on nucleotide binding to rgyr_hel

To investigate the effect of DNA on nucleotide binding to rgyr_hel, we analyzed nucleotide binding in the presence of a 60 bp ssDNA or a 60 bp dsDNA previously used as a model substrate for reverse gyrase (Fig. 2B, C).[8,11,15] The K_d values, together with previously determined values,[8,11] are summarized in Table 1. The predominant effect of ssDNA binding to rgyr_hel is a 10-fold increase in affinity for the ground state ATP analog ADP·BeF$_x$, compared to DNA-free rgyr_hel. In the ssDNA complex, the affinity for ADPNP is also increased, albeit weaker (3-fold). In contrast, the affinities for ADP·MgF$_x$ and ADP are reduced 2-fold in the presence of ssDNA compared to the DNA-free enzyme. DsDNA also promotes binding of ADP·BeF$_x$ (4-fold) and ADPNP (19-fold), but in contrast to ssDNA, the affinity for ADP·MgF$_x$ (1.3-fold) and ADP (2.5-fold) is slightly increased in the dsDNA complex. Overall, rgyr_hel binds ADP·BeF$_x$ with the highest affinity in the DNA-bound states (see below), and this effect is most pronounced in the ssDNA-bound state.

DNA binding

We also analyzed DNA binding to rgyr_hel in all states during the nucleotide cycle. First, K_d values for ssDNA and dsDNA in the presence of saturating ADP·BeF$_x$- and ADP·MgF$_x$-concentrations were determined (Fig. 3A and B). In the nucleotide cycle, rgyr_hel binds ssDNA with the highest affinity in the ADP·BeF$_x$- and ADP·MgF$_x$-states (K_d = 0.044 μM and 0.082 μM, respectively). Starting from the nucleotide-free state, the affinity of rgyr_hel for ssDNA is increased 4.5-fold in the ADP·BeF$_x$-state, remains similar in the ADP·MgF$_x$-state, and decreases, returning to a similar value to the nucleotide-free state, in the ADP state. These data

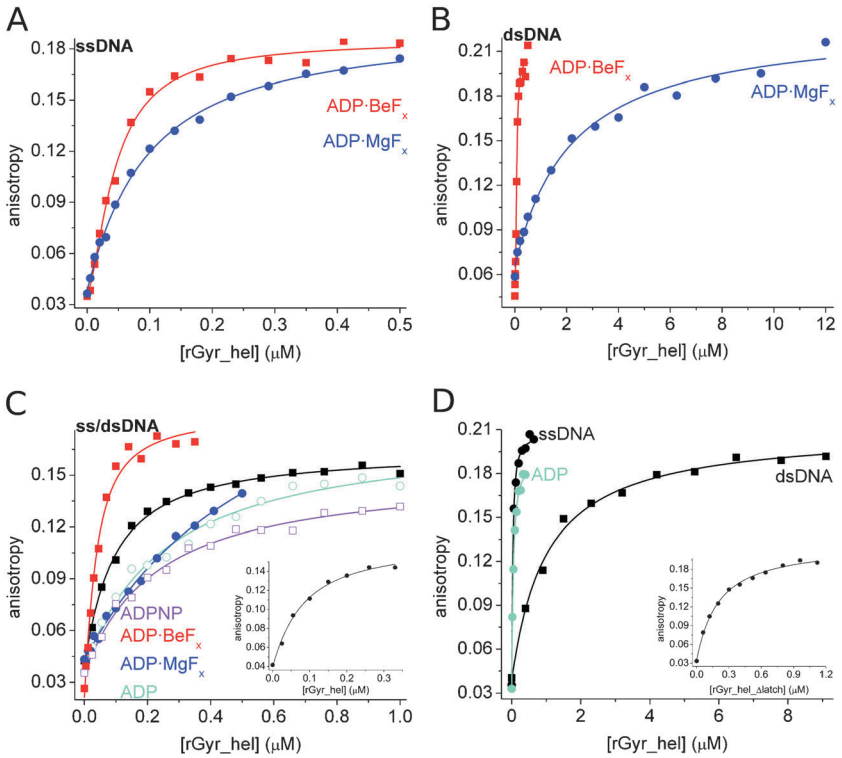

Fig. 3 DNA binding at different stages of the nucleotide cycle. The K_d values for all DNA complexes are summarized in Table 2. (A) Fluorescence equilibrium titrations of ssDNA with rgyr_hel in the presence of 0.5 mM ADP·BeF$_x$ (red, squares) or ADP·MgF$_x$ (blue, circles). $K_{d,ssDNA}$ values are 0.044 ± 0.003 μM (ADP·BeF$_x$) and 0.082 ± 0.007 μM (ADP·MgF$_x$). (B) Fluorescence equilibrium titrations of dsDNA with rgyr_hel in the presence of 0.5 mM ADP·BeF$_x$ (red, squares) or ADP·MgF$_x$ (blue, circles). $K_{d,dsDNA}$ values are 0.072 ± 0.004 μM (ADP·BeF$_x$) and 2.2 ± 0.3 μM (ADP·MgF$_x$). (C) Fluorescence equilibrium titrations of a ss/dsDNA junction in the absence of nucleotide (black, squares), and in the presence of 0.5 mM ADPNP (magenta, open squares), ADP·BeF$_x$ (red, squares), ADP·MgF$_x$ (blue, circles), or ADP (cyan, open circles). The $K_{d,ss/dsDNA}$ values are 0.081 ± 0.006 μM (no nucleotide), 0.21 ± 0.02 μM (ADPNP), 0.026 ± 0.004 μM (ADP·BeF$_x$), 0.57 ± 0.09 μM (ADP·MgF$_x$), and 0.24 ± 0.3 μM (ADP). The inset shows the titration of a DNA containing a 15-base single-stranded bubble of bubble-DNA. The $K_{d,bubble-DNA}$ was 0.069 ± 0.012 μM. (D) Fluorescence equilibrium titrations of DNA in phosphate buffer. The K_d values are 0.021 ± 0.003 μM (ssDNA, black, circles) and 1.0 ± 0.1 μM (dsDNA, black, squares) in the absence of nucleotide, and 0.035 ± 0.004 μM (ssDNA, cyan, circles) in the presence of ADP. The inset shows the corresponding titration of ssDNA with rgyr_hel_Δlatch; the K_d value is 0.19 ± 0.02 μM.

are consistent with ATP binding as a trigger for switching rgyr_hel into a high affinity state for ssDNA, and phosphate release as a trigger for the switch back to a low affinity state for ssDNA. Interestingly, the picture is different for dsDNA. The affinity for dsDNA is also highest in the ADP·BeF$_x$-state (K_d = 0.072 μM), but in the ADP·MgF$_x$-state (K_d = 2.2 μM) it already returns to the lower affinity as observed for the ADPNP- and ADP-states. Thus, in complex with dsDNA the switch towards higher affinity is also coupled to ATP binding, but the switch back to the low affinity state for dsDNA already occurs upon ATP hydrolysis, as evidenced by the 20-fold reduction in dsDNA affinity from the ADP·BeF$_x$-state to the ADP·MgF$_x$-state. Overall, in the nucleotide cycle the high preference of nucleotide-free rgyr_hel for ssDNA over dsDNA (20-fold) is lost upon ATP binding. The ADPNP- and ADP·BeF$_x$-states show only a small (1.6- to 2.4-fold) preference for ssDNA or dsDNA. After ATP-hydrolysis, the high ssDNA preference is regained (27-fold for the ADP·MgF$_x$-state, 13-fold for the ADP-state). All K_d values are summarized in Table 2.

The nucleotides affinities (Table 1) have been determined using mant-nucleotides, and unlabeled DNA. In contrast, DNA affinities (Table 2) have been determined using DNA end-labeled with fluorescein and unmodified adenine nucleotides. As a consequence, comparison has to be performed with

Table 2 DNA binding in different states of the nucleotide cycle

DNA	Nucleotide	$K_{d,DNA}$/μM
ssDNA	—	0.20 ± 0.01[a]
	ADPNP	0.46 ± 0.03[a]
	ADP·BeF$_x$	0.044 ± 0.003
	ADP·MgF$_x$	0.082 ± 0.007
	ADP	0.28 ± 0.01[a]
dsDNA	—	3.9 ± 0.6[a]
	ADPNP	0.19 ± 0.03[a]
	ADP·BeF$_x$	0.072 ± 0.004
	ADP·MgF$_x$	2.2 ± 0.3
	ADP	3.7 ± 0.5[a]
ss/dsDNA junction	—	0.081 ± 0.006
	ADPNP	0.21 ± 0.02
	ADP·BeF$_x$	0.026 ± 0.004
	ADP·MgF$_x$	0.57 ± 0.09
	ADP	0.24 ± 0.5
Bubble-DNA	—	0.069 ± 0.012

[a] From ref. 11.

care, and we therefore limit the comparison to DNA affinities in different nucleotide states, or nucleotide affinities in different DNA-bound states, *i.e.* to data obtained with the same set of modifications. These data point towards a strong to moderate positive coupling of ADPNP-binding, and a moderate coupling of ADP·BeF$_x$-binding to ssDNA and dsDNA binding, both reflecting nucleotide states before ATP hydrolysis. In contrast, the binding of ADP·MgF$_x$ and ADP shows no or slightly negative coupling to DNA binding. Consequently, DNA binding to rgyr_hel favors progression through the nucleotide cycle before ATP hydrolysis by increasing nucleotide affinities, and after hydrolysis by promoting nucleotide release.

Conformational changes in the helicase-like domain

The results on nucleotide and DNA binding to rgyr_hel and their coupling support and refine the previously established function of rgyr_hel as a nucleotide-dependent switch.[8,11] The picture that emerges for ssDNA binding throughout the nucleotide cycle resembles the catalytic cycle of DEAD box proteins (reviewed in ref. 16), the largest family of SF2 helicases. Presumably, the main features of these proteins are also characteristic of rgyr_hel, despite the severe deviations in the sequence of conserved motifs. A conformational change in the helicase-like domain upon nucleotide and DNA binding has been proposed earlier as a first step in the catalytic cycle of reverse gyrase.[6] To investigate the conformational cycle of rgyr_hel, we introduced cysteines into the H1 (S169C) and H2 domains (F332C or S341C, Fig. 4) of rgyr_hel, and performed smFRET experiments with donor/acceptor labeled rgyr_hel. In the absence of DNA, the predominant species is a low FRET efficiency state ($E_{FRET} \approx 0.1$) in the nucleotide-free state, and in the presence of ADPNP, ADP·BeF$_x$, ADP·MgF$_x$ and ADP for rgyr_hel_S169C/F332C (Fig. 5), consistent with an open conformation throughout the nucleotide cycle. Similar results are obtained with rgyr_hel_S169C/S341C (not shown). We have recently determined crystal structures of rgyr_hel (lacking the latch) in five different conformations,[17] and the FRET efficiency observed here for rgyr_hel in all nucleotide states is in agreement with the C_β–C_β distances in these structures. The structures point towards a large inter-domain flexibility, which may explain the broad smFRET histograms. In the following, we therefore restrict the interpretation of the smFRET data to qualitative changes in the main FRET efficiencies. We next studied the influence of DNA on the conformation of rgyr_hel throughout the nucleotide cycle (Supplementary Figure, ESI†). In the presence of ssDNA (Fig. 6A), two predominant species with low and high FRET efficiencies are observed in the ADPNP-state. In contrast, the ADP·BeF$_x$-bound state of rgyr_hel is mainly in a high FRET state, indicative of a closure of the cleft separating H1 and H2. In the presence of dsDNA (Fig. 6B), rgyr_hel is mainly in a high FRET state with ADPNP and ADP·BeF$_x$. In the ADP·MgF$_x$-state, rgyr_hel shows a low FRET efficiency in the presence of either ssDNA or dsDNA (Fig. 6B and C), indicative of re-opening of the inter-domain cleft upon ATP hydrolysis. Thus, the helicase-like domain is "switched on" by a closure of the inter-domain cleft between H1 and H2 before ATP-hydrolysis, similar to DEAD box proteins.[14] However, it is already "switched off" when ATP is hydrolyzed, and returns to the open conformation in the product state (as mimicked by ADP·MgF$_x$). This is in contrast to DEAD box proteins that return to the open conformation only after phosphate release,[13] a step that is coupled to a release of the RNA bound to the helicase core.

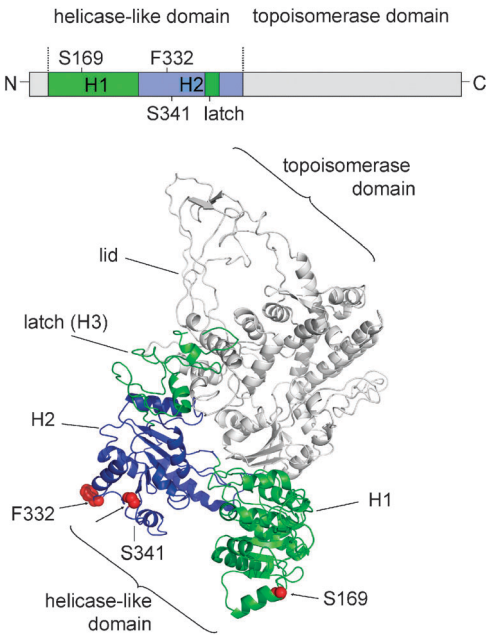

Fig. 4 Donor/acceptor-labeling for smFRET experiments. Scheme of *T. maritima* reverse gyrase, and homology model based on the crystal structure of *Archaeoglobus fulgidus* reverse gyrase,[6] (PDB-ID 1gku). H1 of the helicase-like domain is depicted in green, H2 in blue. The latch domain is shown in green, and the topoisomerase domain in gray. Cysteines were introduced at positions 169 (S169C) in the H1 domain, and at positions 332 (F332C) or 341 (S341C), highlighted in space-filling representation (red).

Rgyr_hel interaction with a ss/dsDNA junction

It has been suggested that reverse gyrase senses ssDNA regions, and that ssDNA sensing is the basis for its protective effect on DNA at high temperatures.[3,4] In-line with this suggestion, it has been demonstrated previously that reverse gyrase more efficiently supercoils DNA plasmids containing a single-stranded bubble.[4] These findings are supported by our results on DNA binding to rgyr_hel that demonstrate its high preference for ssDNA in the nucleotide-free, ADP·MgF$_x$- and ADP-bound states. However, we have shown above that this preference is tremendously reduced in the ADPNP- and ADP·BeF$_x$-bound states. In an intact DNA molecule, a single-stranded region always occurs in context of a ss/dsDNA junction, and we therefore measured the affinity of rgyr_hel for a 20/60 bp ss/dsDNA junction, and for a 57 bp DNA containing an unpaired region of 15 nucleotides (bubble-DNA) (Fig. 3C). The affinities for both DNAs were similar (K_d = 0.081 μM *vs.* 0.069 μM, respectively), and higher than the affinity for either ssDNA or dsDNA, pointing towards a direct interaction of rgyr_hel with the ss/dsDNA junction. The

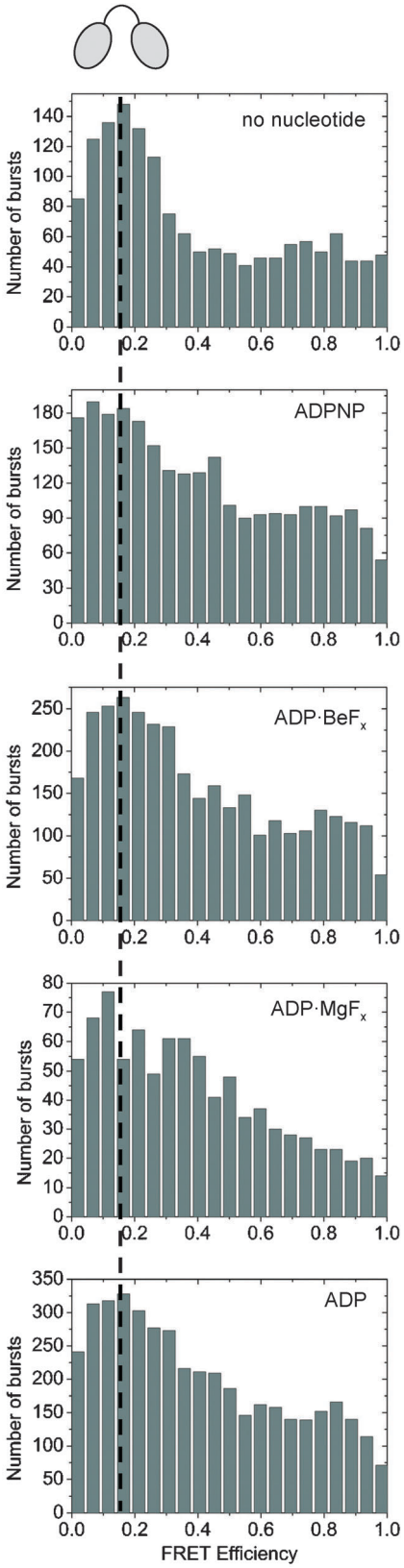

Fig. 5 Conformation of the helicase-like domain in the absence of DNA. smFRET histograms of donor/acceptor-labeled rgyr_hel S169C/F332C in the absence of DNA in all nucleotide states. The main FRET efficiency of ~0.1 is indicative of an open cleft between the H1 and H2 domains.

20/60 ss/dsDNA contains only one single-stranded region at each junction, whereas the bubble-DNA contains two forks with two single-stranded regions, yet the affinities of rgyr_hel for these substrates were similar, indicating that gyr_hel interacts with only one of the two ssDNA regions present in the bubble. For reasons of simplicity, all measurements in the presence of nucleotides were thus performed with the 20/60 ss/dsDNA substrate (Fig. 3C).

Compared to the nucleotide-free state, the affinity of rgyr_hel for the ss/dsDNA junction is reduced 2.6-fold upon addition of ADPNP to K_d = 0.21 μM, and becomes virtually the same as for dsDNA, suggesting that rgyr_hel now engages in contacts with the dsDNA region of this DNA substrate. In the ADP·BeF$_x$-bound state, the K_d value decreases to 0.026 μM, and the preference for the ss/dsDNA junction is thus regained. After ATP hydrolysis, in the ADP·MgF$_x$- and ADP-bound states, the affinity for the ss/dsDNA junction decreases (K_d = 0.57 μM and 0.24 μM), and is now 10-fold higher than for dsDNA, but within two-fold of the affinity for ssDNA, indicating that rgyr_hel contacts the ssDNA region in these states of the nucleotide cycle. Overall, our data thus indicate that rgyr_hel binds to different regions of the ss/dsDNA junction at individual steps in the nucleotide cycle.

Effect of phosphate

DEAD-box helicases have been shown to adopt a closed conformation upon RNA and ATP binding, and return to the open conformation after phosphate release,[13,14,18] the rate-limiting step in their catalytic cycle.[19] To address the difference between our results with rgyr_hel and with DEAD box proteins, the effect of phosphate on binding of rgyr_hel to DNA was further analyzed by performing DNA titrations in a phosphate buffer (12 mM phosphate pH 7.5, 137 mM NaCl, 27 mM KCl, 10 mM $MgCl_2$) (Fig. 3D). Low phosphate concentrations (<1.4 mM) led to the dissociation of DNA from a rgyr_hel/ssDNA complex (not shown), in agreement with a general screening effect of anions on electrostatic interactions involved in DNA binding. At the higher phosphate concentration in the phosphate buffer, however, the affinity of rgyr_hel for ssDNA is increased 10-fold compared to the affinity in Tris/HCl buffer. A smaller increase in affinity was observed for dsDNA (4-fold). In order to distinguish whether the effect of phosphate on DNA affinity is a consequence of specific binding at the nucleotide binding site, the same measurement was repeated with a mutant lacking the latch region, rgyr_hel_Δlatch, that shows uncoupled DNA and nucleotide binding.[11] Here, the increase in affinity for ssDNA in phosphate buffer was only 2-fold, supporting that the effect of the phosphate ion on DNA binding may reflect an interaction in the nucleotide binding site. As these effects are only observed at high phosphate concentrations, they are consistent with a low affinity for phosphate at the nucleotide binding site, and thus a high off-rate. Under physiological conditions, rapid phosphate release after ATP hydrolysis can be inferred, which is in-line with our observation that ATP hydrolysis is the rate-limiting step in the nucleotide cycle. Phosphate binding to rgyr_hel

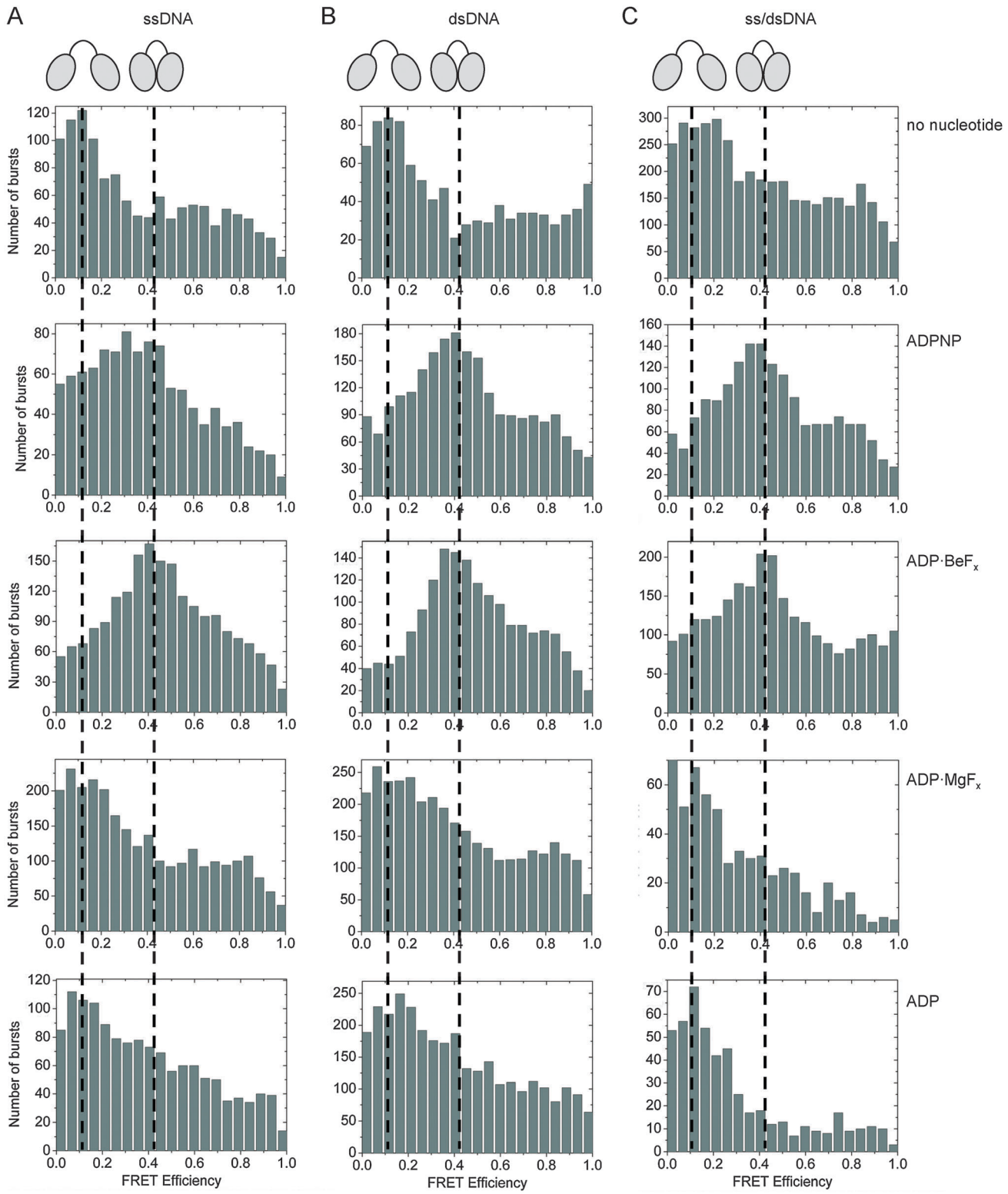

Fig. 6 Conformational changes in the helicase-like domain in the presence of DNA substrates. (A) FRET histograms for rgyr_hel S169C/F332C in the presence of ssDNA, all nucleotide states (no nucleotide, ADPNP, ADP·BeF$_x$, ADP·MgF$_x$, ADP, from top to bottom). (B) FRET histograms for rgyr_hel S169C/F332C in the presence of dsDNA, all nucleotide states (no nucleotide, ADPNP, ADP·BeF$_x$, ADP·MgF$_x$, ADP, from top to bottom). (C) FRET histograms for rgyr_hel S169C/F332C in the presence of ss/dsDNA junction, all nucleotide states (no nucleotide, ADPNP, ADP·BeF$_x$, ADP·MgF$_x$, ADP, from top to bottom). The DNA concentration was 0.5 mM. The nucleotide concentrations were 1 mM (ADP·BeF$_x$, ADP·MgF$_x$, ADP), and 5 mM (ADPNP). The FRET efficiencies for open (~0.1) and closed conformations (~0.4) are indicated by vertical lines, and the conformations are depicted as cartoons. The corresponding data for rgyr_hel_S169C/S341C are shown in the Supplementary Figure (ESI†).

thus selectively increases its affinity for ssDNA, presumably by binding to the nucleotide binding site. The similar DNA affinities in phosphate buffer and with ADP·MgF_x validate that ADP·MgF_x indeed acts as a product state analog.

Conformations in the presence of the ss/dsDNA junction

When we performed smFRET experiments with rgyr_hel in the all nucleotide states in the presence of the ss/dsDNA junction (Fig. 6C), we observed a high FRET state for the ADPNP and ADP·BeF_x-complexes, indicative of the closure of the inter-domain cleft with ATP binding, and a low FRET state for the ADP·MgF_x- and ADP-complexes, again consistent with re-opening of the inter-domain cleft upon ATP hydrolysis. Thus, while rgyr_hel is a conformational switch similar to DEAD box proteins, the inter-domain cleft re-opens already upon ATP hydrolysis, the rate-limiting step in the nucleotide cycle of rgyr_hel. ATP hydrolysis and re-opening are coupled to a loss in dsDNA affinity.

Discussion

Here we have reported equilibrium dissociation constants for all relevant nucleotide- and DNA-bound states during the rgyr_hel catalytic cycle, revealing an intricate coupling between binding of nucleotides and ssDNA, dsDNA, and ss/dsDNA junctions. In addition, we have monitored a conformational change in the helicase-like domain during the catalytic cycle, and show that the cleft between the H1 and H2 domains closes upon binding of ATP and DNA, and re-opens upon ATP hydrolysis, irrespective of the nature of the DNA bound. Our results demonstrate that the helicase-like domain of reverse gyrase changes its affinities for different DNA substrates in a nucleotide-dependent manner, and provide a framework for understanding reverse gyrase mechanism and the contributions of the helicase-like domain for the positive supercoiling of DNA.

How can the thermodynamic data be related to the catalytic cycle of reverse gyrase?

Different models for the cooperation of the helicase-like and the topoisomerase domain in positive supercoiling by reverse gyrase have been put forward.[20] Originally, it was suggested that the topoisomerase domain selectively relaxes negative supercoils accumulating behind the helicase-like domain translocating on DNA,[5] leading to the net effect of positive supercoiling. However, this model would predict a translocase activity for the helicase-like domain and reverse gyrase that has not been detected experimentally. In a second model, suggesting a segregation of DNA in topological domains of unwound and positively supercoiled domains, and rewinding of the separated strands by reverse gyrase, it is unclear how this topological separation may occur. Third, it has been suggested by inference from the homology of the helicase-like domain to SF2 helicases that changes in binding affinities for ssDNA and dsDNA in the helicase-like domain that are coupled to strand passage in the topoisomerase domain may be the basis for reverse gyrase function, but the assignment of nucleotide states and DNA affinities remained unclear.[20,21] Our thermodynamic characterization of nucleotide- and DNA binding to the helicase-like domain of reverse gyrase,[8,11] (this work) supports this model, and allows to assign the nucleotide states and DNA affinities, and to correlate them with the conformation of the helicase-like domain (Fig. 7).

Reverse gyrase has been described as an enzyme that senses single-stranded DNA regions at high temperature and protects cellular DNA from temperature-induced damage.[3,4] Its activity thus most likely starts in or next to the single-stranded regions it binds to. Entering the catalytic cycle, nucleotide-free rgyr_hel strongly binds to ssDNA and to the ss/dsDNA junctions that will be generated by local DNA melting at high temperatures, leading to the initiation of positive supercoiling by reverse gyrase at these junctions. After ATP binding, mimicked by the non-hydrolyzable analog ADPNP, rgyr_hel interacts with dsDNA, which may contribute to DNA binding even in the absence of single-stranded regions. Binding of DNA and ADPNP is coupled to a closure of the inter-domain cleft separating H1 and H2. In a subsequent step closer to ATP hydrolysis, as reflected by the ADP·BeF_x state, all DNAs are bound to rgyr_hel with similar, high affinities. In this state, the cleft between H1 and H2 remains closed. The generally very high DNA affinities of rgyr_hel in the ADP·BeF_x-state will trap reverse gyrase on the DNA. In this state, strong preferences for DNA are transiently lost, possibly facilitating inter-conversion and thus structural changes in the DNA substrate, but a small preference for ssDNA and ss/dsDNA junctions remains, and reverse gyrase thus most likely remains on the single-stranded and junction regions. The preference of rgyr_hel for ssDNA and ss/dsDNA junctions suggests that it stabilizes junctions already present, and may even promote local double-strand destabilization during ATP binding if no junction was present at this stage. The energetic differences between the respective ternary complexes (Fig. 7A), with a $\Delta\Delta G^0$ value of 12 kJ mol^{-1} ($\Delta G^0_{rgyr\_hel–ADPNP–dsDNA} = -63$ kJ mol^{-1}, $\Delta G^0_{rgyr\_hel–ADP·BeFx–ss/dsDNA} = \Delta G^0_{rgyr\_hel–ADP.BeFx–ssDNA} = -75$ kJ mol^{-1}), suggest that rgyr_hel in principle may provide energy for local disruption of 2–3 base pairs[22,23] in this step. After ATP hydrolysis, in the ADP·MgF_x- or ADP·P_i-state, rgyr_hel retains the high affinity for ssDNA, whereas the affinity for dsDNA is reduced, and the enzyme thus preferentially binds to ssDNA. In this step of the nucleotide cycle, the cleft between H1 and H2 re-opens, and product dissociation from the open cleft will be facilitated. Upon phosphate release, rgyr_hel maintains the open conformation, and returns to a low affinity-state for ssDNA in the ADP-state, while the dsDNA affinity is not affected. At the end of the nucleotide cycle, in the ADP (and nucleotide-free) state, rgyr_hel thus again shows a high affinity and high preference for ssDNA. In the ssDNA-bound state, the ADP affinity is reduced, allowing for nucleotide exchange presumably while the enzyme remains bound to the DNA. Thereby, processivity of reverse gyrase may be ensured. At the same time, the helicase-like domain will also sense when the ssDNA region has disappeared due to positive supercoiling, and could provide the signal that reverse gyrase has completed its task. The relevant DNA complexes in the catalytic cycle of rgyr_hel are summarized in Fig. 7B.

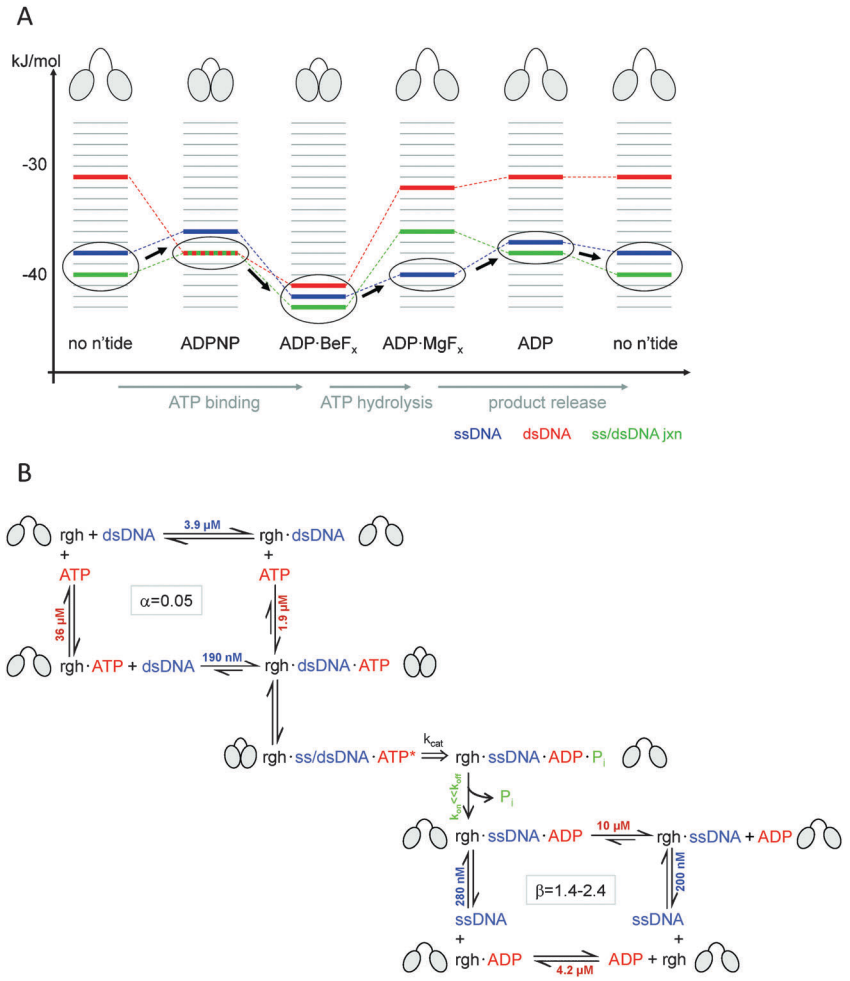

Fig. 7 DNA interactions in the nucleotide cycle of rgyr_hel and their coupling to conformational changes. (A) Energetic scheme for DNA interactions in the nucleotide cycle. Binding energies for different DNAs are depicted in kJ mol^{-1} for all nucleotide states in the catalytic cycle of rgyr_hel. Red lines correspond to dsDNA, blue lines to ssDNA, and green lines to the ss/dsDNA junction. The conformation of the inter-domain cleft between H1 and H2 is indicated by the cartoon at the top. Black ovals and arrows indicate the predominant DNA complex for each nucleotide state, and the progression through the catalytic cycle. (B) Scheme of relevant DNA complexes during the catalytic cycle of rgyr_hel (rgh). Dissociation constants and coupling factors are indicated. The cartoons indicate the conformational state in each complex. In the ATP state, rgyr_hel binds most tightly to dsDNA. Binding of ATP and DNA is strongly coupled (α = 0.05, corresponding to a mutual 20-fold increase in affinity), and lead to a closure of the cleft between the two RecA domains. In a state closer to ATP hydrolysis (indicated by a star), the ss/dsDNA junction is bound with highest affinity. ATP hydrolysis re-opens the cleft between the RecA domains, and rgyr_hel now exhibits a strong preference for ssDNA. ssDNA and ADP dissociations show slight anti-cooperativity (β = 1.4–2.4, corresponding to a 1.4–2.4-fold mutual decrease in affinity).

Similarities and differences to other helicase cores: a possible role for the latch?

It has previously been suggested that a conformational change in the helicase-like domain of reverse gyrase may initiate a movement of the latch, and thereby release the topoisomerase domain for strand passage.[6] Our smFRET data demonstrate that such a change in conformation indeed occurs in rgyr_hel, and provides first experimental evidence for this model. Rgyr_hel undergoes a cycle of nucleotide-dependent conformational changes that are reminiscent of the catalytic cycle of DEAD box proteins. These parallels may point towards a similar communication between the helicase motifs in rgyr_hel as in DEAD box proteins, despite the large differences in sequence. In-line with these similarities, mutations in the conserved SF2 motifs in the helicase-like domain of reverse gyrase have proven deleterious for positive DNA supercoiling.[24] It is currently unclear whether the closure of the inter-domain cleft leads to a similar local destabilization of DNA duplexes as for DEAD box proteins. The closure of the inter-domain cleft in rgyr_hel is paralleled by an increase in affinity for ssDNA, suggesting that this conformational change generates an ssDNA binding site. However, in DEAD box proteins re-opening of this cleft is coupled to phosphate release, a rate-limiting step in the catalytic cycle.[19] In contrast, in rgyr_hel, re-opening of the cleft already occurs upon ATP hydrolysis, which is the rate-limiting step in the rgyr_hel nucleotide cycle. In the post-hydrolysis state, rgyr_hel retains an increased affinity and preference for ssDNA, despite the open conformation of the inter-domain cleft. In contrast to ssDNA binding, dsDNA binding is directly coupled to the conformational change: on

closure of the cleft between H1 and H2, the dsDNA affinity increases (20-fold), and a reciprocal (30-fold) decrease in affinity is observed upon re-opening. We have previously shown that the latch, an insertion into the H2 domain of rgyr_hel, contributes to DNA binding.[11] A deletion of the latch causes a loss of affinity for ssDNA and dsDNA in the nucleotide-free and in the ADPNP state, and for dsDNA in the ADP states, pointing towards specific contributions of the latch to DNA binding at each step of the nucleotide cycle.[11] It is possible that differential contributions of the latch during the nucleotide cycle could account for the observed discrepancies between ssDNA affinity and the conformation of the inter-domain cleft in the helicase-like domain. Future studies will have to address the effect of the latch on DNA binding throughout the nucleotide cycle and its suggested role in guiding DNA during strand passage in the supercoiling reaction.

Conclusion

We have shown that the interaction of the helicase-like domain with DNA during its nucleotide cycle is modulated *via* conformational changes, similar to the switching between open and closed conformers of DEAD box proteins. The modulation of interactions with DNA during the progression through the nucleotide cycle renders the helicase-like domain a central module for the function reverse gyrase. Coordination of conformational changes in the helicase-like domain with strand passage in the topoisomerase domain may guide positive supercoiling. Our results provide a basis for understanding mechanistically how helicase-like domains can be harnessed as modules to support a DNA topoisomerase, and to generate a novel function such as positive supercoiling of DNA.

Abbreviations

ADPNP	5′-adenylyl-β,γ-imidodiphosphate
mant	2′(3′)-*O*-(*N*-methyl-anthraniloyl)
FRET	Förster resonance energy transfer
rgyr	reverse gyrase
rgyr_hel	helicase-like domain of rgyr
rgyr_hel_Δlatch	rgyr_hel lacking the latch domain
SF 2	helicase superfamily 2

Acknowledgements

This work was supported by the Swiss National Science Foundation.

References

1 A. Kikuchi and K. Asai, *Nature*, 1984, **309**, 677–681.
2 P. Forterre, *Trends Genet.*, 2002, **18**, 236–237.
3 M. Kampmann and D. Stock, *Nucleic Acids Res.*, 2004, **32**, 3537–3545.
4 T. S. Hsieh and J. L. Plank, *J. Biol. Chem.*, 2006, **281**, 5640–5647.
5 F. Confalonieri, C. Elie, M. Nadal, C. de La Tour, P. Forterre and M. Duguet, *Proc. Natl. Acad. Sci. U. S. A.*, 1993, **90**, 4753–4757.
6 A. C. Rodriguez and D. Stock, *EMBO J.*, 2002, **21**, 418–426.
7 A. C. Declais, J. Marsault, F. Confalonieri, C. B. de La Tour and M. Duguet, *J. Biol. Chem.*, 2000, **275**, 19498–19504.
8 Y. Del Toro Duany, S. P. Jungblut, A. S. Schmidt and D. Klostermeier, *Nucleic Acids Res.*, 2008, **36**, 5882–5895.
9 J. W. Dolan, N. F. Marshall and J. P. Richardson, *J. Biol. Chem.*, 1990, **265**, 5747–5754.
10 A. J. Dombroski and T. Platt, *Proc. Natl. Acad. Sci. U. S. A.*, 1988, **85**, 2538–2542.
11 A. Ganguly, Y. Del Toro Duany, M. G. Rudolph and D. Klostermeier, *Nucleic Acids Res.*, 2010, DOI: 10.1093/nar/gkq1048.
12 T. Hiratsuka, *Biochim. Biophys. Acta*, 1983, **742**, 496–508.
13 R. Aregger and D. Klostermeier, *Biochemistry*, 2009, **48**, 10679–10681.
14 B. Theissen, A. R. Karow, J. Kohler, A. Gubaev and D. Klostermeier, *Proc. Natl. Acad. Sci. U. S. A.*, 2008, **105**, 548–553.
15 S. P. Jungblut and D. Klostermeier, *J. Mol. Biol.*, 2007, **371**, 197–209.
16 M. Hilbert, A. R. Karow and D. Klostermeier, *Biol. Chem.*, 2009, **390**, 1237–1250.
17 Y. del Toro Duany, D. Klostermeier and M. G. Rudolph, unpublished.
18 A. R. Karow and D. Klostermeier, *Nucleic Acids Res.*, 2009, **37**, 4464–4471.
19 A. Henn, W. Cao, D. D. Hackney and E. M. De La Cruz, *J. Mol. Biol.*, 2008, **377**, 193–205.
20 T. S. Hsieh and J. L. Plank, *J. Biol. Chem.*, 2009, **284**, 30737–30741.
21 T. S. Hsieh and C. Capp, *J. Biol. Chem.*, 2005, **280**, 20467–20475.
22 M. T. Record, S. J. Masur, P. Melancon, J. H. Roe, S. L. Shaner and L. Unger, *Annu. Rev. Biochem.*, 1981, **50**, 997–1024.
23 Lohman, *Annu. Rev. Biochem.*, 1996, **65**, 169–241.
24 C. Bouthier de la Tour, L. Amrani, R. Cossard, K. Neuman, M. C. Serre and M. Duguet, *J. Biol. Chem.*, 2008, **283**, 27395–27402.

Chapter 4. Article

The conformational flexibility of the helicase-like domain from *Thermotoga maritima* reverse gyrase is restricted by the topoisomerase domain.

In this report, the isolated helicase-like domain lacking the latch region has been successfully crystallized in five different conformations. A high flexibility of the linker joining the two RecA folds was detected, although the conformations were not random, but clustered in two main groups. In the absence of the topoisomerase domain the H1 und H2 domains seem to have minimal interactions that hold them together, and only the simultaneous presence of DNA and nucleotide can align them in a fixed conformation. Nevertheless, smFRET data of the same construct reveals that all these conformations are allowed in solution. Here we provide structures revealing the most details of this domain to date. Also the structure of a complex with ADP reveals that the helicase-like domain binds nucleotides using the same network of interactions with the ligand as the other members of the DEAD-box superfamily, although the consensus sequences of the signature motifs strongly vary from the rest. Our structures also revealed a different structure of a motif putatively involved in DNA binding, compared to the structure of *A. fulgidus* reverse gyrase.

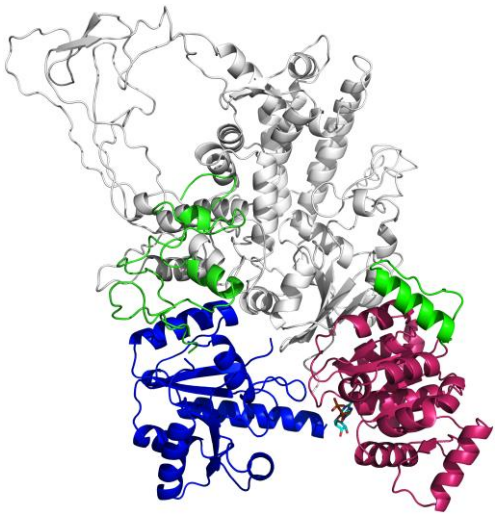

Structure of *T. maritima* reverse gyrase, with the topoisomerase domain generated from homology modeling and the helicase-like domain from the solved crystal structures.

BIOCHEMISTRY
including biophysical chemistry & molecular biology

ARTICLE

pubs.acs.org/biochemistry

The Conformational Flexibility of the Helicase-like Domain from *Thermotoga maritima* Reverse Gyrase Is Restricted by the Topoisomerase Domain

Yoandris del Toro Duany,[†] Dagmar Klostermeier,[*,†,‡] and Markus G. Rudolph[§]

[†]Biozentrum, Department of Biophysical Chemistry, University of Basel, Klingelbergstrasse 70, CH-4056 Basel, Switzerland

[‡]Institute for Physical Chemistry, University of Muenster, Correnssstrasse 30, D-48149 Muenster, Germany

[§]Hoffmann-La Roche AG, Grenzacher Strasse 124, CH-4070 Basel, Switzerland

Supporting Information

ABSTRACT: Reverse gyrase is the only enzyme known to introduce positive supercoils into DNA. Positive supercoiling is achieved by the functional cooperation of a helicase-like and a topoisomerase domain. The isolated helicase-like domain is a DNA-stimulated ATPase, and the isolated topoisomerase domain can relax supercoiled DNA. In the context of reverse gyrase, these individual activities are suppressed or attenuated. The helicase-like domain of *Thermotoga maritima* reverse gyrase is a nucleotide-dependent conformational switch that binds DNA and ATP cooperatively. It provides a nucleotide-dependent DNA-binding site to reverse gyrase and thus serves as a valuable model for the investigation of the effect of nucleotides on DNA processing by reverse gyrase that is key to its supercoiling activity. To improve our understanding of the structural basis for the functional cooperation of a helicase domain with a DNA topoisomerase, we have determined the structures of the isolated helicase-like domain of *T. maritima* reverse gyrase in five different conformations. Comparison of these structures reveals extensive domain flexibility in the absence of conformational restrictions by the topoisomerase that is consistent with single-molecule Förster resonance energy transfer experiments presented here. The structure of the first ADP-bound form provides novel details about nucleotide binding to reverse gyrase. It demonstrates that reverse gyrases use the canonical nucleotide binding mode common to superfamily 2 helicases despite large deviations in the conserved motifs. A characteristic insert region adopts drastically different structures in different reverse gyrases. Counterparts of this insert region are located at very different positions in other DNA-processing enzymes but may point toward a general role in DNA strand separation.

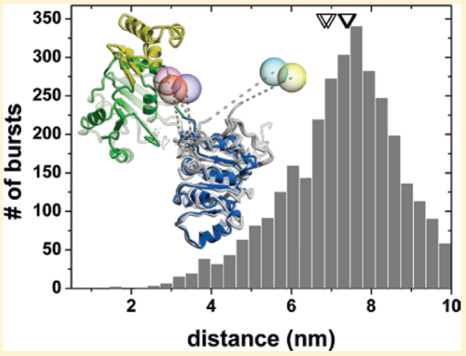

The degree of DNA supercoiling affects central cellular processes such as replication, recombination, and repair.[1] It is regulated by DNA topoisomerases, an enzyme class that catalyzes the interconversion of different topoisomers. Bacterial gyrases introduce negative supercoils in an ATP-dependent process[2] and thereby relieve topological stress ahead of the replication fork. Reverse gyrases catalyze the inverse reaction, namely the introduction of positive supercoils into DNA, in an ATP-dependent fashion. These enzymes are unique to thermophiles and hyperthermophiles where they are thought to exert protective functions for DNA at high temperatures.[3,4] Reverse gyrases share a unique modular structure that combines an N-terminal helicase-like domain with a C-terminal topoisomerase domain.[5] The topoisomerase domain is homologous to prokaryotic and eukaryotic type IA DNA topoisomerases. It has been shown to relax negatively supercoiled DNA in vitro,[6] but this activity is suppressed in reverse gyrase. The helicase-like domain is divided into two subdomains, termed H1 and H2, that both bear similarity to the RecA fold[7] (Figure 1A). H1 and H2 harbor the signature motifs of superfamily 2 (SF2) helicases necessary for ATP and DNA binding, though their sequences substantially differ from the SF2 consensus.[7] The critical role of the helicase-like domain for reverse gyrase activity has been demonstrated by the deleterious effect of mutations in the helicase motifs.[8] The so-called latch domain (Figure 1A), an insertion in H2, allows for communication between the helicase and topoisomerase domains.[9,10] The latch is required for positive DNA supercoiling by *Thermotoga maritima* reverse gyrase, but not for nucleotide binding and hydrolysis.[10]

The helicase-like domain of *T. maritima* reverse gyrase is a nucleotide-dependent conformational switch that binds DNA and ATP with positive cooperativity[11,12] and provides a nucleotide-dependent DNA-binding site to reverse gyrase. The DNA binding properties of the different nucleotide states are masked in the context of reverse gyrase because of additional DNA binding sites.[10,11] The isolated helicase-like domain thus serves as a valuable model for investigation of the effect of nucleotides on

Received: February 15, 2011
Revised: May 10, 2011

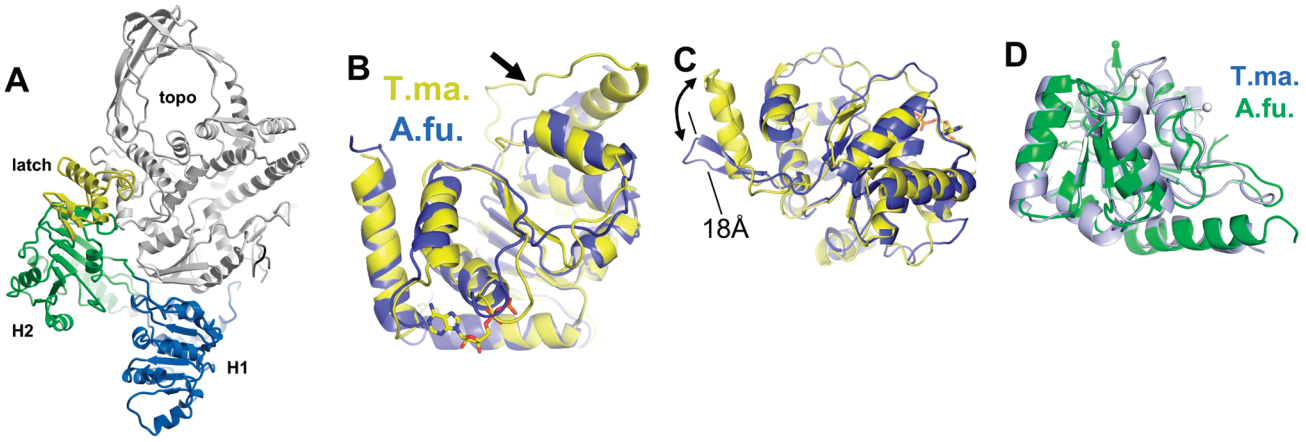

Figure 1. Overview of reverse gyrase. (A) Structure of reverse gyrase from *A. fulgidus* (PDB entry 1GKU). The topoisomerase domain is colored gray. The helicase-like domain is composed of the two RecA-like subdomains H1 (blue) and H2 (green). The latch domain (yellow) is inserted in H2 and allows communication between the helicase and topoisomerase domains. In this study, the isolated helicase-like domain without the latch (rgyr_hel_Δlatch) is used to assess domain flexibility and nucleotide binding. (B) Superposition of H1 of *T. maritima* rgyr_hel_Δlatch (yellow) and *A. fulgidus* (blue) reverse gyrase. The arrow denotes an insert region that varies strongly in sequence length. In *A. fulgidus*, this region forms a β-hairpin, but in *T. maritima*, it is an α-helix−loop motif. (C) View rotated ∼90° about the *z*-axis relative to panel B highlighting the strong deviation of the insert regions. (D) Superposition of H2. *A. fulgidus* reverse gyrase (green) depicted without the latch region (normally inserted at the green sphere). The gray spheres denote a disordered loop in *A. fulgidus* reverse gyrase that could be traced in the *T. maritima* enzyme (blue).

DNA processing by reverse gyrase that is at the heart of its positive supercoiling activity.

The structures of *Archaeoglobus fulgidus* reverse gyrase in the apo and ADPNP-bound forms[7] are the only structural information on reverse gyrases to date. To provide a structural basis for understanding the cooperation of the helicase-like domain with the topoisomerase domain in positive supercoiling, we determined the crystal structure of the helicase-like domain of *T. maritima* reverse gyrase, an enzyme that has been extensively characterized biochemically.[10−13] Three crystal structures with five different conformations of the *T. maritima* reverse gyrase helicase-like domain without the latch domain (rgyr_hel_Δlatch) show large variations in H1 and H2 domain juxtaposition, consistent with single-molecule Förster resonance energy transfer (FRET) experiments.[12] Interestingly, the different conformations cluster around two preferred conformations, none of which resembles the conformation imposed by the topoisomerase domain in full-length reverse gyrase. The structure of the ADP−Mg^{2+} complex of rgyr_hel_Δlatch reveals significant differences and novel features compared to the *A. fulgidus* reverse gyrase−ADPNP complex and offers new insight into the functional communication between SF2 motifs in reverse gyrases. An insert region that has counterparts in other DNA-processing enzymes can adopt very different structures among reverse gyrases and may play an important role in DNA strand separation.

MATERIALS AND METHODS

The helicase-like domain lacking the latch (rgyr_hel_Δlatch) was constructed and purified as described in detail in ref 10. Three diffraction-quality crystal forms for rgyr_hel_Δlatch were obtained at 25 °C using the sitting drop vapor diffusion setup by 1:1 (v/v) mixing of 20 mg/mL protein in 50 mM Tris-HCl (pH 7.5), 0.2 M NaCl, 10 mM $MgCl_2$, 10 mM $Zn(OAc)_2$, and 2 mM β-mercaptoethanol with reservoir solutions consisting of 0.2 M magnesium formate and 20% PEG 3350 (PDB entry 3OIY), 0.2 M Li_2SO_4 and 20% PEG 3350 (PDB entry 3P4X), and 0.1 M HEPES-NaOH (pH 7.5) and 30% PEG 300 (PDB entry 3P4Y). Crystals were cryo-protected with paraffin oil, mounted in an arbitrary orientation, and data were collected at Swiss Light Source beamlines PX-II and PX-III. Intensities were integrated with XDS[14] and scaled with SCALA (PDB entries 3P4X and 3OIY)[15] or SADABS (PDB entry 3P4Y; Bruker). Systematic absences identified space group $P2_12_12_1$ for two nonisomorphous data sets representing apo and ADP-bound structures (two molecules per asymmetric unit), and rare space group *P*2 for a third crystal form (one molecule per asymmetric unit). Phasing and refinement of the apo-$P2_12_12_1$ form (PDB entry 3OIY) were described previously,[10] and the H1 and H2 domains of this structure were used as search models for phasing of the other two data sets by molecular replacement using PHASER.[16] Models were built in COOT[17] and refined with PHENIX[18] using separate TLS descriptions for the H1 and H2 domains. Data collection and refinement statistics are listed in Table 1. The coordinates and structure factors have been deposited in the Protein Data Bank (PDB) (entries 3OIY, 3P4X, and 3P4Y). Figures were created with Bobscript,[19] Raster3D,[20] Pymol (http://www.pymol.org), and ESPript.[21] Single-molecule FRET experiments were performed with rgyr_hel_Δlatch_S169C/F332C labeled with AlexaFluor 488 (donor) and tetramethylrhodamine (acceptor) using a home-built confocal microscope.[22,23] The labeled protein exhibited DNA-stimulated ATPase activity similar to that of the wild type. ATPase hydrolysis was monitored in a coupled enzymatic assay as described previously.[13] FRET data analysis was performed as described previously.[23,24]

RESULTS

Crystals of the helicase-like domain including the latch were obtained but did not diffract X-rays. The latch does not affect the intrinsic ATPase activity of the helicase-like domain and has little effect on nucleotide affinity.[10] A latch deletion mutant (rgyr_hel_Δlatch) still shows DNA-stimulated ATPase activity and thus constitutes a valid model for structural studies. This construct

dx.doi.org/10.1021/bi200236a |*Biochemistry* XXXX, XXX, 000–000

Table 1. Data Collection, Phasing, and Refinement Statistics

	apo, 3OIY[a]	ADP complex, 3P4X	apo, 3P4Y
	Data Collection		
resolution range (Å)[b]	132.7−2.35 (2.44−2.35)	129.7−2.4 (2.5−2.4)	48.8−3.20 (3.3−3.2)
space group	$P2_12_12_1$	$P2_12_12_1$	$P2$
cell dimensions	a = 59.6 Å, b = 126.5 Å, c = 132.7 Å	a = 59.2 Å, b = 111.2 Å, c = 129.7 Å	a = 61.9 Å, b = 59.2 Å, c = 67.7 Å, β = 98.2°
no. of unique reflections[b]	42547 (4453)	34066 (3511)	7475 (376)
multiplicity[b]	7.1 (7.4)	3.6 (3.7)	3.4 (3.7)
completeness (%)[b]	99.6 (100)	99.1 (99.9)	91.4 (99.9)
R_{sym} (%)[b,c]	9.9 (65.9)	6.4 (63.5)	17.5 (65.6)
average $\langle I/\sigma(I)\rangle$[b,c]	9.7 (1.3)	12.0 (1.1)	7.2 (1.6)
	Refinement		
resolution range (Å)[b]	44.4−2.35 (2.41−2.35)	56.0−2.4 (2.5−2.4)	44.3−3.2 (4.0−3.2)
R_{cryst} (%)[b,d]	20.8 (39.4)	18.6 (32.7)	28.6 (33.0)
R_{free} (%)[b,d]	25.1 (41.5)	25.6 (41.4)	29.7 (34.8)
no. of residues/waters	807/99	809/52	407/0
phase error/coordinate error[e]	28.3°/0.38 Å	29.3°/0.36 Å	33.2°/0.49 Å
rmsd for bonds/angles	0.012 Å/1.56°	0.009 Å/1.14°	0.003 Å/0.54°
Ramachandran plot (%)[f]	96.8/3.1/0.1	91.7/8.0/0/0.3	89.4/10.1/0.3/0.3

[a] Data reproduced from ref 10. [b] Values in parentheses correspond to those of the highest-resolution shell. [c] Calculated with XPREP (Bruker). [d] $R_{cryst} = \Sigma||F_o| - |F_c||/\Sigma|F_o|$, where F_o and F_c are the structure factor amplitudes from the data and the model, respectively. R_{free}[41] is R_{cryst} with 5% of the test set structure factors. [e] Based on maximum likelihood after refinement with PHENIX.[18] [f] Calculated using PROCHECK.[42] Numbers reflect the percentage amino acid residues of the core, allowed, additionally allowed, and disallowed regions, respectively.

crystallizes readily, suggesting that the latch may be only loosely connected to H2, consistent with its previously suggested flexibility.[7] Three crystal structures of rgyr_hel_Δlatch were obtained and refined to resolutions of 2.35, 2.4, and 3.2 Å. The structures comprise five independent molecules and provide higher-resolution information about this part of reverse gyrase than what was previously available.

Comparison of *A. fulgidus* and *T. maritima* Subdomains H1 and H2. The core structures of H1 and H2 resemble RecA folds, i.e., a central parallel β-sheet flanked by α-helices on both sides. The H1 domains of *T. maritima* and *A. fulgidus* reverse gyrases superpose with a root-mean-square deviation (rmsd) of 1.8 Å over 187 residues (43% sequence identity). Similarly, the H2 domains superpose with an rmsd of 1.6 Å over 166 residues (39% identical sequences). Notably, an insertion is present in the sequence of *T. maritima* reverse gyrase compared to *A. fulgidus* (Figure S1 of the Supporting Information). At residue Gly239 of H1, 12 residues are inserted and form a loop region (arrow in Figure 1B). This loop and its preceding α-helix form a lid-like structure. In contrast, the corresponding region in *A. fulgidus* reverse gyrase forms a small, two-stranded β-sheet (Figure 1C). In a superposition of the H2 structures, the tips of these structural elements are ∼18 Å from each other (Figure 1C). The sequence of this insertion is quite variable among reverse gyrases, and it may comprise up to 41 residues (Figure S2 of the Supporting Information).

Within the RecA fold of H2 (Figure 1D), the latch domain is inserted at residue Gly389. This domain is present in all reverse gyrases but also varies strongly in both extent and sequence (Figure S2 of the Supporting Information). Comparison of the H2 structures from *A. fulgidus* and *T. maritima* reveals that the deletion of the latch region does not alter the fold of H2.[10]

Flexibility of the Helicase-like Domain. The helicase-like domain is formed by H1 and H2 that are connected by a linker sequence, which spans residues 280−286 in *T. maritima* reverse gyrase. While H2 follows the classic RecA topology with a seven-stranded β-sheet, H1 has only six β-strands. The seventh β-strand, normally formed by parts of the H1−H2 linker region, is not present because of the large displacements of H2 relative to H1. The same topology is present in the *A. fulgidus* enzyme.[7]

In the absence of interactions with the topoisomerase domain, H1 and H2 in rgyr_hel_Δlatch engage in only a few contacts, and the flexible linker allows the relative juxtapositions of H1 and H2 to vary strongly (Figure 2A). No common pattern of H1−H2 interactions is evident, strongly indicating that these modules are conformationally independent in the absence of DNA or the topoisomerase domain. Similarly, in both available structures of *A. fulgidus* reverse gyrase, H1 and H2 are connected by only five hydrogen bonds (different compared to rgyr_hel_Δlatch), and the buried surface area between them covers a mere 430 Å^2. In contrast, the topoisomerase domain interacts extensively with H1 and H2, fixing them in space.

None of the five conformations observed in the rgyr_hel_Δlatch crystal structures represents that of the helicase-like domain in *A. fulgidus* reverse gyrase or compares to the closed conformation of DEAD box helicases in complex with RNA and an ATP analogue, such as Vasa (gray sphere in Figure 2B). However, as reverse gyrase does belong to SF2 but is not a DEAD box protein, a direct comparison with Vasa may not be possible. The location of H2 with respect to H1 is not random but forms two clusters (Figure 2B). Single-molecule FRET experiments with rgyr_hel_Δlatch labeled at cysteines introduced at positions 169 and 332 reveal a mean distance between donor and acceptor dyes of 7.5 nm (Figure 2C,D). The corresponding Cβ−Cβ distances in the crystal structures vary between 6.8 and 7.4 nm, a strong indication that the conformations trapped in the crystal lattice represent conformations that are predominantly populated

dx.doi.org/10.1021/bi200236a |*Biochemistry* XXXX, XXX, 000–000

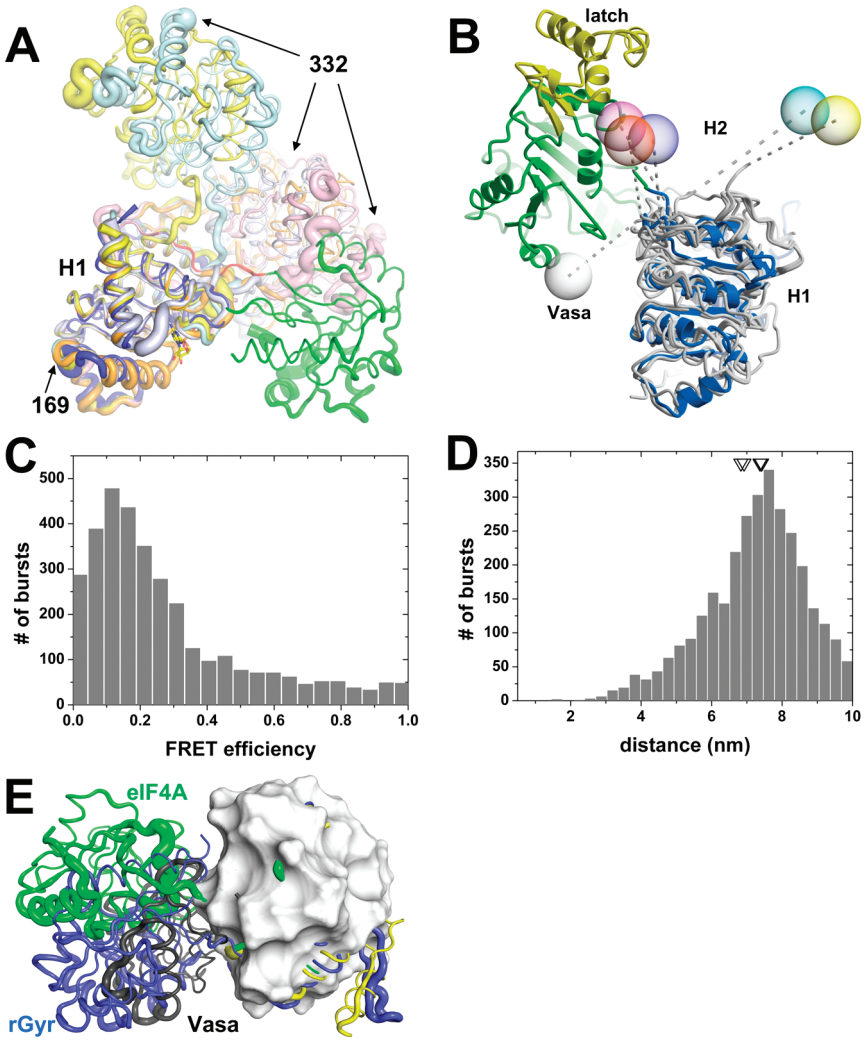

Figure 2. Large domain flexibility in rgyr_hel_Δlatch and comparison with related structures. (A) Superposition of the five different *T. maritima* rgyr_hel_Δlatch conformations onto H1 of *A. fulgidus* reverse gyrase. The location of H2 varies widely because of the lacking restraint by the topoisomerase domain. H2 of *A. fulgidus* reverse gyrase is colored green as a reference. *T. maritima* H2 domains are colored yellow and blue (molecules 1 and 2 of PDB entry 3OIY), cyan and orange (molecules 1 and 2 of PDB entry 3P4X), and pink (PDB entry 3P4Y). Cysteine positions 169 and 332 for fluorescent labeling in FRET experiments are indicated. (B) View rotated 180° about the *y*-axis relative to panel A. The centers of mass of the H2 domains are shown as transparent spheres colored the same as in panel A. Dashed lines connect the centers to the C-termini of H1. The five conformations of rgyr_hel_Δlatch form two clusters. The closed form of the DEAD box RNA helicase Vasa is shown as a gray sphere. This structure is only adopted when RNA and ATP are present. (C) Single-molecule FRET histogram for rgyr_hel_Δlatch (S169C/F332C), labeled with AlexaFluor 488 (donor) and tetramethylrhodamine (acceptor). The mean FRET efficiency is ~0.1. (D) Distance histogram calculated from the data in panel C. The predominant distance between donor and acceptor dyes is 7.5 nm. The empty triangles indicate the Cβ−Cβ distances between the labeled Cys169 and Cys332 residues in the five different structures (PDB entry 3OIY, 7.4 and 6.8 nm; PDB entry 3P4X, 7.4 and 6.9 nm; PDB entry 3P4Y, 7.4 nm) and compare favorably with the mean dye distance in solution. (E) Comparison of the H2 locations of *A. fulgidus* reverse gyrase (blue) with the closed form of Vasa (gray) and the open form of eukaryotic translation initiation factor eIF4A (green) shows large domain movements of the helicase cores. The structures were superposed on H1. The surface of Vasa H1 is shown, highlighting the protruding insert regions unique to reverse gyrases (yellow for *T. maritima* and blue for *A. fulgidus* reverse gyrase).

in solution. rgyr_hel_Δlatch exhibits DNA-stimulated ATPase activity,[10] which shows that DNA can align H1 and H2 for ATP hydrolysis in the absence of the topoisomerase domain. The conformational restriction of H1 and H2 by the topoisomerase domain is inhibitory with respect to ATP hydrolysis but is likely to support reverse gyrase activity. Interestingly, the helicase core of *A. fulgidus* reverse gyrase adopts an intermediate state between closed (Vasa) and open (rgyr_hel_Δlatch). A half-open conformation is also documented for the eIF4A−eIF4G complex[25] (Figure 2E).

Nucleotide Binding to the H1 Domain. The helicase-like domain is responsible for ATP binding and hydrolysis.[11] Although all crystallization setups were performed with ADPNP and Mg^{2+}, only in one instance (PDB entry 3P4X) was a nucleotide observed in the electron density that was assigned as ADP. The affinity of rgyr_hel_Δlatch for ADP is ~5.5-fold higher than for ADPNP,[10] and ADP generated from ADPNP by limited hydrolysis or introduced as an impurity will be preferentially bound. The nucleotide exclusively interacts with H1, forming a total of 11 hydrogen bonds with the adenine base and the diphosphate

dx.doi.org/10.1021/bi200236a |*Biochemistry* XXXX, XXX, 000–000

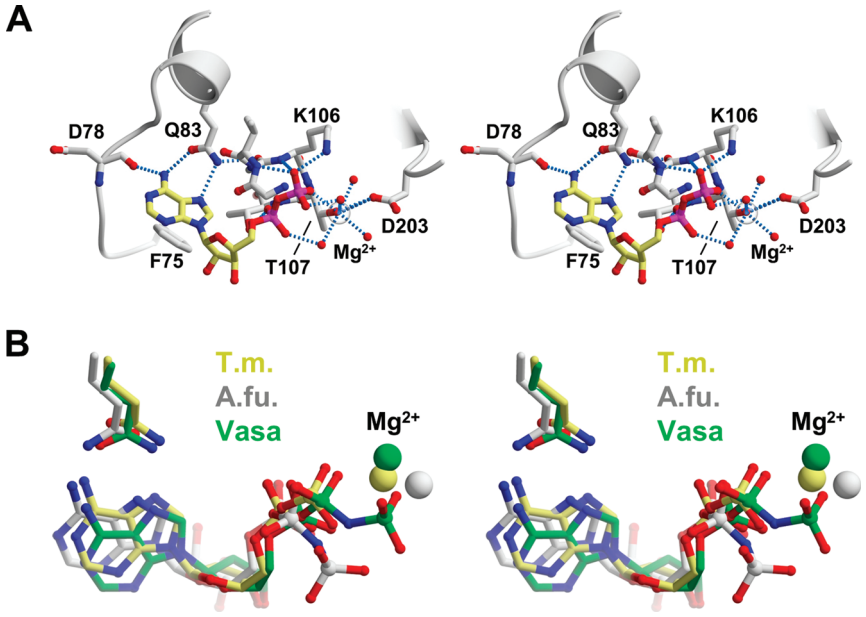

Figure 3. Detailed view of nucleotide binding to reverse gyrase. (A) Stereo figure of the hydrogen bond network of ADP and Mg^{2+} bound to *T. maritima* reverse gyrase. The adenine base is bound by three hydrogen bonds (dashed lines) to the conserved Gln83 of the Q-motif and the backbone carbonyl group of Asp78. A hydrophobic sandwich is formed between adenine and Phe75. The β-phosphate forms hydrogen bonds to the P-loop, and its charge is neutralized by Lys106 and the Mg^{2+}—aquo complex. Mg^{2+} connects the nucleotide with Asp203 of the DDVD motif, a modified DEAD box that is conserved in RNA helicases. (B) Comparison of the nucleotide binding modes of *T. maritima* and *A. fulgidus* reverse gyrases with the DExD/H-helicase Vasa. Mg^{2+} ions are shown as spheres. Note the deviation of the γ-phosphate in *A. fulgidus* reverse gyrase compared to that in Vasa, leading to the absence of interactions with the Mg^{2+} ion.

moiety (Figure 3). Thus, ADP binding will not affect H1—H2 domain flexibility (see above). The ribose is not involved in any interactions with the protein. The lack of interactions with the 2′-OH group of the ribose rationalizes the previous observation that 2′-desoxy-ATP is also accepted as a substrate of *A. fulgidus* reverse gyrase,[9] and the observation that mantADP is a suitable analogue for monitoring adenine nucleotide binding to *T. maritima* reverse gyrase.[11,13] Thus, ribose-modified nucleotides should bind to reverse gyrases in general.

In contrast to the ribose moiety, the adenine base is recognized specifically by a region that bears homology to the Q-motif in DEAD box proteins, consisting of a conserved glutamine residue and a hydrophobic (often aromatic) side chain located 13 residues upstream of the glutamine.[26,27] Such a glutamine is conserved in reverse gyrases, discriminating adenine from other nucleobases via two hydrogen bonds (Figure 3A). A third hydrogen bond is formed between the exocyclic N6 atom of adenine and the main chain carbonyl group of Asp78. The interaction network with adenine is completed by hydrophobic contacts with Phe75 (Val54 in *A. fulgidus* reverse gyrase). This adenine-specific pocket stands in contrast to the observation that *A. fulgidus* reverse gyrase, although preferring ATP, can apparently use all four standard NTPs and dNTP as substrates.[9]

The α- and β-phosphate moieties form hydrogen bonds to the main chain amide nitrogen atoms of P-loop residues Gly103, Gly105, Lys106, Thr107, and Thr108. The charge of the β-phosphate is neutralized by Lys106 and a Mg^{2+} ion. This Mg^{2+} ion is directly bound to the β-phosphate and coordinated octahedrally by the side chain of Thr107 and four water molecules. In DEAD box helicases, the nucleotide-bound Mg^{2+} ion connects the P-loop with the first aspartate residue of the DEAD box. Reverse gyrases possess a modified DEAD box, the DDVD motif, where the valine may also be Ala, Ile, or Ser. Similar to DEAD box proteins, the Mg^{2+}—aquo complex in *T. maritima* rgyr_hel_Δlatch connects the nucleotide with the first aspartate (Asp203) of the DDVD motif. An equivalent interaction is present in the closed exon junction complex[28,29] but absent in DDX19[30] and Vasa.[31] A second link between the P-loop and the DDVD motif is established by a direct hydrogen bond of the Thr107 and Asp203 side chains (Figure 3A). Again, this interaction is present in the exon junction complex but absent in the currently available closed DEAD box helicase structures.

To date, only one other reverse gyrase—nucleotide complex structure is available. In the ADPNP complex of *A. fulgidus* reverse gyrase (PDB entry 1GL9), a minor error is a 180° rotated carboxamide side chain of the conserved glutamine, and the C2 epimeric arabinose was built instead of a ribose[7] (Figure 3B). The P-loops of reverse gyrases adopt different conformations in the apo and nucleotide-bound forms. The Cα—Cα distance between Thr102 (*T. maritima*) and the equivalent Thr80 (*A. fulgidus*) is 5 Å in the apo forms and 2 Å in the nucleotide-bound forms. In both *T. maritima* and *A. fulgidus* reverse gyrase, the P-loop essentially collapsed onto the phosphate part of the nucleotide. Thus, the P-loop may be mobile in the apo form of reverse gyrases and becomes fixed only after nucleotide binding. The locations of the adenine, sugar moiety, and α-phosphate are roughly similar between the *T. maritima* and *A. fulgidus* nucleotide complexes. Large differences are apparent for the locations and coordination of the Mg^{2+} ions and the connection of the P-loop with the DDVD motif. In *T. maritima* rgyr_hel_Δlatch, Thr107 is a direct ligand for the Mg^{2+} ion and binds to Asp203 of the DDVD motif (Figure 3A). By contrast, the analogous Thr85 in *A. fulgidus* only contacts the β-phosphate and is too far from

dx.doi.org/10.1021/bi200236a |*Biochemistry* XXXX, XXX, 000–000

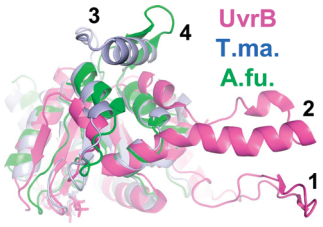

Figure 4. Insertions in UvrB and reverse gyrase helicase-like H2 domains. UvrB (PDB entry 1d9z, magenta) has two insertions (right part of the image) that might contribute to strand separation, a β-hairpin (1) and an α-helix connecting back to H2 via a loop region (2). The UvrB α-helix is located closer to the insertion in the reverse gyrase H2 domains (3 and 4) than the β-hairpin and is structurally similar to *T. maritima* H2 (light blue). Similar to UvrB, *A. fulgidus* reverse gyrase H2 (green) possesses a β-hairpin (4). However, the reverse gyrase insertions are located at very different sites in the H2 structure compared to the UvrB insertions, and their putative involvement in DNA strand separation is currently unconfirmed.

either the Mg^{2+} ion or the DDVD motif. In conclusion, the structures we report here establish that the salient features of nucleotide binding to DEAD box helicases, including the Q-motif, the P-loop, and the connection to the (modified) DEAD box, are present in *T. maritima* reverse gyrase.

DISCUSSION

In this study, the latch region had to be deleted from the *T. maritima* helicase-like domain to obtain diffracting crystals. The latch does not interact with any residues of the nucleotide binding pocket, and the mutant serves as a meaningful model system for nucleotide binding to *T. maritima* reverse gyrase. The fold of the H2 domain remains unaltered upon latch deletion.[10] Furthermore, H2 does not significantly interact with H1 in any of the reverse gyrase structures determined so far.

One of the larger sequence differences between *T. maritima* and *A. fulgidus* reverse gyrases is an insertion of 12 residues at position 240 (*T. maritima* numbering). This insertion effectively replaces a β-hairpin of *A. fulgidus* reverse gyrase with a long α-helix followed by a loop region (Figures 1B,C and 2E). For *A. fulgidus* reverse gyrase, a function of this β-hairpin for strand separation was hypothesized.[7] β-Hairpins that were implicated in strand separation are also present in the H1 domain of SF2 helicases NS3[32] and Hel308[33] and in the SF1 excision repair nuclease UvrB,[34] albeit at quite different locations in the structures. Interestingly, another insertion close to those observed in H1 of *T. maritima* and *A. fulgidus* reverse gyrases is present in UvrB (Figure 4). This insertion adopts a shape similar to that of the insertion in *T. maritima* reverse gyrase, namely a long α-helix that connects back to H1 via a loop region. A multiple-sequence comparison of 19 reverse gyrases (Figure S2 of the Supporting Information) demonstrates that *A. fulgidus* harbors an exceptionally compact reverse gyrase. The insertion in *T. maritima* is the smallest of the set but can comprise up to 42 residues (*Pyrococcus kodakaraensis*, with all pyrococci having >38-residue insertions). Thus, if this region should participate in strand separation, and if the insertion in UvrB has an equivalent function, the task can be achieved not only via very different sequence lengths but also via very different structures. Alternatively, the insertion might undergo a helix loop to β-hairpin transition during catalysis. Whether insertions at this position constitute a general feature of DNA and DExD/H helicases that is involved in nucleic acid strand separation remains to be determined.

While the general features of nucleotide binding to reverse gyrases and DEAD box helicases are the same with the adenine base binding to the Q-motif and the phosphate moiety located in the P-loop, the details of nucleotide binding in reverse gyrases differ from those observed in DEAD box helicases. In the structure of rgyr_hel_Δlatch, Thr107 is a direct Mg^{2+} ligand, a pattern often encountered in P-loop-containing proteins. For example, in the GTP-binding protein Ras, Ser17 of the P-loop binds to the Mg^{2+} ion.[35] With DEAD box and related helicases, the picture is somewhat incoherent. In the human DDX19−ADPNP−RNA complex,[30] the threonine at this position does not interact directly with Mg^{2+}, and in the *Drosophila* Vasa−ADPNP−RNA complex,[31] the interaction is indirectly mediated by a water molecule. By contrast, a direct interaction of the threonine with Mg^{2+} is present in the RNA-bound exon junction complex with either ADPNP[28] or the transition state analogue ADP-AlF_3.[29] All of these complexes are regarded as closed structures, trapped either in a state prior to RNA unwinding or after release of the first strand.

Superposition of the ADP−Mg^{2+} complex with that of closed-form DEAD box helicases predicts a likely position for the γ-phosphate in a reverse gyrase−ATP complex (Figure 3B). The γ-phosphate should follow the extended conformation present in the ATP analogue of the Vasa helicase,[31] and the Mg^{2+} ion should be bound to both the β- and γ-phosphate. Instead, neither the β-phosphate nor the γ-phosphate of the ADPNP in the *A. fulgidus* reverse gyrase structure interacts with Mg^{2+}, but the γ-phosphate takes a very different path pointing into the solvent (Figure 3B).

The helicase-like domain of reverse gyrase is composed of the H1 and H2 domains and resembles the helicase core of DEAD box proteins. An essential feature of these helicases is a bipartite nucleic acid binding site that is generated by both RecA-like domains[31] (reviewed in ref 36). Generation of this binding site requires closure of the interdomain cleft, which also harbors the nucleotide binding site.[28,30,31,37] DEAD box helicases and reverse gyrases share several common denominators. First, the spatial distribution of conserved motifs is similar.[7] Second, mutational studies defined important contributions of these motifs to supercoiling.[8] Third, cooperativity exists between DNA and ATP binding in the helicase-like domain of *T. maritima* reverse gyrase.[11] Fourth, several crystal structures of DEAD box helicases in the absence of either RNA and ATP analogues have shown a plethora of open conformations where the N- and C-terminal RecA-like domains are splayed apart[28,38−40] (unpublished observations, PDB entry 2Z0M). Binding of nucleotide alone does not induce a closure of the cleft between H1 and H2, not in the intact *A. fulgidus* reverse gyrase[7] or in the *T. maritima* rgyr_hel_Δlatch variant (this work), and also not in DEAD box proteins.[22] Taken together, these data suggest similar concerted conformational changes for the helicase domains of reverse gyrase and DEAD box helicases upon ATP and nucleic acid binding. Indeed, single-molecule FRET studies of the isolated reverse gyrase helicase-like domain demonstrate a closure upon nucleotide and DNA binding.[12]

In *T. maritima* reverse gyrase, binding of DNA and nucleotide is less cooperative than in the isolated helicase-like domain, pointing toward an inhibitory effect of the topoisomerase domain for the required closure of the helicase-like domain.[11] It is therefore conceivable that both nucleotide and DNA binding

dx.doi.org/10.1021/bi200236a |*Biochemistry* XXXX, XXX, 000–000

are required to alleviate the conformational restrictions imposed on the helicase-like domain by the topoisomerase domain of reverse gyrase. Likewise, nucleotide hydrolysis by the helicase-like domain is attenuated by the topoisomerase domain in reverse gyrase. The activation of eukaryotic initiation factor eIF4A by eIF4G through the stabilization of a half-open conformation demonstrates that a balance of conformational restriction and conformational plasticity is crucial for DEAD box protein function.[24] Possibly, restriction by the topoisomerase domain impedes rapid alternation between open and closed forms of H1 and H2. In the isolated *T. maritima* helicase-like domain, these restrictions are alleviated, rationalizing its increased ATPase activity. In conclusion, the crystallographic and single-molecule FRET data presented here established the precise nucleotide binding mode of and the conformational space available to the helicase-like domain of reverse gyrase. To guide future studies of the conformational changes upon ATP and DNA binding, further structural information about the complete *T. maritima* reverse gyrase is needed.

■ ASSOCIATED CONTENT

Supporting Information. Supplementary Figures S1 and S2; a structure-sequence comparison of the *A. fulgidus* and *T. maritima* reverse gyrase helicase-like domains and a multiple sequence alignment of reverse gyrase helicase-like domains highlighting the variability of the insertion region. This material is available free of charge via the Internet at http://pubs.acs.org.

■ AUTHOR INFORMATION

Corresponding Author

*Institute for Physical Chemistry, University of Muenster, Corrensstrasse 30, D-48149 Muenster, Germany. Phone: 0049-251 83 23421. Fax: 0049-251-83 29138. E-mail: dagmar.klostermeier@uni-muenster.de.

Funding Sources

This work was supported by the VolkswagenStiftung (D.K.) and the Swiss National Science Foundation (D.K.).

■ ACKNOWLEDGMENT

We thank the staff at SLS beamlines PX-II and PX-III for support during data collection.

■ REFERENCES

(1) Schoeffler, A. J., and Berger, J. M. (2008) DNA topoisomerases: Harnessing and constraining energy to govern chromosome topology. *Q. Rev. Biophys. 41*, 41–101.

(2) Gellert, M., Mizuuchi, K., O'Dea, M. H., and Nash, H. A. (1976) DNA gyrase: An enzyme that introduces superhelical turns into DNA. *Proc. Natl. Acad. Sci. U.S.A. 73*, 3872–3876.

(3) Kampmann, M., and Stock, D. (2004) Reverse gyrase has heat-protective DNA chaperone activity independent of supercoiling. *Nucleic Acids Res. 32*, 3537–3545.

(4) Hsieh, T. S., and Plank, J. L. (2006) Reverse gyrase functions as a DNA renaturase: Annealing of complementary single-stranded circles and positive supercoiling of a bubble substrate. *J. Biol. Chem. 281*, 5640–5647.

(5) Confalonieri, F., Elie, C., Nadal, M., de La Tour, C., Forterre, P., and Duguet, M. (1993) Reverse gyrase: A helicase-like domain and a type I topoisomerase in the same polypeptide. *Proc. Natl. Acad. Sci. U.S.A. 90*, 4753–4757.

(6) Declais, A. C., Marsault, J., Confalonieri, F., de La Tour, C. B., and Duguet, M. (2000) Reverse gyrase, the two domains intimately cooperate to promote positive supercoiling. *J. Biol. Chem. 275*, 19498–19504.

(7) Rodriguez, A. C., and Stock, D. (2002) Crystal structure of reverse gyrase: Insights into the positive supercoiling of DNA. *EMBO J. 21*, 418–426.

(8) Bouthier de la Tour, C., Amrani, L., Cossard, R., Neuman, K. C., Serre, M. C., and Duguet, M. (2008) Mutational analysis of the helicase-like domain of *Thermotoga maritima* reverse gyrase. *J. Biol. Chem. 283*, 27395–27402.

(9) Rodriguez, A. C. (2002) Studies of a positive supercoiling machine. Nucleotide hydrolysis and a multifunctional "latch" in the mechanism of reverse gyrase. *J. Biol. Chem. 277*, 29865–29873.

(10) Ganguly, A., Del Toro Duany, Y., Rudolph, M. G., and Klostermeier, D. (2011) The latch modulates nucleotide and DNA binding to the helicase-like domain of *Thermotoga maritima* reverse gyrase and is required for positive DNA supercoiling. *Nucleic Acids Res. 39*, 1789–1800.

(11) Del Toro Duany, Y., Jungblut, S. P., Schmidt, A. S., and Klostermeier, D. (2008) The reverse gyrase helicase-like domain is a nucleotide-dependent switch that is attenuated by the topoisomerase domain. *Nucleic Acids Res. 36*, 5882–5895.

(12) Del Toro Duany, Y., and Klostermeier, D. (2011) Nucleotide-driven conformational changes in the reverse gyrase helicase-like domain couple the nucleotide cycle to DNA processing. *Phys. Chem. Chem. Phys. 13*, 10009–10019.

(13) Jungblut, S. P., and Klostermeier, D. (2007) Adenosine 5′-O-(3-thio)triphosphate (ATPγS) promotes positive supercoiling of DNA by *T. maritima* reverse gyrase. *J. Mol. Biol. 371*, 197–209.

(14) Kabsch, W. (1988) Evaluation of single crystal X-ray diffraction data from a position sensitive detector. *J. Appl. Crystallogr. 21*, 916–924.

(15) Collaborative Computational Project, Number 4. (1994) The Collaborative Computational Project Number 4, suite programs for protein crystallography. *Acta Crystallogr. D50*, 760–763.

(16) McCoy, A. J., Grosse-Kunstleve, R. W., Adams, P. D., Winn, M. D., Storoni, L. C., and Read, R. J. (2007) Phaser crystallographic software. *J. Appl. Crystallogr. 40*, 658–674.

(17) Emsley, P., Lohkamp, B., Scott, W. G., and Cowtan, K. (2010) Features and development of Coot. *Acta Crystallogr. D66*, 486–501.

(18) Zwart, P. H., Afonine, P. V., Grosse-Kunstleve, R. W., Hung, L. W., Ioerger, T. R., McCoy, A. J., McKee, E., Moriarty, N. W., Read, R. J., Sacchettini, J. C., Sauter, N. K., Storoni, L. C., Terwilliger, T. C., and Adams, P. D. (2008) Automated structure solution with the PHENIX suite. *Methods Mol. Biol. 426*, 419–435.

(19) Esnouf, R. M. (1997) An extensively modified version of MOLSCRIPT that includes greatly enhanced coloring capabilities. *J. Mol. Graphics 15*, 132–134.

(20) Merritt, E. A., and Murphy, M. E. P. (1994) Raster3D Version 2.0: A program for photorealistic molecular graphics. *Acta Crystallogr. D50*, 869–873.

(21) Gouet, P., Courcelle, E., Stuart, D. I., and Metoz, F. (1999) ESPript: Analysis of multiple sequence alignments in PostScript. *Bioinformatics 15*, 305–308.

(22) Theissen, B., Karow, A. R., Kohler, J., Gubaev, A., and Klostermeier, D. (2008) Cooperative binding of ATP and RNA induces a closed conformation in a DEAD box RNA helicase. *Proc. Natl. Acad. Sci. U.S.A. 105*, 548–553.

(23) Gubaev, A., Hilbert, M., and Klostermeier, D. (2009) The DNA-gate of *Bacillus subtilis* gyrase is predominantly in the closed conformation during the DNA supercoiling reaction. *Proc. Natl. Acad. Sci. U.S.A. 106*, 13278–13283.

(24) Hilbert, M., Kebbel, F., Gubaev, A., and Klostermeier, D. (2010) eIF4G stimulates the activity of the DEAD box protein eIF4A by a conformational guidance mechanism. *Nucleic Acids Res. 39*, 2260–2270.

(25) Schütz, P., Bumann, M., Oberholzer, A. E., Bieniossek, C., Trachsel, H., Altmann, M., and Baumann, U. (2008) Crystal structure

of the yeast eIF4A-eIF4G complex: An RNA-helicase controlled by protein-protein interactions. *Proc. Natl. Acad. Sci. U.S.A. 105*, 9564–9569.

(26) Tanner, N. K. (2003) The newly identified Q motif of DEAD box helicases is involved in adenine recognition. *Cell Cycle 2*, 18–19.

(27) Tanner, N. K., Cordin, O., Banroques, J., Doere, M., and Linder, P. (2003) The Q motif: A newly identified motif in DEAD box helicases may regulate ATP binding and hydrolysis. *Mol. Cell 11*, 127–138.

(28) Andersen, C. B., Ballut, L., Johansen, J. S., Chamieh, H., Nielsen, K. H., Oliveira, C. L., Pedersen, J. S., Seraphin, B., Le Hir, H., and Andersen, G. R. (2006) Structure of the exon junction core complex with a trapped DEAD-box ATPase bound to RNA. *Science 313*, 1968–1972.

(29) Nielsen, K. H., Chamieh, H., Andersen, C. B., Fredslund, F., Hamborg, K., Le Hir, H., and Andersen, G. R. (2009) Mechanism of ATP turnover inhibition in the EJC. *RNA 15*, 67–75.

(30) Collins, R., Karlberg, T., Lehtio, L., Schutz, P., van den Berg, S., Dahlgren, L. G., Hammarstrom, M., Weigelt, J., and Schuler, H. (2009) The DEXD/H-box RNA helicase DDX19 is regulated by an α-helical switch. *J. Biol. Chem. 284*, 10296–10300.

(31) Sengoku, T., Nureki, O., Nakamura, A., Kobayashi, S., and Yokoyama, S. (2006) Structural Basis for RNA Unwinding by the DEAD-Box Protein *Drosophila* Vasa. *Cell 125*, 287–300.

(32) Kim, J. L., Morgenstern, K. A., Griffith, J. P., Dwyer, M. D., Thomson, J. A., Murcko, M. A., Lin, C., and Caron, P. R. (1998) Hepatitis C virus NS3 RNA helicase domain with a bound oligonucleotide: The crystal structure provides insights into the mode of unwinding. *Structure 6*, 89–100.

(33) Büttner, K., Nehring, S., and Hopfner, K. P. (2007) Structural basis for DNA duplex separation by a superfamily-2 helicase. *Nat. Struct. Mol. Biol. 14*, 647–652.

(34) Theis, K., Chen, P. J., Skorvaga, M., Van Houten, B., and Kisker, C. (1999) Crystal structure of UvrB, a DNA helicase adapted for nucleotide excision repair. *EMBO J. 18*, 6899–6907.

(35) Bourne, H. R., Sanders, D. A., and McCormick, F. (1990) The GTPase superfamily: A conserved switch for diverse cell functions. *Nature 348*, 125–132.

(36) Hilbert, M., Karow, A. R., and Klostermeier, D. (2009) The mechanism of ATP-dependent RNA unwinding by DEAD box proteins. *Biol. Chem. 390*, 1237–1250.

(37) Bono, F., Ebert, J., Lorentzen, E., and Conti, E. (2006) The crystal structure of the exon junction complex reveals how it maintains a stable grip on mRNA. *Cell 126*, 713–725.

(38) Caruthers, J. M., Johnson, E. R., and McKay, D. B. (2000) Crystal structure of yeast initiation factor 4A, a DEAD-box RNA helicase. *Proc. Natl. Acad. Sci. U.S.A. 97*, 13080–13085.

(39) Story, R. M., Li, H., and Abelson, J. N. (2001) Crystal structure of a DEAD box protein from the hyperthermophile *Methanococcus jannaschii*. *Proc. Natl. Acad. Sci. U.S.A. 98*, 1465–1470.

(40) Cheng, Z., Coller, J., Parker, R., and Song, H. (2005) Crystal structure and functional analysis of DEAD-box protein Dhh1p. *RNA 11*, 1258–1270.

(41) Brünger, A. T. (1992) Free R value: A novel statistical quantity for assessing the accuracy of crystal structures. *Nature 355*, 472–475.

(42) Laskowski, R. A., MacArthur, M. W., Moss, D. S., and Thornton, J. M. (1993) PROCHECK: A program to check the stereochemical quality of protein structures. *J. Appl. Crystallogr. 26*, 283–291.

Chapter 5

The N-terminal putative Zn-finger has a deleterious effect on DNA binding and DNA-stimulated ATPase activity of reverse gyrase helicase-like domain

Introduction

We have previously shown that the deletion of the latch from the isolated helicase-like domain of *T. maritima* reverse gyrase, strongly decreases DNA binding at virtually every step of the nucleotide cycle. Also the DNA-stimulated ATPase activity of the helicase-like domain module is decreased upon latch deletion, and the thermodynamic coupling between ATP hydrolysis and DNA binding practically disappears. Furthermore, our direct affinity measurements demonstrated that the latch is able to bind DNA. From these results a notion emerged on the role of the latch in guiding and presenting the suitable DNA to the topoisomerase domain during the supercoiling reaction, as well as its strong involvement in the reaction the helicase-like domain performs on its own.[47]

The role played by individual regions of the enzyme in specific steps of reverse gyrase catalytic cycle was further addressed by studying the effect of the N-terminal putative Zn-finger on the properties of the helicase core. The crystal structure of *A. fulgidus* reverse gyrase suggests that the first residues in the primary structure of the molecule interact almost exclusively with the C-terminal topoisomerase domain. This N-terminal region was not included in the final refined model due to poor electron density[48]. Nevertheless, although the secondary structure of the segment could not be assigned, the location of the N-terminal putative Zn-finger in close proximity to the topoisomerase domain was confidently determined.

From the exclusive physical interaction of the N-terminal putative Zn-finger with the topoisomerase domain, it is expected to be more strongly involved in the reaction carried out by this module than in the reaction of the helicase-like domain. Topoisomerases are known to possess Zn-fingers in their structure[49], while helicases usually lack them. We therefore set out to determine whether

the presence of the N-terminal putative Zn-finger has indeed no influence on the properties of the helicase-like domain, or if it actually cooperates with the helicase-like domain in the nucleotide-dependent DNA processing performed by this region of the enzyme.

Results

Our biochemical data suggest that the folding of the recA domains contained in the structure of rGyr_hel is not affected in the absence of the topoisomerase domain[50]. The unstimulated steady-state ATPase activities of rGyr and rGyr_hel are virtually the same, what also indicates that rGyr_hel is the only responsible for ATP hydrolysis. Additionally, the crystal structure of rGyr_hel_Δlatch reveals that the latch deletion has no effect on the folding of the H2 domain [51] . CD spectra of these two constructs of the helicase-like domain, along with the spectrum of the same module containing the N-terminal Zn-finger (rGyr_hel_ZnF_1) show no significant difference in the secondary structure (Figure 9). Overall the differences in α-helical content are within the expected range, due to the different length of the constructs and the contribution of the individual residues, therefore the secondary structure seems to remain unaltered.

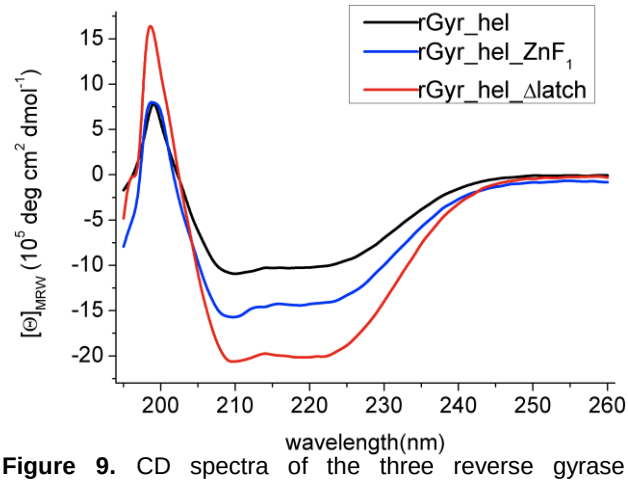

Figure 9. CD spectra of the three reverse gyrase helicase-like constructs assayed so far. The differences in the curves are derived from the different lengths of the polypeptides. No significant difference in secondary structure was detected.

DNA-stimulated ATP hydrolysis under steady-state conditions

Under steady-state conditions, the k_{cat} value for ATP hydrolysis by rGyr_hel_ZnF_1 in the presence of ssDNA is 470 ± 50·$10^{-3}s^{-1}$ (Table I). This

value is intermediate between the ones obtained for the full-length rGyr and rGyr_hel_Δlatch. Compared to rGyr_hel, the ssDNA stimulation of ATP hydrolysis by rGyr_hel_ZnF$_1$ is 2.5-fold lower, but still approximately 3-fold higher than the full-length rGyr. rGyr_hel_Δlatch hydrolyzes ATP at a rate closest to the displayed by rGyr_hel_ZnF$_1$, being only 1.7-fold higher. Overall, ssDNA stimulation of ATP hydrolysis by rGyr_hel_ZnF$_1$ is the lowest of all the helicase-like domain constructs, but still higher than the full-length rGyr (Figure 2).

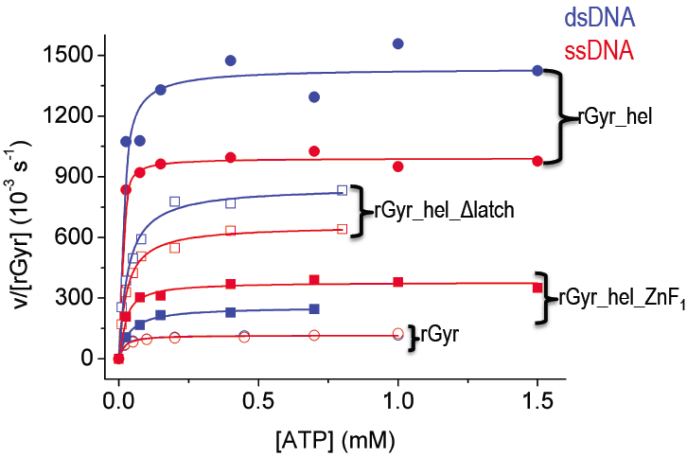

Figure 10. DNA-stimulated ATPase activity of the full-length reverse gyrase and different constructs of the helicase-like domain. There is no overlap between the constructs, showing that for all helicase-like variants, the DNA stimulations occurs to a higher extent as the wild-type full-length enzyme.

Comparison of the $K_{M,ssDNA}$ values indicate a 10-fold decrease of the apparent affinity for ssDNA in rGyr_hel_ZnF$_1$ compared to rGyr_hel, with values of 0.7 ± 0.3 μM and 0.07 ± 0.04 μM, respectively. Interestingly, compared to rGyr and rGyr_hel_Δlatch, which have $K_{M,ssDNA}$ of 0.45 ± 0.06 μM and 0.25 ± 0.03 μM respectively, the apparent affinity for ssDNA in the case of rGyr_hel_ZnF$_1$ was only 1.6-fold smaller than rGyr, and 2.8-fold smaller than rGyr_hel_Δlatch. We have previously reported that the full-length rGyr had an apparent ssDNA affinity lower than rGyr_hel and rGyr_hel_Δlatch[1]. From that we concluded that the presence of the topoisomerase domain had a deleterious effect on the apparent affinity of the helicase-like domain, which is the part of the molecule performing the ATPase reaction. That rGyr_hel_ZnF$_1$ has an apparent affinity for ssDNA even lower than rGyr, leads us to assume a deleterious effect of the N-terminal Zn-finger on the isolated helicase-like domain apparent affinity for ssDNA, even higher than within the context of the full-length enzyme.

Analysis of the stimulation of the ATPase activity by dsDNA reveals a trend similar to what was observed in the case of ssDNA. rGyr_hel_ZnF$_1$ exhibits a k_{cat} of 330 ± 70·10^{-3}s^{-1}, which is 4.4-fold and 2.4-fold slower than the dsDNA-

stimulated ATP hydrolysis rate of rGyr_hel and rGyr_hel_Δlatch, respectively. Compared to rGyr, rGyr_hel_ZnF_1 performs the reaction at a rate 2.2-fold higher. This is again consistent with the dsDNA-stimulation of ATP hydrolysis by rGyr_hel_ZnF_1 being the lowest of all the helicase-like domain constructs but still higher than rGyr, following the same trend as the ssDNA-stimulated ATPase activity.

Analysis of the $K_{M,dsDNA}$ values indicate that rGyr_hel_ZnF_1 has apparent dsDNA affinities 14- and 22-fold smaller than rGyr_hel_Δlatch and rGyr_hel, respectively. This last case is where the apparent affinity for DNA is most drastically impaired by the presence of the N-terminal Zn-finger within the helicase-like domain construct. On the other hand, compared with full-length rGyr, rGyr_hel_ZnF_1 apparent affinity for dsDNA is only 1.8-fold smaller, and these two constructs have apparent dsDNA affinities one order of magnitude smaller than the other two helicase-like constructs.

Overall, the DNA-stimulated ATP hydrolysis is clearly distributed in four different populations, where the constructs lacking the N-terminal Zn-finger show higher DNA-stimulated ATPase rates, in the order rGyr_hel > rGyr_hel_Δlatch > rGyr_hel_ZnF_1 > rGyr (Figure 2). The dsDNA-stimulated ATPase activity represents the biggest gap between the two sub-sets of populations determined by the presence of the N-terminal Zn-finger, indicating a more pronounced effect of this region on dsDNA-stimulated ATPase activity than on ssDNA. Another difference between these sub-sets of constructs, is that for the ones lacking Zn-fingers dsDNA stimulates ATP hydrolysis more or to the same extent as ssDNA, while for the ones bearing the N-terminal Zn-finger it is ssDNA the one that stimulates ATP hydrolysis most.

Global analysis of the apparent DNA affinities reveals a rather similar picture, where the constructs lacking Zn-fingers have higher apparent DNA affinities than the ones bearing the N-terminal Zn-finger. However, the order rGyr_hel > rGyr_hel_Δlatch > rGyr > rGyr_hel_ZnF_1 reveals an inversion of the last two constructs, which also happen to be in an overlapping range. Additionally, although all constructs show higher apparent affinities for ssDNA than dsDNA, the ones without Zn-fingers show a rather small preference for ssDNA, while

the constructs bearing the N-terminal Zn-finger show a marked preference for ssDNA, with a strongly decreased apparent affinity for dsDNA (Table I).

Table I. Steady-state ATPase parameters for rGyr_hel, rGyr_hel_Δlatch, and rGyr_hel_ZnF$_1$. Intrinsic ATPase activity, and influence of DNA on K_M and k_{cat}.

	$k_o(10^{-3}*s^{-1})$	$k_{cat}(10^{-3}*s^{-1})$	$K_M(\mu M)$
rGyr_hel			
DNA-dependent ssATPase			
ssDNA	19 ± 167	1160 ± 188	0.07 ± 0.04
dsDNA	21 ± 54	1450 ± 64	0.18 ± 0.03
ATP-dependent ssATPase			
ATP-ssDNA	0	992 ± 12	4.8 ± 1
ATP-dsDNA	0	1435 ± 57	11 ± 4
rGyr_hel_Δlatch			
DNA-dependent ssATPase			
ssDNA	0 ± 17	780 ± 20	0.25 ± 0.03
dsDNA	0 ± 20	780 ± 40	0.29 ± 0.06
ATP-dependent ssATPase			
ATP-ssDNA	0	660 ± 10	27 ± 2
ATP-dsDNA	0	850 ± 20	30 ± 4
rGyr_hel_ZnF$_1$			
DNA-dependent ssATPase			
ssDNA	0 ± 20	470 ± 50	0.7 ± 0.3
dsDNA	8 ± 3	330 ± 70	4 ± 1
ATP-dependent ssATPase			
ATP-ssDNA	0	380 ± 10	21 ± 4
ATP-dsDNA	0	260 ± 10	36 ± 4

DNA binding

rGyr_hel_ZnF$_1$ binds ssDNA with a 37- and 6.5-fold smaller affinity than rGyr and rGyr_hel, respectively. Compared to rGyr_hel_Δlatch, this affinity is still 3.1-fold smaller, consistent with a deleterious effect of the N-terminal Zn-finger on ssDNA binding by the helicase-like domain.

In the case of dsDNA however, no quantitative analysis of binding to rGyr_hel_ZnF$_1$ was possible. Nevertheless, an anisotropy increase was detected, indicating that dsDNA is weakly bound. This finding is inline with the steady-state ATPase measurements, where rGyr and rGyr_hel_ZnF$_1$ had

apparent dsDNA affinities one order of magnitude smaller than the ones from rGyr_hel and rGyr_hel_Δlatch.

Analysis of DNA binding by rGyr_hel_ZnF$_1$ in the ATP ground state, mimicked by ADPNP, had as result that the affinity for ssDNA remains unaltered while the affinity for dsDNA falls within the measurable range, with a value of 3.1 μM. These results support the previous findings that binding of ssDNA by rGyr_hel is rather insensitive to ADPNP binding, while the affinity for dsDNA is greatly increased[3] (Figure 3).

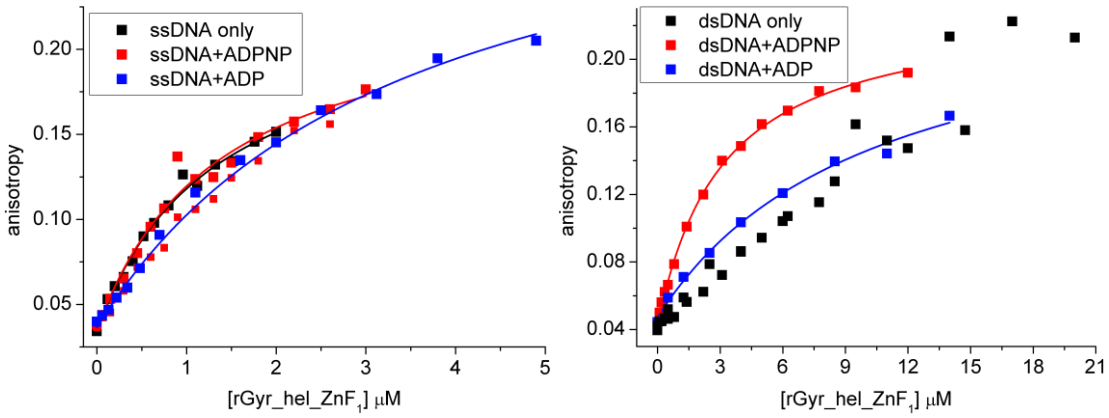

Figure 11. DNA binding to rGyr_hel_ZnF$_1$. **Left**: ssDNA binding. **Right**: dsDNA binding. The K_D values are summarized in Table II.

Also in the ADP-bound state the trend seen with rGyr_hel is roughly maintained, where the affinity for DNA remains similar as in the nucleotide-free state, with a 1.4-fold decrease of the affinity for ssDNA and a 1.05-fold increase of the affinity for dsDNA[4]. For rGyr_hel_ZnF$_1$, ADP has the effect of decreasing 2.6-fold the affinity for ssDNA, while in the case of dsDNA the extent of the increase could not be measured.

These results are consistent with the N-terminal Zn-finger not cooperatively contributing to DNA binding by the helicase-like domain, impairing dsDNA binding the most, supposedly by competing for the substrate (Table II).

Table II. Dissociation constants for DNA binding to all constructs

ssDNA 60mer	rGyr_hel		rGyr_hel_Δlatch	rGyr_hel_ZnF$_1$
	K_D(μM) (Hill analysis)	n	K_D(μM)	K_D(μM)
ssDNA	0.20 ± 0.01	1.4 ± 0.1	0.42 ± 0.07	1.3 ± 0.4
ssDNA+ADPNP	0.46 ± 0.03	1.4 ± 0.1	1.1 ± 0.1	1.3 ± 0.3
ssDNA+ADP	0.28 ± 0.01	1.6 ± 0.1	2.6 ± 0.3	3.4 ± 0.4
dsDNA 60 bp				
dsDNA	3.9 ± 0.6		21 ± 5	n.d.
dsDNA+ADPNP	0.19 ± 0.03		36 ± 8	3.1± 0.2
dsDNA+ADP	3.7 ± 0.5		24 ± 5	10 ± 2

Discussion

Our findings indicate a role of the putative N-terminal Zn-finger on DNA binding in general, with a marked preference for dsDNA. In this case it can be interpreted as a competition with the helicase-like domain for the substrate, which is not surprising since this regions do not engage in intramolecular contacts in rGyr and therefore no direct cooperation is expected. rGyr_hel_ZnF$_1$ still displays the affinity switch first described for rGyr_hel, although although to a lesser extent, due to the negative effect exerted by the N-terminal Zn-finger. These results may indicate a role in vivo for rGyr Zn-fingers in dsDNA binding, in line with its spatial location close to the Rossman fold (domain T1 in *A. fulgidus* reverse gyrase[2], domain I in *E. coli* topoisomerase I[52]) of the topoisomerase module. The structure of a type IA topoisomerase, E. coli topoisomerase III, in complex with an 8-base ssDNA reveals the involvement of domain I in binding the 3'end of the cleaved ssDNA strand[53]. The fact that the homologous region in rGyr, namely domain T1, has the Zn-fingers right at the end of the groove where ssDNA is bound, and given that these Zn-fingers strongly interact with dsDNA, they might contribute to hold the DNA bubble in place by stabilizing the duplex and confining the unwound region to the enzyme active site.

These results also indicate that the Zn-fingers might contribute to rGyr_hel attenuation in the context of the full-length enzyme. Apparently, in rGyr the topoisomerase domain is able to attenuate the helicase-like domain not only by restricting its conformational dynamics, but also by competing for the DNA substrates.

It has been reported that Zn-fingers tend to appear in clusters and they are known to act in tandem[54]. For that reason we also attempted to express the

helicase-like domain with the two flanking Zn-fingers. Unfortunately this mutant was insoluble, and no measurements could be performed.

Overall, our results reconcile apparent contradictions with other studies on helicase-like domains from rGyr of other organisms. It has been reported that the deletion of the topoisomerase domain either decreases or has no effect at all on the helicase-like domain activity, in constructs bearing the N-terminal Zn-finger [55]. We show that the N-terminal Zn-finger has a deleterious effect on DNA binding and DNA-stimulated ATP hydrolysis by the helicase-like domain, presumably by competing for the DNA substrate, rendering most of the steady-state kinetic parameters as reduced as in the context of the full-length enzyme. On the other hand, our structural data of the isolated helicase-like domain have revealed that secondary structure motives involved in DNA binding by rGyr, like the A. fulgidus β-hairpin (aa 201-217)[2] and its homologous in T. maritima α-helix (aa 223-250)[4] are not as conserved among rGyr helicase-like domains as expected. That can also account for moderate functional differences between rGyrs from different sources. Overall, more structural information is required to identify subsets of rGyrs with slight structural differences that account for the functional differences reported.

Chapter 6

Stoichiometry and length-dependence of DNA binding to rGyr_hel

Introduction

We have previously shown that DNA processing by rGyr_hel is coupled to conformational changes driven by ATP hydrolysis [56]. Elucidation of the nucleotide cycle by determining the affinities for nucleotide and DNA in equilibrium implied the use of substrate analogs resembling intermediary states generated during the catalytic cycle. For that reason different DNA constructs of different lengths were used. The approximate dimensions of rGyr_hel in the crystal structure of rGyr are 60 x 70 x 50 Å. This roughly corresponds to a 20.6 bp dsDNA bound along its longest axis, and this number should be higher in the case of ssDNA. That would theoretically allow for simultaneous binding of three rGyr_hel molecules to a 60 bp dsDNA, the standard substrate used to characterize the rGyr_hel nucleotide cycle. Nevertheless, the following equation describing the 1:1 binding mode, shows the hyperbolic dependence of the complex concentration on K_D and the interacting partners. It has as a consequence that small changes in stoichiometry hardly affect the complex concentration, rendering the observed K_D rather insensitive to these small stoichiometry changes.

$$[hel \cdot DNA] = \frac{K_D + [hel] + [DNA]}{2 - \sqrt{\left(\frac{K_D + [hel] + [DNA]}{2}\right)^2 - [hel][DNA]}}$$

Single-molecule measurements on the other hand, clearly differentiate subsets of FRET efficiencies if the enzyme adopts different conformations when it binds different DNA regions of the same construct. We therefore set out to determine the stoichiometry of binding of rGyr_hel to DNA substrates, as well as the minimal length allowing binding of only one enzyme molecule without loss of activity. That way, binding or rGyr_hel to different DNA regions can be distinguished from binding to one region in different conformations, in conditions that show more than one population of FRET efficiencies on single-molecule measurements.

Results

Stoichiometry of binding of rGyr_hel to different DNA substrates in the nucleotide-free state

We have previously reported the rGyr_hel affinity for a 60mer ssDNA to be 0.20 ± 0.01 μM. The stoichiometric titration, using a substrate concentration 10 times higher than the K_D value did not produce the typical kink of the binding isotherm[57]. Only a DNA concentration 20 times higher than the K_D followed the graphic behavior that allowed assigning the stoichiometry of binding, which in this case was roughly two rGyr_hel molecules bound to one molecule of ssDNA (Figure 12).

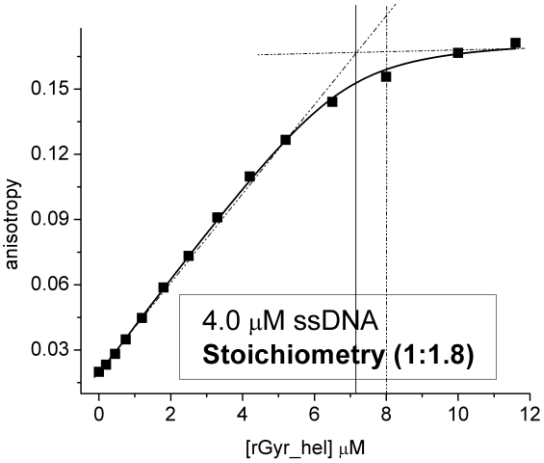

Figure 12. Stoichiometric titration of ssDNA. The stoichiometric equivalence is roughly at 8 μM. It means that two molecules of the protein bind to one molecule of ssDNA.

We have shown that in the nucleotide-free state, rGyr_hel preferentially binds a 60/20mer jxnDNA carrying ssDNA overhangs with both polarities, one at each side of the substrate dsDNA 60/20_mid, *i.e.*, 5'-OH and 3'-OH ends of the backbone chain[1]. We also demonstrated that the simultaneous presence of two ssDNA strands with both polarities at the same fork in a bubbled DNA substrate does not improve binding. It is an indication that in the nucleotide-free state, rGyr_hel interacts with only one of the ssDNA strands of the bubble substrate. Additionally, no significant difference was detected between the binding affinities of rGyr_hel to dsDNA 60/20_mid and the affinity of rGyr_hel for two other constructs of the same length with only one ssDNA overhang, of either 5'-OH (dsDNA 60/20_5) or 3'-OH (dsDNA 60/20_3) polarity (Figure 13). We therefore set out to determine the stoichiometry of binding of rGyr_hel to these substrates (Figure 14). Binding of rGyr_hel to dsDNA 60/20_mid has a

stoichiometry of 4:1. For the other two constructs a smaller ratio of 2.5:1 is obtained.

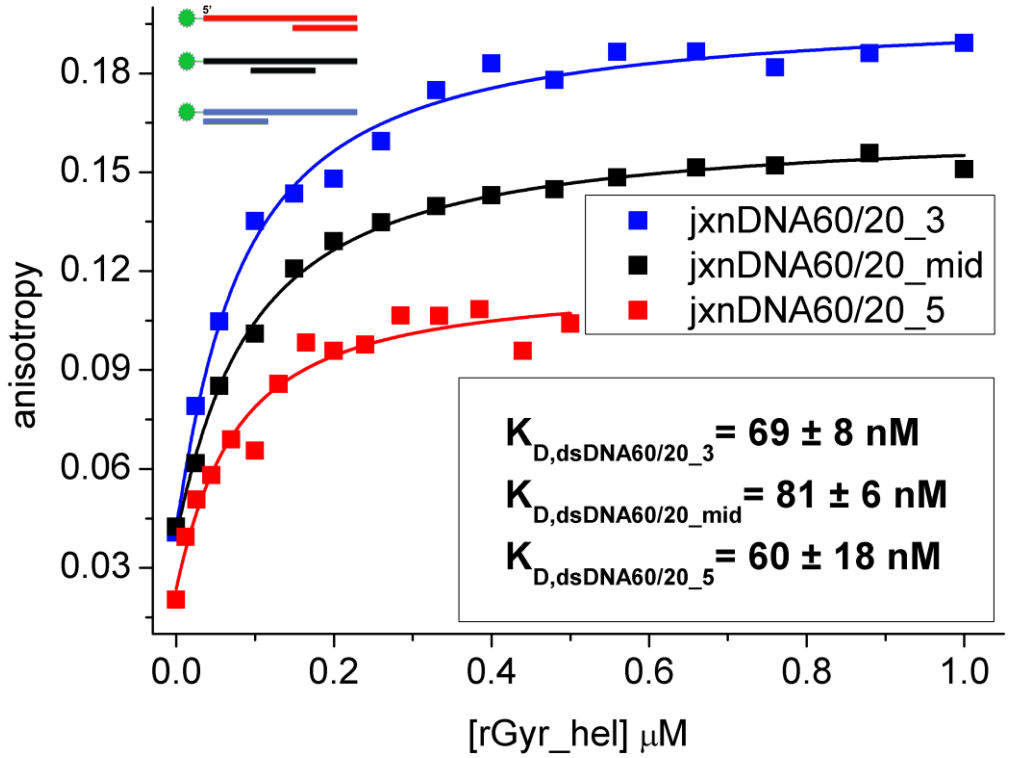

Figure 13. Binding affinities of rGyr_hel to jxnDNA substrates, with either 3', 5', or both ssDNA overhangs. It shows that all DNA constructs are bound by rGyr_hel with virtually the same affinity.

Minimal rGyr_hel jxnDNA substrate

The length dependence of the binding affinity and stoichiometry of rGyr_hel to junction DNAs with a 5'-OH polarity of the ssDNA region was also determined (Figure 15). The K_D values for binding of rGyr_hel to the different length DNAs fluctuate in ratios smaller than 2-fold, consistent with no significant difference in binding. The stoichiometry of binding on the other hand, starts with a ratio

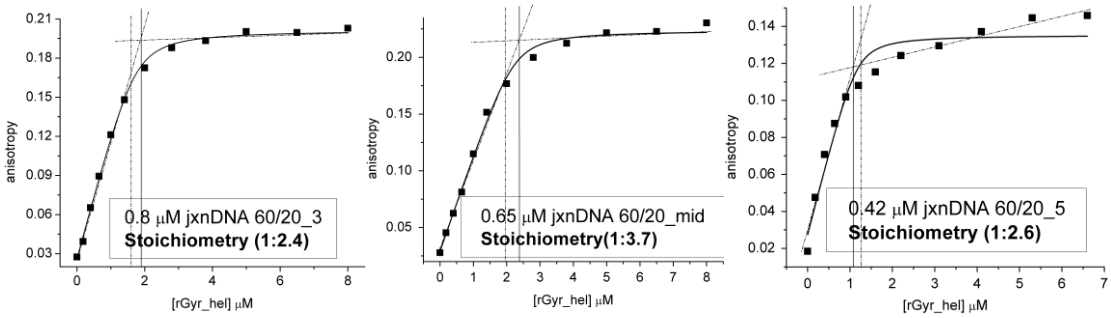

Figure 14. Stoichiometric titrations of 60/20mer junction DNAs. The construct having ssDNA overhangs with both polarities accommodates roughly one rGyr_hel molecule more than the rest.

of 3:1 for the dsDNA 60/20_5 construct, and ends up with a 1:1 binding ratio for the shortest constructs dsDNA 30/20_5 and dsDNA 25/20_5. This result is consistent with small enzyme regions engaging in contact with the ssDNA strands at a junction in the nucleotide-free state. For the DNA constructs with intermediate lengths of the ssDNA overhang, namely dsDNA 40/20_5 and dsDNA 35/20_5, the stoichiometric point could not be detected due to the absence of the expected kink in the graphic behavior. Interestingly, also their affinities for rGyr_hel were the lowest of all the junction constructs.

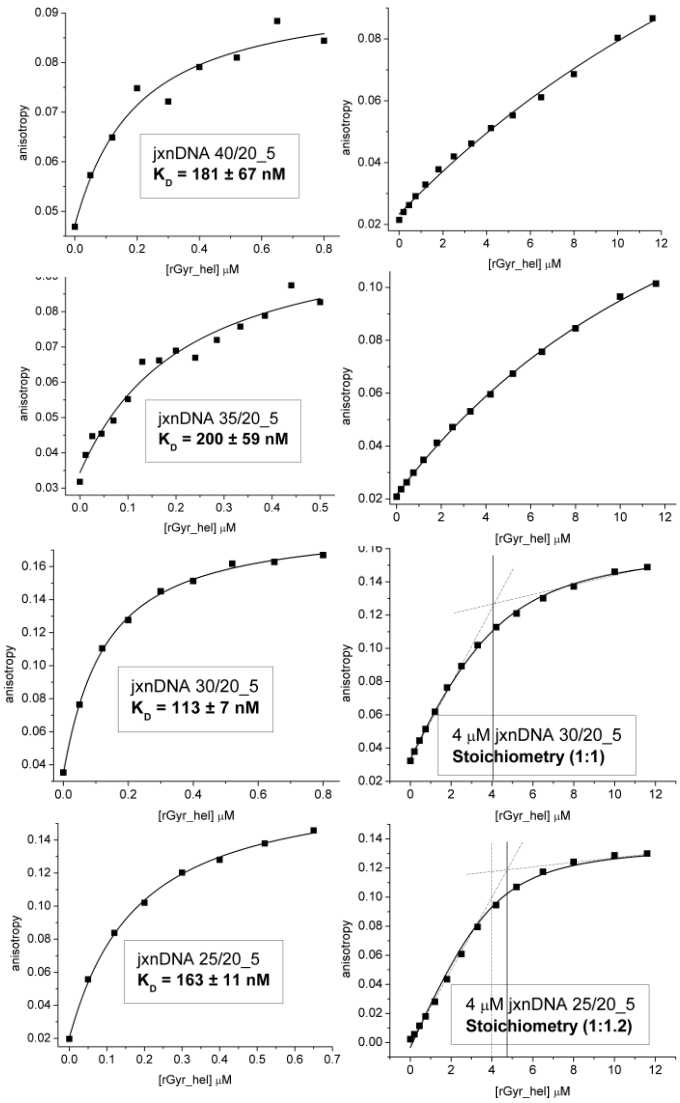

Figure 15. DNA binding (left panel) and stoichiometric titrations for the corresponding construct (right panel).

Apparently, higher DNA:protein ratios should be used to determine the stoichiometry of binding to these jxnDNAs.

Discussion

Binding of rGyr_hel to ssDNA with a stoichiometry of 2:1 is not expected to significantly affect the observed K_D, provided that rGyr_hel does not cooperatively bind DNA. If there were a significant cooperative binding between these interacting partners, binding of the first protein molecule would facilitate binding of a second one to the ssDNA substrate, and at the same time the affinity of both molecules of the enzyme for the substrate would be increased. Cooperativity in binding would imply a mixed effect of higher

stoichiometry and increase of the affinity for DNA, that would be reflected on the K_D value and the shape of the binding isotherm. If alternatively the same protein where faced with a ssDNA segment short enough to accommodate only one protein molecule, the stoichiometry would be forced to remain 1:1, preventing the enzyme from the affinity increase upon interaction with a second molecule of the enzyme. We have previously reported that the shape of the binding isotherm suggests marginal cooperativity between two rGyr_hel molecules bound to the same ssDNA, and the fit with the Hill equation was slightly better than using a 1:1 binding model[2]. Further experiments should address whether the minimal ssDNA substrate, *i.e.*, the substrate that can accommodate only one rGyr_hel molecule, shows a decreased affinity for rGyr_hel that may further support the notion of a functionally relevant cooperative effect. Nevertheless, the 1:1 based model for determination of the K_D should be adjusted to our experimentally determined stoichiometry factor.

The analysis of the junction substrates with different polarities shows that rGyr_hel has no preference for the polarity of the ssDNA overhang at the junction on the nucleotide-free state. It most probably indicates the presence of different regions of the enzyme responsible for binding to each strand, since the spatial distribution of residues that can contact ssDNA of one polarity are not optimally arranged to establish contact with ssDNA of the inverse polarity[58]. These results also indicate that the regions involved in binding to the ssDNA strands cannot simultaneously interact with the strands of both polarities in the open conformation, as we have previously determined via smFRET that this is the conformational state corresponding to this protein:DNA complex[1].

From the stoichiometry of binding of rGyr_hel to the junction substrates we conclude that in the case of dsDNA 60/20_mid, the enzyme binds to both junctions and both ssDNA overhangs. A molecule of the enzyme bound to the dsDNA region is unlikely, due to the low affinity of this complex in the nucleotide-free state. From the other two constructs we conclude that a 40 nt ssDNA region is still long enough to accommodate roughly two rGyr_hel molecules, in addition to the one bound to the junction (Figure 16). The length of the 5’ ssDNA overhang next to a junction can be reduced to 5 nt without

significant change of the affinity for rGyr_hel, which indicate that the interaction with this region does not involve a large protein surface.

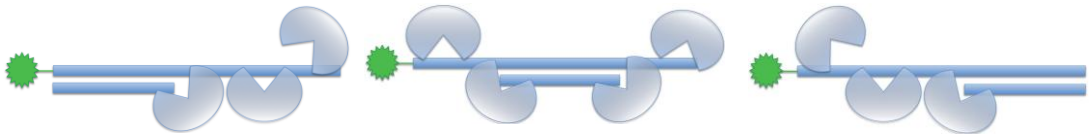

Figure 16. Figure depicting hypothetical binding modes of rGyr_hel to the different 60/20 jxnDNAs. Left: construct with a 3'ssDNA overhang, where approximately 2.5 rGyr_hel molecules bind, one to the junction and the rest to the ssDNA region. Middle: construct with both 3' and 5' ssDNA overhangs, where approximately 4 protein molecules bind, two to the junctions and the others to the ssDNA region. Right: same as in the first case, only the ssDNA directionality is inverted.

Chapter 7. Article

Deletion of the latch from reverse gyrase helicase-like domain restricts the conformational changes associated to nucleotide-dependent DNA processing

We have contributed to demonstrate that the latch, an insertion into the H2 domain of the helicase-like domain, modulates interactions between the topoisomerase and the helicase-like domain during positive DNA supercoiling. We determined the nucleotide cycle from a thermodynamic and conformational point of view for this mutant. It revealed that the reverse gyrase helicase-like domain lacking the latch had significantly different DNA preferences during the nucleotide cycle compared to rGyr_hel. It shows thermodynamically uncoupled ssDNA binding in the ATP-bound state, and even loses the ssDNA high affinity state in the post-hydrolysis or the ADP-bound state, indicating a major role of the latch in ssDNA binding at these stages. Interestingly, jxnDNA binding at the pre-hydrolysis state is the only stage virtually unchanged when compared to rGyr_hel. We show for the first time that at this point of the reaction both mutants are able to unwind DNA. Overall, our results are consistent with a modulatory function of the latch, presenting the 5`-ssDNA strand in the pre-hydrolysis state to the lid in order to perform positive supercoiling.

Deletion of the latch from reverse gyrase helicase-like domain restricts the conformational changes associated with nucleotide-dependent DNA processing.

Yoandris del Toro Duany[1], Agneyo Ganguly[1], and Dagmar Klostermeier[1,2,*]

* corresponding author:

Dagmar Klostermeier, University of Muenster, Institute for Physical Chemistry, Corrensstrasse 30, D-48149 Muenster, Germany

Phone 0049-251 83 23421, FAX 0049-251-83 29138, dagmar.klostermeier@uni-muenster.de

[1] University of Basel, Biozentrum, Dept. of Biophysical Chemistry, Klingelbergstrasse 70, CH-4056 Basel, Switzerland

[2] University of Muenster, Institute for Physical Chemistry, Corrensstrasse 30, D-48149 Muenster, Germany

Funding information: This work was supported by the VolkswagenStiftung (D.K.) and the Swiss National Science Foundation (D.K.).

Keywords: reverse gyrase, helicase, topoisomerase, latch, positive supercoiling, DNA unwinding

Running title: Role of the latch on DNA processing by reverse gyrase helicase-like domain.

Abstract

Reverse gyrase is an enzyme exclusive from thermophilic and hyperthermophilic organisms that plays a DNA-thermoprotective role at high temperatures. Its structural signature is a modular build-up consisting of a topoisomerase domain linked to a helicase-like module, this last one bearing an insertion, the latch domain, optimally suited for interdomain communication. Deletion of the latch from the full-length reverse gyrase abolishes its capacity to positively supercoil DNA, and only relaxation can take place. However, deletion of the latch from the isolated helicase-like domain strongly impairs DNA binding, DNA-stimulated ATP hydrolysis, and thermodynamic coupling between both processes. Here we further address the effect of the latch deletion from *T. maritima* reverse gyrase helicase-like domain. We confirm the big differences in the thermodynamic and conformational properties compared to the helicase-like domain bearing the latch. Nevertheless, at the pre-hydrolysis stage there are virtually no differences between both constructs, indicating a minimal contribution of the latch. However, DNA supercoiling by the full-length reverse gyrase reveal a role of the latch at this stage of the reaction, preventing the topoisomerase domain from resealing the cleaved strand, and therefore from performing only DNA relaxation. Our results are consistent with a role of the ssDNA-bound latch at the pre- and post-hydrolysis states, guiding the lid covalently attached to the same strand to perform the directional strand passage that ensures introduction of positive supercoils into the DNA.

Introduction

Reverse gyrase is a type IA topoisomerase exclusive from thermophilic and hyperthermophilic organisms[1] that introduces positive supercoils into the DNA in an ATP-dependent manner[2]. It has been suggested to play a DNA thermoprotective role *in vivo*, although the deletion of its gene is not a lethal mutation[3]. Nevertheless, reverse gyrase has been demonstrated to have DNA chaperone and renaturase activities[4,5].

The distinctive structural feature of reverse gyrase is its modular build up. It contains an N-terminal helicase-like module fused to a C-terminal topoisomerase domain, homologous to the family IA of topoisomerases[6]. The helicase-like domain of reverse gyrase belongs to the superfamily 2 of helicases (SF2). It comprises two RecA folds, bearing all determinants for nucleotide binding and hydrolysis. It also possesses an insertion in the H2 domain, the so-called latch domain, which has been shown to play a key role in interdomain communication, presumably by guiding and presenting the DNA into the active site of the topoisomerase domain. Furthermore, the latch is also crucial for thermodynamic coupling between DNA binding and nucleotide binding and hydrolysis[7].

We have previously reported that the helicase-like domain of reverse gyrase is a nucleotide-dependent switch, attenuated by the topoisomerase domain in the context of the full-length enzyme[8]. We have also characterized the nucleotide cycle of rGyr_hel, by elucidating the DNA preference at each stage of the cycle from a thermodynamic point of view[9]. In the present study we further analyze the role of the latch region, an insertion on the H2 domain, by studying how its deletion affects the way rGyr_hel interacts with nucleotide

analogs, DNA, the coupling between both processes, and the conformational changes during the reaction. Additionally, we demonstrate for the first time that this construct of the helicase-like domain possesses nucleotide-dependent DNA unwinding activity. Using this approach we have been able to elucidate the nucleotide cycle of the helicase-like domain from *T. maritima* reverse gyrase, when the latch is removed from its structure. It has revealed the stages of the cycle where the reaction is affected most, due to strong involvement of the latch, and answers the question of why the latch deletion from the full-length enzyme abolishes the introduction of positive DNA supercoiling by reverse gyrase.

Material and methods

Cloning and protein purification

rGyr_hel_Δlatch was produced as described[7]. The double Cysteine mutant S169C/F332C was generated according to the Quickchange protocol (Stratagene) and purified as rGyr_hel.

Nucleotides and DNA substrates

Nucleotides were purchased from Jena Biosciences and Biolabs. Unlabeled and labeled oligonucleotides were purchased from Sigma Aldrich and Purimex, respectively. The ssDNA substrate used was: 5'-(fluorescein)-AAG CCA AGC TTC TAG AGT CAG CCC GTG ATA TTC ATT ACT TCT TAT CCT AGG ATC CCC GTT. dsDNA was generated by annealing of the ssDNA substrate with the complementary strand. jxnDNAs were obtain by annealing the ssDNA substrate with 20nt oligonucleotides, complementary to either the

underlined part or the ends. The 5'ssDNA and 3'ssDNA junction DNAs for unwinding assays were obtained by annealing: 5'-(Cy5)-CGT TAC GCA with GAT AAT GCG TAA CG-(Cy3)-3', or 5'-(Cy5)-CGT TAC GCA TTA TC with TGC GTA ACG-(Cy3)-3'.

DNA unwinding assay

DNA unwinding was detected via FRET between the Cy3 and Cy5 dyes. The 5' and 3' ends were labeled with Cy5 and Cy3 respectively, at the duplex side of junction or dsDNA. Unwinding was detected by decrease of the fluorescence emission of the acceptor Cy5 at 666 nm (1 nm bandwidth), after excitation at 554 nm (1 nm bandwidth) on a Fluoromax-3 fluorimeter (Jobin Yvon). 0.5 μM DNA was incubated with 5 μM the enzyme at 37°C for 1 min in buffer 50 mM Tris/HCl, pH 7.5, 0.15 M NaCl, 10 mM $MgCl_2$, 10 μM $Zn(OAc)_2$, 2 mM β-mercaptoethanol, prior to nucleotide addition.

Fluorescence equilibrium titrations

The assay for determination of fluorescently labeled mant-nucleotides binding to rGyr_hel_Δlatch was performed as described[9]. The K_D values were determined with the equation describing a 1:1 binding mode:

$$F = F_0 + \frac{\Delta F_{max}}{[mA]}\left(\frac{[hel] + [mA] + K_D}{2} - \sqrt{\left(\frac{[hel] + [mA] + K_D}{2}\right)^2 - [hel][mA]}\right)$$

where F_0 is the inicial fluorescence of the nucleotide, ΔFmax is the amplitude of the increase upon binding to rGyr_hel_Δlatch, [hel] is rGyr_hel_Δlatch concentration, and [mA] is the labeled nucleotide concentration.

Fluorescein-labeled DNA binding was measured *via* fluorescence anisotropy, at 37°C in buffer 50 mM Tris/HCl, pH 7.5, 0.15 M NaCl, 10 mM $MgCl_2$, 10 µM $Zn(OAc)_2$, 2 mM β-mercaptoethanol. Data was evaluated as previously described[8].

Single-molecule FRET

Measurements and data evaluation were performed as previously described[9].

Plasmid DNA supercoiling

The DNA supercoiling reaction of rGyr_Δlatch was performed at 75°C in buffer 50 mM Tris/HCl, pH 7.5, 0.15 M NaCl, 10 mM $MgCl_2$, 10 µM $Zn(OAc)_2$, 2 mM β-mercaptoethanol, 10% (w/v) polyethylene glycol 8000, as previously described[7].

Results

Nucleotide binding to rGyr_hel_Δlatch

We have previously reported nucleotide and DNA binding data of rGyr_hel_Δlatch, in the cases of ADPNP, ADP, ssDNA, and dsDNA. We further address the nucleotide cycle by characterizing the ADP.BeF_x- and ADP.MgF_x-bound states, as analogs for the pre-hydrolysis and post-hydrolysis prior P_i release states, respectively. We also characterize the interaction of the enzyme with junction DNA (jxnDNA), as an intermediate generated during the catalytic cycle.

In the DNA-free state, rGyr_hel_Δlatch binds the nucleotide analogs ADPNP and ADP with 2.8- and 1.5-fold higher affinities than rGyr_hel, respectively. As

the latch is not involved in nucleotide binding or hydrolysis, this probably reflects an effect of the mutation on the overall protein dynamics. However, binding of the analogs ADP.BeF_x and ADP.MgF_x remains virtually the same as the wild-type isolated helicase-like domain. In general, binding of DNA hardly affects the affinity of rGyr_hel_Δlatch for ADPNP or ADP, but slightly increases the affinity for ADP.BeF_x and decreases the affinity for ADP.MgF_x (Figure 1).

Specifically ssDNA increases 12-fold the affinity for ADP.BeF_x, in line with the effect it has on the wild-type helicase, where it increases 9.5-fold the affinity for ADP.BeF_x. The presence of ssDNA decreases 0.7–fold the affinity for ADP.MgF_x, also in agreement with the 0.7-fold decrease in affinity seen with rGyr_hel. On the other hand, dsDNA increases 1.8–fold and decreases 1.5–fold, the affinity of rGyr_hel_Δlatch for ADP.BeF_x and ADP.MgF_x, respectively. The corresponding values for rGyr_hel are 3.8–fold and 1.3–fold increases in affinity. Overall, these results reveal that the trend observed in rGyr_hel for the effect of DNA on nucleotide analogs binding, is only conserved in the presence of ssDNA for the latch deletion mutant (Table I).

We have also studied the effect of jxnDNA on nucleotide binding, using the 60/20mer previously described[9]. ADPNP and ADP.BeF_x binding to rGyr_hel_Δlatch are 2-fold and 1.7-fold increased by the presence of the jxnDNA, respectively. On the other hand, binding of rGyr_hel_Δlatch to ADP.MgF_x is 2.7-fold decreased by the presence of the jxnDNA, while the affinity for ADP is 1.5-fold increased. Compared to rGyr_hel, the most affected events are ADPNP binding, which is 600–fold increased in the wild-type

helicase; ADP.MgF_x binding, that remains unaltered in rGyr_hel; and ADP binding, which is 4.7-fold increased in the jxnDNA-bound state.

DNA binding to rGyr_hel_Δlatch

In the present study we also investigate DNA binding to rGyr_hel_Δlatch, and how it is influenced by the nucleotide state of the enzyme. For that purpose, the previously described 60mer ssDNA and 60bp dsDNA were used, as well as the 60/20mer jxnDNA (Table II).

We have reported data for rGyr_hel_Δlatch binding to ssDNA and dsDNA, showing that the latch deletion has the overall effect of drastically reducing the affinity for DNA. Compared to rGyr_hel, in the nucleotide-free state the most impaired is dsDNA binding by rGyr_hel_Δlatch, with a 5.4–fold reduced affinity, while in the case of ssDNA the affinity reduction is only 2.1–fold. In the ADPNP-bound state, again dsDNA binding is the most impaired, with a 1.7-reduced affinity compared to the nucleotide-free state, in contrast with the 20-fold increase of affinity experimented by rGyr_hel. ssDNA binding by rGyr_hel_Δlatch is 2.6-fold reduced, following the same trend as rGyr_hel, where ADPNP binding reduces 2.3-fold the affinity for ssDNA. Finally, in the ADP-bound state rGyr_hel_Δlatch binds ssDNA with a 6.2-fold reduced affinity, while dsDNA binding is the same as for the nucleotide-free enzyme. These are the same trends observed in the ADP-bound rGyr_hel, with a 1.4-fold reduced affinity for ssDNA compared to the nucleotide-free state, and practically no effect on dsDNA binding (Figure 2).

Analysis of the effect of the transition state analog ADP.BeF_x on DNA binding resulted on a 1.7-fold reduced affinity for ssDNA and a 5.8-fold increased

affinity for dsDNA. Compared to rGyr_hel, ssDNA binding is the most affected, since the wild-type helicase-like domain experiences a 4.5-fold increase in affinity in this nucleotide state. The trend observed on dsDNA binding is in agreement with the effect observed on rGyr_hel, although the 20-fold increase in affinity in the presence of ADP.BeF_x suggests that the latch deletion reduces the extent of the stimulation of dsDNA binding by this nucleotide analog.

DNA binding by rGyr_hel_Δlatch in the presence of ADP.MgF_x is 9.3- and 1.5-fold decreased, in the cases of ssDNA and dsDNA, respectively. For rGyr_hel the corresponding values are a 2.4-fold increased affinity for ssDNA and a 1.8-fold increased affinity for dsDNA, indicating that this is the nucleotide state where the overall trend most drastically differ between these two constructs. It also implies a crucial role of the latch on ssDNA binding at this point of the cycle.

We also investigated binding of rGyr_hel_Δlatch to the 60/20mer junction DNA in all nucleotide states. In the nucleotide-free state rGyr_hel_Δlatch binds jxnDNA with similar affinity as ssDNA, which means that the enzyme binds to the ssDNA region and the junction is no longer recognized. In the ADPNP-bound state the affinity for the jxnDNA is 2.6–fold decreased compared to the nucleotide-free state, and the value for the dissociation constant is the same as the complex with ssDNA, meaning that again the enzyme is only interacting with the ssDNA region of this substrate. In the ADP.BeF_x–bound state however, the affinity for jxnDNA is 11.4–fold increased, with a K_D value only 2-fold smaller than the corresponding rGyr_hel complex. This is the first stage where rGyr_hel_Δlatch preferably binds a DNA different

from ssDNA. At the post-hydrolysis state prior to P_i release, mimicked by ADP.MgF_x, the preference for the ssDNA is regained, with a 1.3-fold decrease in affinity for the jxnDNA. The K_D value is even slightly higher than the one for ssDNA binding. This scenario does not change in the presence of ADP, where the affinity for jnxDNA is 4-fold decreased and is also within the range of the affinity for ssDNA, and virtually the same value displayed by rGyr_hel.

Overall, rGyr_hel_Δlatch preferably binds ssDNA throughout the nucleotide cycle, except at the pre-hydrolysis state mimicked by ADP.BeF_x, where rGyr_hel_Δlatch preferably binds to the jxnDNA, with an affinity comparable to rGyr_hel binding to jxnDNA in the same nucleotide state. Interestingly, at the post-hydrolysis state prior to Pi release, although the preference for ssDNA is regained, the affinity for the enzyme is so low that it is likely that rGyr_hel_Δlatch disengages from the contact with ssDNA.

Single molecule FRET

It has been previously reported for helicases, the occurrence of a conformational change upon ATP and DNA binding that brings the recA domains closer together, and the enzyme adopts a closed conformation[10]. We have been able to demonstrate that rGyr_hel experiments the same conformational change in the presence of DNA and the nucleotide analogs ADPNP and ADP.BeFx[9]. We also address the question of the conformational change in rGyr_hel_Δlatch by creating the same double Cys mutant previously reported for rGyr_hel, S169C/F332C[9].

We have also reported crystallographic data, indicating that the latch deletion does not affect the proper folding of the H2 domain[7]. We also showed that a

labeled rGyr_hel_Δlatch double Cys mutant exhibits a FRET efficiency peak at approximately 0.15, the same as the FRET efficiency maximum of the equivalent rGyr_hel double Cys mutant. This is a further indication that the latch deletion does not affect the conformation neither in the crystal lattice nor in solution[11].

In the absence of DNA, rGyr_hel_Δlatch shows the same conformation in all nucleotide states as the nucleotide-free enzyme (Figure 3). Binding of any of the DNA substrates in the nucleotide-free state does not induce any detectable conformational change either. In the ADPNP-bound state, binding of DNA to rGyr_hel_Δlatch does not promote the formation of the high FRET species detected on rGyr_hel, providing the first conformational difference between these constructs. This result is also in line with the lack of cooperativity in binding of dsDNA and ADPNP by rGyr_hel_Δlatch. In the presence of ADP.BeF_x however, ssDNA and dsDNA promote closure of the cleft in only a fraction of the rGyr_hel_Δlatch molecules, with both species represented on the histograms as populations of high and low FRET efficiencies. jxnDNA however, is the only construct that can promote full closure of the cleft between the recA domains in this nucleotide state, in agreement with its rGyr_hel-like affinity for jxnDNA. Right after hydrolysis rGyr_hel_Δlatch returns to the open conformation, in line with the behavior seen by rGyr_hel (Figure 4). These experiments indicate that the cooperativity in binding of both types of substrates is completely lost at the beginning of the reaction cycle, and only at the pre-hydrolysis state the expected cooperative effect in binding of both substrate analogs occurs.

DNA unwinding by rGyr_hel_Δlatch

In the accompanying paper we report that rGyr_hel is able to unwind jxnDNA in the presence of ADP.BeF_x. We also tested whether the latch deletion might have an effect on DNA unwinding by the enzyme. For that purpose the rGyr_hel_Δlatch mutant was used, under the same assay conditions as rGyr_hel (Figure 5).

rGyr_hel_Δlatch unwinds the 5'ssDNA junction at the same rate as rGyr_hel, namely 0.02 s^{-1}, indicating that the latch deletion has no effect on the unwinding rate of jxnDNA with this polarity of the ssDNA overhang. On the other hand, unwinding of the 3'ssDNA junction takes place at a rate approximately half so fast as rGyr_hel. In the accompanying paper we demonstrate the involvement of the latch in binding to the 5'ssDNA overhang in a jxnDNA. Probably the latch is not the only region of the molecule engaging in contact with this strand. That is why when the DNA strand with 5'-polarity is the longest of the junction, other regions of the molecule can compensate for the lack of the latch. When the strand with this polarity is short however, as is the case of the 3'ssDNA junction, the contribution of the latch becomes more relevant and the overall unwinding reaction is slowed-down, compared to rGyr_hel.

Plasmid DNA supercoiling by rGyr_hel_Δlatch

Although the supercoiling assay has been performed in many conditions and with several nucleotide analogs, there is no report of this reaction in the presence of ADP.BeF_x or ADP.MgF_x. In this study we also investigate the

supercoiling reaction performed by rGyr_Δlatch in the presence of these transition state analogs (Figure 6).

The control reaction with ATP only showed DNA relaxation, in agreement with previous reports[7]. In the presence of ADP.BeF_x however, in spite of a prominent nicked-DNA band also relaxation was detected. This is in contrast with the reaction performed by rGyr, where only nicked DNA is detected. This result further supports our hypothesis that the latch remains bound to the DNA covalently attached to the lid, preventing from resealing at this stage. Apparently, the strand passage and introduction of positive supercoils at a later stage, depends on the rearrangement of the intact strand and a conformational change where the latch optimally aligns the lid-bound DNA to perform the resealing.

Discussion

We have previously speculated that the helicase-like domain overall increased affinity for nucleotides in the DNA-free state, as a consequence of the latch deletion, might have a dynamic reason. Our smFRET data indeed supports this notion, because the FRET efficiency histograms from rGyr_hel_Δlatch show better defined peaks and less background.

From a thermodynamic point of view, the nucleotide cycle of rGyr_hel_Δlatch starts with binding of ssDNA and ATP. However, neither the affinity increase for both substrates as expected from thermodynamically coupled reactions, nor the associated conformational change reported for rGyr_hel in the DNA-ADPNP-bound state, take place. Only at a later point close to hydrolysis the conformational change that brings the recA domains closer to each other

occurs. This is the first stage of the reaction where rGyr_hel_Δlatch displays a high affinity state for DNA, comparable to rGyr_hel. Apparently, only the isomerized form of the nucleotide ATP*, represented by ADP.BeF_x, and the jxnDNA can promote this conformational change. At this point, the DNA preference changes for jxnDNA and rGyr_hel_Δlatch can promote local unwinding, thus providing the topoisomerase domain with the ssDNA substrate for strand breakage, passage, and reseal[7].

Right after hydrolysis and prior to Pi release however, the reaction critically differs from the proposed cycle for rGyr_hel. Although both constructs display a preference for ssDNA, in the case of rGyr_hel_Δlatch the high affinity state for ssDNA is completely lost, with a K_D value of 3.9 μM, while the nucleotide remains bound with a comparable affinity of 3.5 μM. At this state, rGyr_hel_Δlatch most probably disengages from the contact with DNA, nucleotide, or both (Figure 7).

Role of the latch at every step of rGyr_hel nucleotide cycle

Comparison of our data on DNA and nucleotide analogs equilibrium binding to rGyr_hel_Δlatch and rGyr_hel, as well as smFRET and DNA unwinding measurements, reveal the steps of the nucleotide cycle where the latch plays a crucial role. First, the cooperative binding of dsDNA and ADPNP by rGyr_hel, and the associated conformational change that closes the cleft between the recA domains, completely disappears upon latch deletion. It is in line with a crucial role of the latch in binding dsDNA and contributing to the closure of the cleft in the ADPNP-bound state. At the following step however, mimicked by ADP.BeF_x, thermodynamically and structurally the latch deletion

does not seem to play a major role. Nevertheless, a closer look reveals mild impairment of the jxnDNA unwinding reaction that rGyr_hel_Δlatch performs, compared to rGyr_hel. It seems that the role of the latch at this point consists not that much on taking part of the intrinsic properties of the helicase core, but on communicating the nucleotide state to the topoisomerase domain, presenting the 5'ssDNA strand to it. That might be the reason why rGyr_Δlatch is unable to positively supercoil DNA. Right after hydrolysis and prior Pi release, the loss of the high affinity state for ssDNA also indicates a key role of the latch in binding to it. And finally, at the ADP-bound state, rGyr_hel_Δlatch and rGyr_hel display properties rather similar to the substrate-free enzyme. It is an indication that in the context of the full-length enzyme, at this stage of the cycle the introduction of one turn into the DNA, either to promote relaxation of negatively supercoiled DNA or to introduce positive supercoils has already been done.

Overall, the latch is strongly involved in dsDNA cooperative binding in the ATP-bound state, 5'ssDNA binding and subsequent contribution to jxnDNA unwinding at the pre-hydrolysis state, and ssDNA binding at the post-hydrolysis state prior Pi release.

Implication of the latch in DNA relaxation and supercoiling

In the context of the full-length rGyr, the deletion of the latch has been reported to abolish the capacity to positively supercoil DNA[7]. Our equilibrium binding data indicate that rGyr_hel_Δlatch, unlike rGyr_hel, is unable to remain bound to the same DNA segment after one round of the nucleotide cycle, due to the strong decrease in affinity for ssDNA in the post-hydrolysis

step prior to Pi release. We have previously suggested that rGyr is likely to processively undergo several catalytic cycles bound to the same DNA segment, due to the gradual decrease in affinity for the nucleotide after its hydrolysis while maintaining a constitutively high affinity for ssDNA[9]. In the accompanying paper we demonstrate that strand breakage by the topoisomerase domain only takes place at a point close to ATP hydrolysis. We also demonstrate that rGyr_hel_Δlatch and rGyr_hel behave the same way at this point of the cycle. Nevertheless, a significant difference arose from the supercoiling assays, where the deletion of the latch from the full-length enzyme allows DNA relaxation at the pre-hydrolysis state. This finding indicates that the latch prevents premature strand resealing that would only amount to relaxation due to the structural array of the enzyme domains and DNA at this stage of the reaction. Therefore, the stages of directional strand passage and resealing are where the biggest functional differences between rGyr and rGyr_Δlatch are expected, and it should occur at the post-hydrolysis stage. Given the big difference in ssDNA binding between the two helicase constructs at the ADP.MgF_x-bound state, the latch seems to remain bound to the ssDNA and its conformation is what determines whether the strand reseal actively occurs in the direction of introducing positive supercoils, or if it passively happens in the sense of the gradient, *i.e.*, strand reseal in a direction that leads to relaxation.

Overall, our results indicate that the latch plays a crucial role in promoting cooperative binding of dsDNA in the ATP-bound state, in unwinding and presenting the 5'ssDNA segment to the active tyrosine in the lid at the ATP*-bound state, and in guiding the DNA-bound lid to perform the directional

strand passage that amounts to DNA relaxation and ultimately supercoiling in the ADP·P_i-bound state. Nevertheless, as a compensatory mechanism, the lid seems able to “find” the ssDNA strand without the help of the latch, and that appears to be the reason why rGyr_Δlatch is able to promote relaxation of negatively supercoiled DNA in spite of the severe functional alterations. Even the isolated topoisomerase domain is able to perform DNA relaxation[12]. But the latch seems to be irreplaceable on its function of guiding the DNA-bound lid in a direction that ensures introduction of positive supercoils into the DNA.

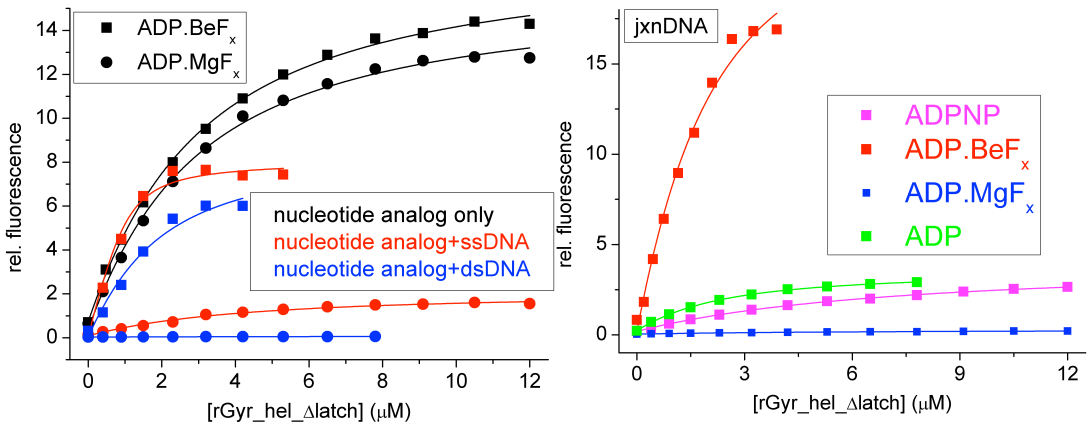

Figure 1

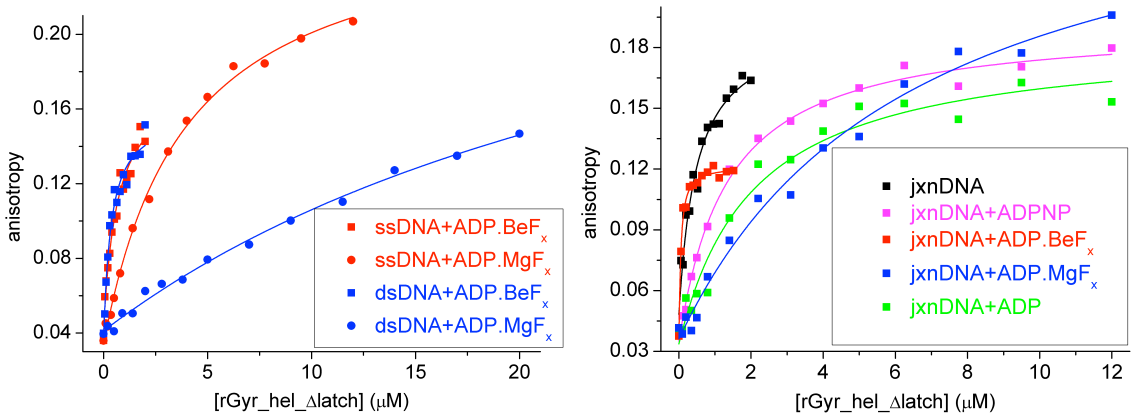

Figure 2

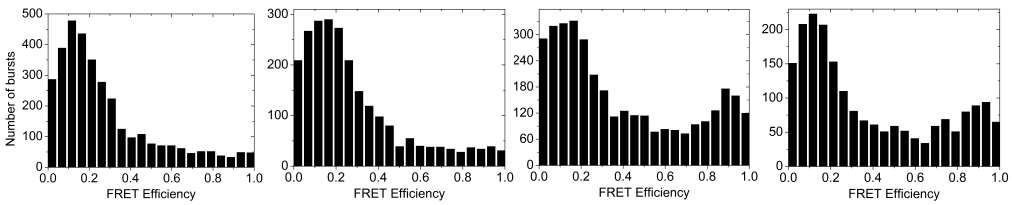

Figure 3

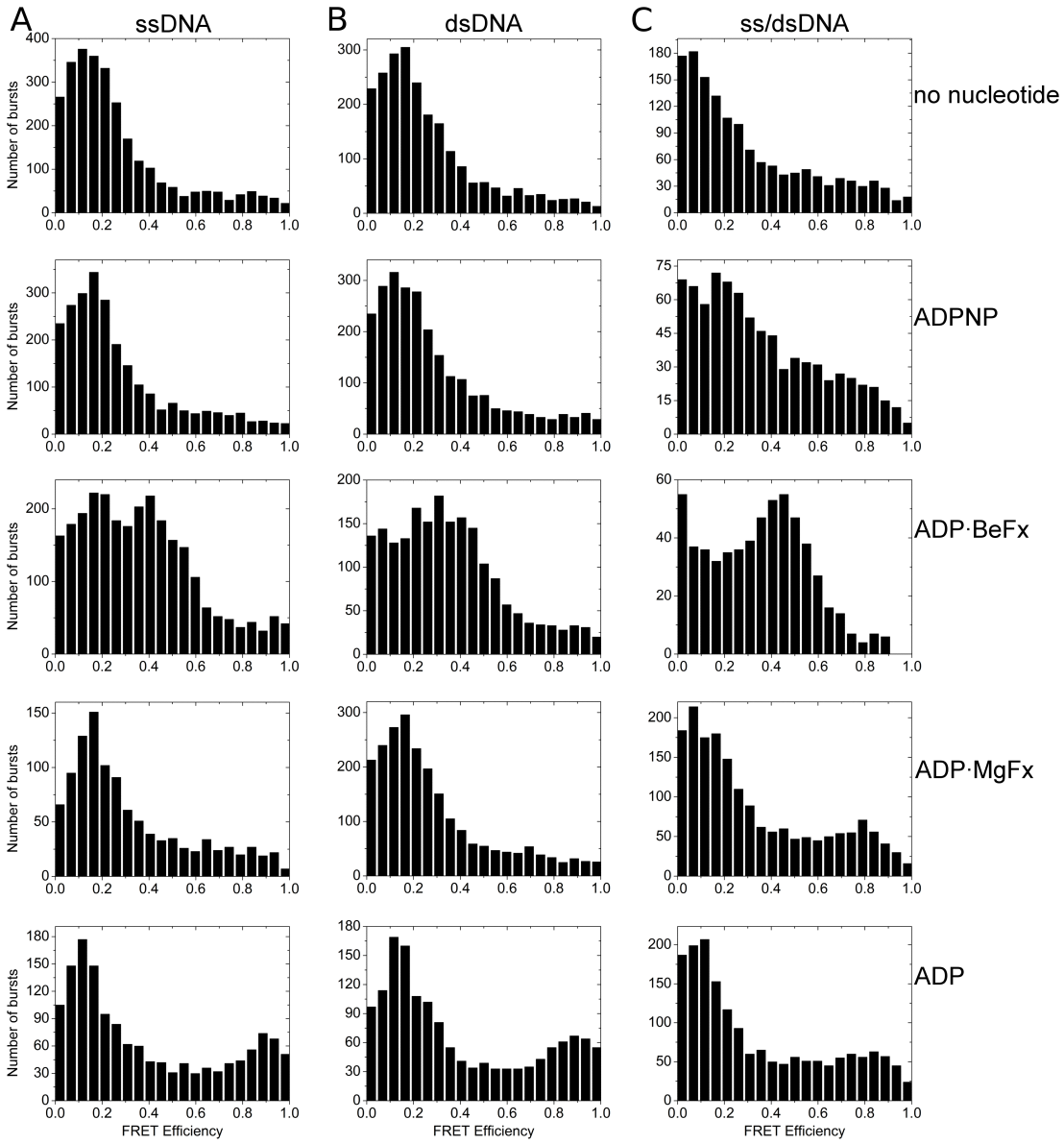
A
ssDNA
B
dsDNA
C
ss/dsDNA
no nucleotide
ADPNP
ADP·BeFx
ADP·MgFx
ADP
Number of bursts
FRET Efficiency

Figure 4

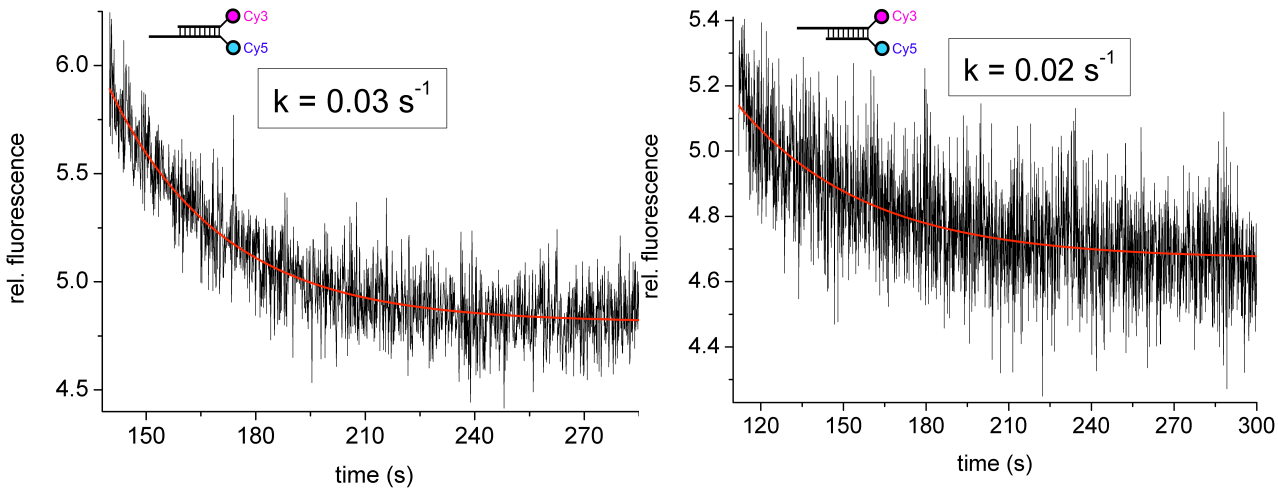

Figure 5

Figure 6

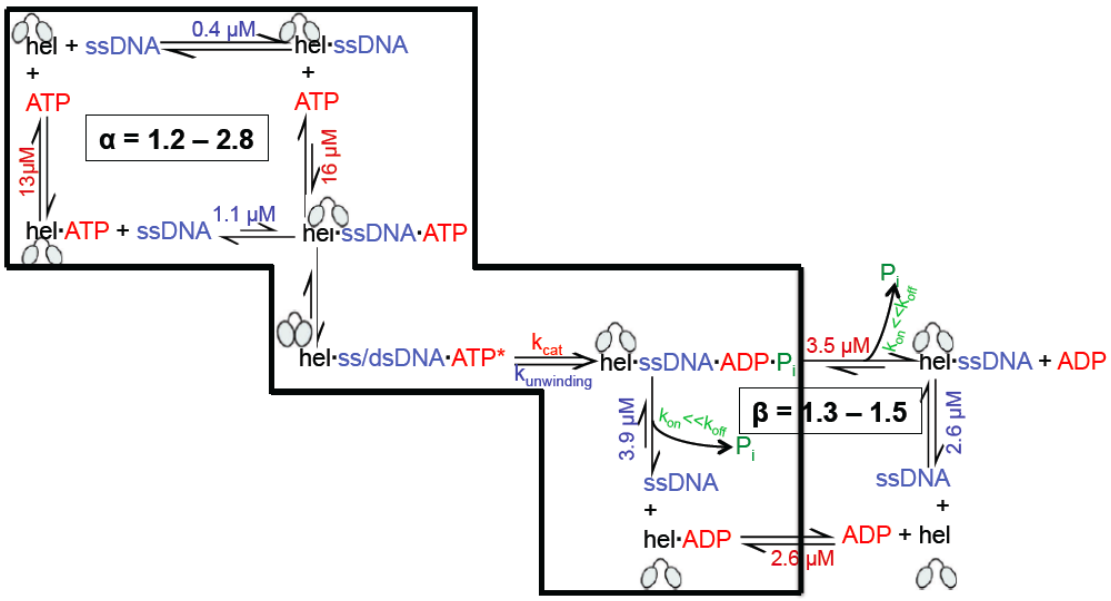
hel + ssDNA
0.4 µM
hel·ssDNA
+
ATP
ATP
α = 1.2 – 2.8
13µM
16 µM
hel·ATP + ssDNA
1.1 µM
hel·ssDNA·ATP
hel·ss/dsDNA·ATP*
k_cat
k_unwinding
hel·ssDNA·ADP·P_i
3.5 µM
P_i
k_on << k_off
hel·ssDNA + ADP
β = 1.3 – 1.5
3.9 µM
k_on << k_off
P_i
2.6 µM
ssDNA
+
hel·ADP
2.6 µM
ADP + hel

Figure 7

Table I

rGyr_hel	$K_{D\ (mantADPNP)}$ µM	$K_{D\ (mantADP.BeFx)}$ µM	$K_{D\ (mantADP.MgFx)}$ µM	$K_{D\ (mantADP)}$ µM
-	36 ± 8	1.9 ± 0.1	2.1 ± 0.1	4.2 ± 0.2
ssDNA	12 ± 2	0.2 ± 0.1	4.5 ± 0.9	10 ± 1
dsDNA	1.9 ± 0.4	0.5 ± 0.2	1.6 ± 0.2	1.7 ± 0.4
dsDNA60/20	0.06 ± 0.02	0.8 ± 0.3	2.1 ± 0.4	0.9 ± 0.1

rGy_hel_Δlatch	$K_{D\ (mantADPNP)}$ µM	$K_{D\ (mantADP.BeFx)}$ µM	$K_{D\ (mantADP.MgFx)}$ µM	$K_{D\ (mantADP)}$ µM
-	13 ± 4	2.4 ± 0.2	2.3 ± 0.2	2.7 ± 0.1
ssDNA	16 ± 8	0.2 ± 0.08	3.5 ± 0.7	2.6 ± 0.7
dsDNA	11 ± 4	1.3 ± 0.7	3.4 ± 0.5	0.9 ± 0.4
dsDNA60/20	6.6 ± 0.4	1.4 ± 0.5	6.2 ± 0.7	1.77 ± 0.08

Table II

ssDNA 60mer	**rGyr_hel**		**rGyr_hel_Δlatch**
	K_D(µM) (Hill analysis)	**n**	**K_D(µM)**
ssDNA	0.20 ± 0.01	1.4 ± 0.1	0.42 ± 0.07
ssDNA+ADPNP	0.46 ± 0.03	1.4 ± 0.1	1.1 ± 0.1
ssDNA+ADP·BeFx	44 ± 3 **nM**	1.5 ± 0.1	0.7 ± 0.2
ssDNA+ADP·MgFx	82 ± 7 **nM**		3.9 ± 0.3
ssDNA+ADP	0.28 ± 0.01	1.6 ± 0.1	2.6 ± 0.3
dsDNA 60mer			
dsDNA	3.9 ± 0.6		21 ± 5
dsDNA+ADPNP	0.19 ± 0.03		36 ± 8
dsDNA+ADP·BeFx	72 ± 4 **nM**	2.4 ± 0.3	0.36 ± 0.08
dsDNA+ADP·MgFx	2.2 ± 0.3		32 ± 7
dsDNA+ADP	3.7 ± 0.5		24 ± 5
jxnDNA 60/20mer			
jxnDNA	81 ± 6 **nM**		0.5 ± 0.1
jxnDNA+ADPNP	0.21 ± 0.02		1.3 ± 0.1
jxnDNA+ADP·BeFx	26 ± 4 **nM**		44 ± 6 **nM**
jxnDNA+ADP·MgFx	0.57 ± 0.09		6.5 ± 1.2
jxnDNA+ADP	0.24 ± 0.04		2.0 ± 0.5

[1] P. Forterre, *Trends Genet.*, 2002, **18**, 236-237
[2] A., Kikuchi *et al., Natur*, 1984, **309**, 677-681
[3] H. Atomi *et al., J. Bacteriol*, 2004, **186**, 4829-4833
[4] M. Kampmann *et al., Nucleic Acids Res.,* 2004, **32**, 3537-3545
[5] T.S. Hsieh *et al., J. Biol. Chem.*, 2006, **281**, 5640-5647
[6] R. Krah *et al., Proc. Natl. Acad. Sci.*, 1996, **96**, 106-110
[7] A. Ganguly *et al., Nucleic Acids Res.*, 2011, **39**, 1789-1800
[8] Y. del Toro Duany *et al., Nucleic Acids Res.*, 2008, **36**, 5882-5895
[9] Y. del Toro Duany *et al., Phys. Chem. Chem. Phys.,* 2011, **13**, 10009-10019
[10] B. Theissen *et al., Proc. Natl. Acad. Sci.*, 2008, **105**, 548-553
[11] Y. del Toro Duany *et al., Biochemistry*, 2011, **50**, 5816-5823
[12] A.C. Declais *et al., J. Biol. Chem.*, 2000, **275**, 19498-19504

Figure 1. Nucleotide analogs binding to rGyr_hel_Δlatch, in the absence and presence of DNA. Left: Fluorescence equilibrium titrations of mant-ADP.BeFx and mant-ADP.MgFx in the absence of DNA, and in the presence of saturating concentrations of ssDNA and dsDNA. Right: Fluorescence equilibrium titrations of mant-ADPNP, mant-ADP.BeFx, mant-ADP.MgFx, and mant-ADP, in the presence of jxnDNA. The K_D values are summarized in Table I.

Figure 2. DNA binding to rGyr_hel_Δlatch, in the absence and presence of nucleotide analogs. Left: Binding of ssDNA (red) and dsDNA (blue), in the presence of ADP.BeFx (squares) and ADP.MgFx (circles). The KD values are summarized in Table II.

Figure 3. smFRET measurements of the rGyr_hel_Δlatch double Cys mutant S169C/F332C, labeled in the H1 and H2 domains, in the presence of all nucleotide analogs.

Figure 4. smFRET measurements of the double-labeled rGyr_hel_Δlatch Cys mutant in all DNA-bound states.

Figure 5. FRET-based unwinding assay for rGyr_hel_Δlatch using DNA substrates with 3' overhang (left panel) and 5' overhang (right panel). It shows virtually no difference in unwinding between the two DNA constructs.

Figure 6. Two-dimensional gel electrophoresis to visualize positive supercoiling. Lanes1, supercoiling in presence of ATP, Lanes 2, supercoiling in presence of ADP.BeFx and Lanes 3, supercoiling in presence of ADP.MgFx.

Figure 7. Schema depicting the elucidated reaction pathway. The most probable outcome from a thermodynamic point of view is highlighted.

Table I. Dissociation constant for all nucleotide analogs, in the absence and presence of DNA.

Table II. Dissociation constants for all DNAs, in the absence and presence on nucleotide analogs.

Chapter 8. Article

Reverse gyrase helicase-like domain unwinds and presents the DNA to the topoisomerase domain during supercoiling

The ATP-driven DNA processing by reverse gyrase is inevitably coupled to conformational changes in the helicase-like domain. We have previously determined the sequence of conformational changes at the ATP-bound, pre- and post-hydrolysis and ADP-bound states with changing DNA preferences along this sequence of steps. Along with the thermodynamic characterization of these complexes, pre-steady state kinetic of complex formation and product release, as well as unwinding kinetics were performed. We demonstrate a DNA unwinding activity for the helicase domain. Furthermore, we assign binding of specific secondary structure motifs to different regions of the DNA at different points of the cycle. Taken together, we propose a detailed catalytic cycle for the supercoiling reaction, based on the helicase-like domain contribution and key role in the overall reaction.

Reverse gyrase helicase-like domain unwinds and presents the DNA to the topoisomerase domain during supercoiling

Yoandris del Toro Duany[1], Agneyo Ganguly[1], and Dagmar Klostermeier[1,2,*]

* corresponding author:

Dagmar Klostermeier, University of Muenster, Institute for Physical Chemistry, Corrensstrasse 30, D-48149 Muenster, Germany

Phone 0049-251 83 23421, FAX 0049-251-83 29138, dagmar.klostermeier@uni-muenster.de

[1] University of Basel, Biozentrum, Dept. of Biophysical Chemistry, Klingelbergstrasse 70, CH-4056 Basel, Switzerland

[2] University of Muenster, Institute for Physical Chemistry, Corrensstrasse 30, D-48149 Muenster, Germany

Funding information: This work was supported by the VolkswagenStiftung (D.K.) and the Swiss National Science Foundation (D.K.).

Keywords: reverse gyrase, helicase, topoisomerase, positive supercoiling, DNA unwinding

Running title: Reverse gyrase helicase-like domain presents the DNA and ensures directionality of strand passage and reseal by the topoisomerase domain.

Abstract

Reverse gyrase is a type IA topoisomerase that positively supercoils DNA at the expense of ATP hydrolysis. It consists of an N-terminal helicase-like domain fused to a C-terminal topoisomerase domain. The helicase-like domain belongs to the superfamily 2 (SF2) of helicases and possesses an insertion on the H2 domain, the latch region. The helicase-like domain is a nucleotide-dependent switch that is attenuated by the topoisomerase domain in reverse gyrase. Its nucleotide-driven DNA processing is coupled to a conformational change consisting on the closure of the cleft between the RecA domains, what generates high affinity states for DNA and nucleotide. The reverse gyrase helicase-like domain transits vectorially through a sequence of DNA preferences along its nucleotide cycle that clearly suggests its capability to locally promote duplex DNA destabilization. Lead by the thermodynamic characterization of the helicase-like domain from *T. maritima* reverse gyrase, we further studied the complexes of the proposed reaction mechanism. We address the formation of the initial complex with substrates, as well as the release of products at the end of the reaction *via* stopped-flow pre steady-state kinetics. We also studied kinetic aspects of the conformational change at the ATP pre-hydrolysis state, and demonstrate for the first time a DNA unwinding activity of the helicase-like domain. Furthermore, smFRET measurements revealed a new conformational state of the latch at the post-hydrolysis stage that suggests a role in guiding the DNA-bound lid to perform strand passage in the direction that ensures positive DNA supercoiling. Overall, from our findings on the full-length reverse gyrase

and mostly from its isolated helicase-like domain, we have been able to propose a detailed catalytic cycle for the supercoiling reaction.

Introduction

Reverse gyrase is an enzyme that introduces positive supercoils into DNA in an ATP-dependent manner [1]. It is exclusive from thermophilic and hyperthermophilic organisms, and it has been suggested to play a role in maintaining genome integrity at high temperatures[2,3]. The structural signature of reverse gyrase is the fusion of a topoisomerase and a helicase-like domain in the same polypeptide chain[4]. This is a unique arrangement in nature, which allows the enzyme to perform the also unprecedented task of positively supercoiling DNA. These two modules interact extensively, and the latch, an insertion in the H2 domain of the helicase-like module, has been demonstrated to be involved in interdomain communication, DNA binding, and thermodynamic coupling between DNA binding and ATP binding and hydrolysis[5].

To date, detailed information on the mechanism of DNA supercoiling by reverse gyrase is unavailable. From the crystal structure of *A. fulgidus* reverse gyrase a putative catalytic cycle has been proposed. It involves a conformational change in the helicase-like domain upon DNA and ATP binding that disengages the lid from its contact with the latch, allowing the topoisomerase domain to perform the strand breakage, passage, and reseal, in a similar way as proposed for the type IA topoisomerases[3]. Unlike other topoisomerases, introduction of supercoils by reverse gyrase always occur in

one direction, and the ATPase activity of the helicase-like domain has been proposed to impose this directionality.

Reverse gyrase helicase-like domain belongs to the superfamily 2 (SF2) of helicases. It consists of two globular domains adopting a RecA fold, joined by a flexible linker. Additionally, the C-terminal RecA domain (H2) possesses an insertion, the so-called latch. We have previously demonstrated that the helicase-like domain from *T. maritima* reverse gyrase acts as a nucleotide-dependent switch that is attenuated in the context of the full-length enzyme[6].

We have also reported a comprehensive thermodynamic characterization of the interaction of rGyr_hel with DNA and nucleotides[7]. There, we demonstrate that upon binding of dsDNA and ADPNP, an ATP ground-state analog, rGyr_hel undergoes a conformational change that brings the RecA domains closer together, increasing the affinity for both substrates by a factor of 20. At the pre-hydrolysis step of the cycle, represented by the ADP·BeF_x-bound state of the enzyme, the affinity for DNA is further increased, with a small preference for jxnDNA, while rGyr_hel remains in the closed conformation. From the DNA affinity switch and the ΔΔG° of this transition (12 kJ/mol) we predicted that rGyr_hel could be able to destabilize 2-3 bp and generate local unwinding of the DNA duplex at this point of the cycle. Right after hydrolysis and prior to P_i release the enzyme returns to the open conformation with high affinity only for ssDNA. After Pi release, the affinity for ssDNA also decreases to a value comparable to rGyr_hel in the nucleotide-free state. We therefore set out to further characterize the complexes and transitions relevant to this cycle.

In the present study we present a comprehensive kinetic dissection of the reaction carried by rGyr_hel. On the nucleotide side we address the interaction with substrate and product and how the relevant DNA, according to our thermodynamic cycle, influences it. On the DNA side we demonstrate for the first time DNA unwinding activity of a reverse gyrase helicase-like module. We also investigate the kinetics of strand release, and identification of the regions of the enzyme involved in binding the ssDNA strands with different polarities at a DNA junction in the pre-hydrolysis state. We finally address the question of the conformational change involving closure of the cleft between the RecA domain *via* kinetic and smFRET experiments.

Material and methods

Cloning and protein purification

RGyr_hel and rGyr_hel_Δlatch were produced as described[6,5]. The helicase-like domain mutant lacking the ninth α-helix (rGyr_hel_Δhelix9) that replaces the β-hairpin in *A. fulgidus* reverse gyrase, was sub-cloned from the rGyr_hel gene contained in the pET28a plasmid. It was constructed by separate amplification *via* PCR of the regions flanking the α-helix9 (aa 223-250) using overlapping primers for the internal sequences, and primers complementary to the end target regions containing the Nco I and Xho I restriction sites. Expression and purification of rGyr_hel_Δhelix9 was performed the same way as rGyr_hel and rGyr_hel_Δlatch. Cysteine mutants were generated according to the Quickchange protocol (Stratagene) and purified as rGyr_hel.

Nucleotides and DNA substrates

Nucleotides were purchased from Jena Biosciences and Biolabs. Unlabeled and labeled oligonucleotides were purchased from Sigma Aldrich and Purimex, respectively. The ssDNA substrate used was: 5'-(fluorescein)-AAG CCA AGC TTC TAG AGT CAG CCC GTG ATA TTC ATT ACT TCT TAT CCT AGG ATC CCC GTT. dsDNA was generated by annealing of the ssDNA substrate with the complementary strand. jxnDNAs were obtain by annealing the ssDNA substrate with 20nt oligonucleotides, complementary to either the underlined part or the ends. The dsDNA containing a fork was obtained by annealing the strands: 5'-(fluorescein)-GTC AGC CCG TGA TAT TCA TTA CTT CTT ATC and GAT AAG AAG TAA TGA ATA TCT GCC CGA CTG. The 5'ssDNA and 3'ssDNA junction DNAs for unwinding assays were obtained by annealing: 5'-(Cy5)-CGT TAC GCA with GAT AAT GCG TAA CG-(Cy3)-3', or 5'-(Cy5)-CGT TAC GCA TTA TC with TGC GTA ACG-(Cy3)-3'.

Stopped-flow nucleotide binding kinetics

Measurements were performed on an Applied Photophysics SX 20 stopped-flow apparatus using 0.1 μM rGyr_hel at 37°C in buffer 50 mM Tris/HCl, pH 7.5, 0.15 M NaCl, 10 mM $MgCl_2$, 10 μM $Zn(OAc)_2$, 2 mM β-mercaptoethanol. Binding and dissociation kinetics of mant-nucleotides was detected *via* FRET between the tryptophans in rGyr_hel structure and the mant group. The excitation wavelength was 280 nm and for detection a long pass cut-off filter for the wavelength 335 nm was used.

Fluorescence time courses of binding kinetics were fitted to the equation:

$$k_{obs} = k_{on}\left[mdADP\right] + k_{off} \qquad (1)$$

describing the dependence of k_{obs} on the association (k_{on}) and dissociation (k_{off}) rate constants.

Time courses of mant-d-ADP fluorescence decay for direct determination of the dissociation rate constant were fitted with the equation:

$$Fl = A \cdot e^{-k_{off} \cdot t} + c \quad (2)$$

where *Fl* is the monitored fluorescence signal, *A* is the amplitude, and *c* the fluorescence value where the plateau is reached. The value for k_{off} determined this way was substituted on equation 1 to obtain a better estimate of the association rate constant.

Kinetic competition assays between mant-d-ADP and ADPNP, were performed by rapid mixing of the enzyme solution with pre-incubated mdADP/ADPNP solutions, of varying ADPNP concentrations and 2 μM mdADP.

Measurements in the presence of DNA were performed with saturating DNA concentrations in both solutions before rapid mixing.

DNA unwinding assay

DNA unwinding was detected via FRET between the Cy3 and Cy5 dyes. The 5' and 3' ends were labeled with Cy5 and Cy3 respectively, at the duplex side of junction or dsDNA. Unwinding was detected by decrease of the fluorescence emission at 666 nm (1 nm bandwidth), after excitation at 554 nm (1 nm bandwidth) on a Fluoromax-3 fluorimeter (Jobin Yvon). 0.5 μM DNA was incubated with 5 μM the enzyme at 37°C in buffer 50 mM Tris/HCl, pH 7.5, 0.15 M NaCl, 10 mM $MgCl_2$, 10 μM $Zn(OAc)_2$, 2 mM β-mercaptoethanol, prior to nucleotide addition.

Kinetic acquisition of fluorescence anisotropy

ssDNA strand release was measured at 37°C in buffer 50 mM Tris/HCl, pH 7.5, 0.15 M NaCl, 10 mM $MgCl_2$, 10 µM $Zn(OAc)_2$, 2 mM β-mercaptoethanol *via* depolarization of the reaction medium. Samples were irradiated with linearly polarized light and the fluorescence emission was monitored in the perpendicular plane.

Fluorescence anisotropy titration

Binding of fluorescein-labeled DNA was measured *via* fluorescence anisotropy, at 37°C in buffer 50 mM Tris/HCl, pH 7.5, 0.15 M NaCl, 10 mM $MgCl_2$, 10 µM $Zn(OAc)_2$, 2 mM β-mercaptoethanol. Data was evaluated as previously described[6].

Single-molecule FRET

Measurements and data evaluation were performed as previously described[7].

Plasmid DNA supercoiling

The DNA supercoiling reaction of rGyr_Δlatch was performed at 75°C in buffer 50 mM Tris/HCl, pH 7.5, 0.15 M NaCl, 10 mM $MgCl_2$, 10 µM $Zn(OAc)_2$, 2 mM β-mercaptoethanol, 10% (w/v) polyethylene glycol 8000, as previously described[5].

Results

Pre steady-state kinetics of rGyr_hel binding to fluorescently labeled nucleotides

The formation of the initial and final complexes of the reaction according to rGyr_hel thermodynamic cycle *i.e.*, APDNP- and ADP-bound states, as well as the effect of the relevant DNAs in each case, were investigated under pre steady-state conditions. Binding of the fluorescently labeled nucleotides mant-ADP and mant-ADPNP to rGyr_hel was monitored in stopped-flow regime *via* FRET, between rGyr_hel tryptophans and the mant group. Measurements with 2'(3')-mant-ADP or 2'(3')-mant-ADPNP yielded double exponential observed binding curves, composed by a fast first order binding rate, and a slow order zero binding rate.

The mant group is known to spontaneously isomerize between positions 2'OH and 3'OH of the ribose ring, having a distribution of 40 % and 60 % in solution[8]. We therefore determined whether this isomerization could account for differential binding of the nucleotide, and as a consequence give rise to the two sets of observed binding rates. The slow phase disappeared after removal of the 3-OH of the mant-ADP ribose ring, indicating that the second phase detected was due to the 2', 3' isomerization of the mant group. We have previously determined the structure of rGyr_hel_Δlatch in complex with ADP, and it shows that the modification in the nucleotide does not affect any native interaction with the enzyme[9].

The observed rate constants for mant-d-ADP binding to rGyr_hel increased linearly in the measured concentration range (figure 1), indicating the presence of a single binding step according to the model:

$$rGyr\_hel + mdADP \underset{k_{off}}{\overset{k_{on}}{\rightleftharpoons}} rGyr\_hel \bullet mdADP$$

Due to the small value and the relatively large error of the dissociation rate constant of mant-d-ADP, we directly measured the rate of mant-d-ADP release from the enzyme (figure 1).

The K_D value calculated from the rate constants obtained by this method was 2.8 µM. This value is within the range of the dissociation constants obtained by the fluorescence equilibrium titrations previously reported. Monitoring of 2'(3')-mant-ADP binding *via* direct excitation of the mant group yielded a K_D value of 1.1 µM[6], while the detection of FRET between the tryptophans and the mant-ADP upon binding to the enzyme gave a K_D value of 4.2 µM[7]. From that result we can conclude that mant-d-ADP is as good as 2'(3')-mant-ADP for studying nucleotide binding to rGyr_hel.

Unstimulated ATP hydrolysis by rGyr_hel

Binding of ADPNP and ATP was measured in competition with the fluorescently labeled mant-d-ADP. Increasing concentrations of ADPNP or ATP were used, while maintaining constant the enzyme and mant-d-ADP concentrations.

Under steady-state conditions, ATP hydrolysis takes place at a rate of 30 ± $2 \cdot 10^{-3}$ s^{-1}. Since the time course for ATP binding reaches a maximum after 100 ms, less than 1 % would be hydrolyzed during this time. The concentration dependence of the observed association rate follows a hyperbolic behavior, indicating the presence of a two-step binding mechanism for ATP that can be described as follows:

$$rGyr\_hel + ATP \underset{k_{-1}}{\overset{k_1}{\rightleftharpoons}} rGyr\_hel \bullet ATP \underset{k_{-2}}{\overset{k_2}{\rightleftharpoons}} rGyr\_hel \bullet ATP*$$

The data was fitted in Scientist, to a two-step sequential binding model (Figure 2), where $k_{-1} >> k_2 >> k_{-2}$.

Overall, the unstimulated ATP hydrolysis reaction can be kinetically expressed as follows:

$$hel + ATP \underset{100\,s^{-1}}{\overset{4.9\cdot10^{6}\,M^{-1}s^{-1}}{\rightleftharpoons}} hel \bullet ATP \underset{0.4\,s^{-1}}{\overset{42\,s^{-1}}{\rightleftharpoons}} hel \bullet ATP^{*} \xrightarrow{20\cdot10^{-3}\,s^{-1}} hel \bullet ADP \underset{1.3\cdot10^{-5}\,M^{-1}s^{-1}}{\overset{36\,s^{-1}}{\rightleftharpoons}} hel + ADP$$

Surprisingly, binding of ADPNP to rGyr_hel showed a linear dependence between the observed rate constants and the ADPNP concentrations within the same range used for ATP, indicating that ADPNP does not undergo the same isomerization step as ATP (Figure 2).

Influence of DNA on nucleotide binding kinetics to rGyr_hel

We have previously determined the DNA preference of rGyr_hel at each step of the catalytic cycle[7]. In this study we also characterize the influence of dsDNA on the ATP ground state mimicked by ADPNP, and the influence of ssDNA on mant-d-ADP.

Saturating concentrations of ssDNA had a small influence on mant-d-ADP binding to rGyr_hel. The rate constant for dissociation of the complex remained virtually unaltered, while the association rate constant was 2.7–fold reduced, when compared to the rate constants in the absence of ssDNA. The calculated K_D had a value of 9.4 μM, which represents a 3.4-fold decrease of the affinity for mant-d-ADP in the presence of ssDNA (Figure 3). The corresponding equilibrium binding titration, namely binding of mant-ADP to rGyr_hel in the presence of ssDNA, gave a K_D value of 10 μM, representing a 2.4-fold decrease of the affinity for 2'(3')-mant-ADP in the presence of ssDNA.

This finding is in agreement with the trend observed by stopped-flow binding kinetics.

On the other hand, in the presence of dsDNA, binding of ADPNP to rGyr_hel in competition with mant-d-ADP, yielded time courses of the fluorescence that could only be fitted to double exponentials. From the 20-fold increase in affinity for ADPNP observed in equilibrium binding, either an increase of the association rate constant, a decrease of the dissociation rate constant, or a mixture of both was expected. Instead, the dependence of the fast phase observed rate constants on ADPNP concentration remained practically the same as for the DNA-free reaction (data shown in supplements), while the observed rate constants for the slow phase were independent of the ADPNP concentration, indicating the occurrence of an order zero simultaneous process. In this experiment rGyr_hel was half-saturated with dsDNA before mixing with ADPNP and mdADP, due to the low affinity for dsDNA on the nucleotide-free state. The dsDNA concentration used, became saturating only after the affinity change upon mixing with ADPNP. Our equilibrium binding measurements suggest a complex kinetic behavior upon mixing of the two solutions. On one hand, binding of mant-d-ADP to either the dsDNA-free or dsDNA-bound enzyme does not make any difference, since rGyr_hel binds mant-d-ADP with practically the same affinity in both states. On the other hand, binding of ADPNP follows two different kinetic behaviors, depending on its binding to either dsDNA-bound or DNA-free enzyme. Binding to the dsDNA-free rGyr_hel occurs with a low affinity, and at the same time it increases the enzyme's affinity for dsDNA, displacing the equilibrium of the DNA half-saturated enzyme, what at the same time increases its own affinity

for the enzyme as more DNA is bound. On the other hand, if it first binds the dsDNA-bound enzyme, it does it with a 20-fold higher affinity, and it all amount to a displacement of the equilibrium rGyr_hel:mdADP. Furthermore, our smFRET measurements suggest that at the same time a conformational change is taking place upon dsDNA and ADPNP binding[7]. Unfortunately, assignment of the second phase to a specific process could not be done in such complex mixture. Only the first collisional state seems to remain unaltered, judging from the resemblance of the fast pseudo first order phase, to the one in the experiments in the absence of DNA.

rGyr_hel unwinds jxnDNA in the presence of ADP.BeF$_x$

After addressing the binding of rGyr_hel to the nucleotides analogs representing the ground-state substrate and product, as well as the effect of the corresponding DNAs at these points of the cycle, the next relevant step according to our thermodynamic cycle would be the pre-hydrolysis state. We have previously predicted that if rGyr_hel were able to destabilize the double helix and therefore promote local DNA unwinding, it should take place at the ADP.BeF$_x$-bound state[7]. The $\Delta\Delta G^0$ for the transition from the ADPNP-bound state to the pre-hydrolysis state, mimicked by ADP.BeF$_x$, has a value of 12 kJ/mol, in theory sufficient to destabilize 2-3 bp[7]. At the same time, the ADPNP-bound state has a preference for dsDNA that switches to jxnDNA at the ADP.BeF$_x$-bound state, thus promoting the generation of the ssDNA substrate for the supercoiling reaction carried by the topoisomerase domain.

The FRET-based unwinding assay under single turnover conditions confirmed previous reports that rGyr_hel is unable to unwind DNA in the presence of

ATP[6]. We therefore performed the assay in the presence of each of the nucleotide analogs used for elucidation of the nucleotide cycle. As predicted, unwinding was detected only in the presence of ADP.BeF_x (Figure 4). We tried to determine whether the full-length rGyr was also able to unwind DNA, but no unwinding could be detected in the presence of any of the nucleotide analogs used (data not shown). To further characterize the unwinding reaction carried out by rGyr_hel on the ADP.BeF_x-bound state, we used jxnDNA substrates with either 3' or 5'ssDNA overhangs, as well as dsDNA. Only the jxnDNAs could be unwound, with the junction carrying the 3'ssDNA overhang having a 3.5-fold higher unwinding rate constant than the junction with the 5'ssDNA overhang (Figure 4).

rGyr_hel binds jxnDNA with no preference for the polarity of the ssDNA overhang

Any protein that interacts with ssDNA has to do it in an asymmetric way due to its intrinsic polar structure[10]. We have previously demonstrated that in the nucleotide-free state, rGyr_hel binds to a DNA bubble with a similar affinity as it binds to a 60/20 jxnDNA bearing two junctions, each with one ssDNA overhang with different directionalities[7]. It indicates that the nucleotide-free rGyr_hel does not bind simultaneously to both ssDNA strands at a fork. We therefore set out to further investigate how rGyr_hel interacts with the ssDNA region next to a junction, this time at the point of the nucleotide cycle where the jxnDNA is preferred, the pre-hydrolysis state. We designed a forked DNA with a 20 bp dsDNA region, and 10 nucleotides non-complementary ssDNA

regions. We also used 60/20mer jxnDNAs, which had either a 3'-OH or a 5'-OH ssDNA end.

There was no difference in binding of rGyr_hel to either the 5'- or the 3'-ssDNA junction, with K_D values of 42 nM and 38 nM, respectively. However, binding of rGyr_hel to the fork DNA yielded a K_D value of 26 nM (Figure 5). This means a 1.5-fold higher affinity for the fork than the junctions with only one ssDNA strand, which indicates that on the ADP.BeF_x–bound state rGyr_hel may simultaneously interact with the ssDNA regions at the fork with both polarities. Put together with the conformational information from our previous smFRET measurements[7], rGyr_hel only interacts with either one of the ssDNA overhangs of a fork in the open conformation of the nucleotide-free state, while it is able to simultaneously bind both ssDNA overhangs of a forked DNA in the closed conformation of the ADP.BeF_x- DNA-bound state. We also tried a 3'ssDNA junction DNA of the same length as the fork substrate, which showed a binding affinity of 113 nM (Figure 5). Overall, rGyr_hel simultaneously binds both ssDNA overhangs at the fork in the ADP.BeF_x–bound state, and with comparable affinities.

Role of the latch and the helix9 in jxnDNA binding

We have shown that the deletion of the latch from the helicase-like domain affects coupling between DNA and nucleotide binding, and the affinity of the enzyme for DNA is in most cases drastically decreased[5]. Only in the ADP.BeF_x-bound state, rGyr_hel_Δlatch binds jxnDNA with rGyr_hel-like affinity, and it is also the only state that can promote full closure of the cleft between the two Rec-A domains. In this nucleotide state, rGyr_hel_Δlatch

shows a 3.5-fold preference for the 3'ssDNA junction over the 5'ssDNA. rGyr_hel binds either of these junction with the same affinity, indicating that the latch is the region responsible of binding to the 5'ssDNA overhang.

We have previously reported the crystal structure of rGyr_hel_Δlatch, where a putative DNA binding motif, a hairpin in H1 in the structure of rGyr from *Archaeoglobus fulgidus*, turned out to be a helix in rGyr from *Thermotoga maritima*. We deleted this region by introducing a sharp bend between the residues 223 and 250 flanking the helix, 4.8 Å apart in the native structure. The overall Δhelix9 mutant binding to DNA was similar to rGyr_hel, with a 2-fold decreased affinity for ssDNA and a 2-fold increased affinity for dsDNA. It indicates that this region may only have a small contribution to ssDNA binding in the nucleotide-free state. This mutant also loses the high affinity for the jxnDNA seen in rGyr_hel, binding to it with an affinity of 0.39 μM, comparable to binding to ssDNA. In the ADP.BeF_x-bound state however, it has an affinity for the 5'ssDNA junction of 43 nM, same as rGyr_hel (Figure 6). The 3'ssDNA junction was bound with an affinity of 82 nM, 2.2-fold weaker than rGyr_hel.

Overall, in the ADP.BeF_x-bound state rGyr_hel binds preferably to the junction, with the latch binding the 5'ssDNA region, and the H1 domain and specifically the helix9 bound to the 3'ssDNA region. The small differences in affinity for the jxnDNAs indicate that the latch and apparently also the helix9 bind weakly to the substrate, in line with our previous report of the direct measurement of the affinity of the latch for DNA [5].

ssDNA strand release by rGyr_hel

For this experiment the fluorescence anisotropy was used in a kinetic way, in order to track ssDNA release from rGyr_hel. That way, the change in size of the fluorescently labeled complex was followed over time.

We tested whether the 60/20mer junction DNA previously used for equilibrium binding titrations could also be unwound by rGyr_hel in the ADP.BeF_x–bound state. The time course of the fluorescence depolarization did not change during the measured time, indicating that a 20 bp dsDNA region cannot be unwound by rGyr_hel.

We also tested the single labeled jxnDNAs used in the FRET-based unwinding assay to determine which strand is first released and which one remains longer bound to the enzyme. When the label was attached to the longest strand, the fluorescence time decay courses could only be described by double exponentials, indicating that the label was sensitive to two processes, which appeared to be the release of both strands (Figure 7). Nevertheless, the rate with the highest amplitude could be assigned to the release of the labeled strand and the smallest amplitude to the complementary unlabeled strand. The two sets of rate constants for the constructs with either 5'-OH or 3'-OH ssDNA overhangs were practically the same. Only the relative amplitudes were significantly different. In the case of the 5'ssDNA junction the highest amplitude corresponded to the fast phase, meaning that the longest 5'ssDNA strand is the first to be released. The 3'ssDNA junction on the other hand, exhibited the highest amplitude for the slow phase, indicating that the longest 3'ssDNA is the last to be released, which corroborates that the complementary strand with 5'ssDNA polarity is released first.

When the label was located in the short strand (9mer), single exponential decay time courses were obtained for the junctions with both ssDNA overhang directionalities, which means that the short strand is only sensitive to its own release (Figure 7). The release rate of the short strand from the 3'ssDNA junction was the same as the highest rate with the smallest amplitude when the longest strand (14mer) was labeled, corroborating that the labeled 14mer indeed senses the release of both strands. The labeled 9mer of the 5'ssDNA junction however, showed an intermediate rate value compared to the two sets of rates from jxnDNA labeled in the complementary strand. The release rate of the shortest strand was nevertheless closer to the lowest rate with the smallest phase, also corroborating that the rate of depolarization for the jxnDNA bearing the label in the short strand, match the rate with the smallest amplitude when the labeled is in the longest strand.

Comparison between the experiments where only the shortest strands were labeled shows that the junction with a 3'ssDNA overhang, having the label in the short strand with 5'-polarity, has a 2-fold faster release rate than the one with the 5'ssDNA overhang labeled in the strand with 3'-polarity. It corroborates that the short strand in a 3'ssDNA junction, *i.e.* the strand with 5'ssDNA polarity, is released faster than the short strand from the 5'ssDNA junction, having a 3'ssDNA polarity.

DNA unwinding by the rGyr_hel_Δhelix9 mutant

We also tested the Δhelix9 mutant for unwinding. Surprisingly, it was able to unwind the jxnDNAs at rates comparable to rGyr_hel, but with inverted preference, *i.e.*, the highest unwinding rate corresponded to the 5'ssDNA

junction. The 3'ssDNA junction was unwound at a rate of 0.02 s^{-1}, and the 5'ssDNA junction at a rate of 0.06 s^{-1}. This result is in agreement with the notion that this helix binds to the 3'ssDNA strand. That way, the interaction of this mutant with the 3'ssDNA junction, with decreased affinity for the 3'ssDNA strand, could account for the decreased unwinding rate, compared to rGyr_hel. In the case of the 5'ssDNA junction however, the lowered affinity for the 3'ssDNA strand due to the absence of the helix9, could account for faster release of the short 3'ssDNA strand, what amounts to an increase in the observed unwinding rate (Figure 8).

Conformational change and tryptophan fluorescence

Tryptophans are known to give fluorescence signals that are highly sensitive to the chemical environment. rGyr_hel has five tryptophans at both sides of the cleft between the two RecA domains, therefore the environmental change after closure of the cleft should be sensed by these residues. In order to ensure that local DNA unwinding had no contribution to the change in fluorescence emission by the tryptophans, ADPNP and dsDNA were used instead of ADP.BeF_x and jxnDNA. As a control where no conformational change takes place thus no change in tryptophan fluorescence is expected, we used ADP instead of ADPNP, while maintaining the dsDNA.

Addition of dsDNA and nucleotide quenched the intrinsic fluorescence emission of Trp. Nevertheless, a change in the environment of the Trp should increase it again, although not to the initial values. As expected, upon addition of ADP no increase in fluorescence was detected. Upon addition of ADPNP however, a single exponential could describe the increment in Tryptophan

emission, which should represent the closure of the cleft between the RecA domains. The observed rate constant for this conformational change had a value of 0.08 s^{-1} (Figure 9). Although this value most probably has the contributions of the rates of closure and re-opening, it sets a minimum for the closure rate constant. It also accounts for the apparent increase in affinity for ADPNP in the presence of dsDNA. Overall, the stimulated nucleotide cycle can be kinetically represented as follows:

$$hel \bullet dsDNA + ADPNP \underset{8.2 s^{-1}}{\overset{1.7 \bullet 10^{7} M^{-1} s^{-1}}{\rightleftharpoons}} hel \bullet dsDNA \bullet ADPNP \overset{0.08 s^{-1}}{\rightleftharpoons} hel \bullet dsDNA \bullet ADPNP \rightarrow \langle ... \rangle \rightleftharpoons hel \bullet ssDNA \bullet ADP \underset{4.8 \bullet 10^{6} M^{-1} s^{-1}}{\overset{45 s^{-1}}{\rightleftharpoons}} hel \bullet ssDNA + ADP$$

Single molecule FRET measurements of thermodynamically relevant complexes

The crystal structures of rGyr_hel_Δlatch revealed conformational states in the open form of the enzyme that cannot be differentiated with the combination of double Cys mutants previously reported [9]. For that reason we created the double mutant S169C/E422C. The main feature of the obtained FRET histograms is a broad peak of the apo form of the enzyme, possibly due to the additional degree of rotational freedom between the positions selected. The latch orientation respective to the H1 domain depends not only on the "hinge motion" of the linker joining H1 and H2, but also on its rotation and eventual movements of the latch relative to the H2 domain.

In the substrate-free form, rGyr_hel shows a low FRET efficiency state of approximately 0.3, that changes to a higher value upon 60/20 jxnDNA and ADP.BeF_x addition. This conformational change is in agreement with the closure of the cleft between the RecA domains. Interestingly, the FRET

efficiency histogram for this complex reveals what appears to be the presence of two populations close to each other. This might be an indication of small conformational differences in binding to the 3' and 5' ssDNA overhangs. We have already demonstrated that the latch is involved in binding to the 5'ssDNA overhang, while the helix9 mostly interacts with the 3'ssDNA overhang. At the post-hydrolysis state however, prior to P_i release, we see a high FRET efficiency peak at approximately 0.6. We have previously demonstrated that at this point of the cycle the RecA domains return to the open conformation with a low FRET efficiency[7]. This result indicates that at this stage the latch remains in a high FRET efficiency state, as if the H2 domain has rotated in a way that its core moves away from the H1 domain while leaving the latch behind. This is the first conformational difference that could account for the high affinity state for ssDNA at this point of the cycle, and this conformation sets the post-hydrolysis state apart from the enzyme free and the pre-hydrolysis state. This seems to be consistent with binding to ssDNA in a conformation where the H2 domain is not aligned as in the apo rGyr structure, but twisted in a way that leaves the latch in close proximity to the H1 domain.

Supercoiling reaction and nucleotide analogs

rGyr is able to introduce positive supercoils into the DNA only in the presence of ATP and ATPγS[11]. It has also been reported to produce relaxed DNA in the presence of ADPNP and ADP [11]. In this study we investigate the effect of the analogs ADP.BeF_x and ADP.MgF_x on the supercoiling reaction performed by rGyr_hel.

In the presence of ADP.BeF_x, rGyr is only able to produce nicked DNA, in agreement with a closed conformation of the helicase-like domain, exposing only a partially unwound DNA to the topoisomerase domain. The fact that the topoisomerase domain seems unable to reseal the DNA strand in this nucleotide state seems to be a consequence of the latch binding to the strand covalently attached to the lid, thus restricting its movement.

In the ADP.MgF_x-bound state however, only relaxation was detected. Since in the previous step only strand breakage takes place, it is expected that at this point directional strand passage and resealing occur.

Nucleotide analogs do not allow for multiple turnovers. Even in the case where the ADP.MgF_x-bound state were able to allow the directional strand passage that amounts to the introduction of positive supercoils, only the simultaneous action of multiple rGyr molecules bound to the same DNA, each one introducing one turn, would produce enough detectable positive supercoiled product. For that reason we performed the assay with a higher protein/DNA ratio. Unfortunately this experiment did not produce different results. Nevertheless, it does not yet discard our hypothesis. The directional strand passage might need as a substrate the DNA-bound enzyme at the ADP.BeF_x stage. Supercoiling assay with a mixture of both analogs might provide a definitive answer to this hypothesis.

Discussion

Intrinsic rGyr_hel ATPase activity

Overall, ATP binding by rGyr_hel involves a two-step binding mechanism with an isomerization step occurring prior hydrolysis, in line with previous reports of DEAD-box helicases[12]. On the other hand, the ADPNP complex does not undergo the isomerization, which probably indicates that this nucleotide analog only resembles the ground state of ATP. Our biochemical data suggest that ADP.BeFx, our choice for the pre-hydrolysis state analog, most probably mimics the ATP isomerized form (ATP*). To complete the cycle we performed this same kind of pre steady-state study on ADP binding to rGyr_hel, which could be described with the classic one step binding mechanism. Comparison with another pre steady-state measurement, namely ATP hydrolysis under single turnover conditions, sets out the hydrolysis step of the reaction as the most likely to be rate-limiting, judging from its significant slower rate constant, compared to binding and release of substrate an product. Finally, ATPase assays under steady-state conditions ultimately proved the hydrolysis step to be rate-limiting, as concluded from the similar rates of these two experiments[6]. Additionally, our smFRET measurements confirmed previous reports that helicases are unable to undergo the well-documented conformational change that brings the RecA domains closer together, only in the presence of nucleotides[13].

Effect of DNA on the kinetics of binding and release of the nucleotides substrate and product

Our nucleotide binding experiments indicate that at the initial collisional step, ADPNP is weakly bound by rGyr_hel, and it is not improved in the presence of dsDNA. The 20-fold increase in the apparent affinity for ADPNP is a

consequence of the conformational change that “traps” the nucleotide on the closed conformation, preventing its release and therefore displacing the equilibrium and increasing the apparent affinity. This effect has been previously described in HIV reverse transcriptase[14]. For now we can only speculate about the implications it might have for the natural substrate ATP. The model of ATP binding to rGyr_hel in the absence of DNA foresees a low populated initial collision complex before isomerization, that in principle can be stabilized after the conformational change upon DNA binding, reducing the energetic barrier for the transition to the activated form and subsequent hydrolysis. Once the ternary complex rGyr_hel/ATP*/jxnDNA is formed, the condition $k_{hydrolysis}$ >>> k_{-2} is likely to be fulfilled, so the complex will not dissociate and the rate of hydrolysis will govern the process. At the end of the cycle, ssDNA increases the rate of ADP dissociation from rGyr_hel, ensuring multiple turnovers at the same DNA binding site while promoting nucleotide exchange.

Nucleotide-dependent DNA processing by rGyr_hel

On the DNA side, the start of the nucleotide cycle according to our previously determined thermodynamic cycle is the ADPNP-bound state. At this point the affinity for dsDNA is 20-fold increased, apparently because, as for ADPNP, the closed conformation rGyr_hel adopts at this stage prevents the DNA from being released, increasing the apparent affinity. At the following step however, the ADP.BeF_x-bound state, the enzyme is able to perform local unwinding of the DNA, what presumably provides the topoisomerase domain with the ssDNA substrate, needed to perform strand breakage with the active tyrosine

at the inner side of the lid. At this point four main steps take place that are hard to put in context. On the one hand we have the conformational change that brings the RecA domains closer in space. On the other hand we have ATP isomerization and hydrolysis, and DNA unwinding. In this scenario the ATP ground-state is able to promote the conformational change if dsDNA is bound, judging from the data obtained with ADPNP. Therefore, DNA and ATP promote closure of the cleft, and the isomerized ATP* promotes DNA unwinding. The actual hydrolysis step however might occur so fast that it probably is also coupled to DNA unwinding. The fact that the unwinding rates are equal or slower than the rate of closure indicates that the conformational change is rate-limiting for the unwinding reaction, but it may as well be an artifact from using the analog ADP.BeF_x. *In vivo*, ATP* appears already in the context of the closed enzyme, and once trapped in that state it can proceed faster to hydrolysis due to the decrease in activation energy. Unlike the actual substrate, ADP.BeF_x has to induce closure itself and cannot proceed to hydrolysis, so under these conditions the rate of closure is the one that dominates the unwinding reaction.

Right after hydrolysis and prior to P_i release, rGyr_hel retains a high affinity state only for ssDNA. Our smFRET data reveal a conformation that sets this complex apart from the others, namely, helicase core in the open form, but with the latch still close to the H1 domain. The previous step, the ADP.BeF_x-bound enzyme, is only able to allow the introduction of a nick into the DNA. Meaning that the directional strand passage and reseal occur at a later stage of the nucleotide cycle. As a bona fide candidate, the conformation of rGyr_hel at the ADP.MgF_x- ssDNA-bound state may suggest a role of the

latch guiding the DNA into the active site of the topoisomerase domain. It could do it either by binding to the 5'end-bound lid or reorienting the intact strand, so that the reseal occurs at the "right" side of the duplex, ensuring the introduction of a positive supercoil.

In the presence of ATP however, DNA unwinding by rGyr_hel has not been detected so far, probably because the locally unwound intermediate is too short lived, compared to the relatively fast DNA-stimulated ATP hydrolysis. The DNA-stimulated steady-state ATPase activity of rGyr_hel is 2 orders of magnitude faster than the fastest DNA unwinding rate measured. That way, the helicase would return to an energetic state that allows for re-annealing before ssDNA could be released from the enzyme. Under physiological conditions, strand release by rGyr would have disastrous consequences. That is the reason why rGyr_hel is optimized for not releasing ssDNA, and only by trapping the enzyme with transition state analogs such an activity could be detected.

Contribution of secondary structure motifs to DNA processing during catalysis

The interaction of H1 with 3'ssDNA seems to be more extensive than the interaction of H2 with the 5'ssDNA, judging from the effect of the deletions of the latch and the helix9. Since the differences in the rate constants for unwinding, strand release, and conformational change fluctuate in a small range, only results between experiments using the same method can be safely compared. Also the labeled jxnDNAs can be destabilized by the presence of the dye, thus the apparent rates can differ between single or double labeled substrates.

Overall, our hypothesis includes binding of the latch to the 5'ssDNA region and binding of the helix9 to the 3'ssDNA region at the junction. The latch seems to bind 5'ssDNA more strongly than the helix9 binds 3'ssDNA, judging from the relative effects on the helicase-like domain affinity for jxnDNA and relative rates of release of the individual strands by rGyr_hel, namely 5'ssDNA>3'ssDNA. Therefore, when rGyr_hel_Δlatch is faced with the 5'ssDNA junction, the overall rate of hydrolysis is the same as rGyr_hel because the first strand to be released is the one with a 5'-polarity and there is no latch to engage in contacts with it. When faced with the 3'ssDNA junction however, the short strand with a 5'-polarity has a smaller interaction surface, and not having the latch has a bigger impact. It seems that the latch is able to bind and "pull away" a strand with a 5'-polarity, either as ssDNA of dsDNA, in line with our direct titrations of the latch binding to DNA [5]. In the case of the helix9 the opposite effect is observed, with an inversion of the relative unwinding rates of 5'ssDNA and 3'ssDNA junctions, compared to rGyr_hel. The decrease of the unwinding rate of the 3'ssDNA junction can be explained by the deletion of the helix9, which fails to "pull" the 3' strand away from the duplex. In the case of the 5'ssDNA junction however, the "pulling" is mainly a responsibility of the latch, and the subsequent step of release of the strand with 3' polarity occurs faster in the absence of the helix9, what accounts for the overall increased unwinding rate.

In the case of the full-length enzyme, the fact that the strand first released (5'ssDNA) is the one that covalently binds to the topoisomerase domain according to the mechanism proposed for type IA topoisomerases, seems to also justify the fact that no unwinding has been detected so far, even in the

presence of ADP.BeF_x. We have thoroughly documented that rGyr_hel is harnessed by the topoisomerase domain[6]. Further thermodynamic and kinetic investigation should be performed on the full-length rGyr to properly predict the energy associated to the transitions that may promote unwinding and how many base pairs it could theoretically unwind. That should provide a reliable substrate length range that after destabilization allows for quantification of strand release, and therefore unwinding rates.

Implications for supercoiling and improved catalytic cycle

Incorporating our results of the isolated helicase-like domain, and interpolating the current knowledge of the mechanism of catalysis by type IA topoisomerases, we are able to propose an improved mechanism of the positive supercoiling reaction performed by reverse gyrase. Using the putative catalytic cycle derived from the only structure available of a full-length reverse gyrase[15], we will attempt to improve it by delineating the events that correlate to each nucleotide-state, as well as the involvement of specific secondary structure motifs, mainly from the helicase-like domain, at each stage of the cycle.

Upon ATP and DNA binding, our smFRET results indicate the occurrence of a conformational change that brings the RecA domains of the helicase-like module together, in line with the proposed model. However, comparison of the $K_{D,dsDNA}$ values for this complex reveals that rGyr and rGyr_hel bind dsDNA with virtually the same affinity, indicating that only the helicase-like domain engages in contact with the DNA, and any contribution of the rest of the molecule, if any, is minimal. Therefore, at this point of the cycle we locate the

dsDNA only in contact with the helicase-like domain, although interaction of the Zn-finger with dsDNA cannot be discarded according to our results (unpublished). Since from this arrangement no contact with the topoisomerase domain is predicted, also no conformational change of the lid in the topoisomerase domain is expected, judging from the crystal structure of the DNA-free E. coli DNA topoisomerase I[16]. Furthermore, at this point no DNA unwinding has been detected, so we leave the bound DNA as a duplex. Last but not least, at this point the latch is strongly involved in contact with dsDNA, as evidenced by the loss of cooperativity between ADPNP and dsDNA binding in the case of the rGyr_hel_Δlatch mutant, with the subsequent decrease in the affinity for dsDNA. We have also directly demonstrated that the latch is able to bind either ssDNA or dsDNA[5].

At the pre-hydrolysis state, represented by ATP* and mimicked by ADP.BeF_x, rGyr_hel still in the closed conformation is able to produce local unwinding of the DNA. At this point we have been able to assign binding of the 5'ssDNA overhang to the latch and binding to the 3'ssDNA overhang to the helix9. These polarities are relative to the same fork of the generated DNA bubble. Our supercoiling results indicate that rGyr is able under these circumstances to introduce a nick in one DNA strand, but unable to reseal it. It might be an indication that at this stage the latch remains bound to the 5'ssDNA overhang, the same strand the lid is covalently bound to, as proposed for type IA topoisomerases[17], and therefore restricts its movement. On the other hand, we locate the 3'end of the cleaved strand further into the domain T1, a Rossman fold that in the crystal structure of E. coli topoisomerase III engages in contact with an 8-base ssDNA[16], that runs along the positively charged

groove between domains T1 and T4, leading right to the Zn-fingers next to it. At this point it is worth mentioning that the Zn-fingers are likely to engage in contact with the DNA, but as our previous unpublished data suggests, this interaction would be with dsDNA, what would account for the reported chaperone effect of reverse gyrase, that binds to nicked regions and prevents thermally induced further unwinding[2]. This may help keep the unwound intermediate located within the active site of the enzyme, preventing local DNA melting to propagate along the duplex.

At the post-hydrolysis state the latch deletion abolishes the high affinity of rGyr_hel for ssDNA, indicating that the latch accounts for it. Since we know that the latch binds to the 5' strand, which is also the strand that remains covalently attached to the active tyrosine of the topoisomerase domain during supercoiling, we might expect that at this point the latch is crucial in guiding the lid for directional strand passage. Also the smFRET measurements reveal a conformation where the latch remains close to the H1 domain. This conformation sets apart this nucleotide state, and accounts for close proximity of the latch and therefore the ssDNA-bound lid, to the 3'end in the T1 domain. In the meantime, the re-opening of the cleft between the RecA domains during this transition should have re-located the intact ssDNA strand bound to helix9, allowing strand resealing in the direction compatible with positive supercoiling.

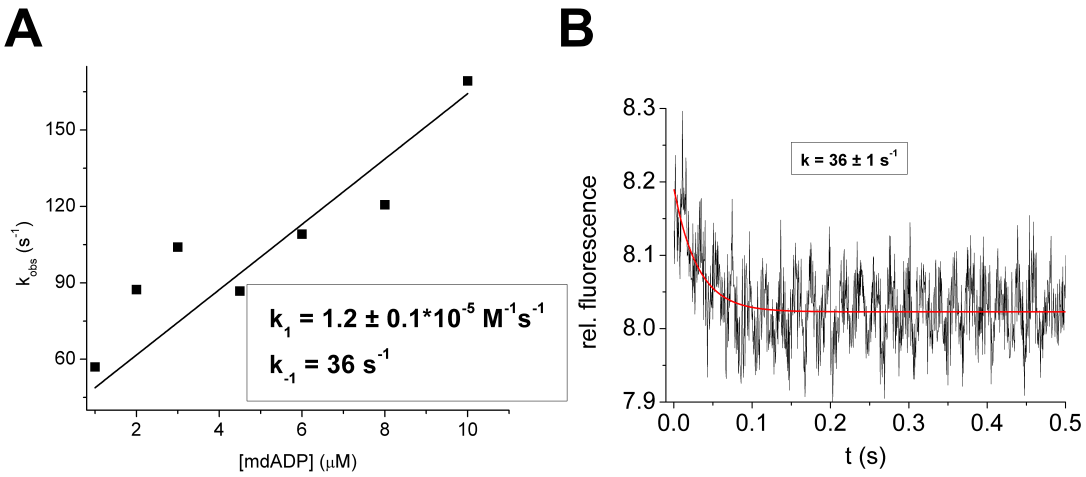

Figure 1

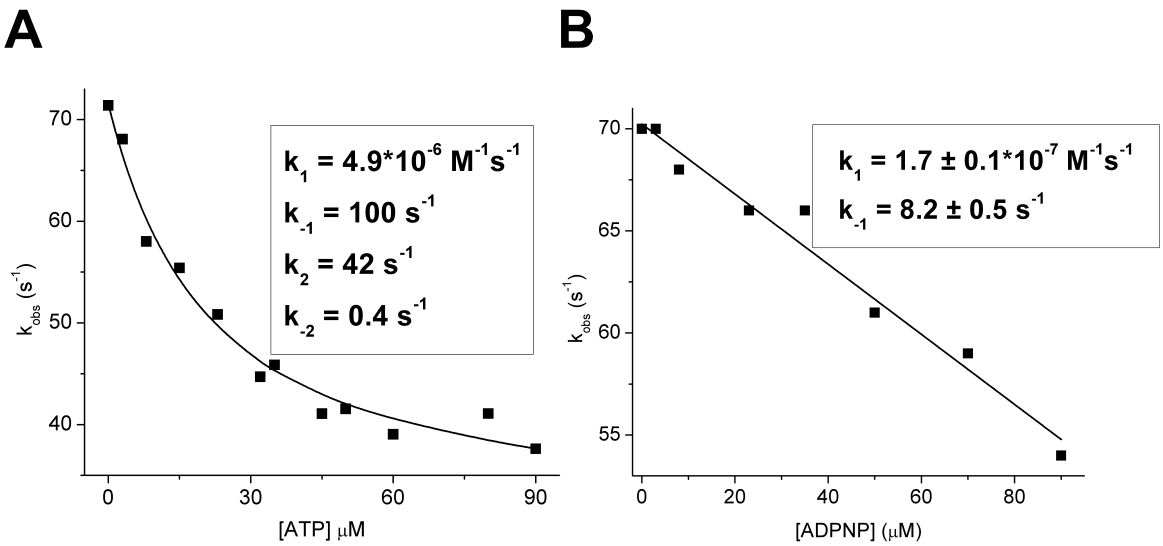

Figure 2

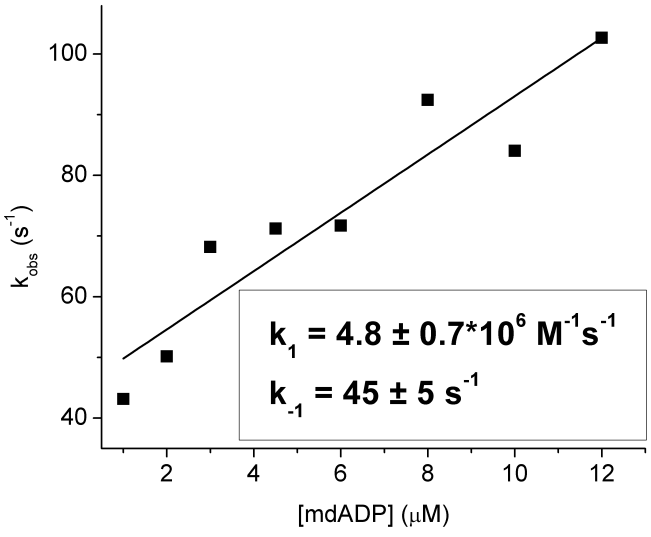

Figure 3

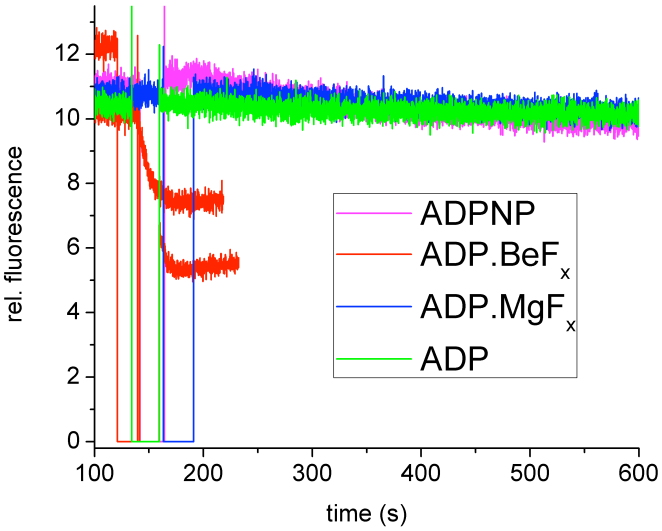
rel. fluorescence
time (s)
ADPNP
ADP.BeF$_x$
ADP.MgF$_x$
ADP

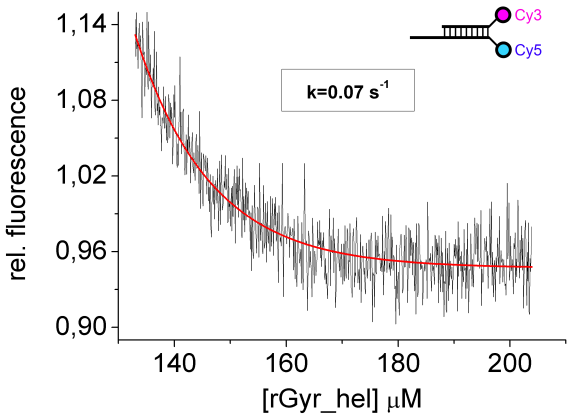
rel. fluorescence
[rGyr_hel] μM
k=0.07 s^{-1}
Cy3
Cy5

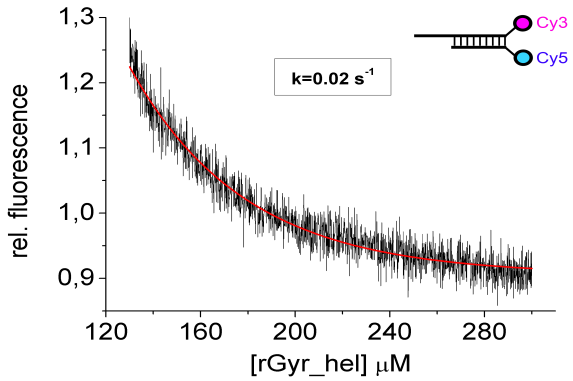
rel. fluorescence
[rGyr_hel] μM
k=0.02 s^{-1}
Cy3
Cy5

Figure 4

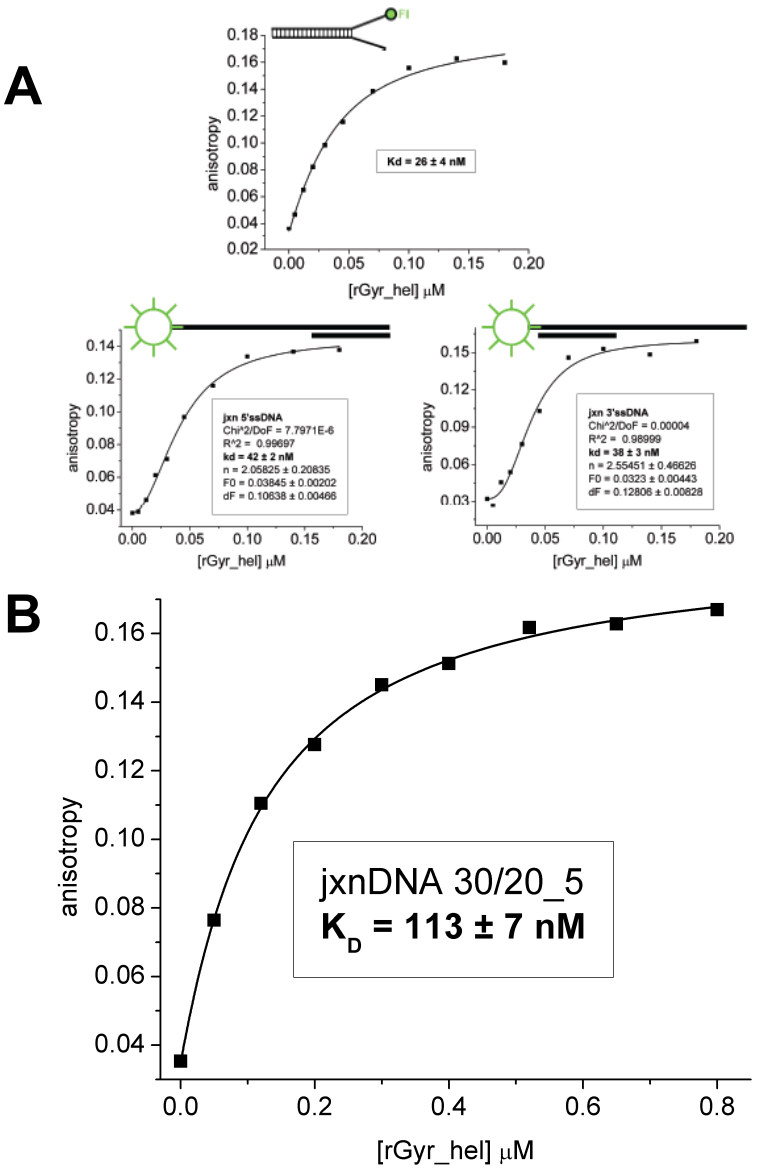
A
anisotropy
[rGyr_hel] μM
Kd = 26 ± 4 nM
jxn 5'ssDNA
Chi^2/DoF = 7.7971E-6
R^2 = 0.99697
kd = 42 ± 2 nM
n = 2.05825 ± 0.20835
F0 = 0.03845 ± 0.00202
dF = 0.10638 ± 0.00466
jxn 3'ssDNA
Chi^2/DoF = 0.00004
R^2 = 0.98999
kd = 38 ± 3 nM
n = 2.55451 ± 0.46626
F0 = 0.0323 ± 0.00443
dF = 0.12806 ± 0.00828
B
anisotropy
[rGyr_hel] μM
jxnDNA 30/20_5
K_D = 113 ± 7 nM

Figure 5

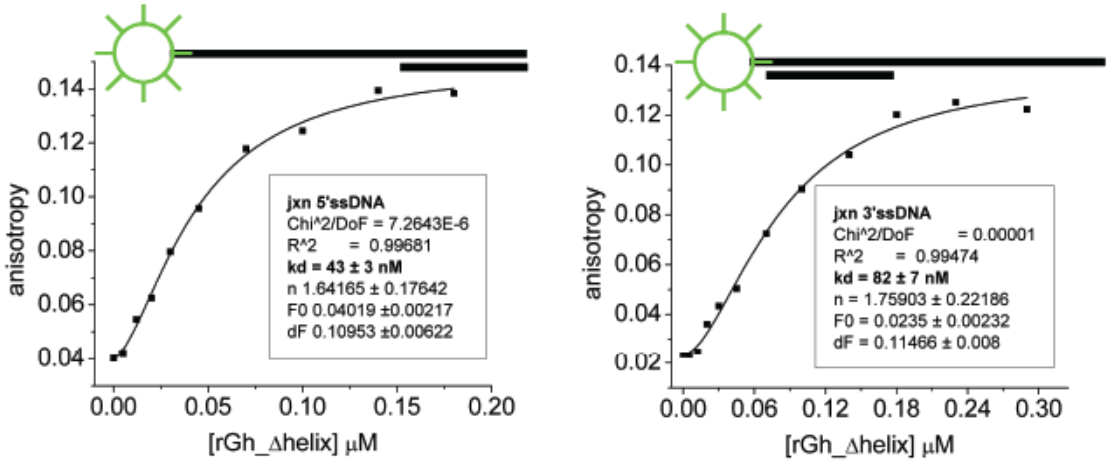

Figure 6

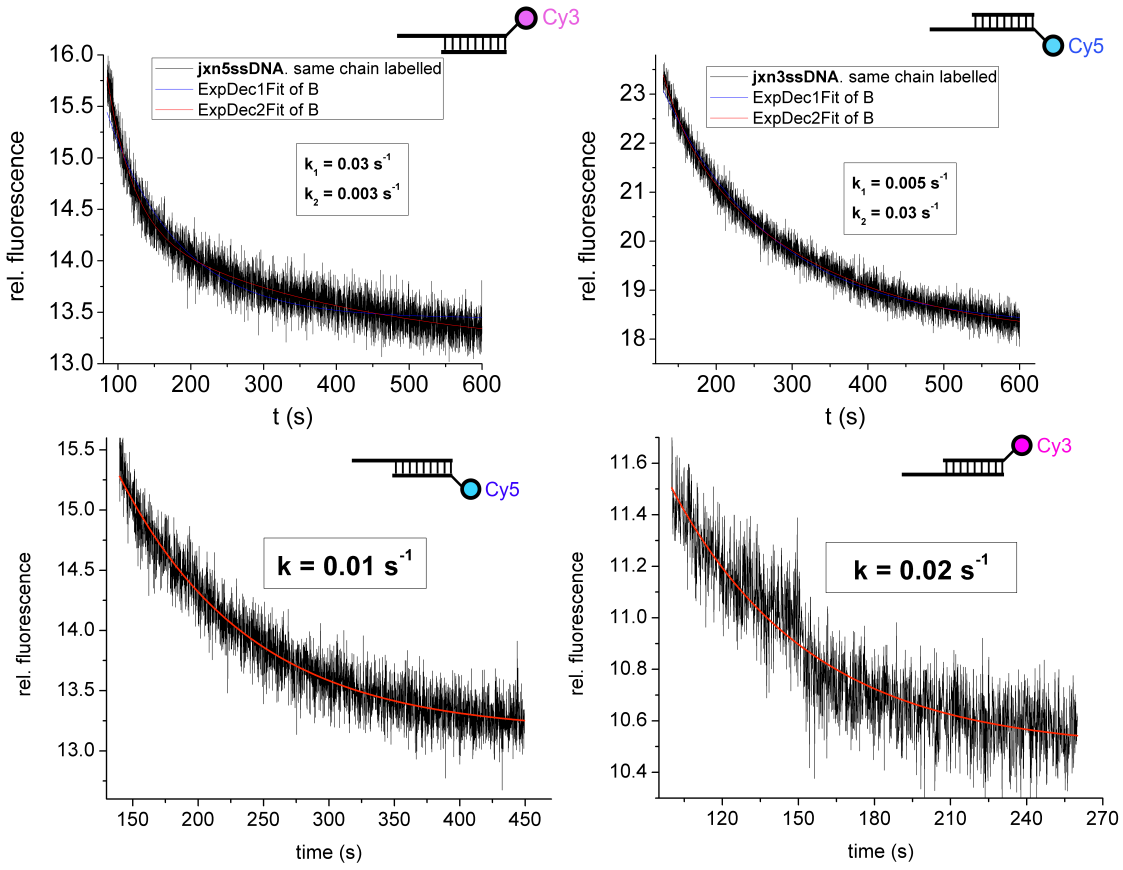

Figure 7

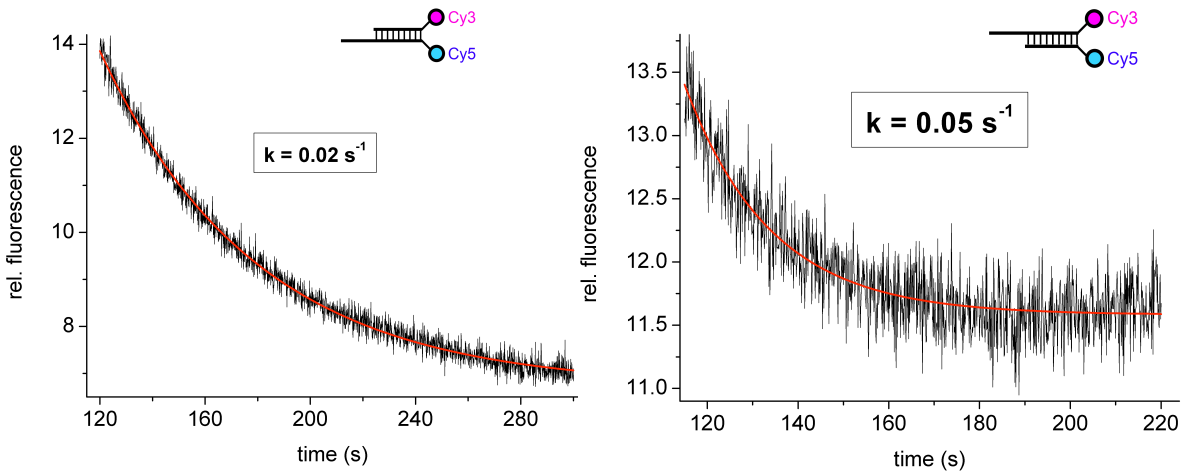

Figure 8

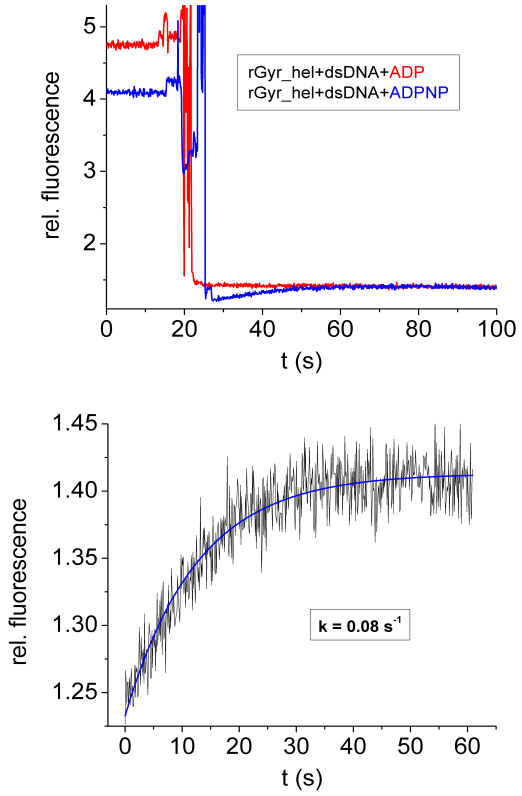

Figure 9

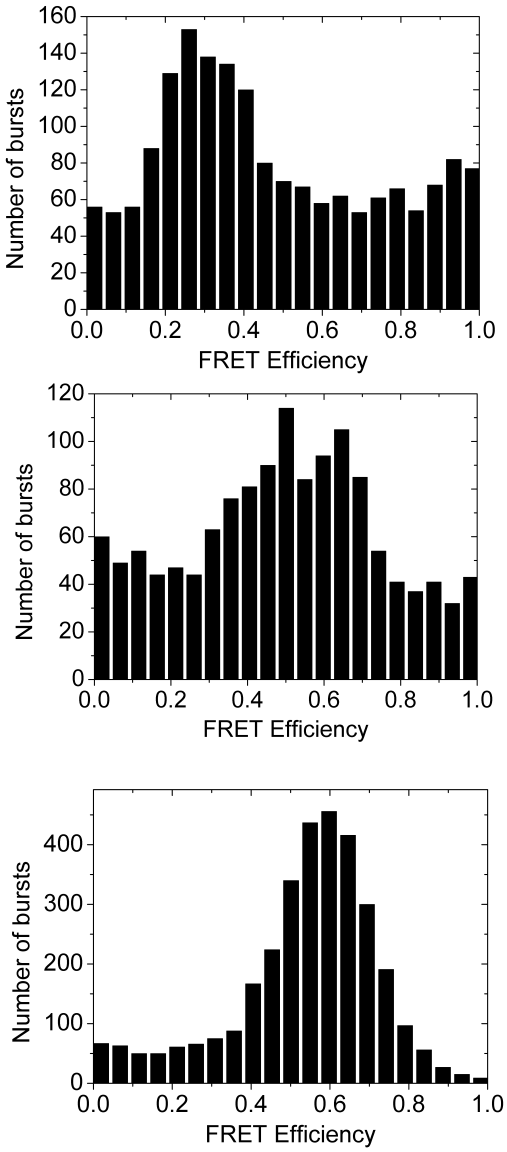

Figure 10

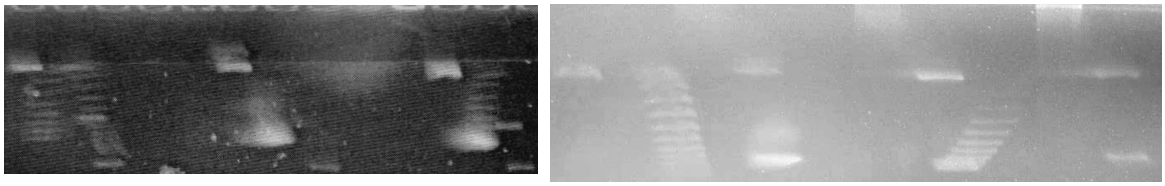

Figure 11

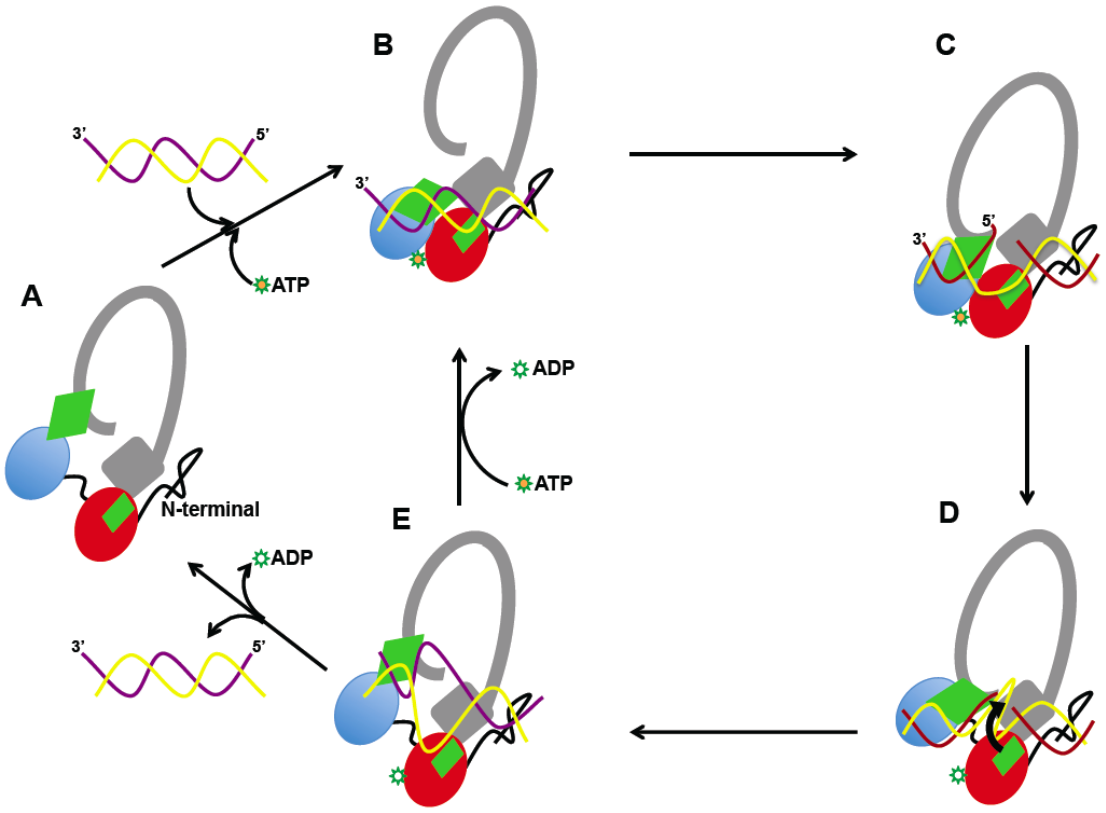

Figure 12

[1] A. Kikuchi *et al., Nature*, 1984, **309**, 677-681
[2] M. Kampmann *et al., Nucleic Acids Res.*, 2004, **32**, 3537-3545
[3] T. S. Hsieh *et al., J. Biol. Chem.*, 2006, **281**, 5640-5647
[4] F. Confalonieriet *et al., Proc. Natl. Acad. Sci.*, 1993, **90**, 4753-4757
[5] A. Ganguly *et al., Nucleic Acids Res.*, 2011, **39**, 1789-1800
[6] Y. del Toro Duany *et al., Nucleic Acids Res.*, 2008, **36**, 5882-5895
[7] Y. del Toro Duany *et al., Phys. Chem. Chem. Phys.,* 2011, **13**, 10009-10019
[8] K.J. Moore *et al., Biochemistry*, 1994, **33**, 14550-14564
[9] Y. del Toro Duany *et al., Biochemistry*, 2011, **50**, 5816-5823
[10] T. M. Lohman *et al., Annu. Rev. Biochem.*, 1996, **65**, 169-214
[11] S.P. Jungblut *et al., J. Mol. Bio.*, 2007, **371**, 197-209
[12] J.M. Keith *et al., Biochemistry*, 1994, **33**, 14550-14564
[13] B. Theissen *et al., Proc. Natl. Acad. Sci.*, 2008, **105**, 548-553
[14] M.W. Kellinger *et al., Proc. Natl. Acad. Sci*., 2010, **107**, 7734-7739
[15] A.C. Rodríguez *et al*., *EMBO J.*, 2002, **21**, 418-426
[16] H. Feinberg, *Nat. struct. Biol*., 1999, **6**, 961-968
[17] J.J. Champoux, *Annu. Rev. Biochem.*, 2001, **70**, 369-413

Figure 1. Stopped-flow measurement of the observed binding rates to mantdATP (A) and its dissociation from the complex (B).

Figure 2. Competition binding of mantdADP with ATP (A) and ADPNP (B).

Figure 3. Stopped-flow measurement of the observed binding rate of mantdADP in presence of saturating concentration of ssDNA.

Figure 4. FRET based DNA unwinding assay. Top: Unwinding by the helicase domain in presence of nucleotide analogues. Unwinding of junction DNA with 5' overhang (middle panel) and with 3' overhang (bottom panel) in presence of ADP.BeFx.

Figure 5. Fluorescence anisotropy titrations of reverse gyrase helicase-like domain with different DNA constructs. A: Top panel, titration with a fork DNA. Bottom panel, titrations with jxnDNAs with 5' (left) and 3' (right) single stranded DNA overhangs. B: control measurements with the junction DNA but with a 5' ssDNA overhang of same length as the fork DNA.

Figure 6. Fluorescence anisotropy titrations of rGyr_hel_Δhelix9 with junction DNAs having 5' and 3' single stranded overhangs in the left and right panels respectively.

Figure 7. Unwinding assays to measure single strand release using DNA substrates fluorescently labeled on one strand.

Figure 8. FRET based unwinding assay for rGyr_hel_Δhelix using DNA substrates with 3' overhang (left panel) and 5' overhang (right panel).

Figure 9. Closure of the cleft followed by change in intrinsic fluoresce from tryptophan residue. The upper panel shows rGyr_hel fluorescence quenching in presence dsDNA and ADP of ADPNP. The lower panel shows an expansion of the event upon ADPNP addition.

Figure 10. Single molecule FRET measurements of rGyr_hel with labels on the latch and the H1 domains. Upper panel shows FRET efficiency histograms for protein only, middle panel shows measurement in presence of jxnDNA and ADP.BeFx and the lower panel shows measurements in presence of ssDNA and ADP.MgFx.

Figure 11. Two-dimensional gel electrophoresis to visualize positive supercoiling. Lanes1, supercoiling in presence of ATP, Lanes 2, supercoiling in presence of ADP.BeFx and Lanes 3, supercoiling in presence of ADP.MgFx. The left panel depicts supercoiling in presence of 1 μM rgyr_wt while the right panel depicts the same reaction in presence of 2 μM enzyme.

Figure 12: improved catalytic cycle for reverse gyrase DNA positive supercoiling reaction. **A**: nucleotide- and DNA-free state, where the helicase-like domain is in an open conformation. **B**: upon addition of DNA and ATP, the helicase-like domain adopts a closed conformation, but only at a later stage closer to hydrolysis (**C**) local DNA unwinding occurs. It exposes the ssDNA region that the topoisomerase domain cleaves. **D**: the intact ssDNA strand is presumably relocated into the topoisomerase domain and the complementary strand is re-sealed, right after ATP hydrolysis. At this point the helicase-like domains adopts the open conformation, with the latch tilted inwards. **E**: the resulting DNA now has an increased linking number, and the enzyme may perform various ATP hydrolysis cycles before releasing the positively supercoiled DNA.

V. Discussion

Many vital processes related to DNA metabolism locally generate positively supercoiled DNA. Mesophilic organisms have developed mechanisms to control the torsional stress, by constitutively having negatively supercoiled DNA and/or by eliminating the positive supercoils as they are being generated. For thermophilic and hyperthermophilic organisms the challenge is different: as at higher temperatures the DNA duplex is highly unstable in the negatively supercoiled form, they need to prevent local unwinding with constitutive levels of relaxed or positively supercoiled DNA. These topological interconversions are controlled by topoisomerases, with reverse gyrase being the only one capable of positively supercoil DNA.

Reverse gyrase is a special case from a reaction mechanistic point of view, as nature instead of a brand-new design, “reuses” pre-existing modules to create a new function and facilitate life at high temperatures. The challenge about the modular build-up of this enzyme is to know how its components are optimized to cooperatively achieve supercoiling. Evidently, some properties of the individual modules are exploited, but others have to be harnessed or even suppressed for the sake of synchronization and timing. Furthermore, extensive communication between the modules is expected during the “team-play” that is the supercoiling reaction.

Characterization of rGyr_hel intrinsic ATPase activity

The steady-state kinetic measurements of the ATPase activity gave us the first experimental evidence regarding the role rGyr_hel plays in the supercoiling reaction. Comparison of the parameters for ATP hydrolysis by rGyr_hel and the full-length enzyme were virtually the same, confirming that the helicase-like domain of *T. maritima* reverse gyrase has all determinants for ATP binding and hydrolysis, and that it is not influenced by the deletion of the topoisomerase domain.

Further kinetic characterization of rGyr_hel ATPase activity included pre steady-state measurement of ADP binding, and ATP binding and hydrolysis. ATP binding to rGyr_hel could be directly measured because this reaction is under the rapid equilibrium system, *i.e.*, the rates of binding and dissociation of substrate and product are very rapid compared to the hydrolysis step. We have reported for the first time that rGyr_hel binds ATP in a two-step sequential mechanism, as previously reported for helicases of the same family[59]. Furthermore, we were also the first to identify the ATP hydrolysis as rate-limiting step for the overall reaction at 37°C, and also demonstrated that our measurements can be extrapolated to physiological temperatures, conclusion deduced from the linearity and the slopes of the Arrhenius and van't Hoff plots. The following scheme summarizes our kinetic characterization of rGyr_hel intrinsic ATPase activity.

$$hel + ATP \underset{100\,s^{-1}}{\overset{4.9\cdot10^{6}\,M^{-1}s^{-1}}{\rightleftharpoons}} hel \bullet ATP \underset{0.4\,s^{-1}}{\overset{42\,s^{-1}}{\rightleftharpoons}} hel \bullet ATP^{*} \xrightarrow{20\cdot10^{-3}\,s^{-1}} hel \bullet ADP \underset{1.3\cdot10^{-5}\,M^{-1}s^{-1}}{\overset{36\,s^{-1}}{\rightleftharpoons}} hel + ADP$$

On the other hand, smFRET measurements revealed that the conformational state of rGyr_hel does not change in the presence of nucleotides, in line with previous reports that the condition for a conformational change of the helicase core is the simultaneous binding of ATP and DNA[44].

Effect of DNA on rGyr_hel nucleotide cycle

The DNA-stimulation of rGyr and rGyr_hel ATPase activity under steady-state conditions revealed that the helicase-like domain is slowed down in the context of the full-length enzyme. This is an indication of a harnessing effect of the topoisomerase domain that makes rGyr_hel transit through the catalytic cycle at rates compatible with the apparently slower strand breakage, passage and resealing performed by the topoisomerase domain. The thermodynamic coupling between DNA binding and ATP hydrolysis, deduced from the increase of rGyr_hel apparent affinity for ATP under DNA saturating conditions, also was strongly reduced in the context of the full-length enzyme.

Nevertheless, there are reports of the topoisomerase domain having the opposite effect over the helicase-like domain in rGyr[55]. Our steady-state ATPase measurements with the mutant rGyr_hel_ZnF$_1$ reconcile these apparent contradictions. The presence of the N-terminal Zn-finger has a deleterious effect on DNA-stimulation of ATP binding and hydrolysis, comparable to the effect the topoisomerase domain exerts on rGyr_hel. These results indicate that rGyr Zn-fingers might strongly contribute to rGyr_hel harnessing in the context of the full-length enzyme, by competing for the DNA substrate, especially dsDNA. Overall, the decision of the start and end points in the rGyr gene sequence chosen to generate the isolated helicase core, as well as the use of rGyr from different organisms, seem to be the main reasons accounting for the apparently contradictory reports between helicase-like domains from reverse gyrases.

A thorough analysis of the effect of DNA on nucleotide binding and release from rGyr_hel also required the acquisition and comparison of thermodynamic parameters that could only be obtained by characterizing the interaction with intermediaries along the reaction path in equilibrium. This was achieved by using a combination of nucleotide analogs that arrest the reaction at different stages, and DNA constructs with the putative modifications introduced by helicases during the catalytic cycle.

The selected intermediates and ground state analogs were not only suited for equilibrium binding measurement, but also kinetic measurements under pre-steady state conditions. In the presence of DNA however, the activation energy for ATP hydrolysis is decreased, in line with the expected effect of thermodynamic coupling. It has as a consequence that the reaction falls into the steady-state system, which would imply the use of all rate constants for individual steps in data analysis, according to the King-Altman method, to extract the individual ATP binding and release rates[39]. Instead, we used a non-hydrolysable analog, ADPNP, which mimics the ATP ground state. Our equilibrium binding measurements revealed that rGyr_hel is a nucleotide-dependent switch that binds 20-fold stronger ADPNP and dsDNA when they are simultaneously present, indicating a strong positive coupling. Although this nucleotide cooperatively binds rGyr_hel in the presence of dsDNA, the

increase in the apparent affinity does not arise from changes in the binding or release rates, but on the conformational change that sequesters this analog, displacing the equilibrium and increasing the apparent affinity. We have been able to confirm *via* smFRET the conformational change that closes the cleft between rGyr_hel recA domains, and also to quantify the rate of the closure *via* direct detection of tryptophans fluorescence.

At the other end of the reaction, we revealed that rGyr_hel affinity for ADP is decreased in the presence of ssDNA, also in line with the expectation for thermodynamic coupling between the end products of any reaction. We demonstrated that this decrease in affinity for ADP in the presence of ssDNA is due mostly to the decrease of the binding rate constant, while the dissociation rate constant remains practically unaltered.

There are some differences between the actual DNA-stimulated ATP hydrolysis reaction and the recreated kinetic path using non-hydrolysable nucleotide analogs. First, ADPNP only resembles the ATP ground state and does not account for the ATP* isomerized stage. Our biochemical data suggest that the analog ADP·BeF_x most like resembles ATP*, but since ADPNP does not turn into ADP·BeF_x we cannot measure the rate for that transition. Also the DNA-stimulated ATP hydrolysis rate cannot be characterized using analogs. Although ATP hydrolysis is the rate-limiting step for rGyr_hel unstimulated reaction, and the k_{cat} for the reaction under steady-state conditions has the same value as the actual hydrolysis rate, is not certain whether it remains rate-limiting under DNA stimulation. Nevertheless, these analogs have kinetically revealed that the conformational change takes place before ATP isomerization, and that the effect of ssDNA on ADP release at the reaction end, is to decrease its binding rate to rGyr_hel. Bearing all this in mind, the DNA-stimulated kinetic cycle derived from the analysis of nucleotide analogs can be summarized as follows:

$$hel \bullet dsDNA + ADPNP \underset{8.2 s^{-1}}{\overset{1.7 \cdot 10^{7} M^{-1} s^{-1}}{\rightleftharpoons}} hel \bullet dsDNA \bullet ADPNP \underset{}{\overset{0.08 s^{-1}}{\rightleftharpoons}} hel \bullet dsDNA \bullet ADPNP \rightarrow \langle ... \rangle \rightleftharpoons hel \bullet ssDNA \bullet ADP \underset{4.8 \cdot 10^{6} M^{-1} s^{-1}}{\overset{45 s^{-1}}{\rightleftharpoons}} hel \bullet ssDNA + ADP$$

Catalytic cycle of rGyr_hel from a thermodynamic point of view

Although kinetically limited, the use of nucleotide analogs and different DNA constructs has proven to be extremely useful in thermodynamic and conformational dynamic studies. This approach allowed us to determine the nucleotide cycle of rGyr_hel, by identification of the reaction pathway with the intermediates of lowest energy along the energetic landscape of all possible routes. We therefore proposed a nucleotide cycle that clearly meets the expectations for a *bona fide* helicase. Fueled and controlled by the nucleotide bound, the enzyme vectorially transits through energetic and conformational states with a sequence of preferences for dsDNA, jxnDNA, and ssDNA at consecutive stages. Furthermore, the rGyr_hel catalyzed reaction also fulfilled the thermodynamic coupling requirements. Since normally ATP hydrolysis is a one-way process for molecular machines, rGyr-DNA complexes with the lowest binding energy and therefore most stable, were chosen at each nucleotide state of the enzyme. From the comparison of the relative binding energies of each ternary complex, we predicted that the transition at the pre-hydrolysis stage on a closed conformation of the enzyme and with the preference switch dsDNA-jxnDNA, in theory provides enough energy to achieve destabilization of 2-3 dsDNA bp. This finding laid the groundwork for us to further address the question of whether rGyr_hel unwinds DNA, by exactly determining the point of the cycle fulfilling the thermodynamic and conformational requirements. Our rGyr_hel nucleotide cycle has been already displayed[40].

Role of the latch in rGyr function

An intriguing structural feature of reverse gyrase structure is the latch domain, which happens to be an insertion into the H2 domain of the helicase-like core. It is homologous to the rho protein[18], a protein known to interact with RNA. From that fact, a possible role in interacting with DNA during supercoiling has been proposed. Furthermore, from its *sui generis* location between the helicase-like domain and the lid of the topoisomerase domain it has also been

suggested to play a key role in interdomain communication. This region sounded so relevant on paper that many groups did set out to determine its actual role in the supercoiling reaction. Most of their studies were performed using the full-length reverse gyrase, which as previously mentioned makes it difficult to dissect the contribution of particular segments of the protein. Nevertheless, a consensus arose that the latch deletion abolishes the rGyr capacity to positively supercoil DNA, and that it was only capable to relax negatively supercoiled DNA.

Our approach consisted on deleting the latch from rGyr_hel (rGyr_hel_Δlatch) and determining how DNA processing, nucleotide binding and hydrolysis, and the thermodynamic coupling between both processes was affected. The first surprise came from the steady-state DNA-stimulated ATPase activity, where the latch deletion mutant showed a 2-fold decreased ATP hydrolysis rate, compared to rGyr_hel. Also the thermodynamic coupling between DNA binding and ATP hydrolysis became virtually inexistent. Further analysis of nucleotide and DNA binding to rGyr_hel_Δlatch revealed an overall decreased affinity for DNA that was hardly influenced by the nucleotide state, unlike rGyr_hel. Also the conformational change reported for rGyr_hel in complex with dsDNA and ADPNP was inexistent. Only in the ADP·BeF_x-jxnDNA-bound state, rGyr_hel_Δlatch behaved as rGyr_hel, in terms of conformational state and affinity for the substrates.

Overall, deletion of the latch has drastic consequences either for the full-length rGyr or the helicase like domain. In the case of the first one its deletion has been described to abolish the introduction of positive supercoils. In the case of the helicase-like domain, it affects its intrinsic DNA and nucleotide binding, the coupling between both processes, as well as its conformational changes. In the following diagram of the H2 domain of the helicase-like module we can see how strategically located the latch is, between the β-strand connected to the consensus sequence V and the α-helix containing the consensus sequence VI. Motif V has been reported in Rep protein to engage in contact with the sugar-phosphate backbone of DNA, and mutational studies with UL5 have revealed decreased affinity of the enzyme for ssDNA and slower ATP hydrolysis rate[60]. Due to the close proximity of motif VI to the

nucleotide and DNA binding sites, reduction of DNA binding, ATP hydrolysis, coupling between both processes, and ligands-induced conformational changes, have also been reported in mutational analysis of several helicases[61]. It seems like smalls movements of the latch in the DNA-bound state indeed may provide feedback to the helicase-like domain by properly aligning or misaligning these motifs, and so control the rate of progression through the nucleotide cycle. On the other hand, the nucleotide state and conformation of the helicase core may also exert the opposite effect and force the latch to bind the "presented" DNA, and so the topoisomerase domain may sense and react "according to the plan" at this stage of the nucleotide cycle.

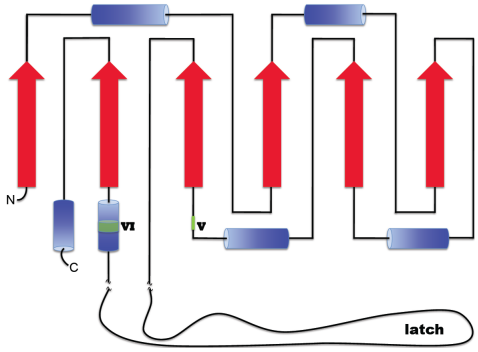

Overall, rGyr_hel_Δlatch has a preference for ssDNA throughout the nucleotide cycle, with the exception of the pre-hydrolysis state, where it prefers jxnDNA. It starts with an uncoupled binding of ADPNP and ssDNA, followed by a high affinity state for jxnDNA at the pre-hydrolysis step in the closed conformation. And finally, right after hydrolysis and prior to Pi release, although the preference for ssDNA is regained, it is bound with such a low affinity that most probably has as a consequence that rGyr_hel_Δlatch disengages from the contact with the DNA. The nucleotide cycle from a thermodynamic point of view was summarized in the schema at the end of the manuscript of Chapter IV.7.

DNA processing by rGyr_hel

After our thorough thermodynamic characterization of the nucleotide cycles of rGyr_hel and rGyr_hel_Δlatch, three steps have been highlighted due to their

potential usefulness in the overall supercoiling reaction. The rGyr_hel ADPNP-bound state has a high affinity for dsDNA and it adopts a closed conformation. The rGyr_hel and rGyr_hel_Δlatch ADP·BeF_x-bound states have high affinities for jxnDNA, are in the closed conformation, and on top of that the formation energy of the complexes are high enough to theoretically promote local destabilization of DNA duplex. The rGyr_hel ADP.MgF_x-bound state is no longer in the closed conformation, but still has a high affinity for ssDNA, and adopts a distinctive conformation, with the latch pointing towards the H1 domain.

First, we tried to demonstrate whether rGyr_hel is able to unwind DNA, and how are the unwinding rates modified by comparison with selected deletion mutants and the full-length rGyr. As predicted, only in the presence of ADP·BeF_x and jxnDNA unwinding was detected. rGyr failed to unwind any DNA with any nucleotide. rGyr_hel on the other hand, was able to unwind a jxnDNA with a 3'ssDNA overhang almost 4-times faster than the jxnDNA with a 5'ssDNA overhang. rGyr_hel_Δlatch however, retained the preference for the jxnDNA with a 3'ssDNA overhang, but it was unwound half as fast as rGyr_hel. We also created another deletion mutant of a region in the H1 domain that was predicted to be involved in DNA binding. Interestingly, this region folded as a β-hairpin in the structure from *A. fulgidus* rGyr, while in the structure we solved for our *T. maritima* helicase-like domain it is a α-helix. This mutant (rGyr_hel_Δhelix9) showed the same unwinding rates as rGyr_hel, but with inverted preferences. Complementary jxnDNA binding assays revealed that even though rGyr_hel has no preference for the ssDNA overhang at a jxnDNA, the latch specifically binds to the 5'ssDNA overhang and the helix9 to the 3'ssDNA overhang. Overall, DNA unwinding tests depend not only on duplex destabilization but on strand release as well. We therefore quantified the rates of strands release from rGyr_hel for the jxnDNAs used. Independent of the substrate, the strand with the 5'-directionality was always the first to be released.

Surprisingly, no DNA unwinding could be detected in the presence of ATP. It might be a consequence of the slow rates of strand release compared to the

rates of DNA-stimulated ATP hydrolysis, which are two orders of magnitude different.

After characterizing the nucleotide cycle of reverse gyrase helicase-like domain, we set out to demonstrate what our results indicate, in the context of the DNA supercoiling reaction by the full-length enzyme. We therefore performed the reaction assay in the presence of the nucleotide analogs ADP·BeF_x and ADP.MgF_x, for the wild-type rGyr and rGyr_Δlatch. Interestingly, the main difference arose from the reaction in the presence of ADP·BeF_x, where rGyr is only able to produce nicked DNA and rGyr_Δlatch is able to relax DNA. It indicates a role of the latch preventing the lid from resealing the broken strand before the conformational change that relocates the intact ssDNA strand in a position suited for positive supercoiling. This conformational state that relocates the intact strand is presumably the one in the presence of ADP.MgF_x.

DNA supercoiling catalytic cycle improved

Our experimental results on the isolated helicase-like domain and the comparison with the full length enzyme, enabled us to provide input to the current knowledge of the mechanism of catalysis by reverse gyrase. We have improved the putative catalytic cycle derived from the only structure available of a full-length reverse gyrase, by elucidating the role the helicase-like domain plays in DNA processing, and how it correlates with the nucleotide cycle. Additionally, the relevance of individual motifs and domains belonging to the helicase-like module at different points of the reaction has also been determined.

Starting with the substrate-free enzyme, the model for the catalytic cycle is represented by the solved crystal structure and therefore has no room for improvement. At this stage the helicase-like domain is in an open conformation, and the latch is located in close proximity to the lid of the topoisomerase domain, what is supposed to restrict its dynamics. Upon binding of ATP and DNA, the helicase-like domain adopts a closed conformation that is expected to release the lid from the interaction with the

latch. Nevertheless, at this stage no local DNA unwinding takes place yet. As the reaction approaches the ATP hydrolysis step, the bound DNA is unwound and the catalytic tyrosine in the lid is able to cleave the exposed ssDNA strand, remaining bound to the 5’ end. Right after hydrolysis the helicase-like domain returns to the open conformation, what presumably allows relocation of the intact ssDNA strand into the cavity of the topoisomerase domain. At this point we succeeded to detect an additional conformational state, where the latch is tilted inwards, which might facilitate ssDNA strand resealing. Finally, the DNA-bound enzyme can undergo additional ATP hydrolysis cycles before releasing the DNA, resulting in the increasing of the linking number in one unit per cycle.

VI. Acknowledgements

This work was performed at Dagmar Klostermeier's group in the Biozentrum of the University of Basel, from 2007 to 2011. It was supported by the Volkswagenstiftung and the SNF.

First of all I want to thank Dagmar for the chance to work on this project. The experience exceeded my expectations, and working under her guidance has actually brought the best out of me. Thanks for all I have learned from you!

I want to thank Prof. Dr. Joachim Seelig for the working environment in the Biophysical Chemistry Department, as well as the input in the departmental seminar. A special thanks goes to Prof. Dr. Nenad Ban, who kindly agreed to be my co-examiner.

I also want to thank the "people of the lab" for the AMAAAZING times we had together these four and something years. It feels not like I'm leaving work colleagues behind, but really close friends that I hope to keep in touch with. I want to thank Stefan Jungblut and Agneyo Ganguly for the teamwork, in and outside the lab. And specially I thank Lenz Steimer for his friendship, his help, his support, and the really special times we had everyday on the coffee break.

Last but not least, I want to thank family and friends, that were not in the lab but contributed to this outcome. Luis Rey Carrera Mannin for the times shared, not only in the disco but also pulling all-nighters to help me meet the "Abgabetermin". Debajyoti Chakrabarti for standing my speech rehearsals, even when he had no clue what I was talking about. Beatrix and Edith Berger for their invaluable support. And last but not least I want to thank my mother, the most important person in my life.

I love U guys (and girls)!

VII. References

[1] P. Forterre, *Trends Genet.*, 2002, **18**, 236–237.3

[2] H. Atomi *et al.*, *J. Bacteriol.*, 2004, **186**, 4829-4833

[3] A. Kikuchi *et al.*, *Nature*, 1984, **309**, 677-681

[4] T. Lindahl, *Nature*, 1993, **362**, 709-715

[5] M. Kampmann, *et al.*, *Nucleic Acids Res.*, 2004, **32**, 3537-3545

[6] T. Hsieh *et al.*, *J. Biol. Chem.*, 2006, **281**, 5640-5647

[7] F. Charbonnier *et al.*, *J. Bacteriol.*, 1992, **174**, 6103-6108

[8] F. Charbonnier *et al.*, *J. Bacteriol.*, 1994, **176**, 1251-1259

[9] J. Champoux, *Annu. Rev. Biochem.*, 2001, **70**, 369-413

[10] M. Duguet, *Nucleic Acids Res.*, 1993, **21**, 463-468

[11] G. Hatfield *et al.*, *Annu. Rev. Genet.*, 2002, **36**, 175-203

[12] K. Drlica, *Trends Genet.*, 1990, **12**, 433-437

[13] F. Crick, *Proc. Natl. Acad. Sci.*, 1976, **73**, 2639-2643

[14] P. Forterre *et al.*, *FEMS Microbiol. Rev.*, 1996, **18**, 237-248

[15] P. Forterre *et al.*, *EMBO J.*, 1985, **4**, 2123-2128

[16] F. Confalonieri *et al.*, *Proc. Natl. Acad. Sci.*, 1993, **90**, 4753-4757

[17] A. Ganguly *et al.*, *Nucleic Acids Res.*, 2011, **39**, 1789-1800

[18] A.C. Rodríguez *et al.*, *EMBO J.*, 2002, **21**, 418-426

[19] A.C. Declais *et al.*, *J. Biol. Chem.*, 2000, **275**, 19498-19504

[20] Y. del Toro Duany *et al.*, *Nucleic Acids Res.*, 2008, **36**, 5882-5895

[21] H. Feinberg *et al.*, *Nature Struct. Biol.*, 1999, **6**, 918-922

[22] S.S. Velankar *et al.*, *Cell*, 1999, **97**, 75-84

[23] A.M. Pyle, *Annu. Rev. Biophys.*, 2008, **37**, 317-336

[24] M. Venkatesan *et al.*, *J. Biol. Chem.*, 1982, **257**, 12426-12434

[25] M.E. Fairman *et al.*, *Science*, 2004, **304**, 730-734

[26] L. Rajkowitsch *et al.*, *RNA Biol.*, 2007, **4**, 118-130

[27] M. Hilbert *et al.*, *J. Biol. Chem.*, 2009, **390**, 1237-1250

[28] N. Tuteja *et al.*, *Eur. J. Biochem.*, 2004, **271**, 1849-1863

[29] T. Lohman *et al.*, *Annu. Rev. Biochem.*, 1996, **65**, 169-214

[30] M.R. Singleton *et al.*, *Annu. Rev. Biochem.*, 2007, **76**, 23-50

[31] J.E. Walker *et al.*, *EMBO J.*, 1982, **1**, 945-951

[32] G.E. Schulz, *Curr. Opin. Struct. Biol.*, 1992, **2**, 61-67

[33] A.E. Gorbalenya *et al.*, *Curr. Opin. Struct. Biol.*, 1993, **3**, 419-429

[34] R.M. Story *et al.*, *Nature*, 1992, **355**, 318-325

[35] A.F. Neuwald *et al.*, *Genome Res.*, 1999, **9**, 27-43

[36] K. Chao *et al.*, *J. Mol. Biol.*, 1991, **221**, 1165-1181

[37] B. Nanduri *et al.*, *Proc. Natl. Acad. Sci.*, 2002, **99**, 14722-14727

[38] S.R. Schmid *et al.*, *Mol. Microbiol.*, 1992, **6**, 283-291

[39] I.H. Segel, *Enzyme kinetics*, 1993, John Wiley & Sons, Inc.

[40] Y. del Toro Duany *et al., Phys. Chem. Chem. Phys.,* 2011, **13**, 10009-10019

[41] F.W. Studier *et al.*, *Protein Expr. and Purif.*, 2005, **41**, 207-234

[42] U.K. Lämmli, *Nature*, 1970, **227**, 680-685

[43] M.M. Bradford, *Anal. Biochem.*, 1976, **72**, 248-254

[44] B. Theissen *et al., Proc. Natl. Acad. Sci.*, 2008, **105**, 548-553

[45] J.K. Weltman *et al.*, *J. Biol. Chem.*, 1973, **248**, 3173-3177

[46] T. Förster, *Naturwissenschaften*, 1946, **33**, 166-175

[47] A. Ganguly *et al.*, *Nucleic Acids Res.*, 2011, **39**, 1789-1800

[48] A.C. Rodríguez *et al.*, *EMBO J.*, 2002, **21**, 418-426

[49] C.D. Lima *et al., J. Mol. Biol*., 1993, **232**, 213-216

[50] Y. del Toro Duany *et al., Nucleic Acids Res*., 2008, **36**, 5882-5895

[51] Y. del Toro Duany *et al., Biochemistry*, 2011, **50**, 5816-5823

[52] H. Feinberg *et al., Nat. Struct. Biol*., 1999, **6**, 961-968

[53] A. Changuela *et al., Nature, 2001*, **411**, 1077-1081

[54] A. Klug, *Annu. Rev. Biochem*., 2010, **79**, 213-231

[55] C. Capp *et al., J. Biol. Chem*., 2010, **285**, 39637-39645

[56] Y. del Toro Duany *et al., Phys. Chem. Chem. Phys.,* 2011, **13**, 10009-10019

[57] Y. del Toro Duany *et al., Nucleic Acids Res.*, 2008, **36**, 5882-5895

[58] T. M. Lohman *et al., Annu. Rev. Biochem.*, 1996, **65**, 169-214

[59] K.J.M. Moore *et al,. Biochemistry*, 1994, **33**, 14550-14564

[60] M.C. Hall *et al*., *Mol. Microbiol*., 1999, **34**, 867-877

[61] A. Pause *et al.*, *EMBO J.*, 1992, **11**, 2643-2654

[49]D.L. Nelson *et al., Lehninger Principles of Biochemistry*, 2009, W.H. Freeman & Co